

AD-A034 788

NAVAL SURFACE WEAPONS CENTER WHITE OAK LAB SILVER SP--ETC F/G 13/13  
A GENERALIZED FINITE DIFFERENCE ELEMENT FOR THE THERMOELASTIC S--ETC(U)  
JUN 76 R J EDWARDS

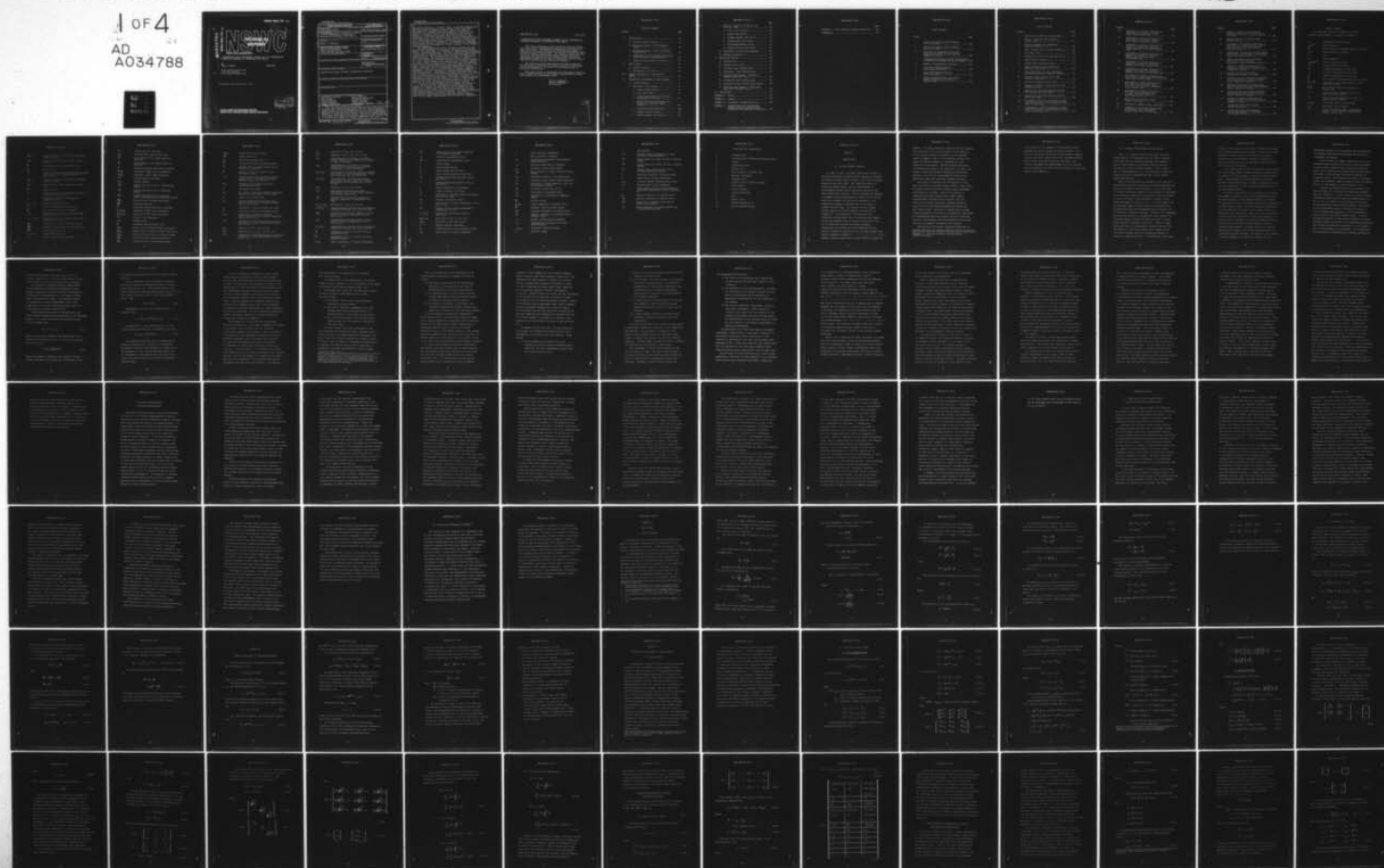
UNCLASSIFIED

NSWC/WOL/TR-76-66

NL

1 OF 4

AD  
A034788



NSWC/WOL/TR 76-66

ADA 034788

NSWC/WOL/TR 76-66

# NSWC

## TECHNICAL REPORT

WHITE OAK LABORATORY

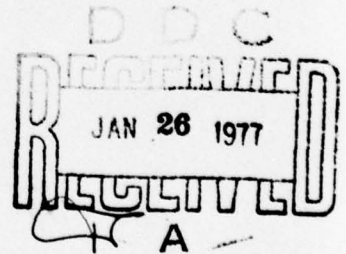
A GENERALIZED FINITE DIFFERENCE ELEMENT FOR THE THERMOELASTIC  
STRUCTURAL RESPONSE OF ANISOTROPIC THIN SHELLS

BY  
Robert J. Edwards

JUNE 1976

NAVAL SURFACE WEAPONS CENTER  
WHITE OAK LABORATORY  
SILVER SPRING, MARYLAND 20910

- Approved for public release; distribution unlimited



NAVAL SURFACE WEAPONS CENTER  
WHITE OAK, SILVER SPRING, MARYLAND 20910

V



UNCLASSIFIED

SECURITY CLASSIFICATION OF THIS PAGE (When Data Entered)

REPORT DOCUMENTATION PAGE		READ INSTRUCTIONS BEFORE COMPLETING FORM
1. REPORT NUMBER NSWC/WOL/TR-76-66	2. GOVT ACCESSION NO.	3. RECIPIENT'S CATALOG NUMBER 9 Technical rept. g
4. TITLE (and Subtitle) A Generalized Finite Difference Element for the Thermoelastic Structural Response of Anisotropic Thin Shells		5. TYPE OF REPORT & PERIOD COVERED
7. AUTHOR(s) Robert J. Edwards		6. PERFORMING ORG. REPORT NUMBER
9. PERFORMING ORGANIZATION NAME AND ADDRESS Naval Surface Weapons Center White Oak Laboratory Silver Spring, Maryland 20910		8. CONTRACT OR GRANT NUMBER(s) 16 F 32 322 17 SF 32 322 507
11. CONTROLLING OFFICE NAME AND ADDRESS		10. PROGRAM ELEMENT, PROJECT, TASK AREA & WORK UNIT NUMBERS SEA 18457/SF32-322-507
14. MONITORING AGENCY NAME & ADDRESS (if different from Controlling Office)		12. REPORT DATE June 1976
		13. NUMBER OF PAGES 312
		15. SECURITY CLASS. (of this report) UNCLASSIFIED
		15a. DECLASSIFICATION/DOWNGRADING SCHEDULE
16. DISTRIBUTION STATEMENT (of this Report) Approved for public release; distribution unlimited		
17. DISTRIBUTION STATEMENT (of the abstract entered in Block 20, if different from Report)		
18. SUPPLEMENTARY NOTES		
19. KEY WORDS (Continue on reverse side if necessary and identify by block number) Structural Analysis      Matrix Methods Thin Shells      Anisotropic Materials Energy Methods      Thermal Stresses Finite Elements      Tensor Analysis Finite Differences      Isoparametric Mapping		
20. ABSTRACT (Continue on reverse side if necessary and identify by block number) Two well established matrix methods for thin shell structural analysis, the finite element method and the finite difference energy method, have been integrated into one unified analytical approach and have been effectively applied to the thermoelastic analysis of anisotropic thin shells. The finite element method is a widely used tool for structural analysis of thin shells due to its ability to model the complex geometries that occur in		

DD FORM 1 JAN 73 1473

EDITION OF 1 NOV 65 IS OBSOLETE  
S/N 0102-014-6601

UNCLASSIFIED

SECURITY CLASSIFICATION OF THIS PAGE (When Data Entered)

UNCLASSIFIED

SECURITY CLASSIFICATION OF THIS PAGE(When Data Entered)

20.

engineering practice. In recent years, it has been demonstrated that the finite difference energy method offers significant advantages over contemporary finite element formulations especially for problems involving geometrical nonlinearities. However, the method suffers from the modeling restrictions imposed by rectangular gridworks which must follow the shell coordinate lines. The results of this research demonstrate that this classic restriction can be removed and that a generalized finite difference energy method can be developed for arbitrary quadrilateral meshes. Furthermore, the formulation is amenable to installation in contemporary, general purpose, finite element computer programs.

The SHEFA generalized finite difference element for the thermoelastic analysis of anisotropic thin shells is developed herein. The term SHEFA is an acronym for SHell ELement based on a FInite difference APproach. The shell reference surface geometry is described in terms of curvilinear surface coordinates using tensor notation. The deformation of the shell is described by the linear strain and curvature change tensors of Sanders. A shell wall model has been developed that is sufficiently general to treat a broad range of wall constructions including layered orthotropic walls, filament wound walls and angle ply composite walls as well as more conventional monocoque construction. The model treats the effects of nonlinear temperature gradients through the shell wall, including material property temperature dependence, and also accounts for coupling between membrane and bending action. Isoparametric mapping techniques have been used to establish a finite difference approximation of the strain and curvature tensors in terms of displacement variables at arbitrarily placed discrete nodes on the shell reference surface. The potential energy of the structural system is then formed in terms of the nodal variables and the equations of motion are obtained by use of the Minimum Potential Energy Theorem.

A series of twelve demonstration problems were solved to verify the accuracy and convergence characteristics of the element in a variety of applications and to demonstrate the generality of the element via several problems that are most efficiently modeled with arbitrary meshes. The SHEFA predictions were verified against classical analytical solutions or experimental results, and in some cases, the results obtained with finite element formulations were available for comparison.

UNCLASSIFIED

SECURITY CLASSIFICATION OF THIS PAGE(When Data Entered)

1 June 1976

A GENERALIZED FINITE DIFFERENCE ELEMENT FOR THE THERMOELASTIC  
STRUCTURAL RESPONSE OF ANISOTROPIC THIN SHELLS

This report describes a newly developed numerical method for predicting the thermoelastic response of anisotropic thin shell structures. The theoretical development and report preparation was sponsored under the Naval Surface Weapons Center Advanced Graduate Study Program. The computer coding and check out of the analysis method was funded under the Structural Technology for Advanced Re-entry Systems (STAR) exploratory development program as one task in the general area of re-entry vehicle structural analysis methods development.

The results of this investigation have been accepted by the University of Maryland as a thesis in partial fulfillment of the requirements of the Doctor of Philosophy Degree in Mechanical Engineering.

The author wishes to acknowledge the programming assistance of Mr. Myles Hurwitz of the Navy Nastran Systems Office, Naval Ship Research and Development Center.

*Leon H. Schindel*  
LEON H. SCHINDEL  
By direction

WOL Section	<input checked="" type="checkbox"/>
WOL Section	<input type="checkbox"/>
WOL Section	<input type="checkbox"/>
DISTRIBUTION/AVAILABILITY CODES	
APPROVAL AND SPECIAL	
A	



## TABLE OF CONTENTS

Chapter	Page
I. INTRODUCTION.....	19
A. Discrete Element Analysis.....	19
B. Historical Review - Finite Element Method.....	22
C. Historical Review - Finite Difference Energy Method.....	40
D. Comparison of Finite Element Method and Finite Difference Energy Method.....	50
E. Objective and Synopsis of Research.....	57
II. SHELL THEORY .....	59
A. Surface Geometry.....	59
B. Deformation of the Shell.....	66
III. GENERAL DESCRIPTION OF THE ANALYSIS METHOD.....	69
IV. THEORETICAL DEVELOPMENT OF SHEFA ELEMENT....	73
A. General Remarks.....	73
B. Thin Shell Strain Energy.....	75
1. Strain Energy Density.....	75
2. Shell Wall Model.....	79
3. Strain-Displacement and Curvature-Displacement Relations.....	87
4. Finite Difference Approximation to Strain and Curvature Change Tensors.....	90
5. Coordinate Transformations.....	106
6. Element Stiffness Matrix.....	117
7. Element Thermal Load Vector.....	121

	Page
C. Potential Energy of Mechanical and Inertial Loads.....	124
1. Total Work Potential.....	124
2. Element Mass Matrix.....	127
3. Element Surface Load Vector.....	133
4. Concentrated Force Vector.....	136
5. Concentrated Moment Vector.....	141
6. Element Gravity Load Vector.....	144
D. Calculation of Structural Response.....	147
E. Boundary Conditions.....	161
V. ANALYTICAL RESULTS.....	166
A. Introduction.....	166
B. Membrane Plate Study.....	170
C. Isotropic Plate Bending Study.....	172
D. Anisotropic Plate Bending Study.....	178
E. Arbitrary Mesh Example - Bending of Rhombic Cantilever Plate.....	181
F. Cylindrical Shell Bending Study.....	183
G. Cylindrical Shell Thermal Stress Study.....	186
H. Arbitrary Mesh Example - Cylindrical Shell With Circular Cutout.....	188
VI. CONCLUSIONS.....	191
APPENDIX A. Tables.....	195
APPENDIX B. Figures.....	205
APPENDIX C. Discussion of Shape Functions.....	249
APPENDIX D. Inverse Functional Relationship Between Surface Coordinates and Parametric Interpolating Coordinates...	259



	Page
APPENDIX E. Shell Reference Surface Geometries....	275
REFERENCES.....	301

## LIST OF TABLES

Tables		Page
1	Curved, Thin Shell, Finite Elements With Four Sides.....	196
2	Curved, Thin Shell, Finite Elements With Three Sides.....	197
3	Abscissae of Integration Points and Weight Coefficients for the Gaussian Quadrature Formula.....	198
4	Correspondence Between Element Interpolating Coordinates and Element Connection Number...	199
5	Summary of Demonstration Problems.....	200
6	Flat Plate Membrane Behavior Displacement Solutions.....	201
7	Flat Plate Membrane Behavior Stress Solutions.....	202
8	Stress Concentrations in an Axially Loaded Cylindrical Shell With a Circular Hole.....	203

## LIST OF FIGURES

Figures		Page
1	STAGS Finite Difference Mesh Schemes.....	206
2	Finite Difference Mesh Scheme by Johnson [110].....	207
3	Discrete Elements for Comparative Study by Bushnell [114].....	208
4	Shell Geometry and Coordinate Systems.....	209
5	Shell Wall Model.....	210
6	Temperature Gradient Through Shell Wall.....	211
7	SHEFA Element Geometry.....	212
8	Element Edge Coordinate System.....	213
9	Sign Conventions for Displacements, Rotations and Stresses.....	214
10	Sign Conventions for Force and Moment Resultants Acting on Reference Surface.....	215
11	Analysis Conditions for Plate Under Parabolic Edge Load.....	216
12	Meshes for Membrane Plate Study.....	217
13	Summary of Analysis Conditions for Plate Bending Problems.....	218
14	Typical Mesh for Plate Bending Problems With Simply-Supported Edges.....	219
15	Typical Mesh for Plate Bending Problems With Fixed Edges.....	220
16	Convergence of Central Deflection vs Mesh Size for Isotropic, Simply-Supported Plate Under Uniform Load.....	221
17	Convergence of Central Deflection vs Mesh Size for Isotropic, Simply-Supported Plate Under Concentrated Load.....	222

Figures		Page
18	Convergence of Central Deflection vs Mesh Size for Isotropic, Clamped Plate Under Uniform Load.....	223
19	Convergence of Central Deflection vs Mesh Size for Isotropic, Clamped Plate Under Concentrated Load.....	224
20	Convergence of Central Deflection vs Degrees of Freedom for Isotropic, Simply-Supported Plate Under Uniform Load.....	225
21	Convergence of Central Deflection vs Degrees of Freedom for Isotropic, Simply-Supported Plate Under Concentrated Load.....	226
22	Convergence of Central Deflection vs Degrees of Freedom for Isotropic, Clamped Plate Under Uniform Load.....	227
23	Convergence of Central Deflection vs Degrees of Freedom for Isotropic, Clamped Plate Under Concentrated Load.....	228
24	Convergence of Central Deflection vs Mesh Size for Simply-Supported Orthotropic Plate Under Uniform Load.....	229
25	Convergence of Central Deflection vs Mesh Size for Anisotropic Plate (10 Layer, +30° Angle-Ply Composite) Under Uniform Load.....	230
26	Convergence of Central Deflection vs Mesh Size for Anisotropic Plate (2 Layer, Cross-Ply Composite) Under Uniform Load.....	231
27	Deflection of Uniformly Loaded Rhombic Cantilever.....	232
28	Cantilevered Rhombic Plate, 13x13 Mesh.....	233
29	Comparison of Predicted Displacements vs Experiment for Cantilevered Rhombic Plate Under Uniform Load.....	234



Figures		Page
30	Summary of Analysis Conditions for Cylindrical Shell With Circumferential Line Load.....	235
31	Typical Mesh for Cylindrical Shell Bending Problem.....	236
32	Convergence of Deflection Under Load vs Mesh Size for Cylindrical Shell With a Load Uniformly Distributed Along a Circular Section.....	237
33	Displacement Distribution for Cylindrical Shell With a Load Uniformly Distributed Along a Circular Section.....	238
34	Moment Distribution for Cylindrical Shell With a Load Uniformly Distributed Along a Circular Section.....	239
35	Summary of Analysis Conditions for Cylindrical Shell With Nonlinear Radial Temperature Gradient.....	240
36	Cylinder With Nonlinear Radial Temperature Gradient, 3x20 Mesh.....	241
37	Material Property Temperature Dependence for Cylindrical Shell With Nonlinear Radial Temperature Gradient.....	242
38	Temperature Distribution Through Shell Wall for Cylindrical Shell With Nonlinear Radial Temperature Gradient.....	243
39	Stress Distribution Through Shell Wall for Cylindrical Shell With Nonlinear Radial Temperature Gradient.....	244
40	Summary of Analysis Conditions for Cylindrical Shell With Circular Cutout Loaded in Tension.....	245
41	Cylindrical Shell With Circular Cutout, 20x20 Mesh.....	246
42	Cylindrical Shell With Circular Cutout, Enlargement of 20x20 Mesh in Vicinity of Hole.....	247



## LIST OF SYMBOLS

The following is a list of symbols used in the analytical developments of Chapters II through IV:

$a$	determinant of metric tensor
$a_{\alpha\beta}, a^{\alpha\beta}$	metric tensors
$\vec{a}_\alpha$	base vectors for Gaussian surface coordinates
$[a_M]$	matrix defined by (IV.194)
$A$	area
$A_\alpha$	Lame' parameters
$b_{\alpha\beta}, b_\beta^\alpha, b^{\alpha\beta}$	initial curvature tensors
$[b]$	matrix defined by (IV.138)
$[B]$	bending compliances for shell wall
$[C]$	coupling compliances for shell wall
$[D]$	membrane compliances for shell wall
$\vec{e}_\alpha$	unit vectors for Gaussian surface coordinates
$\vec{e}_3$ or $\vec{e}_n$	unit vector along outward normal to shell reference surface
$\vec{e}_t, \vec{e}_s$	unit vectors tangent and normal to an element edge
$\{e\}$	physical strain components at point on shell reference surface
$\{\bar{e}\}$	physical strain components at point off shell reference surface
$E_{11}, E_{22}$	orthotropic moduli of elasticity
$E_{12}$	orthotropic shear modulus
$[E]$	matrix relating membrane displacement gradient vector to element displacement vector, see (IV.105)

$E^{\alpha\beta\lambda\rho}$	elastic material constant tensor relating strain to stress
$[E]$	matrix form of elastic material constant tensor
$\vec{F}$	externally applied concentrated force
$\vec{F}_g$	gravity force
$[F]$	matrix relating bending displacement gradient vector to element displacement vector, see (IV.84)
$F_{\alpha\beta\lambda\rho}$	elastic material constant tensor relating stress to strain
$[F]$	matrix form of elastic material constant tensor
$\vec{g}$	gravity vector
$[G]$	matrix form of physical material constants relating strain to stress
$H_i$	weighting coefficients for Gaussian quadrature formula
$H_1, \dots, H_9$	quadratic shape functions
$[H]$	matrix of quadratic shape functions
$\vec{I}_i$	unit vectors for basic coordinates
$[J_1]$	Jacobian matrix for in-plane displacement gradients, see (IV.75)
$[J_2], \dots, [J_5]$	Jacobian matrices for normal displacement gradients, see (IV.92)
$[K_e]$	tensor form of element stiffness matrix
$[\bar{K}_e]$	physical form of element stiffness matrix
$[\bar{K}]$	system stiffness matrix
$L_1, \dots, L_4$	linear shape functions
$[L]$	matrix of linear shape functions

$\bar{m}_e$	element mass per unit area
$\bar{m}_{ns}$	non-structural mass per unit area
$\bar{m}_e^C$	first moment of the element mass per unit area
$\bar{m}_e^R$	second moment of the element mass per unit area
$\hat{M}$	externally applied edge moment resultant
$\tilde{M}_1, \tilde{M}_2$	components of $\hat{M}$ in shell coordinates
$\tilde{M}_t, \tilde{M}_s$	components of $\hat{M}$ in edge coordinates
$\{M\}$	internal moment resultants
$\{M_T\}$	thermal moments
$[\bar{M}_e^T]$	element mass matrix due to translational inertia
$[\bar{M}_e^R]$	element mass matrix due to rotational inertia
$[\bar{M}_e^C]$	element mass matrix due to coupling between translational and rotational inertia
$[\bar{M}_e]$	physical form of element mass matrix
$[\bar{M}]$	system mass matrix
$\hat{N}$	externally applied edge force resultant
$\tilde{N}_1, \tilde{N}_2, \tilde{N}_n$	components of $\hat{N}$ in shell coordinates
$\tilde{N}_t, \tilde{N}_s, \tilde{N}_n$	components of $\hat{N}$ in edge coordinates
$\{N\}$	internal force resultants
$\{N_T\}$	thermal forces
$\bar{p}$	externally applied surface load
$\{P_T\}_e$	tensor form of element thermal load vector
$\{\bar{P}_T\}_e$	physical form of element thermal load vector
$\{\bar{P}_p\}_e$	element load vector due to surface loading
$\{\bar{P}_F\}$	load vector due to concentrated force
$\{\bar{P}_Q\}$	load vector due to concentrated moment

$\{\bar{\mathbf{P}}_g\}_e$	element gravity load vector
$\{\bar{\mathbf{P}}\}$	system load vector
$\{q\}$	system displacement vector
$\bar{Q}$	externally applied concentrated moment
$\{Q\}$	physical form of thermal stress term in constitutive equation
$\bar{\mathbf{r}}$	position vector of a point on shell reference surface
$[R]$	shell geometry matrix relating curvature change vector to bending displacement gradient vector, see (IV.66)
$dS_\alpha$	incremental arc lengths in surface coordinate directions
$dS$	incremental arc length
$\Delta S_\alpha$	arc length in surface coordinate directions between two corner nodes of an element
$\Delta S$	length of an element side
$[S]$	shell geometry matrix relating strain vector to membrane displacement gradient vector, see (IV.59)
$T_k$	temperature at points through shell wall
$\Delta T$	temperature change from reference state
$[T_E]$	transformation relating covariant displacement vector to element displacement vector, see (IV.114)
$[T^H]$	transformation relating normal displacement gradients to element displacement vector, see (IV.102)
$[T_H]$	partition of $[T^H]$ , see (IV.134)
$[\bar{T}_H]$	augmented form of $[T_H]$ , see (IV.140)
$[T^L]$	transformation relating in-plane displacement gradients to element displacement vector, see (IV.78)



$[T_L]$	partition of $[T_E]$ , see (IV.130)
$[\bar{T}_L]$	augmented form of $[T_L]$ , see (IV.139)
$[T_P]$	transformation for rotation of physical elastic constants from material coordinates to shell coordinates
$[T_Q]$	transformation for rotation of physical coefficients of expansion from material coordinates to shell coordinates
$[T_u], [T_w]$	transformations relating covariant displacement vector to physical displacement vector and vice-versa, see (IV.285-IV.288)
$[T^u], [T^w]$	transformations relating contravariant displacement vector to physical displacement vector and vice-versa, see (IV.285-IV.288)
$[T_v]$	partition of $[T_u]$ , see (IV.129)
$[T_w]$	transformation relating the tensor and physical forms of the element displacement vector, see (IV.120)
$[T_w^I]$	transformation relating the tensor and physical components of displacement at a node.
$[T_{w_{12}}], [T_{w_3}]$	partitions of $[T_w]$ , see (IV.120)
$[T_\gamma], [T_e]$	transformations relating tensor and physical components of strain, see (IV.300-IV.302)
$[T_\theta]$	transformation relating covariant rotation vector to element displacement vector, see (IV.141)
$[T_\phi]$	transformation relating physical rotation vector to element displacement vector, see (IV.157)
$[T_\tau], [T_\sigma]$	transformations relating tensor and physical components of stress, see (IV.311-IV.314)
$\bar{u}$	displacement vector at a point on shell reference surface
$\hat{u}$	displacement vector at a point off shell reference surface
$u^\alpha, u_\alpha$	tensor components of in-plane displacement



$u_{\alpha}^K$	nodal values of the tensor components of in-plane displacement
$\{u\}$	covariant displacement vector
$\{\bar{u}\}$	contravariant displacement vector
$U$	strain energy
$U_o$	strain energy density
$\bar{U}$	strain energy per unit area
$\bar{U}_o$	strain energy density per unit area
$\{U\}$	membrane displacement gradient vector, see (IV.57)
$\{V\}$	bending displacement gradient vector, see (IV.64)
$w$	normal component of displacement
$\bar{w}_e$	element weight per unit area
$W$	potential of externally applied mechanical and inertial loads
$\{w\}$	physical displacement vector
$\{W\}$	tensor form of element displacement vector, see (IV.83)
$\{\bar{W}\}$	physical form of element displacement vector, see (IV.119)
$\{W_1\}, \{W_2\}$	nodal point displacement vectors, see (IV.67)
$\{W_{12}\}, \{W_3\}$	partitions of $\{W\}$ , see (IV.116)
$\{\bar{W}_{12}\}$	partition of $\{\bar{W}\}$ , see (IV.119)
$x^{\alpha}$	Gaussian surface coordinates
$x^3$	outward normal to shell reference surface
$x_k^M$	nodal values of surface coordinates

$x^i$	basic Cartesian coordinates
$z$	shell thickness coordinate
$\alpha, \beta$	interpolating coordinates for quadratic shape functions
$\{\alpha\}$	physical coefficients of expansion
$\gamma_{\alpha\beta}$	reference surface strain tensor
$\bar{\gamma}_{\alpha\beta}$	strain tensor at a point off the reference surface
$\Gamma_{\beta\lambda}^{\alpha}$	Christoffel symbols of the second kind
$\{\gamma\}$	reference surface strain tensor components
$\{\bar{\gamma}\}$	components of strain tensor at a point off the reference surface
$\delta_{\beta}^{\alpha}$	Kronecker's delta, see (II.15)
$\epsilon_{\alpha\beta}$	coefficient of expansion tensor
$\{\epsilon\}$	components of coefficient of expansion tensor
$\vec{\theta}$	rotation vector
$\theta_{\alpha}, \theta^{\alpha}$	tensor components of rotation vector
$\vec{\theta}$	alternate form of rotation vector
$\{\theta\}$	covariant components of rotation vector
$\{\theta\}$	physical components of alternate form of rotation vector
$\{\kappa\}$	physical bending strain components
$\lambda, \mu$	interpolating coordinates for linear shape functions
$\nu_{12}, \nu_{21}$	orthotropic Poisson's ratios
$\pi$	potential energy

$\rho$	mass density
$\{\bar{\sigma}\}$	physical stress components at a point off shell reference surface
$\tau^{\alpha\beta}$	stress tensor at a point on shell reference surface
$\bar{\tau}^{\alpha\beta}$	stress tensor at a point off shell reference surface
$\{\bar{\tau}\}$	tensor stress components at a point off shell reference surface
$\phi$	anisotropic material orientation angle
$\Phi$	angle between surface coordinates
$\chi_{\alpha\beta}$	curvature change (bending strain) tensor
$\{\chi\}$	bending strain tensor components
$\psi$	angle between the unit vector tangent to an element edge, and the surface coordinate $x^1$
$\Psi_\alpha$	physical components of rotation vector
$\{\Psi\}$	physical components of rotation vector
$\Omega^{\alpha\beta}$	tensor form of thermal stress term in constitutive equation
$\{\Omega\}$	tensor components of thermal stress term in constitutive equation

SUBSCRIPTS AND SUPERSSCRIPTS

B	bending action
C	coupling between membrane and bending action
e	element
F	concentrated force
g	gravity force
I	inner surface or inertial load
m	material coordinates
M	membrane action
n	normal to shell reference surface
O	outer surface
p	surface pressure
Q	concentrated moment
S	shell
T	thermal force
$T_B$	thermal bending action
$T_M$	thermal membrane action



## CHAPTER I

### INTRODUCTION

#### A. Discrete Element Analysis

In order to obtain solutions to practical problems in structural mechanics, discrete element numerical procedures utilizing the finite element method or the finite difference method are most often used. The classical analysis of continuous systems begins with the establishment of relationships between various quantities associated with small differential elements. Partial differential equations or integral equations governing the behavior of the entire domain are obtained by allowing the dimensions of the differential element to approach zero as the number of elements becomes large. In contrast, discrete element methods begin with the investigation of properties of elements of finite dimensions. The properties are established through direct use of equilibrium and compatibility relationships from the theory of elasticity or by use of variational methods and energy principles. Integrations are replaced by finite summations and the partial differential equations of the continuous domain with infinite degrees of freedom (d.o.f.) are replaced by a system of algebraic equations which have a finite number of degrees of



freedom. If certain continuity, admissibility and completeness conditions [1-7]\* are satisfied in the formulation of the discrete element, the behavior of the discrete system converges to that of the continuous system as the number of discrete elements is increased and their dimensions are decreased. Discrete element methods are in principle applicable to the analysis of the static and dynamic, linear and nonlinear deformation and material behavior of anisotropic, nonhomogeneous bodies of any geometrical shape with arbitrary boundary conditions.

This paper is concerned with the analysis of thin shell structures by discrete element methods. Thin shells are widely used as structural elements where lightweight construction is necessary. Prior to the advent of computerized discrete elements, only simple, highly idealized shell problems could be solved. With the evolution of discrete structural analysis methods, the state of the art has advanced dramatically during the past fifteen years. Solutions to complex shell problems involving geometric and material nonlinearities, anisotropic and inhomogeneous material behavior, discrete stiffening and local reinforcement, arbitrary geometries and boundary conditions and general loadings are now feasible.

Hartung [8,9] has recently conducted assessments of current capability for computer analysis of shell structures.

\*Brackets [ ] indicate references and parentheses ( ) indicate equations

As he points out, the analysis of most practical shell problems can only be treated by discrete methods. The only two such methods which have found widespread application are the finite element and finite difference methods, both of which have been extensively developed. The relative advantages and disadvantages of the two methods will be discussed in a later section following an historical review of both methods.

## B. Historical Review-Finite Element Method

Since its inception about 20 years ago, the finite element method, in conjunction with the digital computer, has evolved into the numerical procedure most commonly used for many classes of structural analysis problems. The wide use of finite element methods is due in large part to their generality, i.e., their ability to model the complex structural configurations that occur in modern engineering practice.

Oden [10] has reviewed the evolution of the concept of representing continuous functions by piecewise approximations which was followed by the introduction, in the early days of aircraft structural analysis, of the practice of representing a structural system by a collection of discrete elements. He cites the works of Kron, Hrennikoff, Courant, Polya, Prager and Synge, as being important. In 1954, Argyris and his coworkers began a series of papers which generalized, extended and unified the fundamental energy principles for the analysis of elastic structures. Reference [11] summarizes this work and presents in considerable detail methods for analyzing complex, discrete aircraft structures in forms easily adapted to automatic computation. Turner, Clough, Martin and Topp [12] are generally credited with the first presentation of the finite element method together with the direct stiffness method for assembling elements to represent a complex structure. It remained for Clough [13]

in 1960 to first coin the term "finite elements" in a paper which addressed plane stress problems. In the last 15 years hundreds of papers have been published on the subject. References [3,14-22] represent important collections of papers and together with [10,23-26] give a good overview of the evolution of the method.

In the 1960's both the force (flexibility) and displacement (stiffness) methods of matrix structural analysis were in common use for the analysis of discrete element systems [14]. These methods are defined simply as a solution procedure formulated directly in terms of unknown forces for the force method and in terms of unknown displacements for the displacement method.

The matrix force method for the analysis of statically indeterminate structures evolved from indeterminate frame and truss analysis in Civil Engineering which is based on the application of the principles of least work, Castigliano's theorem or virtual work. The force method is characterized by the selection of an internal force system which is in equilibrium with the external loads, but since compatibility conditions are not satisfied for this basic system, it is necessary that a redundant load system be selected which in combination with the basic system produces a state of compatible displacement. In modern practice, a rigorous derivation of elements for the force method is based on complementary energy theorems. The method is still popular in certain segments of the aircraft industry but the



displacement method is far more widely used primarily due to problems associated with automating the selection of a redundant load system.

Initial attempts at element formulation for the displacement method utilized the so-called "direct approach" in which element properties were developed through the direct use of equilibrium and compatibility relationships as defined by the pertinent differential equations of elasticity theory. This approach was found to be unsatisfactory for reasonably complex elements because the method failed to yield symmetric stiffness matrices [14].

A rigorous theoretical basis for the formulation of finite elements was introduced when variational methods came into common use. In this context, the finite element displacement method may be viewed as a generalization of the Rayleigh-Ritz method in the calculus of variations. In both methods the total potential energy is formulated and the displacement pattern is expressed in terms of a set of undetermined parameters, which are defined at discrete nodes in the finite element method. A set of simultaneous equations is formed which minimizes the total potential energy with respect to the undetermined parameters. The difference between the two methods is in the manner in which the displacements are prescribed. In the Rayleigh-Ritz procedure the displacements are usually specified by

admissible displacement functions which satisfy the boundary conditions of the entire structure while in the finite element process this specification is piecewise.

The principle of minimum potential energy states: "Of all admissible displacements satisfying the given boundary conditions, those which satisfy the equations of equilibrium are distinguished by a stationary (extreme) value of the potential energy." The potential energy is a minimum for "actual" displacements only in the neighborhood of the stable equilibrium state, where the strain energy is positive definite [27].

Abstracting the discussion of Gallagher [33], the finite element formulation generally adheres to the following sequence. For stable equilibrium the potential energy ( $\pi$ ) is a minimum; thus

$$\delta\pi = \delta U - \delta W = 0 \quad (\text{I.1})$$

where  $U$  is the strain energy of the system and  $W$  is the potential of the applied loads. The strain energy can be cast in the form,

$$U = \frac{1}{2} \int_V \{e\}^T [E] \{e\} dV \quad (\text{I.2})$$

where the integral is taken over the volume ( $V$ ) of the element, the matrix  $[E]$  contains the coefficients of the

the constitutive equations and  $\{e\}$  is a vector of strain measures.

The key operation in the development is then the selection of admissible displacement fields in terms of nodal displacements,  $\{q\}$ . Then by application of the strain-displacement equations, expressions,  $[D]$ , are obtained which relate the strain vector to the nodal displacement vector. Thus

$$\{e\} = [D]\{q\} \quad (I.3)$$

Substituting (I.3) into (I.2) results in the quadratic form,

$$U = \{q\}^T \int_V [D]^T [E] [D] dV \{q\} \quad (I.4)$$

By application of the energy theorem (I.1), the element stiffness matrix,  $[K]$ , is obtained in the form,

$$[K] = \int_V [D]^T [E] [D] dV \quad (I.5)$$

Two significant problems arise in formulating the element stiffness matrix: the choice of admissible displacement functions which preserve the compatibility of displacement in the complete analytical model, and the performance of the integrations required by (I.5), which can be quite difficult in the case of irregular element shapes.

In 1966 a significant innovation in finite element technology, the isoparametric element, was introduced by Irons [28] who recognized the earlier unpublished work of Taig. The essence of the isoparametric concept is the interpolation of both coordinates and displacements by the same interpolation functions which are written in terms of a set of local (mapping) coordinates for the element. The isoparametric mapping leads to two significant advantages. Simple rectangular and triangular shapes can be distorted into irregular shapes (with curved boundaries if desired) which better approximate the complex geometries of practical structures. And the isoparametric formulation permits the element stiffness to be easily established through use of numerical integration.

The isoparametric concept has been extended and successfully applied to a wide range of problems by a number of researchers with Zienkiewicz and his coworkers [23,24,29,30] leading the development. But as Zienkiewicz [30] points out, the isoparametric formulation possesses essential advantages only for the class which embraces all plane and three-dimensional elasticity problems. Its extension to higher-order variational principles is not easy. A useful extension of the method to the plate-shell domain has however been made by Ahmad, et.al. [31,32], who deal with the development of "reduced" solid elements that have been degenerated in the thickness direction to approximate thin and thick shell behavior. The validity



and limitations of this approach will be deferred for later discussion.

A thorough review of the application of the finite element method to general shells\* is contained in the papers by Gallagher [33,34] and the paper by Dawe [50].

As Gallagher [34] points out, the analysis of shells via finite elements is approached in one of three alternative forms:

- (1) In "faceted" form by use of flat elements to approximate curved surfaces.
- (2) By means of "reduced" isoparametric 3-D solid elements which have been specialized to 2-D representations of curved thick or thin shells.
- (3) By curved finite elements that have been formulated directly from the theories of shallow or deep thin shells.

The finite element flat plate technology has been well developed over the past ten years. Numerous "facet" elements [35-40], both quadrilateral and triangular, have been in wide use for shell analysis for a number of years. The "facet" type of element is formulated by superposition of membrane and flexural behavior and by application of appropriate coordinate transformations (see for example, Clough and Johnson [45]).

---

\*The term "general shell" refers to shell problems which require discretization in two surface dimensions. The more restrictive class of shell of revolution problems which requires discretization in only the meridional direction is not being addressed in this paper.

Some of the difficulties and shortcomings of the "facet" model as enumerated by Gallagher [33] are as follows:

- (1) The behavior represented by the differential equations is not approached in the limit of refinement by the flat plate representation.
- (2) The discontinuities of slope between adjacent elements may produce calculated bending moments in regions of the shell where none exist.
- (3) The effects of curvature, in the form of the coupling of membrane and flexural behavior, are absent in the interiors of the individual elements.

In the development of degenerated isoparametric solid elements for thin and thick shell analysis, Ahmad, et.al. [31,32] imposed the requirements that the original normals to the middle surface remain straight and inextensible and the elastic modulus in the normal direction be zero to avoid normal stresses. These assumptions are compatible with thin shell theory and since the surface normals can rotate relative to the middle surface of the shell, shear deformations are approximately included.

For shells where membrane stresses are predominant, good results have been obtained with the Ahmad approach, but where bending effects are important the results have been poor when thickness/length ratios of an element become small [30]. The error arises because constant bending moments can be represented by the deformation

patterns of these elements but for a linearly varying moment excessive shear strain energy is stored [41]. Two approaches have been employed to improve this behavior. The use of approximate integration techniques in order to avoid integrating the excess shear strain energy has been successfully applied by several investigators [32,42,43]. However, Wilson [44] points out that convergence is not assured and the technique is difficult to apply in the general case of curved anisotropic elements. Wilson [44] introduced extra displacement modes (which in general violate interelement compatibility) into the element. The extra modes have the same form as the inherent errors and their magnitudes are determined by requiring that the total strain energy of the element be a minimum. This approach can be very effective but must be used with care [41].

In summary, Wilson [44], Bathe [41] and Zienkiewicz [30] discuss the limitations associated with the use of isoparametric solid elements for shell analysis. These include:

- (1) Solid elements do not represent well the deformation patterns induced by bending moments except for the cubic isoparametric element with four nodes along each side.

- (2) Errors in the shear and normal strains cause the element to be overly stiff.
- (3) If the element is relatively thin, the stiffness coefficients corresponding to the transverse displacement are considerably larger than those associated with the in-plane displacements, which results in numerical ill-conditioning of the stiffness equations.
- (4) A large number of variables have to be included when compared to more conventional analysis methods and excessive amounts of input data are required.
- (5) A single element through the thickness cannot represent a layered, anisotropic shell wall construction.

The first two problems can be treated to some extent by approximate integration techniques or the incompatible mode approach. The alternative of using the cubic element is objectionable due to the relatively large amount of computer time required to form the stiffness equations. Problems three, four and five tend to restrict the application of this method to thick shells.

The development of curved finite elements on the basis of shallow or deep, thin shell theories results in a much more complicated formulation than for the flat plate or "reduced" solid representations previously discussed. Gallagher [33,34] reviews in detail the



following general difficulties:

- (1) The choice of an appropriate shell theory from the many shallow and deep shell theories in the literature.
- (2) The description of the curved geometry, including the definition of the element curvature from the given coordinate data and the derivation of appropriate transformations for the connection of the elements.
- (3) The choice of admissible displacement fields in curvilinear coordinates. Three problems of concern in this respect are the retention of the required interelement continuity of displacement, the representation of all constant states of strain and the assurance of zero-strain energy modes of rigid body displacement.

The representation of rigid body modes by polynomial displacement fields defined in curvilinear coordinates is particularly troublesome, since satisfaction of this condition is approached in the limit only by higher order polynomials [46]. Fonder and Clough [47] have demonstrated that the importance of the zero strain condition under rigid body motion varies significantly with the application.

The net effect of these complications in curved element formulation is that most of those reported in the literature employ higher order polynomial displacement assumptions.

As a consequence, the resulting elements have a relatively large number of degrees of freedom which tends to increase stiffness matrix generation time and the bandwidth of the equations. For higher order facet and curved shell elements, the nodal degrees of freedom frequently exceed six and furthermore do not retain the physical significance that the simpler elements employ; i.e., the degrees of freedom are not translations and physical rotations but are more often translations and their spatial derivatives. This factor complicates their use in general purpose computer programs (see for example [48,49]) both from the standpoint of strategy for assembling the stiffness equations and the need to implement special constraint procedures in order to join the higher order elements to other types of elements with differing nodal degrees of freedom or to join two different surface types. The actual use of higher order shell elements in contemporary general purpose computer codes will be discussed later following a review of the available element technology.

Tables 1 and 2 summarize the major developments in curved, thin shell finite elements using the displacement approach. Many of the developers listed in Tables 1 and 2 have investigated a family of finite elements representing various perturbations on the assumed displacement functions and element assembly procedures. The element description listed in the tables

is for that element in the family which was recommended by the developer as performing best.

Table 1 summarizes the level of sophistication available in four-sided elements [51-63]. There are severe restrictions on the utility of this class of element as regard element shape and surface geometry. Several elements [51-53] are applicable only to cylindrical shells and another [54] is restricted to conical surfaces. Several elements that retain some generality in surface representation [55-60], however, are restricted to regular element shapes whose edges must lie along the curvilinear coordinate lines. The SLADE element by Key and Beisinger [61,62] is an arbitrary curvilinear quadrilateral that treats linear, static and dynamic problems with layered, orthotropic shell walls. The element also treats thermal stresses including material property temperature dependence through the thickness of the shell but the shell geometry is restricted to an axisymmetric reference surface.

The quadrilateral element by Jones [63] is based on the Marguerre shallow shell equations which are equivalent to applying an initial warping to a flat plate to form the curved shell element. This element employs a quadratic form of surface representation which includes cylinders, cones, ellipsoids, hyperboloids and paraboloids. The Jones' element has been developed for problems of small strain, large deflection and nonlinear isotropic, material behavior and hence is probably the most general of the

four-sided elements presently available. It does not however treat layered, anisotropic, shell wall construction or the effects of thermal stresses. Furthermore, Argyris and Scharpf [69], view critically the use of a shallow shell theory in element formulation, particularly with respect to kinematic compatibility between adjoining elements.

Table 2 summarizes the level of sophistication available in three-sided elements [64-72]. The triangular elements possess an inherent generality in shape that makes them quite adaptable to the modeling of irregular domains. However, it takes about twice as many triangular elements to model a structure as it does quadrilateral elements and since element generation times for triangular elements are generally more than half that of a comparable quadrilateral, it will take more computer time to solve a given problem with triangular elements. An optimum modeling would utilize quadrilaterals for the bulk of the mesh with triangular elements being used to fill in irregular regions at the boundaries.

The group of elements [64-68] employ shallow shell theories and generally impose some limitations on surface representation. The shallow shell element by Cowper, et.al. [67,70] appears to be the most useful in this group.

The elements [69-72] are based on deep shell theories, the most sophisticated in this group being the SHEBA element by Argyris and Scharpf [69] and the element by Dupuis and Goel [71]. Both elements satisfy continuity



and rigid-body motion requirements as well as accommodate a completely arbitrary surface geometry. Both element formulations are restricted to isotropic materials and each employ the middle surface as the shell reference surface.

Bushnell [73] presents an excellent review of the behavior of thin shells in practical engineering structures and he reviews modeling requirements for computer codes. As he points out, one of the first requirements of a computer program for shell analysis is the arbitrary location of the reference surface with respect to the wall material and the inclusion of energy coupling between changes in curvature and normal strains. Coupling between membrane and bending energies is present in shells with certain types of composite walls, eccentrically stiffened shells and nonuniformly heated shells with temperature dependent wall materials. Also, the middle surface is often a poor choice for the reference surface, since many practical shells have variable wall thicknesses and local reinforcements which make the middle surface difficult to describe mathematically and which cause its position to change abruptly in space. In such cases, the inner or outer surface of the shell is usually a better choice. Few of the shell elements listed in Tables 1 and 2 have provided for other than single layer wall construction with the reference surface being restricted to the middle surface. Many are restricted to isotropic materials.

A notable exception is the SLADE element by Key and Beisinger [61,62] which permits an arbitrary reference surface with layered, orthotropic walls.

In summarizing the status of curved element development, it is evident that no one element has won wide acceptance and that the quadrilateral elements as a group are not as well developed as the triangular elements. The trend is toward more sophisticated elements with a large number of degrees of freedom and hence increased element generation times. The argument for this approach is that for a given level of accuracy fewer elements will be needed than for the less sophisticated formulations; thus total stiffness matrix generation time and equation solution time will balance out in favor of the sophisticated elements. This argument generally holds up for simple test problems but for the complex structures which occur in engineering practice, the presence of cutouts, stiffeners, thickness variations, severe thermal gradients, and intersections with other components tend to force a minimum level of grid refinement which shifts the tradeoff back towards the simpler elements. This view is supported to some extent by Yates, et.al. [74], who in commenting on future plans for addition of capability to the general purpose code, DAISY, state, "We feel there is plenty of room for improvement in the quality of plate and solid elements.

...In trying more sophisticated plate elements we found none that would improve accuracy without extreme penalties in formation time and reliability."

The curved finite element technology discussed above has remained for the most part in the research stage and has not been widely used by the practical designer and shell analyst. A partial assessment of the utilization of curved finite elements in large scale, general purpose computer codes can be made on the basis of a critical review published in [21]. The ASKA, NASTRAN, DAISY, STARDYNE, STRUDL-II and MARC codes were critically reviewed by experienced users. NASTRAN, DAISY, and STARDYNE have no curved elements for general shell analysis, but rather rely on the "facet" type of element. ASKA has both the SHEBA-3 and SHEBA-6 elements of Argyris and Scharpf [69]. Meijers, the ASKA reviewer [75], states: "SHEBA shell elements are very complicated, require an extremely high amount of computer time and are very restricted in their application to practical problems." STRUDL-II has both triangular and quadrilateral, shallow shell elements; however, the reviewer, Chu [76], states: "...it has also been found that the results obtained from the shell elements, SSCR and SSCT, are not reliable." MARC has implemented one of the family of triangular elements developed by Dupuis and Goel [71]. The reviewer, Ayres [77], reports on satisfactory experience with a three-noded element with nine degrees of freedom per node. The element has been used for

elastic-plastic and creep problems associated with the design of high-temperature pressure vessels. It is interesting to note that the 27 degree of freedom element (T3) implemented in the MARC code was considered to be inferior to more sophisticated 54 degree of freedom elements (T1 and T2) by the element developers [71] on the basis that the T3 elements lead to worse numerical results for a given amount of computer time and generally require relatively fine meshes for convergence.



### C. Historical Review-Finite Difference Energy Method

The finite difference method is generally associated with the concept of directly approximating the spatial derivatives in the partial differential equations of equilibrium which govern the behavior of a physical system. In recent years a variational method for deriving difference equations has come into use which is more closely allied to the finite element method than is the traditional method of finite differences. In the finite difference energy method the domain of interest is subdivided into a set of subareas by means of a finite difference mesh. For each subarea the strain energy density is expressed in terms of displacement components and their derivatives. After approximating the derivatives with finite difference relations, the strain energy of the system together with the work done by applied loads can be summed over the domain to form the total potential energy. As in the finite element method, the use of the minimum potential energy theorem results in a set of algebraic equations in the unknown nodal displacements. The imposition of discrete boundary conditions and the solution of the algebraic equations can be accomplished via the same matrix methods employed in finite element analysis.

The method has been used by mathematicians for many years to solve elliptic partial differential equations. The work by Courant, Friedrichs and Lewy [78] in 1928 is often cited in the literature as being the earliest published use of the method. Forsythe and Wasow [79] in their 1960 text discuss variational methods for setting up difference equations and they cite, as important, the 1953 paper by McNeal [80] which dealt with using network analyzers for solving Laplace's equation.

As was the case with the finite element method, the finite difference energy method was first used to solve structural problems in the aircraft industry. Williams [81], in his 1960 text on Aircraft Structures, discusses the "method of individual displacements" which was combined with an energy approach to solve beam and plate problems. Although the method had in the past yielded useful results via hand calculations, Williams emphasized its great potential for exploiting the capabilities of the digital computers then emerging.

Griffen and Kellogg [82] computerized the method for the solution of axially symmetric and plane elasticity problems and noted that the difference equations obtained were closely related to those obtained by finite element methods.

Havner and Stanton [83] discussed variationally-derived finite difference equations in mixed boundary value problems of plane thermoelastic stress and strain.

As they point out, one possible disadvantage of the variational formulation of difference equations is that prescribed traction and mixed boundary conditions are not explicitly satisfied for a given finite difference network. These boundary conditions arise as distinct conditions only in the continuum problem and are not established separately from the field equations in minimizing the discretized form of the energy function. Hence, the accuracy of the variational approach at or near the boundary might be questioned. The Havner and Stanton paper provides a partial answer to this question for a specific class of problems. A detailed study was made of the boundary discretization error and it was shown that a variationally derived difference equation at the boundary can be represented as a linear combination of the corresponding natural boundary condition and field equation, converging to the discretized natural boundary condition with decreasing grid size. It was also demonstrated numerically that effective control of the boundary discretization error could be obtained with only local changes in grid spacing.

In the mid 1960's a group of researchers at the Lockheed Missiles and Space Company initiated a continuing effort to apply the finite difference energy method to a wide range of axisymmetric and general thin shell problems. Bushnell and his coworkers have developed the method for the analysis of stress, vibration and buckling of ring-

stiffened shells of revolution with various wall instructions. A series of computer codes with the acronym BOSOR (Buckling of Shells of Revolution) have resulted. Almroth and his coworkers have concurrently developed the method for the analysis of general shells, including stress, vibration, buckling and plasticity effects. A series of computer codes with the acronym STAGS (Structural Analysis for General Shells) have evolved. Bushnell and Almroth [84] give a good overview of the BOSOR and STAGS codes and the numerical analysis on which they are based.

References [85-87] describe the initial application of the method to the buckling and free vibration analysis of cylindrical panels. In [88], a linear version of the STAGS code was extended to handle circular or elliptic cutouts in stiffened cylindrical panels. The addition of a capability to treat shells with non-orthogonal Gaussian coordinates was reported in [89] which deals with the nonlinear collapse of elliptic cones. References [90-93] detail various improvements in capability to the STAGS code which include: provision to allow both the temperature and material properties to vary over the surface and through the thickness of the shell, the addition of a bifurcation buckling branch to the code, the extension of the nonlinear version to shells of more general shape with cutouts of arbitrary contour, the addition of inelastic deformation, the capability to handle a finite difference



grid with variable nodal point spacing and the treatment of realistic types of shell wall construction including those which involve anisotropic materials.

STAGS is applicable to four-sided shell panels (or closed shells with two edges) with one rectangular cutout and discrete or smeared stiffeners. Additional cutouts or cutouts of more general shape are handled by specification of a zero modulus of elasticity in the appropriate area. It applies to any shell for which a reference surface and a suitable set of rectangular grid lines can be mathematically defined. In general applications, the user provides a subroutine describing the geometry, but subroutines are included for such standard geometries as cylinder, cone, annular and rectangular plate, sphere, paraboloid, elliptic cylinder, ellipsoid, torus, hyperboloid and elliptic cone. References [94-97] describe research efforts in which the STAGS code has been used to study the stability of various types of shells.

The BOSOR code has undergone an evolution similar to that of STAGS and references [98-109] detail its development. Since the BOSOR code is based on a one-dimensional discretization and deals with the more restrictive class of shell of revolution problems, the history of its development and details of its analytical capabilities will not be discussed.

In the development of the STAGS analysis, various two-dimensional discretization schemes are explored [84]. The shell panel is covered with mesh lines parallel to the shell coordinate lines and the unknowns of the system are the tangential displacements  $u$  and  $v$  and the normal displacement  $w$ . Figure 1 shows three finite-difference schemes that are discussed in [84]. Figure 1a shows the "whole-station" scheme in which  $u$ ,  $v$  and  $w$  are all located at grid points defined by intersections of the coordinate lines. For a typical interior "element" there are nine nodal points which define the  $u$ ,  $v$  and  $w$  displacement fields and the "element area" over which membrane and bending energies are integrated is shaded. The energy integration for all schemes is by one point quadrature in which the functional values and derivatives of displacement are evaluated at the integration point (centroid of area). The whole station scheme of Figure 1a has been discarded because it leads to "jumpy" solutions in some cases and fails completely in cases where the mesh spacing varies.

Figure 1b shows the "whole-station" scheme in which membrane and bending energies are integrated over different areas. Although this scheme has exhibited good numerical behavior it is restricted to shells of such a wall construction that no coupling exists between membrane and bending energies.

The scheme shown in Figure 1c is termed "half-station" because the u and v displacement components are defined at points which lie halfway between the mesh points at which w components of displacement are defined. For a typical interior "element" there are nine nodal points which define the w displacement field and four which define the u, v displacement field. This scheme also gives good numerical results and is applicable to all forms of wall construction since it is not necessary to integrate over different elements of area for membrane and bending energies. The scheme is equivalent to a rectangular finite element in which the u, v displacements vary bilinearly and the w displacement varies biquadratically. Unlike conventional finite elements, however, the w displacement field extends beyond the region of integration into several adjacent elements.

The most obvious limitation of the finite difference energy method as presently implemented in the STAGS code is the restriction on the type of grid and shell shape which can be handled. Complex shell configurations are much easier to model with finite element methods.

Johnson [110] and Jensen [111] have both proposed less restrictive schemes for positioning the discrete points at which unknown displacements are defined. Johnson used Green's Theorem to derive difference relations at the centroid of a quadrilateral area which is defined in

a manner quite similar to the STAGS "half-station" scheme of Figure 1c. The Johnson mesh scheme is shown in Figure 2. As in the STAGS "half station" scheme, the  $u$ ,  $v$  displacements are defined at the centroidal points of the four quadrilateral areas which are formed by the nine nodal points at which  $w$  displacements are defined. The  $u$ ,  $v$  control points then define the quadrilateral element area over which integrations are performed. In generating a structural mesh, a row of  $u$ ,  $v$  control points must be positioned so as to fall on the shell boundary, so that all of the element areas fall within the boundaries of the shell. This is a departure from the STAGS "half-station" scheme where  $w$  control points are positioned on the boundary and the area of boundary elements are appropriately modified. The use of Green's Theorem to obtain finite difference approximations to the first derivatives of  $u$  and  $v$  at the element centroid is straightforward but the determination of difference relations for the second derivatives of  $w$  is quite complex and uses some simplifying assumptions which tend to restrict the generality of the mesh. The procedure relies on a somewhat cumbersome indexing system for the control points and two successive applications of Green's Theorem. The second derivative approximations for  $w$  are actually derived for points in the mesh other than the element centroid, but the assumption is made that the lengths of the line segments connecting



w control points are all of the same order of magnitude ( $\Delta$ ); hence the difference approximations hold also at the element centroid to within an error  $\Delta$ . This method has been programmed for automatic computation and good results were obtained for several example problems.

Jensen [111] has done research on a procedure for generating the required difference relations in terms of the displacements of six arbitrarily placed neighboring nodes. The method is based on the use of the Taylor series expansion and requires special routines for locating and classifying the neighboring nodes, for calculating and storing the inverse nodal matrix for each class of node and for testing for singular nodal matrices, since the set of nearest neighbors in a given grid is sometimes insufficient to determine all the difference expressions needed. When the nodal matrix is singular the node must be reclassified, i.e., a new set of neighbors selected. Another complication is that nodal matrices for points on the boundary of the domain are constructed differently from those in the interior. Jensen experienced difficulties in automating the procedure and it was not implemented in a structural analysis.

In summary, the finite difference energy method has been developed into a powerful analysis tool for certain classes of shell structures, especially for problems involving geometric nonlinearities. It will be compared

to the finite element method in the following section and the advantages and disadvantages of both methods will be discussed.

D. Comparison of Finite Element Method  
And Finite Difference Energy Method

In recent years a number of papers have addressed the problem of comparing various finite element formulations with finite difference energy method formulations. The comparisons are based on a number of specific numerical examples which have been solved by both methods.

Forsberg [112] considered several sample problems including a cylindrical shell roof, a stiffened cylinder with a rectangular cutout and a "pear-shaped" cylinder. For the cylindrical shell roof, comparisons were made between the STAGS finite difference energy method formulation [84] and four finite elements. The finite elements included two flat plates, a 20 degree of freedom quadrilateral [113], a 15 degree of freedom triangle [45], and two curved triangular elements [66,67] based on shallow shell theory, both with 36 degrees of freedom. The STAGS formulation had a more rapid rate of convergence to the analytical solution than the finite elements for both displacement and stress predictions.

In concluding his paper, Forsberg made the following points which apply to the analysis of general shells. For the linear static and dynamic analysis of irregular structures the finite element technique is ideal due to its inherent generality and flexibility in modeling. The finite

difference technique, though not able to treat as general a configuration, is applicable to a wide range of practical structures. The numerical studies indicated a comparable accuracy for the two methods for a given mesh size, however, the finite element method will have far more degrees of freedom and consequently will require considerably more computer time. For an equivalent problem size, the finite difference technique will still require less computer time because the time required to generate the stiffness equations is less. Finite elements have been more extensively used to study material nonlinearities while the finite difference approach has been more highly developed for problems involving geometric nonlinearity.

Hartung, in assessing capability for computer analysis of shell structures, surveyed all available codes and summarized current capability in [8] and reported on the results of comparative analyses for three sample problems representative of current engineering practice in [9]. Solutions were solicited from the structures community for analyses of linear stress, free vibration, bifurcation buckling, elastic and inelastic collapse, and linear and nonlinear transient response. In general there was good agreement among the codes for linear stress, free vibration and bifurcation buckling. The STAGS finite difference energy formulation was the only code for which a solution



was submitted to the elastic and inelastic collapse problems. The linear and nonlinear transient response solutions submitted were primarily from conventional finite difference methods. The agreement between solutions for the linear analysis was good for displacements and membrane strains and only fair for bending strains. The nonlinear results showed virtually no agreement. The conclusions drawn by Forsberg [112] in his comparison of finite element and finite difference energy methods were generally confirmed by the results of the comparative analyses of Hartung [9].

The most rigorous comparison between the finite element and finite difference energy techniques has been carried out by Bushnell [114]. In the previous comparisons by Forsberg and Hartung it was difficult to make quantitative assessments of computer run times because the analyses had been run on various computers and a variety of programming techniques had been used for essentially similar operations (e.g., solution of simultaneous equations). Bushnell inserted curved finite elements into the BOSOR3 computer code, a shell of revolution analyzer which is based on the finite difference energy method. Rates of convergence and computer times were established for linear stresses and displacements, bifurcation buckling loads and free vibration frequencies. The various discrete elements depicted in Figure 3 were compared with respect to convergence rate of mesh spacing, computer times required to form global stiffness, load

geometric and mass matrices, computer times required to factor and solve the systems of algebraic equations, and number of Gaussian integration points required for accurate formation of local matrices. The first three discrete elements shown in Figure 3 are curved finite elements with various displacement assumptions while the fourth is a finite difference element which is the one-dimensional analog of the STAGS "half-station" scheme (Figure 1c) previously discussed.

The rates of convergence were case dependent, the finite difference method showed better performance for vibration frequencies and stress problems not involving rapidly varying edge discontinuity stresses while the finite element method showed more rapidly convergent behavior for buckling loads and static problems involving high stress gradients at a clamped edge.

The finite difference element was clearly superior with respect to computer time. With the finite element models, two to six times as much computer time was required for formation of each of the stiffness, load-geometric and mass matrices. The extra time was associated with coordinate transformations, static reduction and evaluation of element energy density at more than one Gaussian integration point, operations which were not required for the finite difference analysis.

The behavior of the finite element models with a variation in the number of Gauss points used for numerical integration was also studied by Bushnell. The most rapidly convergent solution was obtained by using the minimum number of Gauss points required for eventual convergence to the correct solution. If too few points were used, the calculations converged to the wrong solution. None of the finite elements converged to the proper solution if only one Gauss point was used as was done with the finite difference energy model. The optimum number of Gauss points required for each of the discrete elements is shown in Figure 3.

Although the Bushnell study was restricted to comparisons of one-dimensional discrete elements, he did discuss in some detail the extrapolation of these results to the two-dimensional discrete elements required for the analysis of general shells. He cites four factors of prime importance in numerical analysis of practical structures: ease of application, computer time required to form the various matrices, computer time to decompose the stiffness matrix and solve for eigenvalues, and rate of convergence with increasing number of degrees of freedom.

With respect to ease of application the finite element method is far superior in two-dimensional problems involving irregular grids and arbitrary boundaries.

The saving in computer time for matrix formation which was noted in the one-dimensional case is expected to be even more of an advantage for the finite difference energy method in the two-dimensional case, especially for nonlinear problems. This advantage is anticipated because the order of the element matrices is larger for two-dimensional finite elements and the difference in number of Gauss points between the two methods is greater. For example the finite difference element has 17 degrees of freedom while the finite elements range from 20 to 63 (see Tables 1 and 2 and Figure 1). The number of required Gaussian integration points ranges from 4 for flat plate elements with low order displacement assumptions up to 25 and more for the higher order curved elements [61].

The computer time required to decompose the stiffness matrix and solve for eigenvalues is a significant portion of the total computer time in two-dimensional problems. The simplest finite element formulations lead to coupling over three lines of mesh points and have five unknowns at each node. The STAGS type of finite difference model involves coupling over five lines of mesh points with up to three unknowns per node. The numerical characteristics of these two nodal arrangements lead to computer time ratios which slightly favor the finite difference model. More sophisticated finite elements with midside nodes and/or more degrees of freedom per node require correspondingly



more computer time but presumably fewer elements would be required for convergence to a given degree of accuracy.

The computer times discussed above all depend on the mesh size required to reach a convergent solution. The convergence characteristics of the two methods varied from case to case in all of the comparative studies [9,112,114] and a fair statement would probably be that the two methods are about equal.

A recurring theme in each of the previously discussed comparative studies [8,9,112,114] and several other review articles [73,97] has been the advantage that finite element methods have in modeling complex structures. As Hartung [8] points out in his discussion of areas for further study, if finite difference methods are going to achieve the same versatility for modeling complex structures that the finite element method has achieved, then a capability for handling truly arbitrary meshes must be developed.

## E. Objective And Synopsis Of Research

The objective of this research is to demonstrate that two well accepted matrix methods for thin shell structural analysis, the finite element method and the finite difference energy method, can be integrated into one unified analytical approach and effectively applied to the thermo-elastic analysis of anisotropic thin shells. Since its inception almost 20 years ago the finite element method has evolved into the most widely used tool for structural analysis, primarily due to its generality, i.e., its ability to model the complex geometries that occur in engineering practice. In recent years, the finite difference energy method has been developed to a very high degree, especially for problems involving geometric nonlinearities. Although the method has been demonstrated to have significant advantages over contemporary finite element formulations, it suffers from the modeling restrictions imposed by rectangular grid works. It is the intention of this research to demonstrate that this classic restriction can be removed and that the finite difference energy method can be cast in a formulation which is amenable to insertion in contemporary general purpose finite element computer codes.

In succeeding chapters the details of the analytical development are presented along with the results of several sample calculations. In Chapter II a tensorial description of the geometry of the shell reference surface is presented along with the thin shell theory of Sanders. Chapter III contains a general description of the application of the finite difference energy method to the analysis of thin shells. Chapter IV contains the details of the analytical development of the generalized finite difference element. In Chapter V the analytical results obtained with the element for a number of demonstration problems are compared to theoretical or experimental results and in some cases to the results obtained with finite element formulations. Chapter VI summarizes the results of this research and the Appendices contain the Tables and Illustrations along with further details of the numerical analysis.

## CHAPTER II

## SHELL THEORY

## A. Surface Geometry

A description of the curvilinear surface geometry for shells of arbitrary curvature will be summarized in this section using tensor notation.\* A detailed treatment of this subject is given by Green and Zerna [115] and Sokolnikoff [116].

It is assumed that the reference surface of the shell is defined by curvilinear Gaussian surface coordinates  $x^\alpha$  which are contained in a three-dimensional Euclidean space defined by the basic Cartesian coordinates  $X^1$  (see Figure 4). The curvilinear coordinate lines,  $x^\alpha = \text{constant}$ ,  $x^3 = 0$ , are embedded in the shell reference surface and  $x^3$  is the outward normal to the undeformed reference surface. The position vector of a point,  $P$ , on the reference surface is

---

\*Remarks on notation:

1. Greek indices range over the values 1,2 while Latin indices have the values 1,2,3 unless otherwise noted.
2. Unless specifically suppressed a repeated index in a term represents a summation over the range of the index.
3.  $( )_{,\alpha}$  denotes partial differentiation with respect to  $x^\alpha$ .
4.  $( )|_\alpha$  denotes covariant differentiation with respect to  $x^\alpha$ .



denoted  $\vec{r}$ . The vectors  $\vec{a}_1$  and  $\vec{a}_2$  are the base vectors of the Gaussian surface coordinates and the unit normal vector to the reference surface is  $\vec{e}_3$ . The vectors  $\vec{I}_1$  are the unit vectors in the  $X^1$  directions.

The position vector,  $\vec{r}$ , is related to basic coordinates by,

$$\vec{r} = X^1 \vec{I}_1 \quad (\text{II.1})$$

The covariant base vectors  $\vec{a}_\alpha$  are related to basic coordinates by,

$$\vec{a}_\alpha = X^1_{,\alpha} \vec{I}_1 \quad (\text{II.2})$$

The base vectors  $\vec{a}_\alpha$  are not in general unit vectors, the unit vectors being given by,

$$\vec{e}_\alpha = \frac{\vec{a}_\alpha}{|\vec{a}_\alpha|} = \frac{\vec{a}_\alpha}{\sqrt{\vec{a}_\alpha \cdot \vec{a}_\alpha}} \quad (\text{no sum}) \quad (\text{II.3})$$

The incremental arc length on the shell reference surface is measured by,

$$\begin{aligned} dS^2 &= d\vec{r} \cdot d\vec{r} \\ &= a_{\alpha\beta} dx^\alpha dx^\beta \end{aligned} \quad (\text{II.4})$$

where  $a^{\alpha\beta}$  is the metric tensor of the undeformed reference surface and the right hand expression of (II.4) is called

the first fundamental quadratic form of the surface.

The metric tensor is computed by,

$$\begin{aligned} a_{\alpha\beta} &= \vec{a}_\alpha \cdot \vec{a}_\beta \\ &= X^i_{,\alpha} X^i_{,\beta} \end{aligned} \quad (\text{II.5})$$

An area element on the shell reference surface is,

$$\begin{aligned} dA &= |\vec{a}_1 \times \vec{a}_2| dx^1 dx^2 \\ &= \sqrt{a} dx^1 dx^2 \end{aligned} \quad (\text{II.6})$$

where  $a$  is the determinant of the metric tensor.

An alternate form of (II.4) is,

$$dS^2 = (A_1)^2 dx^1 dx^1 + 2A_1 A_2 \cos\phi dx^1 dx^2 + (A_2)^2 dx^2 dx^2 \quad (\text{II.7})$$

where

$$A_\alpha = \sqrt{a_{\alpha\alpha}} \quad (\text{no sum}) \quad (\text{II.8})$$

$$\cos\phi = \frac{a_{12}}{\sqrt{a_{11}a_{22}}} \quad (\text{II.9})$$

$$\sin\phi = \frac{\sqrt{a}}{\sqrt{a_{11}a_{22}}} \quad (\text{II.10})$$

The quantities  $A_\alpha$ , known as the Lamé parameters, are measures of arc length along the surface coordinate lines and  $\phi$  is the angle between the coordinate lines. For orthogonal coordinates, the angle  $\phi$  is 90 degrees and the component  $a_{12}$  is zero.

The contravariant base vectors are defined by,

$$\vec{a}^1 = \frac{1}{\sqrt{a}} \vec{a}_2 \times \vec{e}_3 \quad (\text{II.11})$$

$$\vec{a}^2 = \frac{1}{\sqrt{a}} \vec{e}_3 \times \vec{a}_1 \quad (\text{II.12})$$

where,

$$\vec{e}_3 = \frac{1}{\sqrt{a}} \vec{a}_1 \times \vec{a}_2 \quad (\text{II.13})$$

The covariant and contravariant base vectors are related by,

$$\vec{a}_\alpha \cdot \vec{a}^\beta = \delta_\alpha^\beta \quad (\text{II.14})$$

where,

$$\delta_\alpha^\beta = \begin{cases} 1, & \alpha = \beta \\ 0, & \alpha \neq \beta \end{cases} \quad (\text{II.15})$$

The components of the associated metric tensor are,

$$a^{\alpha\beta} = \vec{a}^\alpha \cdot \vec{a}^\beta \quad (\text{II.16})$$

The covariant and contravariant base vectors are transformed via the metric tensors. This operation is termed raising and lowering of indices and is given by,

$$\vec{a}^\alpha = a^{\alpha\beta} \vec{a}_\beta \quad (\text{II.17})$$

$$\vec{a}_\alpha = a_{\alpha\beta} \vec{a}^\beta \quad (\text{II.18})$$

The Christoffel symbols of the second kind are defined in terms of the metric tensor and base vectors to be,

$$\Gamma_{\beta\gamma}^\alpha = a^{\alpha\lambda} (\vec{a}_\lambda \cdot \vec{a}_{\beta,\gamma}) \quad (\text{II.19})$$

The covariant form of the initial curvature tensor is defined by,

$$\Gamma_{\alpha\beta}^3 = b_{\alpha\beta} = \vec{e}_n \cdot \vec{a}_{\alpha,\beta} \quad (\text{II.20})$$

The quantities  $b_{\alpha\beta}$  are known as the coefficients of the second fundamental form of the undeformed reference surface and they describe the initial curvature of the surface.

The indices of the tensor  $b_{\alpha\beta}$  may also be raised and lowered via the metric tensor to give the mixed and contravariant forms,



$$b_{\beta}^{\alpha} = a^{\alpha\lambda} b_{\lambda\beta} = a_{\beta\lambda} b^{\lambda\alpha} \quad (\text{II.21})$$

$$b^{\alpha\beta} = a^{\alpha\lambda} b_{\lambda}^{\beta} \quad (\text{II.22})$$

The displacement vector at a point on the shell reference surface is,

$$\begin{aligned} \vec{u} &= u^{\alpha} \vec{a}_{\alpha} + w \vec{e}_n \\ &= u_{\alpha} \vec{a}^{\alpha} + w \vec{e}_n \end{aligned} \quad (\text{II.23})$$

where  $u_{\alpha}$  and  $u^{\alpha}$  are the covariant and contravariant components of in-plane displacement.

The concept of covariant differentiation is utilized in the tensor analysis of the deformation of the shell reference surface. The covariant derivatives of the displacements  $u_{\alpha}$  and  $u^{\alpha}$  are,

$$u_{\alpha}|_{\nu} = u_{\alpha,\nu} - \Gamma_{\alpha\nu}^{\lambda} u_{\lambda} \quad (\text{II.24})$$

$$u^{\alpha}|_{\nu} = u^{\alpha}_{,\nu} + \Gamma_{\lambda\nu}^{\alpha} u^{\lambda} \quad (\text{II.25})$$

and the covariant derivatives of the second order tensors  $b_{\alpha\beta}$  and  $b^{\alpha\beta}$  are,

$$b_{\alpha\beta}|_v = b_{\alpha\beta,v} - \Gamma_{\alpha v}^{\lambda} b_{\lambda\beta} - \Gamma_{\beta v}^{\lambda} b_{\alpha\lambda} \quad (\text{II.26})$$

$$b_{\alpha}^{\beta}|_v = b_{\alpha,v}^{\beta} + \Gamma_{\lambda v}^{\beta} b_{\alpha}^{\lambda} - \Gamma_{\alpha v}^{\lambda} b_{\lambda}^{\beta} \quad (\text{II.27})$$

The practical utilization of the above concepts is demonstrated in Appendix D wherein the tensors necessary to describe the geometry and deformation of the shell reference surface are computed for several classes of shell surfaces.

## B. Deformation of the Shell

Strain displacement relations in arbitrary curvilinear coordinates have been derived by Sanders [117] for thin shells with small reference surface strains and moderately small rotations. The deformation of the shell is defined by the reference surface strain tensor  $\gamma_{\alpha\beta}$  which accounts for stretching or membrane behavior and the curvature change tensor  $\chi_{\alpha\beta}$  which accounts for bending behavior.

The strain tensor at an arbitrary point, Q, which lies off the shell reference surface (see Figure 4) is given by,

$$\bar{\gamma}_{\alpha\beta} = \gamma_{\alpha\beta} + x^3 \cdot \chi_{\alpha\beta} \quad (\text{II.28})$$

where the reference surface tensors  $\gamma_{\alpha\beta}$  and  $\chi_{\alpha\beta}$  are defined by Sanders [117] to be (see also Oden [118]),

$$\gamma_{\alpha\beta} = \frac{1}{2}[u_{\alpha} |_{\beta} + u_{\beta} |_{\alpha} - 2b_{\alpha\beta} w] \quad (\text{II.29})$$

$$\chi_{\alpha\beta} = \frac{1}{2}[\bullet_{\alpha} |_{\beta} + \bullet_{\beta} |_{\alpha} + b_{\beta}^{\lambda} \omega_{\alpha\lambda} + b_{\alpha}^{\lambda} \omega_{\beta\lambda}] \quad (\text{II.30})$$

and

$$\bullet_{\alpha} = -[w,_{\alpha} + b_{\alpha}^{\lambda} u_{\lambda}] \quad (\text{II.31})$$

$$\omega_{\alpha\beta} = \frac{1}{2}[u_{\alpha} |_{\beta} - u_{\beta} |_{\alpha}] \quad (\text{II.32})$$

The quantities  $\bullet_\alpha$  are the covariant components of the rotation vector and describe the rotation of the normal to the deformed reference surface.

The displacement vector at an arbitrary point off the shell reference surface is then defined by,

$$\vec{u} = \vec{u} + x^3 \cdot \vec{\bullet} \quad (\text{II.33})$$

where

$$\vec{\bullet} = \bullet_\alpha \vec{a}^\alpha = \bullet^\alpha \vec{a}_\alpha \quad (\text{II.34})$$

$$\vec{\bullet} = \psi_\alpha \vec{e}_\alpha \quad (\text{II.35})$$

The quantities  $\bullet^\alpha$  are the contravariant components and the quantities  $\psi_\alpha$  are the physical components of the rotation vector.

By use of (II.3), (II.8), (II.17) and (II.34), (II.35) the relationship between physical components and tensor components is found to be,

$$\psi_\alpha = A_\alpha \bullet^\alpha \quad (\text{no sum}) \quad (\text{II.36})$$

$$\psi_\alpha = A_\alpha a^{\alpha\beta} \bullet_\beta \quad (\text{no sum on } \alpha) \quad (\text{II.37})$$



Substituting (II.31) into (II.37) permits the physical components of the rotation vector to be expressed in terms of the covariant components of displacement,

$$\psi_{\alpha} = -A_{\alpha} (a^{\alpha\beta} w_{,\beta} + b^{\alpha\lambda} u_{,\lambda}) \quad (\text{no sum on } \alpha) \quad (\text{II.38})$$

An alternate form of the rotation vector can be defined by,

$$\begin{aligned} \vec{\theta} &= \vec{e}_n \times \vec{\theta} \\ &= -\psi_2 \vec{e}_1 + \psi_1 \vec{e}_2 \end{aligned} \quad (\text{II.39})$$

This form obeys the right hand rule and is more convenient for certain calculations such as the work done by externally applied concentrated or distributed moment loading.

### CHAPTER III

#### GENERAL DESCRIPTION OF THE ANALYSIS METHOD

The strain energy for an arbitrary, thin shell segment may be expressed as [119],

$$U = \iiint U_0 \sqrt{a} \, dx^3 dx^1 dx^2 \quad (\text{III.1})$$

where  $U_0$  is the strain energy density.

Introducing the stress tensor  $\tau^{\alpha\beta}$  and the strain tensor  $\gamma_{\alpha\beta}$ , the strain energy density is [120],

$$U_0 = \frac{1}{2} \bar{\tau}^{\alpha\beta} (\bar{\gamma}_{\alpha\beta} - \epsilon_{\alpha\beta} \cdot \Delta T) \quad (\text{III.2})$$

where the bar indicates quantities at a point which lies off the shell reference surface,  $\epsilon_{\alpha\beta} \cdot \Delta T$  are thermal strains and,

$$\bar{\gamma}_{\alpha\beta} = \gamma_{\alpha\beta} + x^3 \cdot \chi_{\alpha\beta} \quad (\text{III.3})$$

The constitutive equations including thermal effects are,

$$\bar{\tau}^{\alpha\beta} = \mathbf{E}^{\alpha\beta\lambda\rho} (\gamma_{\lambda\rho} - \epsilon_{\lambda\rho} \cdot \Delta T) \quad (\text{III.4})$$

where  $E^{\alpha\beta\lambda\rho}$  and  $\epsilon_{\lambda\rho}$  are the elastic material constants and  $\Delta T$  is the rise in temperature above the reference state.

The strain-displacement relations of Sanders are,

$$\gamma_{\alpha\beta} = \frac{1}{2}[u_{\alpha|\beta} + u_{\beta|\alpha} - 2b_{\alpha\beta}w] \quad (\text{III.5})$$

$$\chi_{\alpha\beta} = \frac{1}{2}[\phi_{\alpha|\beta} + \phi_{\beta|\alpha} + b_{\beta}^{\lambda}w_{\alpha\lambda} + b_{\alpha}^{\lambda}w_{\beta\lambda}] \quad (\text{III.6})$$

By substitution of the constitutive equations (III.4) and strain-displacement relations (III.5) and (III.6) into (III.2) it is possible to express the strain energy density as a functional in terms of the reference surface displacements, the elastic material constants and the temperature rise,

$$U_0 = U_0(u_{\alpha}, w, E^{\alpha\beta\lambda\rho}, \epsilon_{\lambda\rho}, \Delta T) \quad (\text{III.7})$$

The potential energy  $\pi$  is then,

$$\pi = U - W \quad (\text{III.8})$$

where  $W$  is the potential of the externally applied mechanical and inertial loadings.

The integrals appearing in the potential energy expression (III.1) may be evaluated by numerical integration. If the derivatives of displacement which occur in  $\pi$  are replaced by finite difference approximations and a

variational procedure is applied according to the Theorem of Minimum Potential Energy, a set of linear equations in terms of the displacement variables will be obtained. This set of equations can be expressed in the matrix form:

$$[\mathbf{M}]\{\ddot{\mathbf{q}}\} + [\mathbf{K}]\{\mathbf{q}\} = \{\mathbf{P}\} \quad (\text{III.9})$$

or in the absence of inertial loads,

$$[\mathbf{K}]\{\mathbf{q}\} = \{\mathbf{P}\} \quad (\text{III.10})$$

where:  $[\mathbf{M}]$  = Mass matrix

$[\mathbf{K}]$  = Stiffness matrix

$\{\mathbf{q}\}$  = Vector of unknown displacements at discrete points of the finite difference network

$\{\mathbf{P}\}$  = Vector of externally applied thermal or mechanical loads

The solution of (III.9) or (III.10) will yield the time-dependent or static displacements at discrete grid points. The displacements can be converted to strains by using a finite difference form of the strain-displacement relations and the strains can in turn be converted to stresses through the constitutive equations. Equation (III.9) can also be solved for natural frequencies and mode shapes.



Advantages of the above procedure include:

1. Permits point-to-point variation over the shell reference surface of thickness, material properties, and thermal and mechanical loading.
2. Only first and second order derivatives of displacement appear in the potential energy formulation.
3. Only the essential displacement boundary conditions have to be satisfied, the natural force boundary conditions being approximately satisfied via the energy minimization.
4. The stiffness equations are amenable to rapid calculation on modern computers and they are banded; hence large order systems may be economically solved.
5. This approach is based on thin shell theory and should be more accurate than the use of flat finite elements. It should also be competitive with curved finite elements based on shell theory since these elements tend to have a large number of degrees of freedom and therefore the computational time associated with their use can be excessive.

## CHAPTER IV

## THEORETICAL DEVELOPMENT OF SHEFA\* ELEMENT

## A. General Remarks

A thermoelastic analysis method for thin walled shell structures will be formulated using the general tensor notation. After each step of the development the tensor equations will be expanded and recast in a matrix form. The matrix equations will retain all the generality of the tensor equations in that no specialized forms will be substituted which limit the application of the method to a specific class of shell shapes. The only specialized model developed will be that for the shell wall construction and it will be sufficiently general to treat a broad range of anisotropic material configurations including layered orthotropic walls, filament wound walls and angle ply laminates as well as more conventional single layer construction. The model treats the effects of nonlinear temperature gradients through the shell wall including material property temperature dependence and also the coupling between membrane and bending action which results from certain classes of shell wall construction or the use of an arbitrary reference surface (i.e., one not restricted to the shell middle surface).

---

\*The term SHEFA is an acronym for Shell Element based on a Finite difference Approach.

The utility of the matrix notation will be evident as the development progresses. From the standpoint of the theoretician the tensor notation is attractive for its compactness and the ease with which large sets of equations can be manipulated, but the highly condensed form serves to hinder the visibility of the theoretical development. The matrix notation adopted herein serves to provide high visibility and results in a formulation that can be directly programmed for automatic computation without further manipulation. Since this is a matrix method of structural analysis, a specific partitioning of certain variables is necessary in order to facilitate the introduction of numerical approximations, coordinate transformations and transformations from tensor to physical components. Also, since the analysis method is based on a variational procedure, the matrix formulation of the energy equations is done in such a way as to make trivial the final variational operation to obtain the equations of motion.

## B. Thin Shell Strain Energy

1. Strain Energy Density

The strain energy density for a thin shell is, [120],

$$U_o = \frac{1}{2} \bar{\tau}^{\alpha\beta} (\bar{\gamma}_{\alpha\beta} - \epsilon_{\alpha\beta} \cdot \Delta T) \quad (\text{IV.1})$$

or in matrix form,

$$U_o = \frac{1}{2} \{\bar{\tau}\}^T [\{\bar{\gamma}\} - \{\epsilon\} \cdot \Delta T] \quad (\text{IV.2})$$

where,

$\bar{\tau}^{\alpha\beta}$ ,  $\bar{\gamma}_{\alpha\beta}$  = Stress, strain tensors at a point off the shell reference surface

$\epsilon_{\alpha\beta}$  = Tensor of thermal expansion coefficients

$\Delta T$  = Temperature change from reference state

and

$$\{\bar{\tau}\}^T = [\bar{\tau}^{11}, \bar{\tau}^{22}, \bar{\tau}^{12}] \quad (\text{IV.3})$$

$$\{\bar{\gamma}\}^T = [\bar{\gamma}_{11}, \bar{\gamma}_{22}, 2\bar{\gamma}_{12}] \quad (\text{IV.4})$$

$$\{\epsilon\}^T = [\epsilon_{11}, \epsilon_{22}, 2\epsilon_{12}] \quad (\text{IV.5})$$

The thermoelastic constitutive equations relating the stress and strain tensors are:



$$\bar{\gamma}_{\alpha\beta} = \mathbf{F}_{\alpha\beta\lambda\rho} \bar{\tau}^{\lambda\rho} + \epsilon_{\alpha\beta} \cdot \Delta T \quad (\text{IV.6})$$

$$\bar{\tau}^{\alpha\beta} = \mathbf{E}^{\alpha\beta\lambda\rho} \bar{\gamma}_{\lambda\rho} - \Omega^{\alpha\beta} \quad (\text{IV.7})$$

$$\Omega^{\alpha\beta} = \mathbf{E}^{\alpha\beta\lambda\rho} \epsilon_{\lambda\rho} \cdot \Delta T \quad (\text{IV.8})$$

or in matrix form:

$$\{\bar{\gamma}\} = [\mathbf{F}] \{\bar{\tau}\} + \{\epsilon\} \cdot \Delta T \quad (\text{IV.9})$$

$$\{\bar{\tau}\} = [\mathbf{E}] \{\bar{\gamma}\} - \{\Omega\} \quad (\text{IV.10})$$

$$\{\Omega\} = [\mathbf{E}] \{\epsilon\} \cdot \Delta T \quad (\text{IV.11})$$

$$[\mathbf{E}] = [\mathbf{F}]^{-1} \quad (\text{IV.12})$$

where

$\mathbf{E}^{\alpha\beta\lambda\rho}$ ,  $\mathbf{F}_{\alpha\beta\lambda\rho}$  = material elastic constant tensors

and,

$$[\mathbf{E}] = \begin{bmatrix} \mathbf{E}^{1111} & \mathbf{E}^{1122} & \mathbf{E}^{1112} \\ \mathbf{E}^{2211} & \mathbf{E}^{2222} & \mathbf{E}^{2212} \\ \mathbf{E}^{1211} & \mathbf{E}^{1222} & \mathbf{E}^{1212} \end{bmatrix} \quad (\text{IV.13})$$

$$[\mathbf{F}] = \begin{bmatrix} \mathbf{F}_{1111} & \mathbf{F}_{1122} & 2 \mathbf{F}_{1112} \\ \mathbf{F}_{2211} & \mathbf{F}_{2222} & 2 \mathbf{F}_{2212} \\ 2 \mathbf{F}_{1211} & 2 \mathbf{F}_{1222} & 4 \mathbf{F}_{1212} \end{bmatrix} \quad (\text{IV.14})$$

The strain tensor ( $\bar{\gamma}_{\alpha\beta}$ ) at a point off of the reference surface is related to the reference surface strain tensor ( $\gamma_{\alpha\beta}$ ) and curvature change tensor ( $\chi_{\alpha\beta}$ ) by,

$$\bar{\gamma}_{\alpha\beta} = \gamma_{\alpha\beta} + x^3 \cdot \chi_{\alpha\beta} \quad (\text{IV.15})$$

or in matrix form,

$$\{\bar{\gamma}\} = \{\gamma\} + x^3 \cdot \{\chi\} \quad (\text{IV.16})$$

where:

$$\{\gamma\}^T = [\gamma_{11}, \gamma_{22}, 2\gamma_{12}] \quad (\text{IV.17})$$

$$\{\chi\}^T = [\chi_{11}, \chi_{22}, 2\chi_{12}] \quad (\text{IV.18})$$

$x^3$  = coordinate normal to reference surface (positive  
in direction of outward normal)

Substituting equations (IV.10) and (IV.16) into equation (IV.2) gives for the strain energy density,

$$\begin{aligned} U_o &= \left[ \frac{1}{2} \{\gamma\}^T [E] \{\gamma\} + \frac{1}{2} x^3 (\{\chi\}^T [E] \{\gamma\} + \{\gamma\}^T [E] \{\chi\}) \right. \\ &\quad + \frac{1}{2} (x^3)^2 \{\chi\}^T [E] \{\chi\} ] + [ -\{\Omega\}^T \{\gamma\} - x^3 \{\Omega\}^T \{\chi\} \\ &\quad - \frac{1}{2} (\Delta T)^2 \{\epsilon\}^T [E] \{\epsilon\} ] \\ &= [U_o^M + U_o^C + U_o^B] + [U_o^{TM} + U_o^{TB} + C_1] \\ &= U_o^S + U_o^T \end{aligned} \quad (\text{IV.19})$$

where,

$$U_o^S = \text{Strain energy of the shell}$$

$$U_o^T = \text{Work done by thermal forces}$$

$$U_o^M = \frac{1}{2} \{\gamma\}^T [\mathbf{E}] \{\gamma\} \quad (\text{IV.20})$$

= Strain energy due to membrane action

$$U_o^C = \frac{1}{2} x^3 (\{\chi\}^T [\mathbf{E}] \{\gamma\} + \{\gamma\}^T [\mathbf{E}] \{\chi\}) \quad (\text{IV.21})$$

= Strain energy due to coupled membrane and bending action

$$U_o^B = \frac{1}{2} (x^3)^2 \{\chi\}^T [\mathbf{E}] \{\chi\} \quad (\text{IV.22})$$

= Strain energy due to bending action

$$U_o^{TM} = - \{\Omega\}^T \{\gamma\} = - \{\epsilon\}^T [\mathbf{E}] \{\gamma\} \cdot \Delta T \quad (\text{IV.23})$$

= Strain energy due to thermal membrane action

$$U_o^{TB} = - x^3 \{\Omega\}^T \{\chi\} = - x^3 \{\epsilon\}^T [\mathbf{E}] \{\chi\} \cdot \Delta T \quad (\text{IV.24})$$

= Strain energy due to thermal bending action

$$C_1 = - \frac{1}{2} (\Delta T)^2 \{\epsilon\}^T [\mathbf{E}] \{\epsilon\} \quad (\text{IV.25})$$

= Thermal constant which does not contribute to the stiffness equations\*.

---

\*Since  $C_1$  is not a function of the displacements, it vanishes when the potential energy is minimized.

Thus,

$$U_o^S = \frac{1}{2} \left\{ \frac{-Y}{X} \right\}^T \left[ \begin{array}{c|c} -\frac{\mathbf{E}}{x^3 \cdot \mathbf{E}} & -\frac{x^3 \cdot \mathbf{E}}{(x^3)^2 \cdot \mathbf{E}} \end{array} \right] \left\{ \frac{-Y}{X} \right\} \quad (\text{IV.26})$$

$$U_o^T = \frac{1}{2} \left\{ \frac{-\Omega}{x^3 \cdot \Omega} \right\}^T \left\{ \frac{-Y}{X} \right\} \quad (\text{IV.27})$$

## 2. Shell Wall Model

Integrating through the shell wall,

$$\begin{aligned} \bar{U}_o &= \int U_o dx^3 \\ &= \frac{1}{2} \left\{ \frac{-Y}{X} \right\}^T \cdot \left[ \begin{array}{c|c} -\frac{D}{C} & -\frac{C}{B} \end{array} \right] \left\{ \frac{-Y}{X} \right\} - \left\{ \frac{N_T}{M_T} \right\}^T \left\{ \frac{-Y}{X} \right\} \\ &= \frac{1}{2} \{\gamma\}^T [D] \{\gamma\} + \frac{1}{2} \{\chi\}^T [C] \{\gamma\} + \{\gamma\}^T [C] \{\chi\} \\ &\quad + \frac{1}{2} \{\chi\}^T [B] \{\chi\} - \{N_T\}^T \{\gamma\} - \{M_T\}^T \{\chi\} \end{aligned} \quad (\text{IV.28})$$

where,

$$[D] = \int [\mathbf{E}] dx^3 \quad (\text{IV.29})$$

$$[C] = \int [\mathbf{E}] x^3 dx^3 \quad (\text{IV.30})$$

$$[B] = \int [\mathbf{E}] (x^3)^2 dx^3 \quad (\text{IV.31})$$

$$\{N_T\} = \int \{\Omega\} dx^3 = \int [\mathbf{E}] \{\epsilon\} \cdot \Delta T \cdot dx^3 \quad (\text{IV.32})$$

$$\{M_T\} = \int \{\Omega\} x^3 dx^3 = \int [\mathbf{E}] \{\epsilon\} \cdot \Delta T \cdot x^3 dx^3 \quad (\text{IV.33})$$



The final form of the shell compliances (IV.29) - (IV.31) thermal forces (IV.32) and moments (IV.33) depends on the shell wall construction, the materials used, their degree of anisotropy and temperature dependence, the orientation of the natural material axes with respect to the shell coordinates, and the nature of the thermal environment.

For convenience, the symbol  $z$  will be used interchangeably with the normal coordinate,  $x^3$ , in the following analytical development (see Figure 5a).

A general model that will treat a broad range of shell walls and thermal environments is one that accounts for a layered construction with each layer being a different planarly orthotropic, temperature dependent material whose natural axes do not necessarily coincide with the Gaussian surface (shell) coordinates (see Figure 5).

For each orthotropic layer the physical material properties (with respect to the natural material axes) are,

$$[G]_m = \begin{bmatrix} \frac{E_{11}}{1-\nu_o^2} & \frac{\nu_{12}E_{22}}{1-\nu_o^2} & 0 \\ \frac{\nu_{21}E_{11}}{1-\nu_o^2} & \frac{E_{22}}{1-\nu_o^2} & 0 \\ 0 & 0 & E_{12} \end{bmatrix}, \quad \{\alpha\}_m = \begin{Bmatrix} \alpha_{11} \\ \alpha_{22} \\ 0 \end{Bmatrix}$$

(IV.34)

where,

$$v_o^2 = v_{12}v_{21} \quad (\text{IV.35})$$

and by symmetry in the constitutive relations,

$$v_{12} = v_{21} \frac{E_{11}}{E_{22}} \quad (\text{IV.36})$$

The spatial variation of temperature is assumed not to change with the local surface coordinates and to be constant through the thickness of each layer. Hence, nonlinear gradients through the shell thickness can be approximated by a series of finite steps. It is assumed that the temperature gradient through the shell wall is defined by a set of discrete temperatures,  $T_K$ , ( $K = 1, M$ ), which are given at normal coordinate locations,  $z_K$ , ( $K = 1, M$ ), (see Figure 6). This gradient is defined at the element level and is given at the element centroid location. The average layer temperature,  $T_n$ , must then be obtained by interpolation of the temperature gradient through the wall. It is further assumed that the material property matrices  $[G]_m$  and  $\{\alpha\}_m$  are temperature dependent and that they have been obtained by interpolating the appropriate set of material properties at the average layer temperature.

As an example, using linear interpolation the average layer temperature is,

$$T_n = T_K + (T_{K+1} - T_K) \frac{(z_C^n - z_K)}{(K+1 - K)} \quad (\text{IV.37})$$

where

$$z_C^n = \frac{1}{2}(z_I^n + z_O^n) \quad (\text{IV.38})$$

Having computed the matrices  $[G]_m$  and  $\{\alpha\}_m$  for each layer in the material coordinate system  $(x_m^K)$  it is now necessary to rotate them through the anisotropic material orientation angle,  $\phi$ , into the shell coordinates  $(x_S^K)$ . The angle  $\phi$  can change from layer to layer.

$$[G]_S = [T_P][G]_m[T_P]^T \quad (\text{IV.39})$$

$$\{\alpha\}_S = [T_Q]\{\alpha\}_m \quad (\text{IV.40})$$

where the transformation matrices (see [121]) are,

$$[T_P]^T = \begin{bmatrix} c^2 & s^2 & cs \\ s^2 & c^2 & -cs \\ -2cs & 2cs & c^2 - s^2 \end{bmatrix} \quad (\text{IV.41})$$

$$[T_Q] = \begin{bmatrix} c^2 & s^2 & -cs \\ s^2 & c^2 & cs \\ 2cs & -2cs & c^2 - s^2 \end{bmatrix} \quad (\text{IV.42})$$

$$C = \cos\phi, S = \sin\phi \quad (\text{IV.43})$$

The physical matrices  $[G]_S$  and  $\{\alpha\}_S$  in shell coordinates must now be transformed to tensor quantities to permit their use in the general tensor formulation. (See Section IV.D, equations (IV.323) and (IV.310)).

$$[E] = [T_\sigma][G]_S[T_\gamma] \quad (\text{IV.44})$$

$$\{\epsilon\} = [T_\gamma]^{-1}\{\alpha\}_S \quad (\text{IV.45})$$

where:

$$[T_\sigma] = \begin{bmatrix} \sqrt{\frac{a_{11}}{a_{11}}} & 0 & 0 \\ 0 & \sqrt{\frac{a_{22}}{a_{22}}} & 0 \\ 0 & 0 & \sqrt{\frac{a_{11}}{a_{22}}} \end{bmatrix} \quad (\text{IV.46})$$

$$[T_\gamma] = \begin{bmatrix} \frac{1}{a_{11}} & 0 & 0 \\ 0 & \frac{1}{a_{22}} & 0 \\ 0 & 0 & \frac{1}{\sqrt{a_{11}a_{22}}} \end{bmatrix} \quad (\text{IV.4.})$$



Thus,

$$[E] = \begin{bmatrix} \frac{1}{a_{11}} \sqrt{\frac{a_{11}}{a_{11}}} G_{11} & \frac{1}{a_{22}} \sqrt{\frac{a_{11}}{a_{11}}} G_{12} & \frac{1}{a_{11}} \sqrt{\frac{a_{11}}{a_{22}}} G_{13} \\ \frac{1}{a_{11}} \sqrt{\frac{a_{22}}{a_{22}}} G_{21} & \frac{1}{a_{22}} \sqrt{\frac{a_{22}}{a_{22}}} G_{22} & \frac{1}{a_{22}} \sqrt{\frac{a_{22}}{a_{11}}} G_{23} \\ \frac{1}{a_{11}} \sqrt{\frac{a_{11}}{a_{22}}} G_{31} & \frac{1}{a_{22}} \sqrt{\frac{a_{11}}{a_{22}}} G_{32} & \frac{1}{a_{22}} \sqrt{\frac{a_{11}}{a_{11}}} G_{33} \end{bmatrix}_s$$

(IV.48)

$$\{\epsilon\} = \begin{Bmatrix} \epsilon_{11} \\ \epsilon_{22} \\ 2\epsilon_{12} \end{Bmatrix} = \begin{Bmatrix} a_{11}\alpha_{11} \\ a_{22}\alpha_{22} \\ \sqrt{a_{11}a_{22}}\alpha_{12} \end{Bmatrix}_s \quad \text{(IV.49)}$$

Having completed the preliminary calculations for each layer, the integration of the material properties through the thickness can be performed to obtain the compliances for the shell wall.

$$\begin{aligned}
 [D] &= \int [E] dz \\
 &= \sum_{n=1}^N [E]_n \int_{z_I^n}^{z_o^n} dz \\
 &= \sum_{n=1}^N [E]_n (z_o^n - z_I^n) \quad (IV.50)
 \end{aligned}$$

$$\begin{aligned}
 [C] &= \int [E] z dz \\
 &= \sum_{n=1}^N [E]_n \int_{z_I^n}^{z_o^n} z dz \\
 &= \frac{1}{2} \sum_{n=1}^N [E]_n ((z_o^n)^2 - (z_I^n)^2) \quad (IV.51)
 \end{aligned}$$

$$\begin{aligned}
 [B] &= \int [E] z^2 dz \\
 &= \sum_{n=1}^N [E]_n \int_{z_I^n}^{z_o^n} z^2 dz \\
 &= \frac{1}{3} \sum_{n=1}^N [E]_n ((z_o^n)^3 - (z_I^n)^3) \quad (IV.52)
 \end{aligned}$$

The thermal forces and moments are,

$$\begin{aligned}
 \{N_T\} &= \int \{\Omega\} dz \\
 &= \sum_{n=1}^N \{\Omega\}_n \int_{z_I^n}^{z_O^n} dz \\
 &= \sum_{n=1}^N [E]_n \{\epsilon\}_n (z_O^n - z_I^n) \cdot \Delta T \quad (IV.53)
 \end{aligned}$$

$$\begin{aligned}
 \{M_T\} &= \int \{\Omega\} z dz \\
 &= \sum_{n=1}^N \{\Omega\}_n \int_{z_I^n}^{z_O^n} z dz \\
 &= \frac{1}{2} \sum_{n=1}^N [E]_n \{\epsilon\}_n \cdot ((z_O^n)^2 - (z_I^n)^2) \cdot \Delta T \quad (IV.54)
 \end{aligned}$$

Inherent in the philosophy of usage of the above material model is the concept that spatial variations of temperature with the surface coordinates  $(x_s^1, x_s^2)$  are accounted for by the element discretization. Thus in selecting the nodal point mesh, care should be taken to insure that surface temperature variations and the consequent material degradation and thermal loading effects can be adequately

approximated. Similar care should be taken in selecting the layer discretization through the thickness. Discretization strategy requirements such as these are inherent in numerical methods of analysis, both finite element and finite difference, and should not be viewed as undue restrictions on the method of analysis.

### 3. Strain-Displacement and Curvature

#### Displacement Relations

The reference surface strain tensor,  $\gamma_{\alpha\beta}$ , is related to the components of the reference surface displacement vector,  $\vec{u} = u_{\alpha} \vec{a}^{\alpha} + w \vec{e}_n$  by,

$$\gamma_{\alpha\beta} = \frac{1}{2}(u_{\alpha|\beta} + u_{\beta|\alpha} - 2wb_{\alpha\beta}) \quad (\text{IV.55})$$

The tensor form can be expanded and recast in the following matrix form,

$$\{\gamma\} = [S]\{U\} \quad (\text{IV.56})$$

where,

$$\{U\}^T = [u_1 | u_{1,1} | u_{1,2} | u_2 | u_{2,1} | u_{2,2} | w] \quad (\text{IV.57})$$

$$\{\gamma\}^T = [\gamma_{11}, \gamma_{22}, 2\gamma_{12}] \quad (\text{IV.58})$$



$$[S] = \begin{bmatrix} -\Gamma_{11}^1 & 1 & 0 & -\Gamma_{11}^2 & 0 & 0 & -b_{11} \\ -\Gamma_{22}^1 & 0 & 0 & -\Gamma_{22}^2 & 0 & 1 & -b_{22} \\ -2\Gamma_{12}^1 & 0 & 1 & -2\Gamma_{12}^2 & 1 & 0 & -2b_{12} \end{bmatrix} \quad (\text{IV.59})$$

The curvature change tensor,  $\chi_{\alpha\beta}$ , is related to the displacement components by,

$$\chi_{\alpha\beta} = \frac{1}{2}(\bullet_{\alpha} |_{\beta} + \bullet_{\beta} |_{\alpha} + b_{\beta}^{\mu} \omega_{\alpha\mu} + b_{\alpha}^{\mu} \omega_{\beta\mu}) \quad (\text{IV.60})$$

where,

$$\begin{aligned} \bullet_{\alpha} &= -(w_{,\alpha} + b_{\alpha}^{\mu} u_{\mu}) \\ &= \text{shell rotation tensor} \end{aligned} \quad (\text{IV.61})$$

$$\omega_{\alpha\beta} = \frac{1}{2}(u_{\alpha} |_{\beta} - u_{\beta} |_{\alpha}) \quad (\text{IV.62})$$

The tensor form can be expanded and recast in the following matrix form,

$$\{\chi\} = [R]\{V\} \quad (\text{IV.63})$$

where,

$$\{V\}^T = [u_1 | u_{1,1} | u_{1,2} | u_2 | u_{2,1} | u_{2,2} | w_1 | w_2 | w_{11} | w_{12} | w_{22}] \quad (\text{IV.64})$$

$$\{X\}^T = [x_{11}, x_{22}, x_{12}] \quad (\text{IV.65})$$

$$[R]^T = \begin{bmatrix} b_1^1 r_{11}^1 + b_1^2 r_{21}^1 & b_2^1 r_{12}^1 + b_2^2 r_{22}^1 & b_1^1 r_{12}^1 + b_1^2 r_{22}^1 \\ -b_1^1 |_1 & -b_2^1 |_2 & +b_2^1 r_{11}^1 + b_2^2 r_{21}^1 \\ & & -b_1^1 |_2 - b_2^1 |_1 \\ \hline -b_1^1 & 0 & -b_2^1 \\ \hline \frac{1}{2} b_1^2 & -\frac{3}{2} b_2^1 & -\frac{3}{2} b_1^1 + \frac{1}{2} b_2^2 \\ \hline b_1^1 r_{11}^2 + b_1^2 r_{21}^2 & b_2^1 r_{12}^2 + b_2^2 r_{22}^2 & b_1^1 r_{12}^2 + b_1^2 r_{22}^2 \\ -b_1^2 |_1 & -b_2^2 |_2 & +b_2^1 r_{11}^2 + b_2^2 r_{21}^2 \\ & & -b_1^2 |_2 - b_2^2 |_1 \\ \hline -\frac{3}{2} b_1^2 & \frac{1}{2} b_2^1 & -\frac{3}{2} b_2^2 + \frac{1}{2} b_1^1 \\ \hline 0 & -b_2^2 & -b_1^2 \\ \hline r_{11}^1 & r_{22}^1 & 2r_{12}^1 \\ \hline r_{11}^2 & r_{22}^2 & 2r_{12}^2 \\ \hline -1 & 0 & 0 \\ \hline 0 & 0 & -2 \\ \hline 0 & -1 & 0 \end{bmatrix} \quad (\text{IV.66})$$

The matrices [S] and [R] are functions of the shell geometry only and are completely general, not being restricted to any particular shell shape. If the [S] and [R] matrices are programmed for automatic computation in this form, various shell geometries can be handled at execution time by appropriate computation of the entries in [S] and [R]. For any particular class of shells of interest (e.g., cylindrical, spherical, conical) it is only necessary to compute the Christoffel symbols  $\Gamma_{\beta\rho}^{\alpha}$ , the second fundamental form  $b_{\beta}^{\alpha}$ , and its covariant derivative  $b_{\beta}^{\alpha}|_{\rho}$ , and the metric tensor  $a_{\alpha\beta}$ , in order to completely define the [S] and [R] matrices. In Appendix E, Tables E.1 through E.5, concise summaries of these tensors are given for conical, cylindrical and spherical shells as well as for flat plates in both polar and Cartesian coordinates.

#### 4. Finite Difference Approximation to Strain and Curvature Change Tensors

It is now necessary to introduce a finite approximation to the reference surface strain and curvature change tensors. The approximation will be a generalized finite difference procedure which will be developed in the same general way as a finite element. That is, the strain energy will be integrated over a finite region (element) and the total energy obtained by summing on the number of elements. The finite difference element differs from the conventional

finite element in that the displacement field for the normal component of displacement is defined such that it extends beyond the region of integration (element) into several adjacent elements. The displacement fields for the tangential components of displacement are contained within the region of integration.

The computational procedure is termed generalized because unlike conventional finite difference methods the discrete approximation formulated herein does not rely on nodal point meshes which coincide with shell surface coordinate lines, but rather it is developed for arbitrary grids. The removal of this classic restriction which is inherent in conventional finite difference methods makes this generalized finite difference scheme competitive with the finite element method in its ability to model complex geometries. The generalized finite difference element geometry is depicted in Figures 4 and 7.

The tangential components of displacement,  $u_1$  and  $u_2$ , are assumed to be a bilinear function of the local element coordinates  $\lambda$  and  $\mu$ . These displacement fields are defined over the region contained within the solid line of Figure 7, and include the discrete values of displacement,  $u_1^K$  and  $u_2^K$ ,  $K = 1, 4$ . This region is also the area over which the strain energy will be integrated; hence it is the "element area" in conventional finite element terminology. In matrix form, the displacement approximations are,



$$u_1 = [L]\{w_1\} , \quad u_2 = [L]\{w_2\} \quad (\text{IV.67})$$

where,

$$\begin{aligned} [L] &= \text{linear shape functions*} \\ &= [L_1, L_2, L_3, L_4] \end{aligned} \quad (\text{IV.68})$$

$$\begin{aligned} \{w_N\}^T &= \text{discrete nodal point displacement vector} \\ &= [u_N^1, u_N^2, u_N^3, u_N^4], \quad N=1,2 \end{aligned} \quad (\text{IV.69})$$

and,

$$\begin{aligned} L_1 &= \frac{1}{4}(1-\lambda)(1-\mu) \\ L_2 &= \frac{1}{4}(1+\lambda)(1-\mu) \\ L_3 &= \frac{1}{4}(1+\lambda)(1+\mu) \\ L_4 &= \frac{1}{4}(1-\lambda)(1+\mu) \end{aligned} \quad (\text{IV.70})$$

The displacement gradients with respect to the element coordinates  $(\lambda, \mu)$  are then obtained by differentiating (IV.67),

$$\begin{aligned} u_{N,\lambda} &= [L_{,\lambda}]\{w_N\} \\ u_{N,\mu} &= [L_{,\mu}]\{w_N\} \quad N=1,2 \end{aligned} \quad (\text{IV.71})$$

---

\*The linear shape functions are described in detail in Appendix C.

In order to proceed with the discrete approximation it is necessary to obtain the displacement gradients with respect to the Gaussian surface coordinates. This can be accomplished by utilizing the isoparametric mapping techniques of Zienkiewicz and his coworkers, [23,24,29,30]. Let the Gaussian surface coordinates be bilinear functions of the local element coordinates ( $\lambda$  and  $\mu$ ) using the same shape functions as for the tangential displacements. In matrix form, this approximation is,

$$x^M = [L]\{x_K^M\} \quad (\text{IV.72})$$

where,

$\{x_K^M\}^T$  = vector of nodal point Gaussian coordinates

$M = 1, 2$  = coordinate direction

$K = 1, \dots, 4$  = nodal point number

then by differentiating (IV.72),

$$x_{,\lambda}^M = [L_{,\lambda}]\{x_K^M\}$$

$$x_{,\mu}^M = [L_{,\mu}]\{x_K^M\} \quad (\text{IV.73})$$

The spatial derivatives of the displacement functions with respect to local coordinates are related to the displacement gradients (referred to Gaussian surface coordinates  $x^1, x^2$ ) by the familiar first order Jacobian matrix,

$$\begin{Bmatrix} u_{N,\lambda} \\ u_{N,\mu} \end{Bmatrix} = [J_1] \begin{Bmatrix} u_{N,1} \\ u_{N,2} \end{Bmatrix} \quad (\text{IV.74})$$

where,

$$[J_1] = \begin{bmatrix} x_{,\lambda}^1 & x_{,\lambda}^2 \\ x_{,\mu}^1 & x_{,\mu}^2 \end{bmatrix} \quad (\text{IV.75})$$

By substituting (IV.73) into (IV.75) the Jacobian can be expressed in terms of the shape functions and nodal point Gaussian coordinates,

$$[J_1] = \begin{bmatrix} L_{,\lambda} \\ L_{,\mu} \end{bmatrix} [x_k^1 : x_k^2], \quad k=1,\dots,4 \quad (\text{IV.76})$$

where by differentiation of (IV.70),

$$\begin{aligned} L_{1,\lambda} &= -\frac{1}{4}(1-\mu) & , & & L_{1,\mu} &= -\frac{1}{4}(1-\lambda) \\ L_{2,\lambda} &= \frac{1}{4}(1-\mu) & , & & L_{2,\mu} &= -\frac{1}{4}(1+\lambda) \\ L_{3,\lambda} &= \frac{1}{4}(1+\mu) & , & & L_{3,\mu} &= \frac{1}{4}(1+\lambda) \\ L_{4,\lambda} &= -\frac{1}{4}(1+\mu) & , & & L_{4,\mu} &= \frac{1}{4}(1-\lambda) \end{aligned} \quad (\text{IV.77})$$

The displacement gradients with respect to the Gaussian coordinates are then obtained from the inverse of (IV.74),

AD-A034 788

NAVAL SURFACE WEAPONS CENTER WHITE OAK LAB SILVER SP--ETC F/G 13/13  
A GENERALIZED FINITE DIFFERENCE ELEMENT FOR THE THERMOELASTIC S--ETC(U)

JUN 76 R J EDWARDS

UNCLASSIFIED

NSWC/WOL/TR-76-66

NL

2 OF 4

AD  
A034788



Header frame with text and icon	Figure 1	Figure 2	Figure 3	Figure 4	Figure 5	Figure 6	Figure 7	Figure 8	Figure 9	Figure 10	Figure 11	Figure 12	Figure 13
Figure 14	Figure 15	Figure 16	Figure 17	Figure 18	Figure 19	Figure 20	Figure 21	Figure 22	Figure 23	Figure 24	Figure 25	Figure 26	Figure 27
Figure 28	Figure 29	Figure 30	Figure 31	Figure 32	Figure 33	Figure 34	Figure 35	Figure 36	Figure 37	Figure 38	Figure 39	Figure 40	Figure 41
Figure 42	Figure 43	Figure 44	Figure 45	Figure 46	Figure 47	Figure 48	Figure 49	Figure 50	Figure 51	Figure 52	Figure 53	Figure 54	Figure 55
Figure 56	Figure 57	Figure 58	Figure 59	Figure 60	Figure 61	Figure 62	Figure 63	Figure 64	Figure 65	Figure 66	Figure 67	Figure 68	Figure 69
Figure 70	Figure 71	Figure 72	Figure 73	Figure 74	Figure 75	Figure 76	Figure 77	Figure 78	Figure 79	Figure 80	Figure 81	Figure 82	Figure 83
Figure 84	Figure 85	Figure 86	Figure 87	Figure 88	Figure 89	Figure 90	Figure 91	Figure 92	Figure 93	Figure 94	Figure 95	Figure 96	Figure 97
Figure 98	Figure 99	Figure 100	Figure 101	Figure 102	Figure 103	Figure 104	Figure 105	Figure 106	Figure 107	Figure 108	Figure 109	Figure 110	Figure 111



$$\begin{Bmatrix} u_{N,1} \\ u_{N,2} \end{Bmatrix} = [J_1]^{-1} \begin{Bmatrix} u_{N,\lambda} \\ u_{N,\mu} \end{Bmatrix}$$

$$= [T^L] \{w_N\} \quad (\text{IV.78})$$

where the relations (IV.71) have been used to arrive at,

$$[T^L] = [J_1]^{-1} \begin{bmatrix} L \\ L_{,\lambda} \\ L_{,\mu} \end{bmatrix} \quad (\text{IV.79})$$

The matrix equation which relates the strain vector,  $\{\gamma\}$ , and displacement gradient vector,  $\{U\}$ , can now be recast in the following form. Let,

$$\{U\} = [F]\{W\} \quad (\text{IV.80})$$

Then by substituting (IV.80) into (IV.56),

$$\begin{aligned} \{\gamma\} &= [S]\{U\} \\ &= [S][F]\{W\} \end{aligned} \quad (\text{IV.81})$$

where,

$$\{U\}^T = [u_1, u_{1,1}, u_{1,2}, u_2, u_{2,1}, u_{2,2}, w] \quad (\text{IV.82})$$

$$\{W\}^T = [u_1^1, u_2^1, u_1^2, u_2^2, u_1^3, u_2^3, u_1^4, u_2^4 | w^5, w^6, \dots, w^{13}] \quad (\text{IV.83})$$

$$[F] = \begin{bmatrix} L_1 & 0 & L_2 & 0 & L_3 & 0 & L_4 & 0 & 0 & 0 \longrightarrow 0 \\ T_{11}^L & 0 & T_{12}^L & 0 & T_{13}^L & 0 & T_{14}^L & 0 & 0 & 0 \longrightarrow 0 \\ T_{21}^L & 0 & T_{22}^L & 0 & T_{23}^L & 0 & T_{24}^L & 0 & 0 & 0 \longrightarrow 0 \\ 0 & L_1 & 0 & L_2 & 0 & L_3 & 0 & L_4 & 0 & 0 \longrightarrow 0 \\ 0 & T_{11}^L & 0 & T_{12}^L & 0 & T_{13}^L & 0 & T_{14}^L & 0 & 0 \longrightarrow 0 \\ 0 & T_{12}^L & 0 & T_{22}^L & 0 & T_{23}^L & 0 & T_{24}^L & 0 & 0 \longrightarrow 0 \\ 0 & 0 & 0 & 0 & 0 & 0 & 0 & 0 & 1 & 0 \longrightarrow 0 \end{bmatrix} \quad (\text{IV.84})$$

The normal component of displacement,  $w$ , is assumed to be a biquadratic function of the local element coordinates  $\alpha$  and  $\beta$ . The displacement field is defined over the region contained within the dashed line of Figure 7 and includes the discrete values of displacement  $w^k$ ,  $k = 5, 13$ . The  $w$  displacement field thus extends beyond the "element area" into several adjacent elements.

In matrix form, the displacement approximation is,

$$w = [H]\{W_3\} \quad (\text{IV.85})$$

where,

$$\begin{aligned} [H] &= \text{quadratic shape functions}^* \\ &= [H_1, H_2, \dots, H_9] \end{aligned} \quad (\text{IV.86})$$

$$\begin{aligned} \{W_3\}^T &= \text{discrete nodal point displacement vector} \\ &= [w^5, w^6, \dots, w^{13}] \end{aligned} \quad (\text{IV.87})$$

and,

$$\begin{aligned} H_1 &= (1-\alpha^2)(1-\beta^2) \\ H_2 &= \frac{1}{4} \alpha(1-\alpha)\beta(1-\beta) \\ H_3 &= -\frac{1}{2}(1-\alpha^2)\beta(1-\beta) \\ H_4 &= -\frac{1}{4}\alpha(1+\alpha)\beta(1-\beta) \\ H_5 &= \frac{1}{2}\alpha(1+\alpha)(1-\beta^2) \\ H_6 &= \frac{1}{4}\alpha(1+\alpha)\beta(1+\beta) \\ H_7 &= \frac{1}{2}(1-\alpha^2)\beta(1+\beta) \\ H_8 &= -\frac{1}{4}\alpha(1-\alpha)\beta(1+\beta) \\ H_9 &= -\frac{1}{2}\alpha(1-\alpha)(1-\beta^2) \end{aligned} \quad (\text{IV.88})$$

---

\*The quadratic shape functions are described in detail in Appendix C.

The displacement gradients with respect to the element coordinates  $(\alpha, \beta)$  are obtained by differentiating (IV.85),

$$\begin{aligned}w_{,\alpha} &= [H_{,\alpha}]\{w_3\} \\w_{,\beta} &= [H_{,\beta}]\{w_3\} \\w_{,\alpha\alpha} &= [H_{,\alpha\alpha}]\{w_3\} \\w_{,\alpha\beta} &= [H_{,\alpha\beta}]\{w_3\} \\w_{,\beta\beta} &= [H_{,\beta\beta}]\{w_3\}\end{aligned}\tag{IV.89}$$

Again using the isoparametric mapping technique, let the shell coordinates be biquadratic functions of the element coordinates  $(\alpha, \beta)$  using the same shape functions as for the normal displacement. In matrix form this approximation is,

$$x^M = [H]\{x_K^M\}\tag{IV.90}$$

where,

$\{x_K^M\}$  = vector of nodal point shell coordinates

$M = 1, 2$  = coordinate direction

$K = 5, \dots, 13$  = nodal point number



Then by differentiating (IV.90),

$$\begin{aligned}
 x_{,\alpha}^M &= [H_{,\alpha}]\{x_K^M\} \\
 x_{,\beta}^M &= [H_{,\beta}]\{x_K^M\} \\
 x_{,\alpha\alpha}^M &= [H_{,\alpha\alpha}]\{x_K^M\} \quad K=5,\dots,13 \\
 x_{,\alpha\beta}^M &= [H_{,\alpha\beta}]\{x_K^M\} \\
 x_{,\beta\beta}^M &= [H_{,\beta\beta}]\{x_K^M\}
 \end{aligned} \tag{IV.91}$$

The spatial derivatives of the normal displacement function with respect to local coordinates  $\alpha, \beta$  are related to the displacement gradients (referred to shell coordinates  $x^1, x^2$ ) by the second order Jacobian matrix,

$$\begin{bmatrix} w_{,\alpha} \\ w_{,\beta} \\ \hline w_{,\alpha\alpha} \\ w_{,\alpha\beta} \\ w_{,\beta\beta} \end{bmatrix} = \begin{bmatrix} J_2 & \text{null} \\ \hline J_3 & J_4 \end{bmatrix} \begin{bmatrix} w_{,1} \\ w_{,2} \\ \hline w_{,11} \\ w_{,12} \\ w_{,22} \end{bmatrix} = [J_5] \begin{bmatrix} w_{,1} \\ w_{,2} \\ \hline w_{,11} \\ w_{,12} \\ w_{,22} \end{bmatrix} \tag{IV.92}$$

where,

$$[J_5] \left[ \begin{array}{cc|ccc} x_{,\alpha}^1 & x_{,\alpha}^2 & 0 & 0 & 0 \\ x_{,\beta}^1 & x_{,\beta}^2 & 0 & 0 & 0 \\ \hline x_{,\alpha\alpha}^1 & x_{,\alpha\alpha}^2 & (x_{,\alpha}^1)^2 & 2 \cdot x_{,\alpha}^1 \cdot x_{,\alpha}^2 & (x_{,\alpha}^2)^2 \\ x_{,\alpha\beta}^1 & x_{,\alpha\beta}^2 & x_{,\alpha}^1 \cdot x_{,\beta}^1 & x_{,\alpha}^1 \cdot x_{,\beta}^2 & x_{,\alpha}^2 \cdot x_{,\beta}^2 \\ & & & + x_{,\beta}^1 \cdot x_{,\alpha}^2 & \\ x_{,\beta\beta}^1 & x_{,\beta\beta}^2 & (x_{,\beta}^1)^2 & 2 \cdot x_{,\beta}^1 \cdot x_{,\beta}^2 & (x_{,\beta}^2)^2 \end{array} \right] \quad (\text{IV.93})$$

By substituting (IV.91) into (IV.93) the Jacobian can be expressed in terms of the shape functions and nodal point coordinates,

$$[J_2] = \begin{bmatrix} H_{,\alpha} \\ H_{,\beta} \end{bmatrix} [x_K^1 | x_K^2], \quad K=5, \dots, 13 \quad (\text{IV.94})$$

$$[J_3] = \begin{bmatrix} H_{,\alpha\alpha} \\ H_{,\alpha\beta} \\ H_{,\beta\beta} \end{bmatrix} [x_K^1 | x_K^2], \quad K=5, \dots, 13 \quad (\text{IV.95})$$

$$[J_4] = \begin{bmatrix} (J_2)_{11} \cdot (J_2)_{11} & 2 \cdot (J_2)_{11} \cdot (J_2)_{12} & (J_2)_{12} \cdot (J_2)_{12} \\ (J_2)_{11} \cdot (J_2)_{21} & (J_2)_{11} \cdot (J_2)_{22} & (J_2)_{12} \cdot (J_2)_{22} \\ & + (J_2)_{21} \cdot (J_2)_{12} & \\ (J_2)_{21} \cdot (J_2)_{21} & 2 \cdot (J_2)_{21} \cdot (J_2)_{22} & (J_2)_{22} \cdot (J_2)_{22} \end{bmatrix}$$

(IV.96)

where by differentiation of (IV.88)

$$H_{1,\alpha} = -2\alpha(1-\beta^2)$$

$$H_{2,\alpha} = \frac{1}{4}\beta(1-\beta)(1-2\alpha)$$

$$H_{3,\alpha} = \alpha\beta(1-\beta)$$

$$H_{4,\alpha} = -\frac{1}{4}\beta(1-\beta)(1+2\alpha)$$

$$H_{5,\alpha} = \frac{1}{2}(1-\beta^2)(1+2\alpha)$$

$$H_{6,\alpha} = \frac{1}{4}\beta(1+\beta)(1+2\alpha)$$

$$H_{7,\alpha} = -\alpha\beta(1+\beta)$$

$$H_{8,\alpha} = -\frac{1}{4}\beta(1+\beta)(1-2\alpha)$$

$$H_{9,\alpha} = -\frac{1}{2}(1-\beta^2)(1-2\alpha) \quad \text{(IV.97)}$$

$$H_{1,\beta} = -2\beta(1-\alpha^2)$$

$$H_{2,\beta} = \frac{1}{4}\alpha(1-\alpha)(1-2\beta)$$

$$H_{3,\beta} = -\frac{1}{2}(1-\alpha^2)(1-2\beta)$$

$$H_{4,\beta} = -\frac{1}{4}\alpha(1+\alpha)(1-2\beta)$$

$$H_{5,\beta} = -\alpha\beta(1+\alpha)$$

$$H_{6,\beta} = \frac{1}{4}\alpha(1+\alpha)(1+2\beta)$$

$$H_{7,\beta} = \frac{1}{2}(1-\alpha^2)(1+2\beta)$$

$$H_{8,\beta} = -\frac{1}{4}\alpha(1-\alpha)(1+2\beta)$$

$$H_{9,\beta} = \alpha\beta(1-\alpha) \quad (\text{IV.98})$$

and,

$$H_{1,\alpha\alpha} = -2(1-\beta^2)$$

$$H_{2,\alpha\alpha} = -\frac{1}{2}\beta(1-\beta)$$

$$H_{3,\alpha\alpha} = \beta(1-\beta)$$

$$H_{4,\alpha\alpha} = -\frac{1}{2}\beta(1-\beta)$$

$$H_{5,\alpha\alpha} = (1-\beta^2)$$

$$H_{6,\alpha\alpha} = \frac{1}{2}\beta(1+\beta)$$

$$H_{7,\alpha\alpha} = -\beta(1+\beta)$$

$$H_{8,\alpha\alpha} = \frac{1}{2}\beta(1+\beta)$$

$$H_{9,\alpha\alpha} = (1-\beta^2) \quad (\text{IV.99})$$



$$H_{1,\beta\beta} = -2(1-\alpha^2)$$

$$H_{2,\beta\beta} = -\frac{1}{2}\alpha(1-\alpha)$$

$$H_{3,\beta\beta} = (1-\alpha^2)$$

$$H_{4,\beta\beta} = \frac{1}{2}\alpha(1+\alpha)$$

$$H_{5,\beta\beta} = -\alpha(1+\alpha)$$

$$H_{6,\beta\beta} = \frac{1}{2}\alpha(1+\alpha)$$

$$H_{7,\beta\beta} = (1-\alpha^2)$$

$$H_{8,\beta\beta} = -\frac{1}{2}\alpha(1-\alpha)$$

$$H_{9,\beta\beta} = \alpha(1-\alpha) \quad (\text{IV.100})$$

$$H_{1,\alpha\beta} = 4\alpha\beta$$

$$H_{2,\alpha\beta} = \frac{1}{4}(1-2\alpha)(1-2\beta)$$

$$H_{3,\alpha\beta} = \alpha(1-2\beta)$$

$$H_{4,\alpha\beta} = -\frac{1}{4}(1+2\alpha)(1-2\beta)$$

$$H_{5,\alpha\beta} = -\beta(1+2\alpha)$$

$$H_{6,\alpha\beta} = \frac{1}{4}(1+2\alpha)(1+2\beta)$$

$$H_{7,\alpha\beta} = -\alpha(1+2\beta)$$

$$H_{8,\alpha\beta} = -\frac{1}{4}(1-2\alpha)(1+2\beta)$$

$$H_{9,\alpha\beta} = \beta(1-2\alpha) \quad (\text{IV.101})$$

The displacement gradients referred to shell coordinates are then obtained from the inverse of (IV.92),

$$\begin{bmatrix} w_{,1} \\ w_{,2} \\ w_{,11} \\ w_{,12} \\ w_{,22} \end{bmatrix} = [J_5]^{-1} \begin{bmatrix} w_{,\alpha} \\ w_{,\beta} \\ w_{,\alpha\alpha} \\ w_{,\alpha\beta} \\ w_{,\beta\beta} \end{bmatrix}$$

$$= [T^H]\{w_3\} \quad (\text{IV.102})$$

where the relations (IV.89) have been used to arrive at,

$$[T^H] = [J_5]^{-1} \begin{bmatrix} H_{,\alpha} \\ H_{,\beta} \\ H_{,\alpha\alpha} \\ H_{,\alpha\beta} \\ H_{,\beta\beta} \end{bmatrix} \quad (\text{IV.103})$$

A convenient form for the inverse of the Jacobian is,

$$[J_5]^{-1} = \left[ \begin{array}{c|c} J_2^{-1} & \text{null} \\ \hline J_4^{-1} J_3 J_2^{-1} & J_4^{-1} \end{array} \right] \quad (\text{IV.104})$$



## 5. Coordinate Transformations

It is necessary at this point in the analytical development to introduce several coordinate transformations which will be useful in deriving the final physical form of structural matrices and load vectors. These transformations relate the tensor and physical components of the displacement or rotation vectors at an arbitrary point in the element domain to the element displacement vector. The element displacement vector consists of a specific partitioning of the discrete displacement components which are defined at the 13 nodal points shown in Figure 7. Equation (IV.83) defines the covariant tensor form of the element displacement vector; the physical form will be derived in this section. The shape function approximations (IV.67) and (IV.85) will be employed in several alternative matrix forms as required by various partitionings of the displacement variables.

The physical components of displacement,  $\{w\}$ , at an arbitrary point on the shell reference surface are related to the covariant components,  $\{u\}$ , by the transformation (see IV.285),

$$\{w\} = [T_u]\{u\} \quad (\text{IV.110})$$

where,

$$\{w\}^T = [u, v, w] \quad (\text{IV.111})$$

$$\{u\}^T = [u_1, u_2, w] \quad (\text{IV.112})$$



$$[T_u] = \begin{bmatrix} A_1 a^{11} & A_1 a^{12} & 0 \\ A_2 a^{21} & A_2 a^{22} & 0 \\ 0 & 0 & 1 \end{bmatrix} \quad (\text{IV.113})$$

The covariant components of displacement,  $\{u\}$ , at an arbitrary point in the displacement field of an element are related to the covariant components,  $\{w\}$ , of the element displacement vector by the previously introduced shape functions (IV.67) and (IV.86) as follows.

Let,

$$\{u\} = [T_E]\{w\} \quad (\text{IV.114})$$

or in partitioned form,

$$\begin{Bmatrix} u_1 \\ u_2 \\ \hline w \end{Bmatrix} = \begin{bmatrix} T_L & | & \text{NULL} \\ \hline \text{NULL} & | & H \end{bmatrix} \begin{Bmatrix} w_{12} \\ \hline w_3 \end{Bmatrix} \quad (\text{IV.115})$$

where by (IV.83),

$$\begin{aligned} \{w\}^T &= [w_{12} \mid w_3] \\ &= [u_1^1, u_2^1, \dots, u_1^4, u_2^4 \mid w^5, \dots, w^{13}] \end{aligned} \quad (\text{IV.116})$$

and by use of (IV.67) and (IV.86),

$$[T_E] = \left[ \begin{array}{cccc|c} L_1 & 0 & L_2 & 0 & L_3 & 0 & L_4 & 0 & \text{NULL} \\ 0 & L_1 & 0 & L_2 & 0 & L_3 & 0 & L_4 & \\ \hline & & & & \text{NULL} & & & & H_1, \dots, H_9 \end{array} \right]$$

(IV.117)

The covariant tensor form of the element displacement vector,  $\{W\}$ , is related to the physical form,  $\{\bar{W}\}$ , by the transformation,

$$\{W\} = [T_W]\{\bar{W}\} \quad (\text{IV.118})$$

where by the use of the inverse of (IV.113),

$$\begin{aligned} \{\bar{W}\}^T &= [\bar{W}_{12} \mid W_3] \\ &= [u^1, v^1, \dots, u^4, v^4 \mid w^5, \dots, w^{13}] \end{aligned} \quad (\text{IV.119})$$

$$\begin{aligned} [T_W] &= \text{Diagonal } [T_{W_{12}} \mid T_{W_3}] \\ &= \text{Diagonal} [[T_W^1], \dots, [T_W^4] \mid [T_W^5], \dots, [T_W^{13}]] \end{aligned} \quad (\text{IV.120})$$

$$[T_W^I] = \begin{bmatrix} A_1 & a_{21}/A_2 \\ a_{12}/A_1 & A_2 \end{bmatrix}, \quad I = 1, \dots, 4$$

$$= [1], \quad I = 5, \dots, 13 \quad (\text{IV.121})$$

The covariant tensor components of displacement,  $\{u\}$ , at an arbitrary point in the displacement field are then related to the physical components,  $\{\bar{w}\}$ , of the element displacement vector by substitution of (IV.118) into (IV.114) which gives,

$$\{u\} = [T_E][T_W]\{\bar{w}\} \quad (\text{IV.122})$$

The physical components of displacement,  $\{w\}$ , at an arbitrary point in the displacement field are similarly related to the physical components,  $\{\bar{w}\}$ , of the element displacement vector by substituting (IV.122) into (IV.110) to give,

$$\{w\} = [T_u][T_E][T_W]\{\bar{w}\} \quad (\text{IV.123})$$

Later in the analytical development the partitions of the above transformations which pertain to the in-plane components of displacement will be needed. These are obtained as follows.

Let the in-plane partition of (IV.110), (IV.115) and (IV.118) be,

$$\begin{Bmatrix} u \\ v \end{Bmatrix} = [T_V] \begin{Bmatrix} u_1 \\ u_2 \end{Bmatrix} \quad (\text{IV.124})$$

$$\begin{Bmatrix} u_1 \\ u_2 \end{Bmatrix} = [T_L] \{w_{12}\} \quad (\text{IV.125})$$

$$\{w_{12}\} = [T_{W_{12}}] \{\bar{w}_{12}\} \quad (\text{IV.126})$$

Then by substitution of (IV.126) into (IV.125),

$$\begin{Bmatrix} u_1 \\ u_2 \end{Bmatrix} = [T_L][T_{W_{12}}] \{\bar{w}_{12}\} \quad (\text{IV.127})$$

and by substitution of (IV.127) into (IV.124),

$$\begin{Bmatrix} u \\ v \end{Bmatrix} = [T_V][T_L][T_{W_{12}}] \{\bar{w}_{12}\} \quad (\text{IV.128})$$

where

$$[T_V] = \begin{bmatrix} A_1 & a^{11} & A_1 & a^{12} \\ A_2 & a^{21} & A_2 & a^{22} \end{bmatrix} \quad (\text{IV.129})$$



$$[T_L] = \begin{bmatrix} L_1 & 0 & L_2 & 0 & L_3 & 0 & L_4 & 0 \\ 0 & L_1 & 0 & L_2 & 0 & L_3 & 0 & L_4 \end{bmatrix} \quad (\text{IV.130})$$

$$\{w_{12}\}^T = [u_1^1, u_2^1, \dots, u_1^4, u_2^4] \quad (\text{IV.131})$$

$$\{\bar{w}_{12}\}^T = [u^1, v^1, \dots, u^4, v^4] \quad (\text{IV.132})$$

$$[T_{W_{12}}] = \text{Diagonal } [[T_W^1], \dots, [T_W^4]] \quad (\text{IV.133})$$

The first derivatives of the normal displacement at an arbitrary point in the displacement field of an element are related to the discrete normal components,  $\{W_3\}$ , of the element displacement vector by extracting a partition of (IV.102) and using (IV.189) to give,

$$\begin{aligned} \begin{Bmatrix} w_{,1} \\ w_{,2} \end{Bmatrix} &= [J_2]^{-1} \begin{Bmatrix} w_{,\alpha} \\ w_{,\beta} \end{Bmatrix} \\ &= [J_2]^{-1} \begin{bmatrix} H_{,\alpha} \\ H_{,\beta} \end{bmatrix} \{W_3\} \\ &= [T_H] \{W_3\} \end{aligned} \quad (\text{IV.134})$$

Utilizing the last two transformations it is possible to express the covariant components of the rotation vector,  $\{\epsilon\}$ , at an arbitrary point in the element domain in terms of the physical components,  $\{\bar{W}\}$ , of the element displacement vector as follows. The rotation vector is,

$$\bar{\epsilon} = \epsilon_1 \bar{a}^1 + \epsilon_2 \bar{a}^2 \quad (\text{IV.135})$$

where by (II.31),

$$\epsilon_\alpha = -w_{,\alpha} - b_\alpha^\beta u_\beta \quad (\text{IV.136})$$

Recasting in matrix form gives,

$$\{\epsilon\} = \begin{Bmatrix} \epsilon_1 \\ \epsilon_2 \\ 0 \end{Bmatrix} = -[\bar{b}] \begin{Bmatrix} u_1 \\ u_2 \\ 0 \end{Bmatrix} - \begin{Bmatrix} w_{,1} \\ w_{,2} \\ 0 \end{Bmatrix} \quad (\text{IV.137})$$

where,

$$[\bar{b}] = \begin{bmatrix} b_1^1 & b_1^2 & 0 \\ b_2^1 & b_2^2 & 0 \\ 0 & 0 & 0 \end{bmatrix} \quad (\text{IV.138})$$

Since by (IV.125),

$$\begin{Bmatrix} u_1 \\ u_2 \\ 0 \end{Bmatrix} = \begin{bmatrix} T_L \\ \hline \text{NULL} \end{bmatrix} \{w_{12}\}$$

$$= [\bar{T}_L] \{w_{12}\} \quad (\text{IV.139})$$

and by (IV.134),

$$\begin{Bmatrix} w_{,1} \\ w_{,2} \\ 0 \end{Bmatrix} = \begin{bmatrix} T_H \\ \hline \text{NULL} \end{bmatrix} \{w_3\}$$

$$= [\bar{T}_H] \{w_3\} \quad (\text{IV.140})$$

then substituting (IV.139) and (IV.140) into (IV.137) results in the transformation,

$$\begin{aligned} \{\bullet\} &= -[\bar{b}][\bar{T}_L]\{w_{12}\} - [\bar{T}_H]\{w_3\} \\ &= [-[\bar{b}][\bar{T}_L] \mid -[\bar{T}_H]] \left\{ \begin{matrix} w_{12} \\ w_3 \end{matrix} \right\} \\ &= [T_\bullet] \{w\} \end{aligned} \quad (\text{IV.141})$$

Transforming (IV.141) to physical components by use of (IV.118) gives,

$$\{\bullet\} = [T_{\bullet}] [Tw] \{\bar{W}\} \quad (\text{IV.142})$$

In a similar manner the physical components of the rotation vector,  $\{\Psi\}$ , at an arbitrary point in the element displacement field may be expressed in terms of the physical components,  $\{\bar{W}\}$ , of the element displacement vector.

The physical rotation vector is,

$$\bar{\Theta} = \Psi_1 \bar{e}_1 + \Psi_2 \bar{e}_2 \quad (\text{IV.143})$$

where by (II.38),

$$\Psi_1 = -A_1 [a^{11}_{w,1} + a^{12}_{w,2} + b^{11}_{u_1} + b^{12}_{u_2}] \quad (\text{IV.144})$$

$$\Psi_2 = -A_2 [a^{21}_{w,1} + a^{22}_{w,2} + b^{21}_{u_1} + b^{22}_{u_2}] \quad (\text{IV.145})$$

Recasting in matrix form gives,

$$\{\Psi\} = \begin{Bmatrix} \Psi_1 \\ \Psi_2 \end{Bmatrix} = [d_v] \begin{Bmatrix} u_1 \\ u_2 \end{Bmatrix} + [d_w] \begin{Bmatrix} w_{,1} \\ w_{,2} \end{Bmatrix} \quad (\text{IV.146})$$



where,

$$[d_v] = \begin{bmatrix} d_v^1 \\ d_v^2 \end{bmatrix} = \begin{bmatrix} -A_1 b^{11} & -A_1 b^{12} \\ -A_2 b^{21} & -A_2 b^{22} \end{bmatrix} \quad (\text{IV.147})$$

$$[d_w] = \begin{bmatrix} d_w^1 \\ d_w^2 \end{bmatrix} = \begin{bmatrix} -A_1 a^{11} & -A_1 a^{12} \\ -A_2 a^{21} & -A_2 a^{22} \end{bmatrix} \quad (\text{IV.148})$$

Then by substitution of (IV.125) and (IV.134) into (IV.146),

$$\{\Psi\} = [d_v][T_L]\{W_{12}\} + [d_w][T_H]\{W_3\} \quad (\text{IV.149})$$

or alternatively,

$$\begin{aligned} \{\Psi\} &= [[d_v][T_L] \quad [d_w][T_H]] \left\{ \begin{matrix} W_{12} \\ W_3 \end{matrix} \right\} \\ &= [T_\Psi]\{W\} \end{aligned} \quad (\text{IV.150})$$

Transforming (IV.150) to physical components by use of (IV.118) gives,

$$\{\Psi\} = [T_\Psi][T_W]\{\bar{W}\} \quad (\text{IV.151})$$

Another form of the rotation vector which is defined by  $\vec{\nu} = \vec{e}_n \times \vec{\omega}$  (see II.39), is more useful in deriving physical load vectors. It also can be expressed in terms of the

physical components,  $\{\bar{W}\}$ , of the element displacement vector as follows.

The alternate form of the physical rotation vector is,

$$\bar{\theta} = -\psi_2 \bar{e}_1 + \psi_1 \bar{e}_2 \quad (\text{IV.152})$$

Recasting in matrix form and using (IV.144) and (IV.145) yields,

$$\{\theta\} = \begin{Bmatrix} \theta_1 \\ \theta_2 \end{Bmatrix} = [C_V] \begin{Bmatrix} u_1 \\ u_2 \end{Bmatrix} + [C_W] \begin{Bmatrix} w_{,1} \\ w_{,2} \end{Bmatrix} \quad (\text{IV.153})$$

where,

$$[C_V] = \begin{bmatrix} C_V^1 \\ -C_V^2 \end{bmatrix} = \left[ \begin{array}{c|c} A_2 b^{21} & A_2 b^{22} \\ \hline -A_1 b^{11} & -A_1 b^{12} \end{array} \right] \quad (\text{IV.154})$$

$$[C_W] = \begin{bmatrix} C_W^1 \\ -C_W^2 \end{bmatrix} = \left[ \begin{array}{c|c} A_2 a^{21} & A_2 a^{22} \\ \hline -A_1 a^{11} & -A_1 a^{12} \end{array} \right] \quad (\text{IV.155})$$

Then by substituting (IV.125) and (IV.134) into (IV.153),

$$\{\theta\} = [C_V][T_L]\{w_{12}\} + [C_W][T_H]\{w_3\} \quad (\text{IV.156})$$

or alternatively,

$$\begin{aligned} \{ \boldsymbol{\sigma} \} &= \begin{bmatrix} [c_v][T_L] & ; & [c_w][T_H] \end{bmatrix} \left\{ \begin{matrix} W \\ -\frac{1}{W} \frac{1}{3} \end{matrix} \right\} \\ &= [T_{\boldsymbol{\sigma}}] \{ W \} \end{aligned} \quad (\text{IV.157})$$

Transforming (IV.157) to physical components by use of (IV.118) results in,

$$\{ \boldsymbol{\sigma} \} = [T_{\boldsymbol{\sigma}}][T_W]\{\bar{W}\} \quad (\text{IV.158})$$

#### 6. Element Stiffness Matrix

In section IV.B.1, it was shown that the strain energy density for a thin shell is the sum of energies associated with membrane, bending and coupled membrane and bending action. From (IV.19),

$$\begin{aligned} U_o^S &= U_o^M + U_o^C + U_o^B \\ &= \frac{1}{2} \{ \gamma \}^T [E] \{ \gamma \} + \frac{1}{2} x^3 (\{ \chi \}^T [E] \{ \gamma \} + \{ \gamma \}^T [E] \{ \chi \}) \\ &\quad + \frac{1}{2} (x^3)^2 \{ \chi \}^T [E] \{ \chi \} \end{aligned} \quad (\text{IV.159})$$

In section IV.B.2, an analytical model for the shell wall construction was introduced and the strain energy density was integrated through the shell wall to obtain the

strain energy density per unit area. From (IV.28),

$$\begin{aligned}
 \bar{U}_0^S &= \int U_0^S dx^3 \\
 &= \frac{1}{2} \{\gamma\}^T [D] \{\gamma\} + \frac{1}{2} (\{\chi\}^T [C] \{\gamma\} + \{\gamma\}^T [C] \{\chi\}) \\
 &\quad + \frac{1}{2} \{\chi\}^T [B] \{\chi\} \quad (IV.160)
 \end{aligned}$$

In section IV.B.3, matrix forms of the strain-displacement and curvature-displacement relations were introduced in which, for later convenience in the analytical development, the shell geometry was effectively isolated from the displacements and displacement gradients. In section IV.B.4, a finite difference approximation to the strain and curvature tensors was described. The method closely parallels that used for the development of conventional finite elements except that the concept of displacement fields which overlap into several adjacent elements was introduced. By substitution of (IV.81) and (IV.106) into (IV.160) the strain energy for the finite difference element now takes the form,

$$\begin{aligned}
 U_e^S &= \frac{1}{2} \int \int \{W\}^T \left[ [F]^T [S]^T [D] [S] [F] \right. \\
 &\quad + [E]^T [R]^T [C] [S] [F] + [F]^T [S]^T [C] [R] [E] \\
 &\quad \left. + [E]^T [R]^T [B] [R] [E] \right] \{W\} \sqrt{a} dx^1 dx^2 \\
 &= \frac{1}{2} \{W\}^T [K_e] \{W\} \quad (IV.161)
 \end{aligned}$$



Transforming the tensor form of the element displacement vector,  $\{W\}$ , which appears in (IV.161) to the physical form,  $\{\bar{W}\}$ , by use of (IV.118) results in,

$$\begin{aligned} U_e^S &= \frac{1}{2} \{\bar{W}\}^T [T_W]^{-T} [K_e] [T_W] \{\bar{W}\} \\ &= \frac{1}{2} \{\bar{W}\}^T [\bar{K}_e] \{\bar{W}\} \end{aligned} \quad (\text{IV.162})$$

As outlined in Chapter III, the equations of motion (III.9) and (III.10) are arrived at by use of the Theorem of Minimum Potential Energy. By minimizing the strain energy (IV.162) with respect to the discrete variables of the element displacement vector,  $\{\bar{W}\}$ , the physical form of the element stiffness matrix is found to be,

$$[\bar{K}_e] = [T_W]^T [K_e] [T_W] \quad (\text{IV.163})$$

where the tensor form of the element stiffness matrix is given by,

$$[K_e] = \int \int [K_M + K_C^T + K_C + K_B] \sqrt{a} \, dx^1 \, dx^2 \quad (\text{IV.164})$$

and by inspection of (IV.161),

$$\begin{aligned} [K_M] &= [F]^T [S]^T [D] [S] [F] \\ [K_C] &= [F]^T [S]^T [C] [R] [E] \\ [K_B] &= [E]^T [R]^T [B] [R] [E] \end{aligned} \quad (\text{IV.165})$$

The subscripts M, B, C refer to stiffnesses associated with membrane, bending and coupled membrane and bending energies.

The integration of expression (IV.164) can be approximated by Gaussian quadrature and gives,

$$\begin{aligned}
 [K_e] &= \int_{-1}^1 \int_{-1}^1 [K_M + K_C^T + K_C + K_B] \sqrt{a} \cdot |J_1| d\lambda d\mu \\
 &= \sum_{i=1}^M \sum_{j=1}^M H_i H_j [f_k(\lambda_j, \mu_i)] \quad (IV.166)
 \end{aligned}$$

where,

$$[f_k(\lambda_j, \mu_i)] = \left[ [K_M + K_C^T + K_C + K_B] \cdot \sqrt{a} \cdot |J_1| \right]_{\lambda=\lambda_j, \mu=\mu_i} \quad (IV.167)$$

$H_i, H_j$  = Weighting coefficients

$\lambda_j, \mu_i$  = Abscissae of the integration points

$|J_1|$  = Determinant of the Jacobian matrix (IV.75)

The weighting coefficients and the positions of the integration points are given in Table 3 for integration orders M=1 through M=5, [24].

The system stiffness matrix appearing in (III.9) and (III.10) is then obtained by summation of the element stiffness matrices (IV.163).

7. Element Thermal Load Vector

In section IV.B.1, it was shown that the thermal work density for a thin shell is the sum of strain energies associated with thermal membrane forces and thermal bending forces. From (IV.19),

$$\begin{aligned} U_O^T &= U_O^{TM} + U_O^{TB} \\ &= - \Delta T \{\epsilon\}^T [E] \{\gamma\} - \Delta T \{\epsilon\}^T [E] \{\chi\} \cdot x^3 \end{aligned} \quad (IV.168)$$

In section IV.B.2, an analytical model for the shell wall construction was introduced and the work density was integrated through the shell wall to obtain the thermal work density per unit area. From (IV.28),

$$\begin{aligned} \bar{U}_O^T &= \int U_O^T dx^3 \\ &= - \{N_T\}^T \{\gamma\} - \{M_T\}^T \{\chi\} \end{aligned} \quad (IV.169)$$

In sections IV.B.4 and IV.B.5, a numerical approximation to the reference surface strain and curvature tensors was developed. By substitution of (IV.81) and (IV.106) into (IV.169) the thermal work for the finite difference element can now be expressed in the form,

$$\begin{aligned}
 U_e^T &= \int \int \left[ \{N_T\}^T [S][F] + \{M_T\}^T [R][E] \right] \{W\} \sqrt{a} \, dx^1 \, dx^2 \\
 &= \{\mathbf{P}_T\}_e^T \{W\} \quad (\text{IV.170})
 \end{aligned}$$

Transforming the tensor form of the element displacement vector,  $\{W\}$ , which appears in (IV.170) to the physical form,  $\{\bar{W}\}$ , by use of (IV.118) results in,

$$\begin{aligned}
 U_e^T &= \{\mathbf{P}_T\}_e^T [T_W] \{\bar{W}\} \\
 &= \{\mathbf{P}_T\}_e^T \{\bar{W}\} \quad (\text{IV.171})
 \end{aligned}$$

By minimizing the thermal work (IV.171) with respect to the discrete variables of the element displacement vector,  $\{\bar{W}\}$ , the physical form of the element thermal load vector is found to be,

$$\{\bar{\mathbf{P}}_T\}_e = [T_W]^T \{\mathbf{P}_T\}_e \quad (\text{IV.172})$$

where the tensor form of the element thermal load vector is given by,

$$\{\mathbf{P}_T\}_e = \int \int \{P_T^M + P_T^B\} \sqrt{a} \, dx^1 \, dx^2 \quad (\text{IV.173})$$

and by inspection of (IV.170)



$$\begin{aligned}\{P_T^M\} &= [F]^T [S]^T \{N_T\} \\ \{P_T^B\} &= [E]^T [R]^T \{M_T\}\end{aligned}\quad (\text{IV.174})$$

The superscripts M, B refer to thermal loads associated with membrane and bending energies.

The integration of expression (IV.173) can be approximated by Gaussian quadrature and gives,

$$\begin{aligned}\{P_T\}_e &= \int_{-1}^1 \int_{-1}^1 \{P_T^M + P_T^B\} \sqrt{a} \cdot |J_1| \cdot d\lambda d\mu \\ &= \sum_{i=1}^M \sum_{j=1}^M H_i H_j \{f_{P_T}(\lambda_j, \mu_i)\}\end{aligned}\quad (\text{IV.175})$$

where,

$$\{f_{P_T}(\lambda_j, \mu_i)\} = \left\{ \{P_T^M + P_T^B\} \sqrt{a} \cdot |J_1| \right\}_{\lambda=\lambda_j, \mu=\mu_i} \quad (\text{IV.176})$$

The thermal contribution to the system load vector appearing in (III.10) is then obtained by summation of the element thermal load vectors (IV.172).

# C. Potential Energy of Mechanical and Inertial Loads

## 1. Total Work Potential

The total potential energy of various mechanical and inertial loadings is,

$$U_{TOT}^W = \sum_{I=1}^{N_p} (U_e^P)_I + \sum_{J=1}^{N_F} U_J^F + \sum_{K=1}^{N_Q} U_K^Q + \sum_{L=1}^{N_e} (U_e^G + U_e^I)_L \quad (IV.177)$$

The work term  $U_e^P$  is due to a uniformly distributed surface load ( $\vec{p}$ ) acting on the element reference surface,  $N_p$  is the number of elements with surface loading and,

$$U_e^P = \int \int (\vec{p} \cdot \vec{u}) \sqrt{a} \, dx^1 \, dx^2 \quad (IV.178)$$

where

$$\vec{p} = p_1 \vec{e}_1 + p_2 \vec{e}_2 + p_n \vec{e}_n \quad (IV.179)$$

$$\vec{u} = u \vec{e}_1 + v \vec{e}_2 + w \vec{e}_n \quad (IV.180)$$

= Physical displacement vector at  
reference surface (see IV.110)

The work term  $U_J^F$  is due to a concentrated force ( $\vec{F}$ ) acting at a discrete nodal point (J),  $N_F$  is the number of concentrated loads acting and,

$$U_J^F = (\vec{F} \cdot \vec{u})_J \quad (\text{IV.181})$$

where

$$\vec{F}_J = (F_1 \vec{e}_1 + F_2 \vec{e}_2 + F_n \vec{e}_n)_J \quad (\text{IV.182})$$

$$\vec{u}_J = (u \vec{e}_1 + v \vec{e}_2 + w \vec{e}_n)_J \quad (\text{IV.183})$$

= Physical displacement vector at nodal point J

The work term  $U^Q$  is due to a concentrated moment ( $\vec{Q}$ ) acting at a discrete nodal point (K),  $N_Q$  is the number of concentrated moments acting and,

$$U_K^Q = (\vec{Q} \cdot \vec{\vartheta})_K \quad (\text{IV.184})$$

where,

$$\vec{Q}_K = (Q_1 \vec{e}_1 + Q_2 \vec{e}_2)_K \quad (\text{IV.185})$$

$$= (\vartheta_1 \vec{e}_1 + \vartheta_2 \vec{e}_2)_K \quad (\text{IV.186})$$

= Physical rotation vector at nodal point K

The work term  $U_e^g$  is due to a gravity force ( $\vec{F}_g$ ) acting over the volume of the element,  $N_E$  is the total number of elements and,

$$U_e^g = \iiint (\vec{F}_g \cdot \vec{u}) \sqrt{a} \, dx^1 \, dx^2 \, dx^3 \quad (\text{IV.187})$$

An approximation to (IV.187) is,

$$U_e^g \approx \iint (\bar{w}_e \vec{g} \cdot \vec{u}) \sqrt{a} \, dx^1 \, dx^2 \quad (\text{IV.188})$$

where

$\bar{w}_e$  = element weight per unit area

$\vec{g}$  = gravity vector

$$\vec{u} = \bar{u} \vec{e}_1 + \bar{v} \vec{e}_2 + \bar{w} \vec{e}_n \quad (\text{IV.189})$$

= physical displacement vector at a point  
off the reference surface

The work term  $U_e^I$  is due to inertial loads acting over the volume of the element and is obtained by applying the well known principle of D'Alembert,

$$U_e^I = - \int_V \rho \left( \frac{\partial^2 \vec{u}}{\partial t^2} \cdot \vec{u} \right) dV \quad (\text{IV.190})$$

where,

$\rho$  = mass density



2. Element Mass Matrix

The potential energy of inertia forces is by (IV.190),

$$U_e^I = -\int_V U_o^I dV \quad (\text{IV.191})$$

where,

$$U_o^I = \rho \left( \frac{d^2 \vec{u}}{dt^2} \cdot \vec{u} \right) \quad (\text{IV.192})$$

and by (II.33),

$$\vec{u} = (u_\alpha + x^3 \bullet_\alpha) \vec{a}^\alpha + w \vec{e}_n \quad (\text{IV.193})$$

Expanding the work potential density,  $U_o$ , and recasting in matrix form gives,

$$\begin{aligned} U_o^I &= \rho \{ \ddot{u}_1, \ddot{u}_2, \ddot{w} \}^T \begin{bmatrix} a^{11} & a^{12} & 0 \\ a^{21} & a^{22} & 0 \\ 0 & 0 & 1 \end{bmatrix} \begin{Bmatrix} \bar{u}_1 \\ \bar{u}_2 \\ w \end{Bmatrix} \\ &= \rho \{ \ddot{u} \}^T [a_M] \{ \bar{u} \} \end{aligned} \quad (\text{IV.194})$$

where the relation,  $\vec{a}^\alpha \cdot \vec{a}^\beta = a^{\alpha\beta}$ , has been used.

In terms of reference surface displacements,  $\{u\}$ , and rotations,  $\{\bullet\}$ , the work potential is by use of (IV.193),

$$U_e^I = \int_V [U_o^{IT} + U_o^{IC} + U_o^{IR}] dv \quad (IV.195)$$

where,

$$U_o^{IT} = \rho \{\ddot{u}\}^T [a_M] \{u\} \quad (IV.196)$$

= translation work density

$$U_o^{IR} = \rho (x^3)^2 \{\ddot{\bullet}\}^T [a_M] \{\bullet\} \quad (IV.197)$$

= rotational work density

$$U_o^{IC} = \rho \cdot x^3 [\{\ddot{\bullet}\}^T [a_M] \{u\} + \{\ddot{u}\} [a_M] \{\bullet\}] \quad (IV.198)$$

= coupled translational and rotational work density

$$\{u\}^T = [u_1, u_2, w] \quad (IV.199)$$

$$\{\bullet\}^T = [\bullet_1, \bullet_2, 0] \quad (IV.200)$$

$$\{\bar{u}\} = \{u\} + x^3 \{\bullet\} \quad (IV.201)$$

Considering first the translational inertia (IV.196) and introducing the transformation (IV.122) from  $\{u\}$  to the physical components,  $\{\bar{W}\}$ , of the element displacement vector results in,

$$\begin{aligned} U_I^T &= \iiint \rho \{\ddot{\bar{W}}\}^T [T_W] [T_E]^T [a_M] [T_E] [T_W] \{\bar{W}\} \sqrt{a} dx^1 dx^2 dx^3 \\ &= \{\ddot{\bar{W}}\}^T [\bar{M}_e^T] \{\bar{W}\} \end{aligned} \quad (IV.202)$$

By minimizing the inertial expression (IV.202) with respect to the discrete variables of the element displacement vector,  $\{\bar{W}\}$ , the element mass matrix due to translational inertia is obtained in the form,

$$[\bar{M}_e^T] = \iint [\bar{M}^T] \bar{m}_e \sqrt{a} dx^1 dx^2 \quad (\text{IV.203})$$

where,

$$[\bar{M}^T] = [T_W]^T [T_E]^T [a_M] [T_E] [T_W] \quad (\text{IV.204})$$

$$\begin{aligned} \bar{m}_e &= \bar{m}_{ns} + \int \rho dx^3 \\ &= \bar{m}_{ns} + \sum_{n=1}^N \rho_n (z_o^n - z_I^n) \end{aligned} \quad (\text{IV.205})$$

$m_e$  = total mass per unit area

$\bar{m}_{ns}$  = non-structural mass per unit area\*

$z_o, z_I$  = layer thickness coordinates

(see Figure 5b)

$N$  = number of layers through shell wall

The integration of expression (IV.203) can be approximated by Gaussian quadrature and gives for the mass matrix due to translational inertia,

---

\*The non-structural mass per unit area term is provided as a convenience to the analyst. It is useful in accounting for the inertial effects of appendages to the shell.

$$\begin{aligned}
[\bar{M}_e^T] &= \int_{-1}^1 \int_{-1}^1 [\bar{M}^T] \bar{m}_e \cdot \sqrt{a} \cdot |J_1| d\lambda d\mu \\
&= \sum_{i=1}^M \sum_{j=1}^M H_i H_j [f_{M^T}(\lambda_j, \mu_1)] \quad (IV.206)
\end{aligned}$$

where,

$$[f_{M^T}(\lambda_j, \mu_1)] = \left[ [\bar{M}^T] \bar{m}_e \cdot \sqrt{a} \cdot |J_1| \right]_{\lambda=\lambda_j, \mu=\mu_1} \quad (IV.207)$$

Considering next the rotational inertia (IV.197) and introducing the transformation (IV.142) from  $\{\bullet\}$  to the physical components,  $\{\bar{W}\}$ , of the element displacement vector results in,

$$\begin{aligned}
U_I^R &= \iiint \rho(x^3)^2 \{\ddot{W}\}^T [T_W]^T [T_{\bullet}]^T [a_M] [T_{\bullet}] [T_W] \{\bar{W}\} \sqrt{a} dx^1 dx^2 dx^3 \\
&= \{\ddot{W}\}^T [M_e^R] \{\bar{W}\} \quad (IV.208)
\end{aligned}$$

By minimizing the inertial work expression (IV.208) with respect to the discrete variables of the element displacement vector,  $\{\bar{W}\}$ , the element mass matrix due to translational inertia is obtained in the form,

$$[\bar{M}_e^R] = \iint [\bar{M}^R] \bar{m}_e^R \sqrt{a} dx^1 dx^2 \quad (IV.209)$$

where,



$$[\bar{M}^R] = [T_W]^T [T_{\bullet}]^T [a_M] [T_{\bullet}] [T_W] \quad (\text{IV.210})$$

$$\begin{aligned} \bar{m}_e^R &= \int \rho (x^3)^2 dx^3 \\ &= \frac{1}{3} \sum_{n=1}^N \rho_n ((z_O^n)^3 - (z_I^n)^3) \end{aligned} \quad (\text{IV.211})$$

Integrating (IV.209) by Gaussian quadrature gives,

$$\begin{aligned} [\bar{M}_e^R] &= \int_{-1}^1 \int_{-1}^1 [\bar{M}^R] \bar{m}_e^R \cdot \sqrt{a} \cdot |J_1| d\lambda d\mu \\ &= \sum_{i=1}^M \sum_{j=1}^M H_i H_j [f_{M^R}(\lambda_j, \mu_i)] \end{aligned} \quad (\text{IV.212})$$

where,

$$[f_{M^R}(\lambda_j, \mu_i)] = \left[ [\bar{M}^R] \bar{m}_e^R \cdot \sqrt{a} \cdot |J_1| \right]_{\lambda=\lambda_j, \mu=\mu_i} \quad (\text{IV.213})$$

Considering now the coupling between translational and rotational inertia (IV.198) and using the transformations (IV.122) and (IV.142) gives,

$$\begin{aligned} U_I^c &= \iiint \rho x^3 \left[ \{\ddot{W}\}^T [T_W]^T [T_{\bullet}]^T [a_M] [T_E] [T_W] \{\bar{W}\} \right. \\ &\quad \left. + \{\ddot{W}\}^T [T_W]^T [T_E]^T [a_M] [T_{\bullet}] \{\bar{W}\} \right] \sqrt{a} dx^1 dx^2 dx^3 \\ &= \{\ddot{W}\}^T \left[ [\bar{M}_e^c] + [\bar{M}_e^c]^T \right] \{\bar{W}\} \end{aligned} \quad (\text{IV.214})$$

By minimizing the inertial work expression (IV.214) with respect to the discrete variables of the element displacement vector,  $\{\bar{W}\}$ , the element mass matrix due to coupling between translational and rotational inertia is obtained in the form,

$$[\bar{M}_e^c] = \iint [\bar{M}^c] \bar{m}_e^c \sqrt{a} \, dx^1 \, dx^2 \quad (\text{IV.215})$$

where,

$$[\bar{M}^c] = [T_W]^T [T_\bullet]^T [a_M] [T_E] [T_W] \quad (\text{IV.216})$$

$$\begin{aligned} \bar{m}_e^c &= \int \rho \cdot x^3 dx^3 \\ &= \frac{1}{2} \sum_{n=1}^N \rho_n ((z_o^n)^2 - (z_I^n)^2) \end{aligned} \quad (\text{IV.217})$$

Integrating (IV.215) by Gaussian quadrature gives,

$$\begin{aligned} [\bar{M}_e^c] &= \int_{-1}^1 \int_{-1}^1 [\bar{M}^c] \bar{m}_e^c \cdot \sqrt{a} \cdot |J_1| \, d\lambda \, d\mu \\ &= \sum_{i=1}^M \sum_{j=1}^M H_i H_j [f_{M^c}(\lambda_j, \mu_i)] \end{aligned} \quad (\text{IV.218})$$

where,

$$[f_{MC}(\lambda_j, \mu_1)] = \left[ [\bar{M}^C] \bar{m}_e^C \cdot \sqrt{a} \cdot |J_1| \right]_{\lambda=\lambda_j, \mu=\mu_1} \quad (\text{IV.219})$$

The element mass matrix which accounts for the effects of translational inertia, rotational inertia and the coupling between translational and rotational inertia is then the summation of (IV.206), (IV.212) and (IV.218),

$$[\bar{M}_e] = [\bar{M}_e^T] + [\bar{M}_e^C] + [\bar{M}_e^C]^T + [\bar{M}_e^R] \quad (\text{IV.220})$$

The system mass matrix appearing in (III.9) is then obtained by summation of the element mass matrices.

### 3. Element Surface Load Vector

The potential of a uniformly distributed surface load,  $\bar{p}$ , acting on the element reference surface is by (IV.178),

$$U_e^p = \iint (\bar{p} \cdot \bar{u}) \sqrt{a} \, dx^1 dx^2 \quad (\text{IV.221})$$

Carrying out the dot product operation and recasting in matrix form results in,

$$U_e^p = \iint \{\bar{p}\}^T \{w\} \sqrt{a} \, dx^1 dx^2 \quad (\text{IV.222})$$

where by use of (IV.179) and (IV.180),

$$\{\bar{p}\}^T = [p_1 + p_2 \cos \phi, p_2 + p_1 \cos \phi, p_n] \quad (\text{IV.223})$$

$$\{w\}^T = [u, v, w] \quad (\text{IV.224})$$

since,

$$\begin{aligned} \hat{e}_i \cdot \hat{e}_j &= 1, & i=j \\ \hat{e}_i \cdot \hat{e}_j &= \cos \phi, & i \neq j \\ \cos \phi &= \frac{a_{12}}{\sqrt{a_{11} a_{22}}} \end{aligned} \quad (\text{IV.225})$$

Introducing the transformation (IV.123) into (IV.222) results in,

$$\begin{aligned} U_e^p &= \iint \{\bar{p}\}^T [T_u][T_E][T_W] \{\bar{W}\} \sqrt{a} \, dx^1 dx^2 \\ &= \{\bar{P}_p\}_e^T \{\bar{W}\} \end{aligned} \quad (\text{IV.226})$$

By minimizing the mechanical work expression (IV.226) with respect to the discrete variables of the element displacement vector,  $\{\bar{W}\}$ , the element load vector due to



surface loading is obtained in the form,

$$\{\bar{P}_p\}_e = \iint \{P_p\} \sqrt{a} \, dx^1 \, dx^2 \quad (\text{IV.227})$$

where

$$\{P_p\} = [T_W]^T [T_E]^T [T_W]^T \{\bar{p}\} \quad (\text{IV.228})$$

Integrating (IV.227) by Gaussian quadrature gives,

$$\begin{aligned} \{\bar{P}_p\}_e &= \int_{-1}^1 \int_{-1}^1 \{P_p\} \sqrt{a} \cdot |J_1| \, d\lambda \, d\mu \\ &= \sum_{i=1}^M \sum_{j=1}^M H_i H_j \{f_{P_p}(\lambda_j, \mu_i)\} \end{aligned} \quad (\text{IV.229})$$

where

$$\{f_{P_p}(\lambda_j, \mu_i)\} = \left\{ \{P_p\} \cdot \sqrt{a} \cdot |J_1| \right\}_{\lambda=\lambda_j, \mu=\mu_i} \quad (\text{IV.230})$$

The surface load contribution to the system load vector appearing in (III.10) is then obtained by summation of the element surface load vectors.

4. Concentrated Force Vector

The potential of a concentrated force,  $\bar{F}$ , acting at a discrete nodal point, J, that lies within element K is by (IV.181),

$$U_J^F = (\bar{F} \cdot \bar{u})_J \quad (\text{IV.231})$$

Carrying out the dot product operation recasting in matrix form results in,

$$U_J^F = \{\bar{F}\}_J^T \{W\}_J \quad (\text{IV.232})$$

where by use of (IV.182) and (IV.183),

$$\{\bar{F}\}^T = [F_1 + F_2 \cos \phi, F_2 + F_1 \cos \phi, F_n] \quad (\text{IV.233})$$

Introducing the transformation (IV.123) into (IV.232) results in,

$$U_J^F = \{\bar{P}_F\}_J^T \{\bar{W}\}_K \quad (\text{IV.234})$$

where

$$\{\bar{P}_F\}_J = [T_w]_K^T [T_E]_J^T [T_u]_J^T \{\bar{F}\}_J \quad (\text{IV.235})$$

By minimizing the mechanical work expression (IV.234) with respect to the discrete variables of the element displacement vector,  $\{\bar{W}\}$ , the element load vector due to a concentrated force (IV.235) is obtained. The subscript  $J$  locates the point of application of the concentrated force vector within the particular element  $K$  and is identified by the element connection sequence number which ranges from 1 to 13. The location of node  $J$  in the several coordinate systems associated with element  $K$  (see Figure 7) is,

$$\begin{aligned} x^1 &= x_J^1, & x^2 &= x_J^2 \\ \lambda &= \lambda_J, & \mu &= \mu_J \\ \alpha &= \alpha_J, & \beta &= \beta_J \end{aligned} \quad (\text{IV.236})$$

The discrete values of  $\lambda_J, \mu_J$  and  $\alpha_J, \beta_J$  which correspond to the element connection sequence numbers  $J=1, \dots, 13$  are given in Table 4. When the point  $J$  is one of the connection points 1 through 4, the values of  $\alpha_J$  and  $\beta_J$  must be determined numerically from the known values of  $x_J^1$  and  $x_J^2$  by use of the shape function relations (IV.90),

$$\begin{aligned} x_J^1 &= [H_L(\alpha_J, \beta_J)]\{x_L^1\} \\ &L=5, \dots, 13 \\ x_J^2 &= [H_L(\alpha_J, \beta_J)]\{x_L^2\} \end{aligned} \quad (\text{IV.237})$$

When the point J is one of the connection points 6 through 13, the values of  $\lambda_K$  and  $\mu_K$  must be determined numerically from the known values of  $x_J^1$  and  $x_J^2$  by use of the shape function relations (IV.72),

$$\begin{aligned} x_J^1 &= [L_L(\lambda_J, \mu_J)]\{x_L^1\} \\ x_J^2 &= [L_L(\lambda_J, \mu_J)]\{x_L^2\} \end{aligned} \quad \begin{matrix} L=1, \dots, 4 \\ \text{(IV.238)} \end{matrix}$$

The inverse functional relationship between  $\alpha, \beta$  and  $x^1, x^2$  or  $\lambda, \mu$  and  $x^1, x^2$  cannot be derived analytically but Newton's method can be used to rapidly converge on values of  $\alpha_J, \beta_J$  or  $\lambda_J, \mu_J$  when given the discrete values  $x_J^1, x_J^2$ . The details of this calculation are given in Appendix D.

For the convenience of the analyst, several alternative forms of force discretization will be derived.

A force resultant applied along one edge of an element's reference surface is with respect to the element edge coordinate system (see Figure 8),

$$\vec{N} = \tilde{N}_s \vec{e}_s + \tilde{N}_t \vec{e}_t + \tilde{N}_n \vec{e}_n \quad \text{(IV.239)}$$

and with respect to the surface coordinate system,

$$\vec{N} = \tilde{N}_1 \vec{e}_1 + \tilde{N}_2 \vec{e}_2 + \tilde{N}_n \vec{e}_n \quad \text{(IV.240)}$$



Let the unit vector tangent to the edge of the shell,  $\vec{e}_t$ , be located with respect to the surface coordinate,  $x^1$ , by the angle,  $\psi$ , which has the positive sense indicated in Figure 8. The tangent vector is then,

$$\vec{e}_t = \cos\psi \vec{e}_1 + \sin\psi \vec{e}_2 \quad (\text{IV.241})$$

and the unit vector normal to the edge of the shell is,

$$\vec{e}_s = \vec{e}_t \times \vec{e}_n = \sin\psi \vec{e}_1 - \cos\psi \vec{e}_2 \quad (\text{IV.242})$$

It follows that the transformation relating force resultant components in surface coordinates to components in edge coordinates is,

$$\begin{Bmatrix} \tilde{N}_1 \\ \tilde{N}_2 \\ \tilde{N}_n \end{Bmatrix} = \begin{bmatrix} \sin\psi & \cos\psi & 0 \\ -\cos\psi & \sin\psi & 0 \\ 0 & 0 & 1 \end{bmatrix} \begin{Bmatrix} \tilde{N}_s \\ \tilde{N}_t \\ \tilde{N}_n \end{Bmatrix} \quad (\text{IV.243})$$

The angle  $\psi$  may be approximated as follows. In the surface coordinate directions the incremental arc lengths between points L and M are (see Figure 8 and (II.7)),

$$\Delta S_1 = (A_1 x^1)_M - (A_1 x^1)_L \quad (\text{IV.244})$$

$$\Delta S_2 = (A_2 x^2)_M - (A_2 x^2)_L \quad (\text{IV.245})$$

The length of the element side is approximately,

$$\Delta S_K = [(\Delta S_1)^2 + 2(\Delta S_1 \Delta S_2) \cos \phi + (\Delta S_2)^2]^{1/2} \quad (\text{IV.246})$$

where,

$$\cos \phi = \left( \frac{a_{12}}{\sqrt{a_{11} a_{22}}} \right)_K \quad (\text{IV.247})$$

The angle  $\psi$  is then defined by,

$$\sin \psi_K = \frac{\Delta S_2}{\Delta S_K}, \quad \cos \psi_K = \frac{\Delta S_1}{\Delta S_K} \quad (\text{IV.248})$$

The total force acting at the midside of the element (point K of Figure 8) is then,

$$\begin{aligned} \vec{F}_K &= \Delta S_K (\vec{N}) \\ &= F_1 \vec{e}_1 + F_2 \vec{e}_2 + F_n \vec{e}_n \end{aligned} \quad (\text{IV.249})$$

where

$$F_1 = \Delta S_K \cdot \tilde{N}_1 \quad \text{or} \quad \Delta S_K (\tilde{N}_S \sin \psi + \tilde{N}_t \cos \psi)$$

$$F_2 = \Delta S_K \cdot \tilde{N}_2 \quad \text{or} \quad \Delta S_K (-\tilde{N}_S \cos \psi + \tilde{N}_t \sin \psi)$$

$$F_n = \Delta S_K \cdot \tilde{N}_n \quad (\text{IV.250})$$

The calculation of the load vector for  $\vec{F}_K$  then follows from (IV.233) and (IV.235).

The contribution from concentrated loads or force resultants to the system load vector appearing in (III.10) is then obtained by summation of the corresponding element load vectors.

### 5. Concentrated Moment Vector

The potential of a concentrated moment,  $\vec{Q}$ , acting at a discrete node, K, that lies within element J is by (IV.184),

$$U_K^Q = (\vec{Q} \cdot \vec{\vartheta})_K \quad (\text{IV.251})$$

where by use of (II.38) and (II.21),

$\vec{\vartheta}_K$  = rotation vector at node K

$$\vartheta_1 = [A_2 a^{21}_{w,1} + A_2 a^{22}_{w,2} + \frac{A_2}{A_1} b^2_1 u + b^2_2 v] \quad (\text{IV.252})$$

$$\vartheta_2 = - [A_1 a^{11}_{w,1} + A_1 a^{12}_{w,2} + b^1_1 u + \frac{A_1}{A_2} b^1_2 v] \quad (\text{IV.253})$$

since from (IV.286)

$$u = A_1 u^1, \quad v = A_2 u^2 \quad (\text{IV.254})$$

Carrying out the dot product operation and recasting in matrix form results in,

$$U_K^Q = \{\tilde{Q}\}_K^T \{\vartheta\}_K \quad (\text{IV.255})$$

where by use of (IV.185) and (IV.186),

$$\{\tilde{Q}\}^T = [\tilde{Q}_1 + \tilde{Q}_2 \cos\phi, \tilde{Q}_2 + \tilde{Q}_1 \cos\phi] \quad (\text{IV.256})$$

$$\{\vartheta\}^T = [\vartheta_1, \vartheta_2] \quad (\text{IV.257})$$

Introducing the transformation (IV.157) into (IV.255) results in,

$$U_K^Q = \{\bar{P}_Q\}_K^T \{\bar{W}\}_K \quad (\text{IV.258})$$

where

$$\{\bar{P}_Q\}_K = [T_W]_J^T [T_\vartheta]_K^T \{\tilde{Q}\}_K \quad (\text{IV.259})$$

By minimizing the mechanical work expression (IV.258) with respect to the discrete variables of the element displacement vector,  $\{\bar{W}\}$ , the element load vector due to a concentrated moment (IV.259) is obtained.

The subscript K locates the point of application of the concentrated moment vector within the particular element J and is identified by the element connection sequence



number which ranges from 1 to 13. The location of node K in the several coordinate systems associated with element K (see Figure 7) is given in Table 4.

For the convenience of the analyst, several alternative forms of moment discretization will be derived as was done for the concentrated force vector.

A moment resultant applied along one edge of an element's reference surface is with respect to the element edge coordinate system (see Figure 8),

$$\vec{M} = \tilde{M}_s \vec{e}_s + \tilde{M}_t \vec{e}_t \quad (\text{IV.260})$$

and with respect to the surface coordinate system,

$$\vec{M} = \tilde{M}_1 \vec{e}_1 + \tilde{M}_2 \vec{e}_2 \quad (\text{IV.261})$$

Defining the vectors,  $\vec{e}_s$  and  $\vec{e}_t$ , in the same manner as was done in the preceding section, it follows that the transformation relating moment resultants in surface coordinates to moment resultants in edge coordinates is,

$$\begin{Bmatrix} \tilde{M}_1 \\ \tilde{M}_2 \end{Bmatrix} = \begin{bmatrix} \sin\psi & \cos\psi \\ -\cos\psi & \sin\psi \end{bmatrix} \begin{Bmatrix} \tilde{M}_s \\ \tilde{M}_t \end{Bmatrix} \quad (\text{IV.262})$$

Approximating the angle  $\psi$  and the length of the element side,  $\Delta S_K$ , as in the preceding section, the total moment

acting at the midside of the element (point K of Figure 8) is then,

$$\begin{aligned}\vec{Q}_K &= \Delta S_K (\vec{M}) \\ &= \tilde{Q}_1 \vec{e}_1 + \tilde{Q}_2 \vec{e}_2\end{aligned}\quad (\text{IV.263})$$

where,

$$\begin{aligned}\tilde{Q}_1 &= \Delta S_K \cdot \tilde{M}_1 \text{ or } \Delta S_K (\tilde{M}_s \sin\psi + \tilde{M}_t \cos\psi) \\ \tilde{Q}_2 &= \Delta S_K \cdot \tilde{M}_2 \text{ or } \Delta S_K (-\tilde{M}_s \cos\psi + \tilde{M}_t \sin\psi)\end{aligned}\quad (\text{IV.264})$$

The calculation of the load vector for  $\vec{Q}_K$  then follows from (IV.256) and (IV.259).

The contribution from concentrated moments or moment resultants to the system load vector appearing in (III.10) is then obtained by summation of the corresponding element load vector.

## 6. Element Gravity Load Vector

The potential of a gravity force,  $\vec{F}_g$ , acting over the volume of the element is by (IV.188),

$$U_e^g \approx \iiint (\vec{w}_e \cdot \vec{g} \cdot \vec{u}) \sqrt{a} \, dx^1 \, dx^2 \quad (\text{IV.265})$$

where,

$$\vec{g} = g_1 \vec{e}_1 + g_2 \vec{e}_2 + g_n \vec{e}_n \quad (\text{IV.266})$$

= gravity vector (g units)

$$\begin{aligned} \bar{w}_e &= w_{NS} + \int \rho_w dx^3 \\ &= w_{NS} + \sum_{n=1}^N \rho_w (z_0^n - z_I^n) \end{aligned} \quad (\text{IV.267})$$

= element weight per unit area

$w_{NS}$  = non-structural weight per unit area

$\rho_w$  = weight density

Carrying out the dot product operation in (IV.265) and recasting in matrix form results in,

$$U_e^g = \iint \{\vec{g}\}^T \{w\} \sqrt{a} dx^1 dx^2 \quad (\text{IV.268})$$

where by use of (IV.189) and (IV.266),

$$\{\vec{g}\}^T = \bar{w}_e [g_1 + g_2 \cos\phi, g_2 + g_1 \cos\phi, g_n] \quad (\text{IV.269})$$

Introducing the transformation (IV.123) into (IV.268) results in,

$$\begin{aligned} U_e^g &= \iint \{\vec{g}\}^T [T_u][T_E][T_W] \{\bar{w}\} \sqrt{a} dx^1 dx^2 \\ &= \{\bar{P}_g\}_e^T \{\bar{w}\} \end{aligned} \quad (\text{IV.270})$$

By minimizing the work expression (IV.270) with respect to the discrete variables of the element displacement vector,  $\{\bar{W}\}$ , the element load vector due to gravity loading is obtained in the form,

$$\{\bar{P}_g\}_e = \iint \{P_g\} \sqrt{a} \, dx^1 \, dx^2 \quad (\text{IV.271})$$

where,

$$\{P_g\} = [T_W]^T [T_E]^T [T_u]^T \{\bar{g}\} \quad (\text{IV.272})$$

Integrating (IV.271) by Gaussian quadrature gives,

$$\begin{aligned} \{\bar{P}_g\}_e &= \int_{-1}^1 \int_{-1}^1 \{P_g\} \sqrt{a} \cdot |J_1| \, d\lambda \, d\mu \\ &= \sum_{i=1}^M \sum_{j=1}^M H_i H_j \{f_{P_g}(\lambda_j, \mu_i)\} \end{aligned} \quad (\text{IV.273})$$

where,

$$\{f_{P_g}(\lambda_j, \mu_i)\} = \left\{ \{P_g\} \sqrt{a} \cdot |J_1| \right\}_{\lambda=\lambda_j, \mu=\mu_i} \quad (\text{IV.274})$$

The gravity load contribution to the system load vector appearing in (III.10) is obtained by summation of the element gravity load vectors.



## D. Calculation of Structural Response

In this section, transformations between tensor quantities and physical quantities are defined and the equations for calculating strains, stresses, forces and moments from the element displacement vector are developed.

The displacement vector at a point on the reference surface of the shell is from (II.23),

$$\vec{u} = u^\alpha \vec{a}_\alpha + w \vec{e}_n = u_\alpha \vec{a}^\alpha + w \vec{e}_n \quad (\text{IV.275})$$

where  $\vec{a}_\alpha$  and  $\vec{a}^\alpha$  are the covariant and contravariant base vectors of the Gaussian surface coordinates and  $\vec{e}_n$  is the unit vector normal to the reference surface.

The unit vectors in the  $\vec{a}_\alpha$  and  $\vec{a}^\alpha$  directions are by (II.3), (II.5) and (II.18),

$$\vec{e}_\alpha = \frac{\vec{a}_\alpha}{A_\alpha} = \frac{a_{\alpha\beta}}{A_\alpha} \vec{a}^\beta \quad (\text{no sum on } \alpha) \quad (\text{IV.276})$$

where the Lamé' parameters are,

$$A_\alpha = \sqrt{a_{\alpha\alpha}} \quad (\text{no sum}) \quad (\text{IV.277})$$

By substitution of (IV.276) into (IV.275) the displacement vector can thus be written in the alternative physical forms,

$$\vec{u} = u^1 A_1 \vec{e}_1 + u^2 A_2 \vec{e}_2 + w \vec{e}_n \quad (\text{IV.278})$$

$$\vec{u} = A_1 (a^{11} u_1 + a^{12} u_2) \vec{e}_1 + A_2 (a^{21} u_1 + a^{22} u_2) \vec{e}_2 + w \vec{e}_n \quad (\text{IV.279})$$

$$\vec{u} = u \vec{e}_1 + v \vec{e}_2 + w \vec{e}_n \quad (\text{IV.280})$$

The rotation vector at a point on the reference surface is by (II.34),

$$\vec{\theta} = \theta^\alpha \vec{a}_\alpha = \theta_\alpha \vec{a}^\alpha \quad (\text{IV.281})$$

By substitution of (IV.276) into (IV.281) it can be expressed in the alternative physical forms,

$$\vec{\theta} = \theta^1 A_1 \vec{e}_1 + \theta^2 A_2 \vec{e}_2 \quad (\text{IV.282})$$

$$= A_1 (a^{11} \theta_1 + a^{22} \theta_2) \vec{e}_1 + A_2 (a^{21} \theta_1 + a^{22} \theta_2) \vec{e}_2 \quad (\text{IV.283})$$

$$= \psi_1 \vec{e}_1 + \psi_2 \vec{e}_2 \quad (\text{IV.284})$$

The sign convention for reference surface displacements and rotations is shown in Figure 9.

From an inspection of (IV.278), (IV.279) and (IV.280) the physical components of the reference surface displacement vector,  $\{w\}$ , are related to the covariant components,  $\{u\}$ , and

contravariant components,  $\{\tilde{u}\}$ , by the transformations,

$$\{w\} = [T_u]\{u\} = [T^u]\{\tilde{u}\} \quad (\text{IV.285})$$

or,

$$\begin{Bmatrix} u \\ v \\ w \end{Bmatrix} = \begin{bmatrix} A_1 a^{11} & A_1 a^{12} & 0 \\ A_2 a^{21} & A_2 a^{22} & 0 \\ 0 & 0 & 1 \end{bmatrix} \begin{Bmatrix} u_1 \\ u_2 \\ w \end{Bmatrix} = \begin{bmatrix} A_1 & 0 & 0 \\ 0 & A_2 & 0 \\ 0 & 0 & 1 \end{bmatrix} \begin{Bmatrix} u^1 \\ u^2 \\ w \end{Bmatrix}$$

(IV.286)

Conversely,

$$\{u\} = [T_u]^{-1}\{w\} = [T_w]\{w\}$$

$$\{\tilde{u}\} = [T^u]^{-1}\{w\} = [T^w]\{w\} \quad (\text{IV.287})$$

or

$$\begin{Bmatrix} u_1 \\ u_2 \\ w \end{Bmatrix} = \begin{bmatrix} A_1 & \frac{a_{21}}{A_2} & 0 \\ \frac{a_{12}}{A_1} & A_2 & 0 \\ 0 & 0 & 1 \end{bmatrix} \begin{Bmatrix} u \\ v \\ w \end{Bmatrix}$$

(IV.288)

$$\begin{Bmatrix} u^1 \\ u^2 \\ v \end{Bmatrix} = \begin{bmatrix} \frac{1}{A_1} & 0 & 0 \\ 0 & \frac{1}{A_2} & 0 \\ 0 & 0 & 1 \end{bmatrix} \begin{Bmatrix} u \\ v \\ w \end{Bmatrix} \quad (\text{IV.288 cont.})$$

The displacement vector at a point located a distance  $z$  from the reference surface is by (II.33) and (II.34),

$$\begin{aligned} \vec{\bar{u}} &= \vec{u} + z \vec{\Theta} \\ &= (u^\alpha + z \Theta^\alpha) \vec{a}_\alpha + w \vec{e}_n \\ &= (u_\alpha + z \Theta_\alpha) \vec{a}^\alpha + w \vec{e}_n \end{aligned} \quad (\text{IV.289})$$

Introducing the unit vectors (IV.276) into (IV.289) leads to the alternative physical forms,

$$\vec{\bar{u}} = (u^1 + z \Theta^1) A_1 \vec{e}_1 + (u^2 + z \Theta^2) A_2 \vec{e}_2 + w \vec{e}_n \quad (\text{IV.290})$$

$$\begin{aligned} \vec{\bar{u}} &= [A_1 (a^{11} u_1 + a^{21} u_2) + z \cdot A_1 (a^{11} \Theta_1 + a^{21} \Theta_2)] \vec{e}_1 \\ &\quad + [A_2 (a^{12} u_1 + a^{22} u_2) + z \cdot A_2 (a^{12} \Theta_1 + a^{22} \Theta_2)] \vec{e}_2 \\ &\quad + w \vec{e}_n \end{aligned} \quad (\text{IV.291})$$

$$\vec{\bar{u}} = (u + z \Psi_1) \vec{e}_1 + (v + z \Psi_2) \vec{e}_2 + w \vec{e}_n \quad (\text{IV.292})$$

$$\vec{\bar{u}} = \bar{u} \vec{e}_1 + \bar{v} \vec{e}_2 + \bar{w} \vec{e}_n \quad (\text{IV.293})$$



From inspection of (IV.292) and (IV.293) the reference surface displacements and rotations are related to the displacements off the reference surface by,

$$\{\bar{w}\} = \{w\} + z \{\Psi\} \quad (\text{IV.294})$$

or

$$\begin{Bmatrix} \bar{u} \\ \bar{v} \\ \bar{w} \end{Bmatrix} = \begin{Bmatrix} u \\ v \\ w \end{Bmatrix} + z \begin{Bmatrix} \Psi_1 \\ \Psi_2 \\ 0 \end{Bmatrix} \quad (\text{IV.295})$$

where the physical components of the rotation vector are related to the tensor components by inspection of (IV.290) and (IV.291),

$$\{\Psi\} = [T_u]\{\bullet\} = [T^u]\{\tilde{\bullet}\} \quad (\text{IV.296})$$

or

$$\begin{Bmatrix} \Psi_1 \\ \Psi_2 \\ 0 \end{Bmatrix} = \begin{bmatrix} A_1 a^{11} & A_1 a^{12} & 0 \\ A_2 a^{21} & A_2 a^{22} & 0 \\ 0 & 0 & 1 \end{bmatrix} \begin{Bmatrix} \bullet_1 \\ \bullet_2 \\ 0 \end{Bmatrix} = \begin{bmatrix} A_1 & 0 & 0 \\ 0 & A_2 & 0 \\ 0 & 0 & 1 \end{bmatrix} \begin{Bmatrix} \bullet^1 \\ \bullet^2 \\ 0 \end{Bmatrix} \quad (\text{IV.297})$$

Conversely,

$$\{\bullet\} = [T_u]^{-1}\{\psi\} = [T_w]\{\psi\}$$

$$\{\tilde{\theta}\} = [T^u]^{-1}\{\psi\} = [T^w]\{\psi\} \quad (\text{IV.298})$$

or

$$\begin{Bmatrix} \bullet_1 \\ \bullet_2 \\ 0 \end{Bmatrix} = \begin{bmatrix} A_1 & \frac{a_{21}}{A_2} & 0 \\ \frac{a_{12}}{A_1} & A_2 & 0 \\ 0 & 0 & 1 \end{bmatrix} \begin{Bmatrix} \psi_1 \\ \psi_2 \\ 0 \end{Bmatrix}$$

$$\begin{Bmatrix} \bullet^1 \\ \bullet^2 \\ 0 \end{Bmatrix} = \begin{bmatrix} \frac{1}{A_1} & 0 & 0 \\ 0 & \frac{1}{A_2} & 0 \\ 0 & 0 & 1 \end{bmatrix} \begin{Bmatrix} \psi_1 \\ \psi_2 \\ 0 \end{Bmatrix} \quad (\text{IV.299})$$

The physical components of the strain tensor at a point off the reference surface are related to the covariant tensor components by the well known transformation (see [27]),

$$\{\bar{e}\} = [T_Y]\{\bar{\gamma}\} \quad (\text{IV.300})$$

or

$$\begin{Bmatrix} \bar{e}_{11} \\ \bar{e}_{22} \\ \bar{e}_{12} \end{Bmatrix} = \begin{bmatrix} 1/a_{11} & 0 & 0 \\ 0 & 1/a_{22} & 0 \\ 0 & 0 & 1/\sqrt{a_{11}a_{22}} \end{bmatrix} \begin{Bmatrix} \bar{\gamma}_{11} \\ \bar{\gamma}_{22} \\ 2\bar{\gamma}_{12} \end{Bmatrix}$$

(IV.301)

and conversely,

$$\{\bar{\gamma}\} = [T_{\gamma}]^{-1} = [T_e]\{\bar{e}\} \quad (\text{IV.302})$$

or

$$\begin{Bmatrix} \bar{\gamma}_{11} \\ \bar{\gamma}_{22} \\ 2\bar{\gamma}_{12} \end{Bmatrix} = \begin{bmatrix} a_{11} & 0 & 0 \\ 0 & a_{22} & 0 \\ 0 & 0 & \sqrt{a_{11}a_{22}} \end{bmatrix} \begin{Bmatrix} \bar{e}_{11} \\ \bar{e}_{22} \\ \bar{e}_{12} \end{Bmatrix}$$

(IV.303)

Similarly, the physical components of the reference surface strain tensor and curvature change (or bending strain) tensor are,

$$\{e\} = [T_{\gamma}]\{\gamma\} \quad (\text{IV.304})$$

$$\{\kappa\} = [T_{\gamma}]\{\chi\} \quad (\text{IV.305})$$

Conversely,

$$\{\gamma\} = [T_\gamma]^{-1}\{\epsilon\} = [T_e]\{\epsilon\} \quad (\text{IV.306})$$

$$\{\chi\} = [T_\gamma]^{-1}\{\kappa\} = [T_e]\{\kappa\} \quad (\text{IV.307})$$

The coefficient of thermal expansion tensor  $\{\epsilon\}$  and physical vector  $\{\alpha\}$  are also related by the same transformations,

$$\{\alpha\} = [T_\gamma]\{\epsilon\} \quad (\text{IV.308})$$

or

$$\begin{pmatrix} \alpha_{11} \\ \alpha_{22} \\ \alpha_{12} \end{pmatrix} = [T_\gamma] \begin{pmatrix} \epsilon_{11} \\ \epsilon_{22} \\ \epsilon_{12} \end{pmatrix} \quad (\text{IV.309})$$

Conversely,

$$\{\epsilon\} = [T_\gamma]^{-1}\{\alpha\} = [T_e]\{\alpha\} \quad (\text{IV.310})$$

The physical components of the stress tensor are related to the contravariant tensor components by the well known transformation (see [27]),

$$\{\bar{\sigma}\} = [T_\tau]\{\bar{\tau}\} \quad (\text{IV.311})$$



or

$$\begin{Bmatrix} \bar{\sigma}_{11} \\ \bar{\sigma}_{22} \\ \bar{\sigma}_{12} \end{Bmatrix} = \begin{bmatrix} \sqrt{\frac{a_{11}}{a_{11}}} & 0 & 0 \\ 0 & \sqrt{\frac{a_{22}}{a_{22}}} & 0 \\ 0 & 0 & \sqrt{\frac{a_{22}}{a_{11}}} \end{bmatrix} \begin{Bmatrix} \bar{\tau}_{11} \\ \bar{\tau}_{22} \\ \bar{\tau}_{12} \end{Bmatrix} \quad (\text{IV.312})$$

Conversely,

$$\{\bar{\tau}\} = [T_{\tau}]^{-1}\{\bar{\sigma}\} = [T_{\sigma}]\{\bar{\sigma}\} \quad (\text{IV.313})$$

or

$$\begin{Bmatrix} \bar{\tau}_{11} \\ \bar{\tau}_{22} \\ \bar{\tau}_{12} \end{Bmatrix} = \begin{bmatrix} \sqrt{\frac{a_{11}}{a_{11}}} & 0 & 0 \\ 0 & \sqrt{\frac{a_{22}}{a_{22}}} & 0 \\ 0 & 0 & \sqrt{\frac{a_{11}}{a_{22}}} \end{bmatrix} \begin{Bmatrix} \bar{\sigma}_{11} \\ \bar{\sigma}_{22} \\ \bar{\sigma}_{12} \end{Bmatrix} \quad (\text{IV.314})$$

The sign convention for stresses is shown in Figure 9.

The tensor form of the constitutive equations are thus related to the physical form as follows. The tensor form is by (IV.10) and (IV.11),

$$\{\bar{\tau}\} = [\mathbf{E}]\{\bar{\gamma}\} - \{\Omega\} \quad (\text{IV.315})$$

where,

$$\{\Omega\} = [\mathbf{E}]\{\epsilon\} \cdot \Delta T \quad (\text{IV.316})$$

Transforming to physical quantities by use of (IV.302)  
(IV.310) and (IV.313) gives,

$$\{\bar{\sigma}\} = [T_\tau][\mathbf{E}][T_e]\{\bar{\epsilon}\} - [T_\tau][\mathbf{E}][T_e]\{\alpha\} \cdot \Delta T \quad (\text{IV.317})$$

or

$$\{\bar{\sigma}\} = [G]\{\bar{\epsilon}\} - \{Q\} \quad (\text{IV.318})$$

where,

$$\{Q\} = [G]\{\alpha\} \cdot \Delta T \quad (\text{IV.319})$$

By inspection of (IV.317) through (IV.319) the  
following relations thus hold,

$$[G] = [T_\tau][\mathbf{E}][T_e] \quad (\text{IV.320})$$

or

$$[G] = \begin{bmatrix} a_{11}\sqrt{\frac{a_{11}}{a_{11}}} \mathbf{E}^{1111} & a_{22}\sqrt{\frac{a_{11}}{a_{11}}} \mathbf{E}^{1122} & a_{11}\sqrt{\frac{a_{22}}{a_{11}}} \mathbf{E}^{1112} \\ a_{11}\sqrt{\frac{a_{22}}{a_{22}}} \mathbf{E}^{2211} & a_{22}\sqrt{\frac{a_{22}}{a_{22}}} \mathbf{E}^{2222} & a_{22}\sqrt{\frac{a_{11}}{a_{22}}} \mathbf{E}^{2212} \\ a_{11}\sqrt{\frac{a_{22}}{a_{11}}} \mathbf{E}^{1211} & a_{22}\sqrt{\frac{a_{22}}{a_{11}}} \mathbf{E}^{1222} & a_{22}\sqrt{\frac{a_{11}}{a_{11}}} \mathbf{E}^{1212} \end{bmatrix} \quad (\text{IV.321})$$

and,

$$\{Q\} = [T_T]\{\Omega\} \quad (\text{IV.322})$$

Conversely,

$$[E] = [T_\sigma][G][T_\gamma] \quad (\text{IV.323})$$

or,

$$[E] = \begin{bmatrix} \frac{1}{a_{11}} \sqrt{\frac{a_{11}}{a_{11}}} G_{11} & \frac{1}{a_{22}} \sqrt{\frac{a_{11}}{a_{11}}} G_{12} & \frac{1}{a_{11}} \sqrt{\frac{a_{11}}{a_{22}}} G_{13} \\ \frac{1}{a_{11}} \sqrt{\frac{a_{22}}{a_{22}}} G_{21} & \frac{1}{a_{22}} \sqrt{\frac{a_{22}}{a_{22}}} G_{22} & \frac{1}{a_{22}} \sqrt{\frac{a_{22}}{a_{11}}} G_{23} \\ \frac{1}{a_{11}} \sqrt{\frac{a_{11}}{a_{22}}} G_{31} & \frac{1}{a_{22}} \sqrt{\frac{a_{11}}{a_{22}}} G_{32} & \frac{1}{a_{22}} \sqrt{\frac{a_{11}}{a_{11}}} G_{33} \end{bmatrix} \quad (\text{IV.324})$$

and

$$\{\Omega\} = [T_\sigma]\{Q\} \quad (\text{IV.325})$$

The physical strain components,  $\{\bar{e}\}$ , at an arbitrary point located a distance  $z$  from the shell reference surface are from (II.28),

$$\{\bar{e}\} = \{e\} + z\{\kappa\} \quad (\text{IV.326})$$

The physical reference surface strain components,  $\{e\}$ , are related to the physical components,  $\{\bar{W}\}$ , of the element displacement vector by substituting the transformations (IV.81) and (IV.118) into equation (IV.300),

$$\{e\} = [T_Y][S][F][T_W]\{\bar{W}\} \quad (\text{IV.327})$$

The physical bending strain components,  $\{\kappa\}$ , are related to the physical components,  $\{\bar{W}\}$ , of the element displacement vector by substituting the transformation (IV.106) and (IV.118) into (IV.305),

$$\{\kappa\} = [T_Y][R][E][T_W]\{\bar{W}\} \quad (\text{IV.328})$$

Substituting (IV.327) and (IV.328) into (IV.326) gives for the total strains,

$$\begin{aligned} \{\bar{e}\} &= [T_Y][S][F][T_W]\{\bar{W}\} \\ &+ z[T_Y][R][E][T_W]\{\bar{W}\} \end{aligned} \quad (\text{IV.329})$$

and the strains associated with stress are,

$$\{\bar{e}_s\} = \{\bar{e}\} - \{\alpha\} \cdot \Delta T \quad (\text{IV.330})$$

Substituting (IV.329) into the constitutive equation (IV.318) gives for the physical stress components,



$$\begin{aligned}
\{\bar{\sigma}\} &= [G][T_Y][S][F][T_W]\{\bar{W}\} \\
&+ z[G][T_Y][R][E][T_W]\{\bar{W}\} \\
&- [G]\{\alpha\} \cdot \Delta T
\end{aligned}
\tag{IV.331}$$

The force resultants acting on a differential element of the shell reference surface (see Figure 10) are defined to be,

$$\{\bar{N}\} = \int \{\bar{\sigma}\} dx^3 \tag{IV.332}$$

where

$$\{\bar{N}\}^T = [\bar{N}_1, \bar{N}_2, \bar{N}_{12}] \tag{IV.333}$$

Substituting (IV.331) into (IV.332) and integrating through the shell thickness gives,

$$\begin{aligned}
\{\bar{N}\} &= [\bar{D}][T_Y][S][F][T_W]\{\bar{W}\} \\
&+ [\bar{C}][T_Y][R][E][T_W]\{\bar{W}\} - \{\bar{N}_T\}
\end{aligned}
\tag{IV.334}$$

where,

$$[\bar{D}] = \int [G] dx^3 \tag{IV.335}$$

$$[\bar{C}] = \int [G] x^3 dx^3 \tag{IV.336}$$

$$\{\bar{N}_T\} = \int [G]\{\alpha\} \cdot \Delta T \cdot dx^3 \tag{IV.337}$$

The moment resultants acting on a differential element of the shell reference surface (see Figure 10) are defined by,

$$\{\bar{M}\} = \int \{\bar{\sigma}\} x^3 dx^3 \quad (\text{IV.338})$$

where

$$\{\bar{M}\}^T = [\bar{M}_1, \bar{M}_2, \bar{M}_{12}] \quad (\text{IV.339})$$

Substituting (IV.331) into (IV.338) and integrating through the shell thickness gives,

$$\begin{aligned} \{\bar{M}\} = & [\bar{C}][T_Y][S][F][T_W]\{\bar{W}\} \\ & + [\bar{B}][T_Y][R][E][T_W]\{\bar{W}\} - \{\bar{M}_T\} \end{aligned} \quad (\text{IV.340})$$

where,

$$[B] = \int [G] \cdot (x^3)^2 dx^3 \quad (\text{IV.341})$$

$$\{\bar{M}_T\} = \int [G]\{\alpha\} \cdot \Delta T \cdot x^3 dx^3 \quad (\text{IV.342})$$

The physical shell wall compliances (IV.335), (IV.336), (IV.341) and physical thermal forces and moments (IV.337) and (IV.342) are computed in the same manner as the corresponding tensor quantities were computed in equations (IV.50) through (IV.54) except  $[G]$  is substituted for  $[E]$ , and  $\{\alpha\}$  is substituted for  $\{\epsilon\}$ .

## E. Boundary Conditions

When a variational procedure is used to obtain a stationary value of the total potential energy, the Euler differential equations of equilibrium and the "natural" force boundary conditions are obtained. For the solution of a specific structural problem the "essential" displacement boundary conditions must be imposed on the equilibrium equations (see [122]).

Analogously, the minimum potential energy principle used herein to derive the matrix equations of motion requires only that the essential displacement boundary conditions be satisfied through imposition of constraints on the appropriate nodal point degrees of freedom. Force boundary conditions are satisfied through application of the consistent external loads which were derived in section IV.C. The term "consistent" was coined by Archer [123] in referring to mass matrices which have been derived from strain energy considerations and employ the same displacement functions as were used in deriving the stiffness matrix. Consistent mass matrices and load vectors are distinguished from lumped approaches where the analyst using engineering judgement apportions the mass or loading among the discrete nodes of the element.

The displacement boundary conditions in thin shell problems consist of either enforced translational components and/or rotational components. Since the translations appear as nodal point degrees of freedom it is a straight

forward procedure to impose this type of constraint, the procedure being a standard operation in finite element technology (see [37], [38]).

The imposition of prescribed values of rotation, however, is not so straightforward since the shell rotations do not appear as nodal point degrees of freedom in the analysis. At an arbitrary point on the shell reference surface the components of the rotation vector may be expressed explicitly as a function of the reference surface displacements and their spatial derivatives at the arbitrary point. By use of the same interpolating functions used to formulate the element stiffness matrix, the rotation components may be expressed as a function of the discrete nodal displacements at neighboring grid points. The resulting equations of constraint thus involve multiple degrees of freedom at several discrete nodal points. The derivation of the multipoint constraint equations required to impose a prescribed value of rotation is described below. The procedure for imposing multipoint constraints is detailed in [37] and [38].

The physical rotation vector at a point,  $K$ , lying along one side of the reference surface of element  $J$  is with respect to the element edge coordinate system (see Figure 8),



$$\vec{\vartheta}_K = (\vartheta_s \vec{e}_s + \vartheta_t \vec{e}_t)_K \quad (\text{IV.343})$$

and with respect to the surface coordinate system,

$$\vec{\vartheta}_K = (\vartheta_1 \vec{e}_1 + \vartheta_2 \vec{e}_2)_K \quad (\text{IV.344})$$

Let the unit vector tangent to the edge of the shell,  $\vec{e}_t$ , be located with respect to the surface coordinate,  $x^1$ , by the angle,  $\psi$ , which has the positive sense indicated in Figure 8. The tangent vector is then,

$$\vec{e}_t = \cos\psi \vec{e}_1 + \sin\psi \vec{e}_2 \quad (\text{IV.345})$$

and the unit vector normal to the edge of the shell is,

$$\vec{e}_s = \vec{e}_t \times \vec{e}_n = \sin\psi \vec{e}_1 - \cos\psi \vec{e}_2 \quad (\text{IV.346})$$

It follows that the transformation relating rotation components in surface coordinates to rotation components in edge coordinates is,

$$\begin{Bmatrix} \vartheta_1 \\ \vartheta_2 \end{Bmatrix} = \begin{bmatrix} \sin\psi & \cos\psi \\ -\cos\psi & \sin\psi \end{bmatrix} \begin{Bmatrix} \vartheta_s \\ \vartheta_t \end{Bmatrix} \quad (\text{IV.347})$$

The angle  $\psi$  may be approximated as outlined in section IV.C.4, equations (IV.245) through (IV.248).

The rotation vector at a discrete node which lies within element number J and is identified by element connection point K is,

$$\vec{\vartheta}_K = [\vartheta_1 \vec{e}_1 + \vartheta_2 \vec{e}_2]_K \quad (\text{IV.348})$$

where by (II.38) and (II.39),

$$(\vartheta_1)_K = (A_2(a^{21}_{w,1} + a^{22}_{w,2} + b^{21}_{u_1} + b^{22}_{u_2}))_K \quad (\text{IV.349})$$

$$(\vartheta_2)_K = (-A_1(a^{11}_{w,1} + a^{12}_{w,2} + b^{11}_{u_1} + b^{12}_{u_2}))_K \quad (\text{IV.350})$$

Introducing the transformation (IV.156) and (IV.126) into (IV.349) gives,

$$(\vartheta_1)_K = [c^1_v][T_L]_K [T_{w_{12}}]_J \{\bar{w}_{12}\}_J + [c^1_w]_K [T_H]_K \{w_3\}_J \quad (\text{IV.351})$$

$$(\vartheta_2)_K = [c^2_v][T_L]_K [T_{w_{12}}]_J \{\bar{w}_{12}\}_J + [c^2_w]_K [T_H]_K \{w_3\}_J \quad (\text{IV.352})$$

For specified values of rotation components in the shell coordinate system (i.e.,  $\vartheta_1 = \vartheta_1^0$  and/or  $\vartheta_2 = \vartheta_2^0$ ) at node K of element J, the two equations of multipoint constraint relating the shell rotations to the physical displacement components at the other nodes within element J are,

$$(\vartheta_1^0)_K - [\bar{C}_V^1]_K \{\bar{W}_{12}\}_J - [\bar{C}_W^1]_K \{W_3\}_J = 0 \quad (\text{IV.353})$$

$$(\vartheta_2^0)_K - [\bar{C}_V^2]_K \{W_{12}\}_J - [\bar{C}_W^2]_K \{W_3\}_J = 0 \quad (\text{IV.354})$$

where for  $\alpha = 1, 2$ ,

$$[\bar{C}_V^\alpha]_K = [C_V^\alpha]_K [T_L(\lambda_K, \mu_K)] [T_W]_J \quad (\text{IV.355})$$

$$[\bar{C}_W^\alpha]_K = [C_W^\alpha]_K [T_H(\alpha_K, \beta_K)] \quad (\text{IV.356})$$

For specified values of rotation components in the element edge coordinate system (i.e.,  $\vartheta_s = \vartheta_s^0$  and/or  $\vartheta_t = \vartheta_t^0$ ) the two equations of multipoint constraint are,

$$(\vartheta_s^0)_K \sin \psi_K + (\vartheta_t)_K \cos \psi_K - [\bar{C}_V^1]_K \{\bar{W}_{12}\}_J - [\bar{C}_W^1]_K \{W_3\}_J = 0 \quad (\text{IV.357})$$

$$-(\vartheta_s^0)_K \cos \psi_K + (\vartheta_t)_K \sin \psi_K - [\bar{C}_V^2]_K \{\bar{W}_{12}\}_J - [\bar{C}_W^2]_K \{W_3\}_J = 0 \quad (\text{IV.358})$$

## CHAPTER V

## ANALYTICAL RESULTS

## A. Introduction

The SHEFA finite difference element formulated in Chapter IV was installed in the NASTRAN\* general purpose, finite element computer program [37,38]. A series of demonstration problems were solved to verify the accuracy and convergence characteristics of the element in a variety of applications and to demonstrate the generality of the element via several problems that are most efficiently modeled with arbitrary meshes. The SHEFA solutions were verified against theoretical or experimental results and in some cases the results obtained with various finite element formulations were available for comparison.

The 12 demonstration problems are summarized in Table 5. Problem 1, the stretching of an isotropic square plate under parabolically distributed edge loads, was selected to study the membrane behavior of the element. Problems 2 through 5 are a study of the bending behavior of the SHEFA element for an isotropic square plate with two different boundary conditions (fixed and simply supported edges) and two lateral loadings (concentrated load at center

---

\* NASTRAN is an acronym formed from NASA Structural Analysis.



and uniformly distributed load). Problems 6 through 8 demonstrate the versatility of the wall model and the accuracy of the element when applied to the bending of plates with anisotropic wall construction. The plate of problem 6 has a single layer, orthotropic wall and that for problem 7 has an anisotropic composite wall composed of ten orthotropic plies alternately oriented at  $+30^\circ$  and  $-30^\circ$  to the plate axes. The anisotropic wall construction for problem 8 is two orthotropic plies alternately oriented at  $0^\circ$  and  $90^\circ$  to the plate axes. The unsymmetrical nature of this layup causes coupling between membrane and bending action and results in both bending and stretching of the plate when it is subjected to a uniform lateral load. Problem 9 illustrates the modeling versatility of the SHEFA element in accommodating a non-rectangular grid pattern which follows the natural boundaries of a cantilevered, rhombic plate under uniform load. With problem 10 the ability of the SHEFA element to predict severe displacement and stress gradients was demonstrated for the case of localized bending of a cylindrical shell by a concentrated line load. Problem 11 further demonstrates the versatility of the SHEFA wall model in treating the effects of thermal stresses due to a nonlinear radial temperature gradient through the wall of a cylindrical shell, including the effects of temperature dependent material properties. The stress concentrations caused by a circular cutout in a cylindrical shell subjected to axial tension loading were studied in problem 12. This problem requires a very fine

grid adjacent to the hole in order to predict the severe stress gradients caused by the cutout. For efficiency in modeling, an arbitrary mesh which does not coincide with the shell coordinate lines was used which further demonstrates the generality of the SHEFA element.

The computation of the SHEFA element stiffness matrix was discussed in Section IV.B.6 where it was shown that the total stiffness matrix is the sum of stiffnesses associated with membrane ( $K_M$ ), bending ( $K_B$ ) and coupled membrane and bending ( $K_C$ ) energies. The integration of the energy per unit area over the surface of the element is approximated by Gaussian quadrature, the weighting coefficients and positions of the integration points being given in Table 3 for integration orders 1 through 5.

The finite difference energy method, as implemented by Bushnell and Almroth [84] for rectangular meshes, uses first order integration (one integration point) with satisfactory results. As pointed out in Section I.D, the use of one point integration offers a significant computational advantage over the finite element method which requires at least four integration points for flat plate elements with low order displacement assumptions and up to 25 points for the higher order curved shell elements. For example, the curved quadrilateral with 36 degrees of freedom by Key and Beisinger [62] uses 5 x 5 Gaussian quadrature (25 integration points) and the curved triangular element with 36 degrees of freedom by

Cowper, et. al. [69] uses a newly developed 13 point integration formula.

In performing the calculations for the membrane plate study (Problem 1) it was determined that 2 x 2 Gaussian quadrature (four integration points) was required to accurately evaluate the membrane stiffness,  $K_M$ . The plate bending study (Problems 2-5) confirmed that one integration point was adequate for the accurate evaluation of the bending stiffness,  $K_B$ . Accordingly, the computations for the remaining demonstration problems were performed using four point integration for the membrane stiffness and one point integration for the bending stiffness and load vectors. In the case where coupling occurred between membrane and bending energies (Problem 8), four point integration was also used for the coupling stiffness,  $K_C$ . The generalized finite difference energy method, in having to employ four point integration for a portion of the element stiffness calculations, thus incurs a computational penalty when compared to the conventional finite difference energy method. Since the membrane stiffness is not as complicated as the bending stiffness, the penalty is somewhat mitigated. Furthermore, the generalized method retains a computational advantage when compared to the finite element method, since the number of integration points required is still fewer than the number required by the curved shell elements.

## B. Membrane Plate Study

Problem 1, a flat plate subjected to parabolically distributed end loads as shown in Figure 11, was used by Gallagher [57] to evaluate the membrane behavior of a rectangular shell element previously discussed in Chapter I (see Table 1). The calculations by Gallagher were repeated with the SHEFA element and the results of both discrete methods were compared to the analytical solution by Timoshenko and Goodier [124]. This solution is based on an assumed stress function and the use of the Principle of Least Work. As Gallagher points out, the analytical solution is not exact since it is based on only three undetermined parameters in the assumed stress function but it does represent a highly accurate basis for comparison.

The three mesh refinements used to study the convergence of deflections and stresses are shown in Figure 12. Also shown are the discretized nodal point loads used to approximate the parabolic edge load. Due to double symmetry only one quadrant of the plate was analyzed. The boundary conditions on the quadrant meshed and the plate dimensions and material properties are shown in Figure 11.

The distribution of displacements occurring on the loaded edge, at the points labeled 1 through 9 in Figure 12, are tabulated in Table 6. The results obtained with the SHEFA element are virtually the same as the results of Gallagher for all three meshes. At the point of maximum



displacement (point 1) the numerical results for even the coarsest grid work are nearly identical to the classical solution. The improvement in the overall distribution of displacements with mesh refinement is due in part to the improvement in load discretization which accompanies a refinement in mesh.

The distribution of stresses at the centroids of elements closest to the loaded edge, points labeled a through n in Figure 12, are tabulated in Table 7. Again, the results obtained with the SHEFA element are very nearly the same as the results of Gallagher for all three meshes. For the coarsest mesh the stresses are not as accurate as the displacements but the finer grids give stress results which are very close to the classical solution.

## C. Isotropic Plate Bending Study

Clough and Tocher [125] conducted a thorough plate bending study of the relative accuracy provided by seven different finite elements. Three rectangular and four triangular plate bending elements were considered. The convergence of the central deflection was studied for each element using eight different isotropic, rectangular plate systems and five different mesh patterns.

A portion of this study (Problems 2-5) was repeated with the SHEFA element for an isotropic, square plate with two different boundary conditions (fixed and simply supported edges) and two lateral loadings (concentrated load at center and uniformly distributed load). Due to double symmetry only one quadrant of the plate was analyzed. The boundary conditions on the quadrant meshed, the plate dimensions, the loadings and the material properties are shown in Figure 13.

The convergence of the central deflection was studied by using a series of progressively finer  $N \times N$  mesh patterns in the analysis of each case. The mesh size "N" refers to the number of elements along one side of a quadrant of the plate. Typical element patterns and nodal point arrangements for an N of seven are shown in Figure 14 for the simply supported edge condition and in Figure 15 for the fixed edge boundary condition. In both Figures 14 and 15 some nodes lie outside of the physical confines of the plate

quadrant being analyzed. Only  $w$  degrees of freedom are defined at these points and they are eliminated in the solution process via the multipoint constraints used to impose specified values of shell rotations (see Section IV.E).

Figures 16 through 19 show the convergence of the central deflection with refinement in the mesh size. The quantity plotted in these figures is the deflection coefficient, a dimensionless number which is related to the central deflection  $w_c$ , the plate dimension  $a$ , the loading  $P$  or  $q$  and the flexural rigidity  $D$ , which is defined by

$$D = \frac{Et^3}{12(1-\nu^2)} \quad (V.1)$$

where,

$E$  = Modulus of elasticity

$\nu$  = Poisson's ratio

$t$  = plate thickness

Figures 20 through 23 show the convergence of the central deflection with an increase in the number of simultaneous equations that must be solved for a given mesh size. These figures are a replot of Figures 16-19 wherein the mesh size has been converted to the equivalent number of degrees of freedom associated with each element type after boundary conditions are imposed. This type of plot is more representative of the computational effort expended in obtaining a data point.

The "exact" deflection coefficients shown in Figures 16-23 are from the classical plate bending solutions by Timoshenko [128]. Error bands of  $\pm 5\%$  with respect to the classical solution are shown as a basis of comparison. In all cases the SHEFA element exhibited smoothly convergent behavior toward the classical solution. Acceptable accuracy was achieved with a mesh size of five or twenty degrees of freedom. The convergence was somewhat faster for the simply supported plates (Figures 16,17,20,21) than for the fixed edge plates (Figures 18,19,22,23).

The slower convergence of the fixed edge case is due to the method of imposing rotational constraints that is required by the finite difference energy method (see Section IV.E). Since the rotations do not appear as nodal point degrees of freedom they must be enforced through a multipoint constraint relation involving displacement components at several neighboring nodes adjacent to the boundary. The discretization of the boundary conditions could probably be improved by a local refinement of the mesh spacing in the vicinity of the boundary.

For both edge conditions the concentrated load cases (Figures 17,19,21,23) converged faster than the uniform load cases (Figures 16,18,20,22). This is to be expected since the discretization of the concentrated load is exact, while the uniform load is approximated by concentrated forces at the  $w$  nodes. The discretization of the uniform load for the coarser meshes is fairly crude and causes the slower convergence.



Along with the results of the SHEFA element, the results of four elements from the Clough and Tocher study are also plotted in Figures 16-23. The "ACM" element is the Adini-Clough-Melosh rectangle based on a 12 term polynomial displacement assumption. The "M" element is the Melosh rectangle which is based on physical reasoning and the use of beam displacement functions. The "P" element is the Papenfuss rectangle which is based on an incomplete bicubic polynomial displacement assumption which completely satisfies displacement and slope compatibility along the edges. The "HCT" element is the Hsieh-Clough-Tocher triangle which is formed from three subtriangles in such a way as to lead to full slope and displacement compatibility between adjacent elements. The mesh patterns for the HCT triangle were the same as for the rectangular elements except two triangles were used to represent each rectangle. The M, P and ACM rectangular plate bending elements are not of much interest from a practical viewpoint since they are restricted in their ability to model complex shapes. However, they do serve to show the effect of the assumed displacement functions on convergence for elements with the same number of degrees of freedom. The M and ACM elements converge quite rapidly but the P element converges to an overly stiff result.

The HCT triangular plate bending element is of practical interest since it has been proposed as a facet element for the analysis of thin shells of arbitrary shape by Clough and Johnson [45]. The flexural stiffness of the

facet element is represented by the HCT triangle and for the membrane stiffness a plane stress element [12] is used. Except for the simply supported plate under a concentrated load, the HCT element is converging faster than the SHEFA element on a mesh size basis (Figures 16-19). However, on a degree of freedom basis the SHEFA element is converging faster than the HCT element for the simply supported plates (Figures 20,21) and at about the same rate as HCT for the fixed edge plates (Figures 22,23).

For the case of the simply-supported plate under uniform load (Figures 16 and 20), the results of the KB1 and KB6 quadrilateral shell elements by Key and Beisinger [61, 62] and the results of the Q-19 quadrilateral plate bending element [126] are also plotted. The KB6 shell element (see Table 1) has 36 degrees of freedom and employs 12 term polynomial assumptions for the displacements  $u$ ,  $v$  and  $w$ . The KB1 element, having 28 degrees of freedom, employs bilinear assumptions for the displacements  $u$ ,  $v$  and rotations  $\psi_1$ ,  $\psi_2$  and bicubic assumptions for  $w$ . The Q-19 flat plate element by Clough and Fellipa [127] is a quadrilateral based on four triangles of the HCT type. It provides for slope and displacement compatibility between adjacent elements and has 12 degrees of freedom remaining after 7 internal degrees of freedom are removed by static condensation. For this case the KB6 and Q-19 elements converge faster than the SHEFA element on both a mesh size and a degree of freedom basis. The KB1

element converges faster than SHEFA on a mesh size basis and at about the same rate as SHEFA on a degree of freedom basis. The rapidly convergent behavior of the KB6 and Q-19 elements in comparison to the SHEFA element is in part associated with the manner of discretization of the uniform load and also is due to a greater sophistication in element formulation.

## D. Anisotropic Plate Bending Study

Three anisotropic square plates with uniform lateral loading (Problems 6-8 of Table 5), for which analytical solutions are available, were selected to demonstrate the versatility of the SHEFA wall model. Due to double symmetry only one quadrant of the plates was analyzed. The boundary conditions on the quadrant meshed, the plate dimensions, the loading, the wall constructions and the material properties are shown in Figure 13. Problems 6 and 7 are simply supported plates while problem 8 has a boundary condition termed hinge-restrained, a form of simple support in which the in-plane components of displacement are also constrained. The wall construction for problem 6 is one orthotropic layer while that of problem 7 is an anisotropic composite wall composed of 10 orthotropic plies of equal thickness alternately oriented at  $-30^\circ$  and  $+30^\circ$  to the plate axes as shown in Figure 13. Problem 8 has an anisotropic composite wall consisting of two orthotropic plies of equal thickness alternately oriented at  $0^\circ$  and  $90^\circ$  to the plate axes and is also shown in Figure 13. The asymmetry in the cross-ply construction causes coupling between membrane and bending action and results in both bending and stretching of the plate when it is subjected to uniform lateral loading.



The convergence of the central deflection was studied by using a series of  $N \times N$  mesh patterns as was done for the isotropic plate bending problems. Figures 24 through 26 show the convergence of the central deflection with refinement in the mesh size. The quantity plotted is a dimensionless deflection coefficient which is defined in each figure. It is a function of the central deflection  $w_c$ , the plate dimensions  $a$  and  $t$ , the uniform loading  $q$  and the orthotropic material properties,

$E_{11}, E_{22}$  = Modulus of elasticity in the 1,2  
material directions shown in Figure 13

$G_{12}$  = Shear modulus in 1-2 plane

$\nu_{12}, \nu_{21}$  = Poisson's ratios in the 1-2 plane

Due to symmetry in the constitutive relations the orthotropic Poisson's ratios are related by,

$$\nu_{12} = \nu_{21} \frac{E_{11}}{E_{22}} \quad (V.2)$$

The "exact" deflection coefficient shown in Figure 24 is the classical plate bending solution by Lekhnitski [129]. The "exact" deflection coefficients shown in Figures 25 and 26 are by Fortier [130] who used the Ritz method and

trigonometric displacement assumptions to arrive at convergent solutions for a variety of unsymmetrically layered, anisotropic, square plates. In all three cases the SHEFA element showed a smooth convergence toward the "exact" solution and acceptable accuracy was obtained with a mesh size of five.

For the case of the single layer orthotropic wall the results of the Q-19 quadrilateral plate bending element [126] are also plotted. The comparison between the Q-19 and SHEFA results is essentially the same as for the corresponding isotropic plate (Problem 2).

E. Arbitrary Mesh Example - Bending  
of Rhombic Cantilever Plate

The bending of a rhombic cantilever plate by a uniform pressure load was also included in the Clough and Tocher Study [125]. The plate geometry, loading and isotropic material properties are shown in Figure 27. The finite element analyses by Clough and Tocher were all conducted with an 8x6 mesh which is shown by the dotted lines of Figure 27. The sloping boundaries of the plate were treated as stepped in the rectangular element analyses while the triangular elements fitted the boundaries exactly. Experimental results were available for the points labeled 1 through 6 in Figure 27. The finite element displacements at these points were obtained by interpolation of the nodal point deflection data and the results are tabulated in Figure 27 for the ACM, M and P rectangular elements and the HCT triangular element.

In order to obtain a representative comparison between the finite element and SHEFA solutions, a mesh size of 13x13 was selected as shown in Figure 28. This mesh has approximately the same number of degrees of freedom as the finite element meshes and also has nodes at the points where experimental deflections were measured so that comparisons can be made without interpolating. The w degrees of freedom at the nodes which lie outside of

the plate domain are eliminated via the multipoint constraints used to enforce the fixed edge boundary condition. The element layout of Figure 28, which follows the natural boundaries of the rhombic plate, illustrates the arbitrary meshing capability of the SHEFA element.

The SHEFA and finite element deflections together with the experimental results are tabulated in Figure 27. As discussed previously in the isotropic plate bending study, the M, P and ACM rectangles are not of practical interest but the HCT triangle is a representative facet type element for thin shell analysis. All of the numerical solutions are in good agreement with the experimental results, the P element being somewhat stiff as pointed out previously. The SHEFA and HCT results are about the same. The distribution of displacement predicted by the SHEFA element along the edges normal to the fixed support and along the plate centerline are shown in Figure 29. The experimental measurements are also shown.



## F. Cylindrical Shell Bending Study

A curved shell problem, in which flexural behavior is significant, is the cylindrical shell with a uniformly distributed, circumferential line load as shown in Figure 30. Since this is an axisymmetric problem with a plane of symmetry, only a portion of the shell need be meshed. The boundary conditions on the portion meshed, the shell dimensions and the isotropic material properties are also shown in Figure 30. The convergence of the deflection under the load was studied by using a series of progressively finer  $3 \times N$  mesh patterns. A typical example of the element pattern and nodal point arrangement for an  $N$  of 20 is shown in Figure 31. As described previously in section V.C, the  $w$  degrees of freedom at nodes lying outside the shell boundary are eliminated when the boundary conditions are imposed.

Figure 32 shows the convergence of the deflection under the load with a refinement in the mesh size. The quantity plotted is a dimensionless deflection coefficient which depends on the deflection under the load  $w_0$ , the loading  $P$ , the flexural rigidity  $D$  which is given by (V.1) and a parameter  $\beta$  which is defined by,

$$\beta^4 = \frac{Et}{4R^2D} = \frac{3(1-\nu)}{R^2t^2} \quad (V.3)$$

The "exact" deflection coefficient shown in Figure 32 is from the classical solution by Timoshenko [128] of the governing differential equation for symmetrical deformation of circular cylindrical shells. Acceptable accuracy was achieved even for the coarsest mesh size ( $N=4$ ). One solution, for a mesh of 8, was available for the rectangular shell element of Gallagher [57]. It also is shown in Figure 32 and is virtually the same as the SHEFA solution.

In Figure 33 the variation of normal displacement along the length of the shell is plotted in non-dimensional form. The deflection ( $w$ ) and length coordinate ( $z$ ) are normalized with respect to the deflection under the load ( $w_0$ ) and the half length of the shell ( $L$ ). The SHEFA deflections for the 3x20 mesh are superimposed on the classical solution by Timoshenko. The agreement between the two predictions is excellent. The slight departure between the two solutions near the boundary is to be expected since the Timoshenko solution is for an infinite cylinder while the SHEFA solution is for a finite length cylinder with simply supported ends.

The variation of the meridional moment resultant along the length of the shell is plotted in non-dimensional form in Figure 34. The moment resultant ( $M$ ) and length coordinate ( $z$ ) are normalized with respect to the moment resultant under the load ( $M_0$ ) and the half length of the shell ( $L$ ). The SHEFA results for the 3x20 mesh are shown

along with the classical solution. Again, the agreement between the two solutions is excellent and there is no departure between the two solutions near the boundary because the moment decays more rapidly than does the deflection.

## G. Cylindrical Shell Thermal Stress Study

A curved shell problem that further demonstrates the versatility of the SHEFA wall model is the unrestrained cylindrical shell shown in Figure 35. It has a non-linear radial temperature gradient through the shell wall that is everywhere constant with respect to the surface coordinates. Since the problem is axisymmetric and has a plane of symmetry, only a portion of the shell was meshed. The boundary conditions on the portion meshed and the shell dimensions are also shown in Figure 35. The mesh used for analysis is shown in Figure 36 and the isotropic material properties, which are a function of temperature, are shown in Figure 37. The temperature distribution through the shell wall is shown in Figure 38. The shell wall was divided into 20 equal layers in order to model the effects of the material property temperature dependence and the thermal gradient on the compliances (IV.50)-(IV.52) and the thermal forces (IV.53) and thermal moments (IV.54).

Since the shell is completely unrestrained the stress distribution at locations sufficiently removed from the ends of the shell is governed by membrane shell theory. In a membrane state of stress the total strains (IV.329) in both the circumferential and meridional directions



are constant through the thickness, but the strains associated with stress (IV.330) of course vary through the thickness, since the free thermal strains vary according to the temperature distribution.

The variation of meridional and circumferential stresses through the thickness of the shell is shown in Figure 39. The SHEFA results at the extreme outer and inner fibers and at the center of each layer are superimposed on the results obtained with membrane shell theory. The SHEFA stress distribution is for elements near the center of the shell where end effects have decayed to zero. The theoretical results were obtained with an analysis method [131] based on membrane shell theory and employing a layered shell wall model to account for material property temperature dependence and thermal gradient effects. The results with both methods were essentially identical.

#### H. Arbitrary Mesh Example - Cylindrical Shell With Circular Cutout

A curved shell problem with severe stress concentrations is that of a cylindrical shell with a circular cutout loaded in axial tension as shown in Figure 40. The problem has two planes of symmetry which require the analysis of only one-quarter of the shell with appropriate boundary conditions. However, a very fine grid adjacent to the hole is required in order to predict the severe stress gradients caused by the cutout. If the entire quadrant of the shell were meshed, a problem with several thousand degrees of freedom would have to be solved. Since the perturbations in the membrane stress field due to the hole decay rapidly, it is only necessary to mesh a small portion of the shell quadrant. The theoretical solution by Van Dyke [132] indicates that the stress concentrations at the hole decay to a membrane state in about three to four hole radii. Accordingly, a portion equal to about seven hole radii on a side was selected for analysis. The boundary conditions on the portion meshed, the shell dimensions and the isotropic material properties are shown in Figure 40.

Two element discretizations were used in studying the stress concentrations at the hole, a 10x10 mesh and a 20x20 mesh. The element pattern and nodal point arrangement is shown in Figure 41 for the 20x20 mesh. An enlargement of this mesh in the vicinity of the hole is shown in Figure 42. An irregular grid work was used in which the mesh lines correspond roughly to a polar coordinate system about the hole rather than following the shell coordinate lines.

The predicted stress concentrations at the two points on the hole boundary labeled A and B in Figure 40 are given in Table 8 for an applied axial stress of 10,000 psi. The hoop stress peaks at point A and the axial stress peaks at point B. Outer and inner surface stresses as well as membrane and bending stresses are tabulated for two analytical solutions, four finite element solutions and the two SHEFA solutions. The analytical solutions are by Van Dyke [132] and Lekkerkerker [133]. Solutions are also available for the KB1 and KB6 quadrilateral shell elements by Key and Beisinger [61,62]. They used two element discretizations which cover a full quadrant of the shell. The coarse mesh had 176 nodal points, 148 elements and the fine mesh had 589 nodal points, 533 elements. In the KB6 analyses the number of degrees of freedom was 1534 for the coarse mesh and 5301

for the fine mesh, while for the KB1 analyses, the numbers were about ten percent smaller. The two SHEFA meshes, covering a smaller portion of the shell quadrant as shown in Figure 40, had 100 elements, 265 nodal points and 329 degrees of freedom for the 10x10 mesh and 400 elements, 925 nodal points and 1263 degrees of freedom for the 20x20 mesh. If the discrete element meshes are all compared on the basis of the smaller region of analysis used for the SHEFA calculations, the mesh gradations were such that the two finite element meshes each have about 20 percent fewer elements but more degrees of freedom than the SHEFA meshes.

The two SHEFA analyses were essentially the same and the results lie within the spread of the two analytical solutions except for the bending components of the stresses which are slightly higher than the Lekkerkerker prediction. Since stresses are only computed at the centroids of the SHEFA elements, the values in Table 8 were obtained by extrapolation.

The two KB6 analyses showed an increase in the stresses in going from the coarse mesh to the fine mesh. The fine mesh results were approximately the same as the Van Dyke solution. The two KB1 analyses also showed an increase in the stresses for the finer mesh and the results are approximately the same as those obtained by Lekkerkerker. The KB1 and KB6 stresses in Table 8 were also obtained by extrapolation of element centroidal stress data.



AD-A034 788

NAVAL SURFACE WEAPONS CENTER WHITE OAK LAB SILVER SP--ETC F/G 13/13  
A GENERALIZED FINITE DIFFERENCE ELEMENT FOR THE THERMOELASTIC S--ETC(U)  
JUN 76 R J EDWARDS

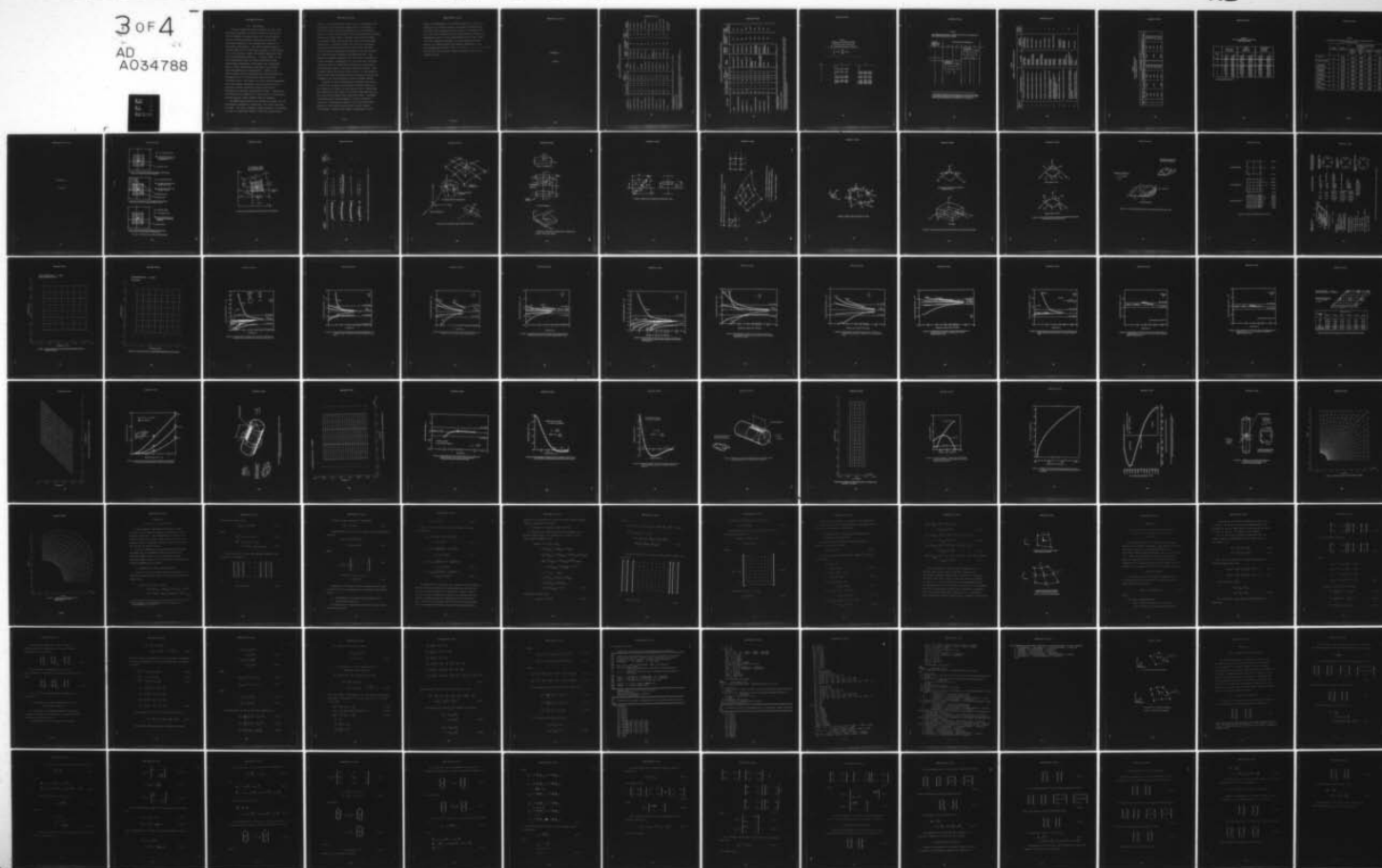
UNCLASSIFIED

NSWC/WOL/TR-76-66

NL

3 OF 4

AD  
A034788



## VI. CONCLUSIONS

Two well established matrix methods for thin shell structural analysis, the finite element method and the finite difference energy method, have been integrated into one unified analytical approach and have been effectively applied to the thermoelastic analysis of anisotropic thin shells. The finite element method is a widely used tool for structural analysis of thin shells due to its ability to model the complex geometries that occur in engineering practice. In recent years, it has been demonstrated that the finite difference energy method offers significant advantages over contemporary finite element formulations, especially for problems involving geometrical nonlinearities. However, the method suffers from the modeling restrictions imposed by rectangular grid works which must follow the shell coordinate lines. The results of this research demonstrate that this classic restriction can be removed and that a generalized finite difference energy method can be developed for arbitrary quadrilateral meshes. Furthermore, the formulation is amenable to installation in contemporary, general purpose, finite element computer programs.

The SHEFA generalized finite difference element for the thermoelastic analysis of anisotropic thin shells has been developed. The shell reference surface geometry is described in terms of curvilinear surface coordinates using tensor

notation. The deformation of the shell is described by the linear strain and curvature change tensors of Sanders. A shell wall model has been developed that is sufficiently general to treat a broad range of wall constructions including layered orthotropic walls, filament wound walls and angle ply composite walls as well as more conventional monocoque construction. The model treats the effects of nonlinear temperature gradients through the shell wall, including material property temperature dependence, and also accounts for coupling between membrane and bending action. Iso-parametric mapping techniques have been used to establish a finite difference approximation of the strain and curvature tensors in terms of displacement variables at arbitrarily placed discrete nodes on the shell reference surface. The potential energy of the structural system is then formed in terms of the nodal variables and the equations of motion are obtained by use of the Minimum Potential Energy Theorem.

A series of twelve demonstration problems were solved to verify the accuracy and convergence characteristics of the element in a variety of applications and to demonstrate the generality of the element via several problems that are most efficiently modeled with arbitrary meshes. The SHEFA predictions were verified against classical analytical solutions or experimental results and in some cases were compared to the results obtained with finite element formulations. Based on the limited comparisons of this

study, the performance of the SHEFA element was found to be comparable to the facet element of Clough and Johnson [45] and the curved rectangular shell element of Gallagher [57]. Some flat finite elements and the quadrilateral elements for axisymmetric shells of Key and Beisinger [61,62] were found to be more rapidly convergent for plate bending problems. However, the SHEFA element gave results comparable to the more sophisticated finite element formulations of Key and Beisinger for the case of an axially loaded cylindrical shell with a circular cutout.



APPENDIX A

TABLES

TABLE 1  
CURVED, THIN SHELL, FINITE ELEMENTS WITH FOUR SIDES

DEVELOPER	REF. NO.	NO. OF NODES	NO. OF D.O.F.	NO. OF POLYNOMIAL TERMS $w, u, v, \psi_1, \psi_2$	SHELL THEORY	SURFACE APPROXIMATION	DISPLACEMENT CONTINUITY SATISFIED	RIGID BODY MODES SATISFIED	ELEMENT PLANFORM
1. BOGNER, ET. AL.	51	4	48	16 16	UNKNOWN	CYLINDRICAL	YES	NO	RECTANGLE
2. CANTIN & CLOUGH	52	4	24	16 4	NOVOZHILOV	CYLINDRICAL	NO	YES	RECTANGLE
3. OLSON & LINDBERG	53	4	28	12 8	LOVE	CYLINDRICAL	NO	YES <sup>(1)</sup>	RECTANGLE
4. YANG & KIM	54	4	48	16 16	UNKNOWN	CONICAL	YES	NO	TRAPEZOID
5. CONNOR & BREBBIA	55	4	20	12 4	MARGUERRE <sup>(2)</sup>	QUADRATIC	NO	NO	PARALLELOGRAM
6. BERGAN & CLOUGH	56	4	20	10 4	MARGUERRE <sup>(2)</sup>	CUBIC	YES	YES <sup>(1)</sup>	RECTANGLE
7. GALLAGHER & YANG	57, 58	4	24	16 4	NOVOZHILOV	PRINCIPAL CURVATURES	NO	NO	RECTANGLE
8. GREENE, ET. AL.	59	4	40	16 16	NOVOZHILOV	QUADRATIC	YES	NO	RECTANGLE
9. WEMPNER, ET. AL.	60	4	20	4 4 4	WEMPNER <sup>(3)</sup>	GAUSSIAN	NO	NO	PARALLELOGRAM
10. KEY & BEISINGER	61, 62	4	36	12 12	WASHIZU <sup>(3)</sup>	AXISYMMETRIC	YES	YES <sup>(1)</sup>	QUADRILATERAL
11. JONES	63	4	48	16 16	MARGUERRE <sup>(2)</sup>	QUADRATIC	YES	NO	EIGHT-SIDED POLYGON

(1) REPRESENTATION OF RIGID BODY MODES DEMONSTRATED NUMERICALLY VIA EIGENVALUES OF STIFFNESS MATRIX.

(2) SHALLOW SHELL THEORY

(3) THESE SHELL THEORIES ALSO INCLUDE TRANSVERSE SHEAR DEFORMATIONS BUT A DISCRETE EQUIVALENT OF THE KIRCHOFF HYPOTHESIS IS INTRODUCED TO ASSURE THAT THE KIRCHOFF THEORY IS APPROACHED IN THE LIMIT AS THE MESH IS REFINED.

TABLE 2  
CURVED, THIN SHELL, FINITE ELEMENTS WITH THREE SIDES

DEVELOPER	REF. NO.	NO. OF NODES	NO. OF D.O.F.	NO. OF POLYNOMIAL TERMS			SHELL THEORY	SURFACE APPROXIMATION	DISPLACEMENT CONTINUITY SATISFIED	RIGID BODY MODES SATISFIED
				w	u,v	$\psi_1, \psi_2$				
1. UTKU	64	3	15	3	3	3	MARGUERRE <sup>(2)</sup>	QUADRATIC	YES	NO
2. STRICKLAND & LODEN	65	3	15	9	3		NOVOZHILOV <sup>(2)</sup>	QUADRATIC	NO	NO
3. BONNES, ET. AL.	66	6	36	12	12		REISSNER <sup>(2)</sup>	QUADRATIC	NO	NO
4. COWPER, ET. AL.	67,70	3	36	21	10		NOVOZHILOV <sup>(2)</sup>	GAUSSIAN	YES	YES <sup>(1)</sup>
5. DHATT	68	3	27	9	10	6	REISSNER, <sup>(2,3)</sup> WASHIZU	QUADRATIC	YES	YES <sup>(1)</sup>
6. ARGYRIS & SCHARPF	69	6	63	21	21		ARGYRIS	NINE POINT LAGRANGIAN	YES	YES
7. COWPER, ET. AL.	70	3	36	21	10		DONNELL-VLASOV, KOITER-SANDERS	GAUSSIAN	YES	YES <sup>(1)</sup>
8. DUPUIS & GOEL	71	3	54	18	18		KOITER	TEN POINT LAGRANGIAN	YES	YES
9. THOMAS & GALLAGHER	72	4	36	10	10		KOITER	GAUSSIAN	YES	NO

(1) REPRESENTATION OF RIGID BODY MODES DEMONSTRATED NUMERICALLY VIA EIGENVALUES OF STIFFNESS MATRIX.

(2) SHALLOW SHELL THEORY

(3) THESE SHELL THEORIES ALSO INCLUDE TRANSVERSE SHEAR DEFORMATIONS BUT A DISCRETE EQUIVALENT OF THE KIRCHHOFF HYPOTHESIS IS INTRODUCED TO ASSURE THAT THE KIRCHHOFF THEORY IS APPROACHED IN THE LIMIT AS THE MESH IS REFINED.



TABLE 3  
 ABSCISSAE OF INTEGRATION POINTS  
 AND WEIGHT COEFFICIENTS FOR  
 THE GAUSSIAN QUADRATURE FORMULA

$$\int_{-1}^1 f(x) dx = \sum_{i=1}^N H_i f(a_i)$$

N	$\pm a$	H
1	0.0	1.0
2	0.57735 02691 89626	1.0
3	0.77459 66692 41483 0.0	0.55555 55555 55556 0.88888 88888 88889
4	0.86113 63115 94053 0.33998 10435 84856	0.34785 48451 37454 0.65214 51548 62546
5	0.90617 98459 38664 0.53846 93101 05683 0.0	0.23692 68850 56189 0.47862 86704 99366 0.56888 88888 88889



TABLE 4  
CORRESPONDENCE BETWEEN ELEMENT INTERPOLATING COORDINATES  
AND ELEMENT CONNECTION NUMBER

ELEMENT CONNECTION NUMBER, K	INTERPOLATING COORDINATES			
	$\lambda_K$	$\mu_K$	$a_K$	$\beta_K$
1	-1	-1	DETERMINE NUMERICALLY* FROM: $x^1_k = [H_L(a_k, \beta_k)] \{x^1_L\}$ $x^2_k = [H_L(a_k, \beta_k)] \{x^2_L\}$ $k = 1, \dots, 4$ $L = 5, \dots, 13$	
2	1	-1		
3	1	1		
4	-1	1		
5	0	0	0	0
6	DETERMINE NUMERICALLY* FROM: $x^1_k = [L_L(\lambda_k, \mu_k)] \{x^1_L\}$ $x^2_k = [L_L(\lambda_k, \mu_k)] \{x^2_L\}$ $k = 5, \dots, 13$ $L = 1, \dots, 4$		-1	-1
7			0	-1
8			1	-1
9			1	0
10			1	1
11			0	1
12			-1	1
13			-1	0

\*A NUMERICAL METHOD FOR DETERMINING THE INVERSE FUNCTIONAL  
RELATIONSHIP BETWEEN SURFACE COORDINATES AND PARAMETRIC  
INTERPOLATING COORDINATES IS PRESENTED IN APPENDIX D.

TABLE 5  
SUMMARY OF DEMONSTRATION PROBLEMS

PROBLEM NO.	PROBLEM DESCRIPTION	LOADING	BOUNDARY CONDITIONS	NO. OF LAYERS IN WALL
1	STRETCHING OF ISOTROPIC, SQUARE PLATE	PARABOLIC EDGE LOADS	2 FREE EDGES 2 LOADED EDGES	1
2	BENDING OF ISOTROPIC, SQUARE PLATE	UNIFORM PRESSURE	SIMPLE SUPPORT	1
3	BENDING OF ISOTROPIC, SQUARE PLATE	CONCENTRATED LOAD AT CENTER	SIMPLE SUPPORT	1
4	BENDING OF ISOTROPIC, SQUARE PLATE	UNIFORM PRESSURE	FIXED EDGES	1
5	BENDING OF ISOTROPIC, SQUARE PLATE	CONCENTRATED LOAD AT CENTER	FIXED EDGES	1
6	BENDING OF ORTHOTROPIC, SQUARE PLATE	UNIFORM PRESSURE	SIMPLE SUPPORT	1
7	BENDING OF ANISOTROPIC, SQUARE PLATE ( $\pm 30^\circ$ ANGLE PLY COMPOSITE)	UNIFORM PRESSURE	SIMPLE SUPPORT	10
8	COMBINED BENDING AND STRETCHING OF ANISOTROPIC, SQUARE PLATE (CROSS PLY COMPOSITE)	UNIFORM PRESSURE	HINGE-RESTRAINED	2
9	BENDING OF ISOTROPIC, RHOMBIC PLATE	UNIFORM PRESSURE	3 FREE EDGES 1 FIXED EDGE	1
10	BENDING OF ISOTROPIC, CYLINDRICAL SHELL	LINE LOAD AROUND CIRCUMFERENCE	ENDS SIMPLY SUPPORTED	1
11	THERMAL STRESSES IN CYLINDRICAL SHELL WITH ISOTROPIC, TEMPERATURE DEPENDENT PROPERTIES	NONLINEAR RADIAL TEMPERATURE GRADIENT	FREE ENDS	20
12	STRESS CONCENTRATIONS IN ISOTROPIC CYLINDRICAL SHELL WITH CIRCULAR HOLE	AXIAL TENSION	END LOADS	1

TABLE 6  
FLAT PLATE MEMBRANE BEHAVIOR  
DISPLACEMENT SOLUTIONS

POINT NO.	ANALYTICAL SOLUTION	DISPLACEMENT, $u$ , ( $10^{-3}$ IN.)					
		SHEFA SOLUTION			GALLAGHER SOLUTION		
		4-ELEMENT	16-ELEMENT	64-ELEMENT	4-ELEMENT	16-ELEMENT	64-ELEMENT
1	1.4764	1.4727	1.4756	1.4764	1.4729	1.4757	1.4769
2				1.4542			1.4550
3	1.3895		1.3891	1.3883		1.3892	1.3899
4				1.2813			1.2842
5	1.1428	1.1491	1.1442	1.1373	1.1490	1.1442	1.1425
6				0.9620			0.9712
7	0.7786		0.7873	0.7643		0.7873	0.7795
8				0.5462			0.5972
9	0.3674	0.4958	0.4161	0.3620	0.4956	0.4159	0.3862

TABLE 7  
FLAT PLATE MEMBRANE BEHAVIOR  
STRESS SOLUTIONS

	ANALYTICAL SOLUTION		SHEFA ELEMENT SOLUTION		GALLAGHER ELEMENT SOLUTION	
POINT	$\sigma_y$	$\sigma_x$	$\sigma_y$	$\sigma_x$	$\sigma_y$	$\sigma_x$
a	78.7	909.6	102.33	854.02	102.35	854.04
b	18.8	456.2	32.94	479.36	32.94	479.29
c	217.8	975.0	224.59	959.95	224.64	960.03
d	171.6	852.6	177.12	837.82	177.18	837.90
e	91.9	609.4	95.42	597.16	95.48	597.26
f	14.9	249.2	21.99	271.57	22.02	271.40
g	310.2	993.5	316.38	989.43	309.27	989.70
h	293.3	962.5	300.90	958.27	293.60	958.54
i	261.4	900.0	270.42	895.98	262.80	896.27
j	213.8	806.9	226.22	803.03	218.93	803.06
k	157.4	683.1	170.54	678.87	163.53	679.18
l	97.0	528.1	107.51	525.83	101.14	525.38
m	41.9	342.6	41.53	315.78	43.78	341.85
n	5.6	126.6	4.11	115.82	8.12	139.32

VALUES SHOWN ARE LB/IN.<sup>2</sup>

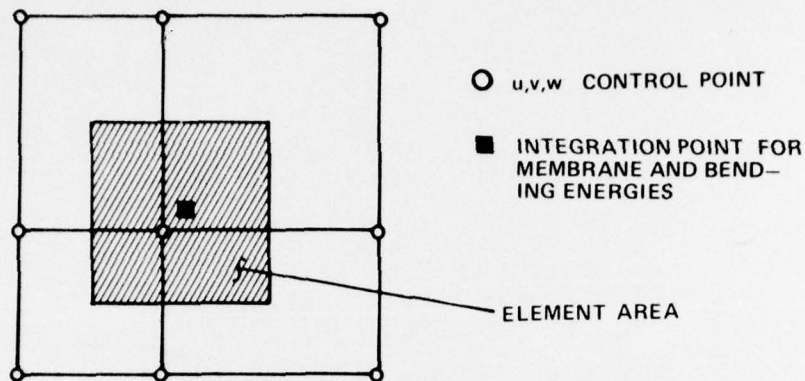


TABLE 8  
STRESS CONCENTRATIONS IN AN AXIALLY LOADED CYLINDRICAL SHELL  
WITH A CIRCULAR HOLE

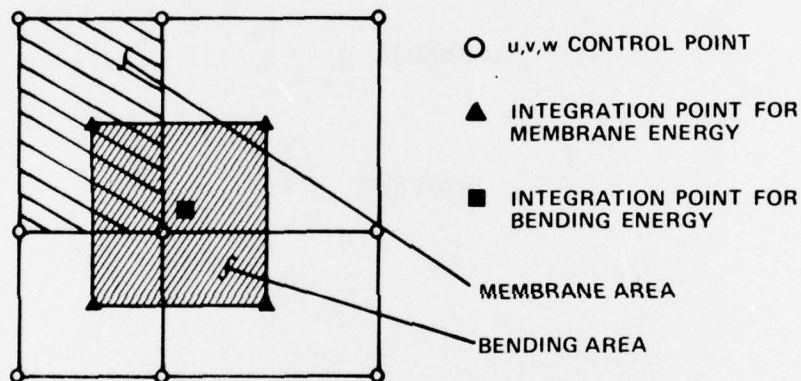
	STRESS LOCATION	STRESS DIRECTION	STRESSES AT HOLE DUE TO AN APPLIED AXIAL STRESS OF 10,000 PSI			
			OUTER SURFACE STRESS PSI	INNER SURFACE STRESS PSI	MEMBRANE STRESS PSI	BENDING STRESS PSI
VAN DYKE	A B	HOOP AXIAL	- 4410 30100	- 20590 41900	- 12500 36000	8090 - 5900
LEKKER KERKER	A B	HOOP AXIAL	- 5500 33500	- 22000 45600	- 13750 39550	8250 - 6050
SLADE-KB6 COARSE MESH	A B	HOOP AXIAL	- 2740 28900	- 18860 39900	- 10800 34400	8060 - 5500
SLADE-KB6 FINE MESH	A B	HOOP AXIAL	- 3680 30400	- 19920 41400	- 11800 35900	8120 - 5500
SLADE-KB1 COARSE MESH	A B	HOOP AXIAL	- 3970 30720	- 19000 42020	11485 36370	7515 - 5650
SLADE-KB1 FINE MESH	A B	HOOP AXIAL	- 4690 33380	- 21010 45060	12850 39220	8160 - 5840
SHEFA 10 X 10 MESH	A B	HOOP AXIAL	- 4000 31000	- 20800 44000	- 12400 37500	8400 - 6500
SHEFA 20 X 20 MESH	A B	HOOP AXIAL	- 4400 31500	- 21000 44500	- 12700 38000	8300 - 6500

APPENDIX B

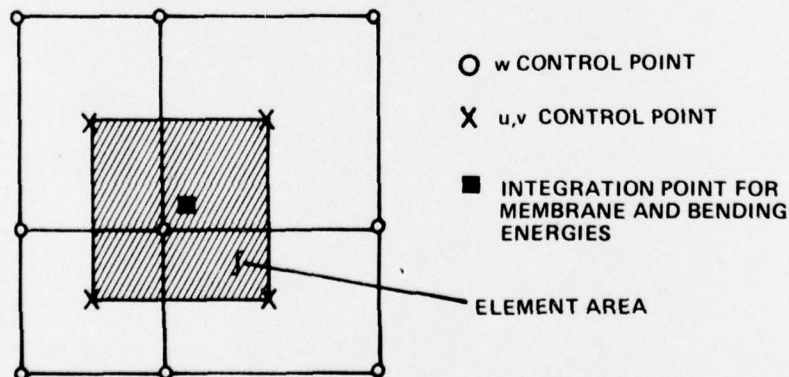
FIGURES



A. WHOLE-STATION SPACING WITH MEMBRANE AND BENDING ENERGIES INTEGRATED OVER SAME AREA



B. WHOLE STATION SPACING WITH MEMBRANE AND BENDING ENERGIES INTEGRATED OVER DIFFERENT AREAS



C. HALF-STATION SPACING WITH MEMBRANE AND BENDING ENERGIES INTEGRATED OVER THE SAME AREA

FIGURE 1 STAGS FINITE DIFFERENCE MESH SCHEMES



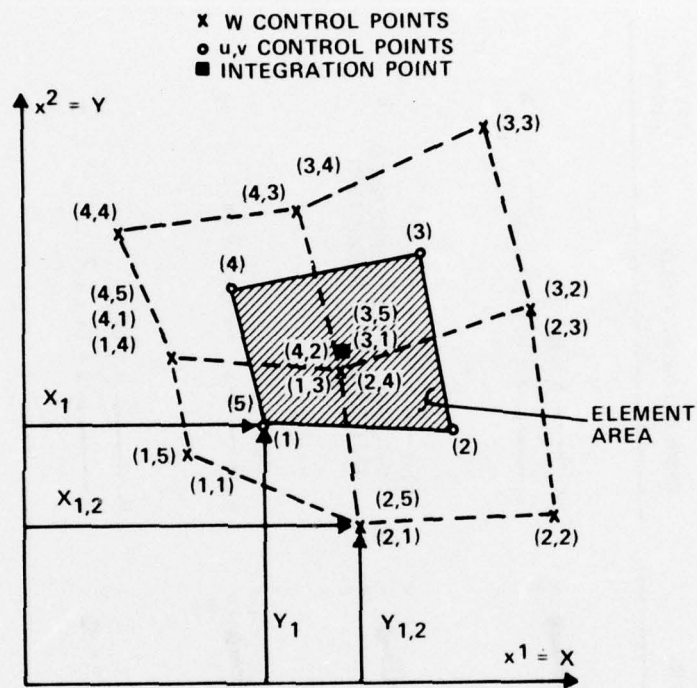


FIGURE 2 FINITE DIFFERENCE MESH SCHEME BY JOHNSON [110]




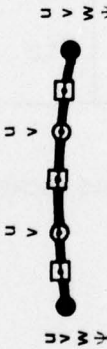


ELEMENT NUMBER	SCHEMATIC	DISPLACEMENT FIELD	MATRIX ORDER	GAUSS POINTS REQUIRED
1		$u, v \rightarrow a + bs$ $w \rightarrow a + bs + cs^2 + ds^3$	8	2
2		$u, v, w \rightarrow a + bs + cs^2 + ds^3$ INTERNAL D.O.F. CONDENSED OUT BY STATIC REDUCTION	8	3
3		$u, v, w \rightarrow a + bs + cs^2 + ds^3$	12	3
4		$u, v \rightarrow a + bs$ $w \rightarrow a + bs + cs^2$	7	1

FIGURE 3 DISCRETE ELEMENTS FOR COMPARATIVE STUDY BY BUSHNELL, [114]

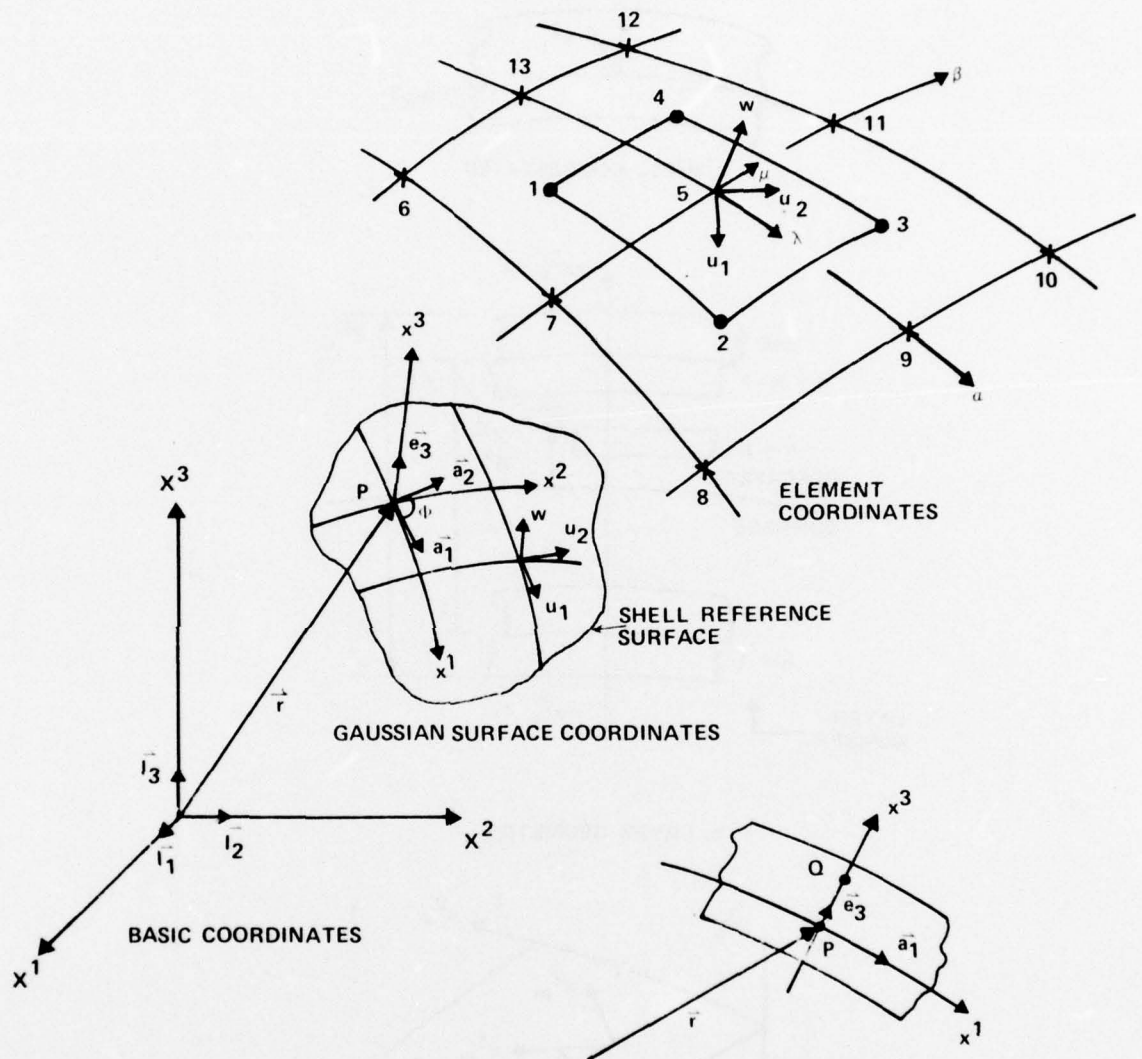


FIGURE 4 SHELL GEOMETRY AND COORDINATE SYSTEMS



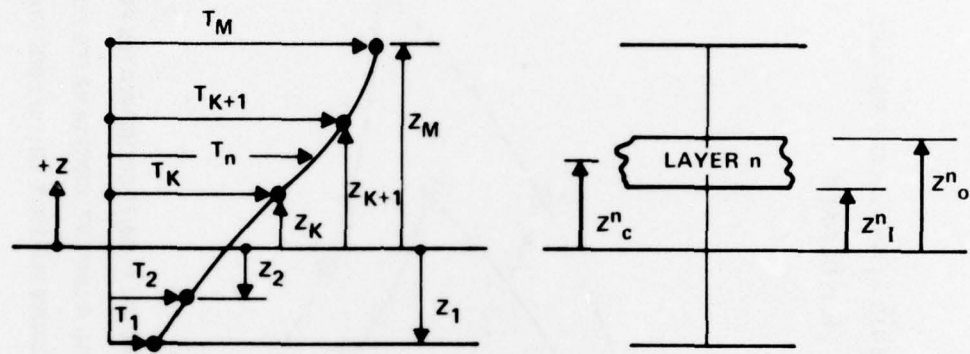


FIGURE 6 TEMPERATURE GRADIENT THROUGH SHELL WALL



X - POINTS AT WHICH TANGENTIAL DISPLACEMENTS,  $u_1$  AND  $u_2$ , ARE DEFINED  
 ⊙ - POINTS AT WHICH NORMAL DISPLACEMENT,  $w$ , IS DEFINED

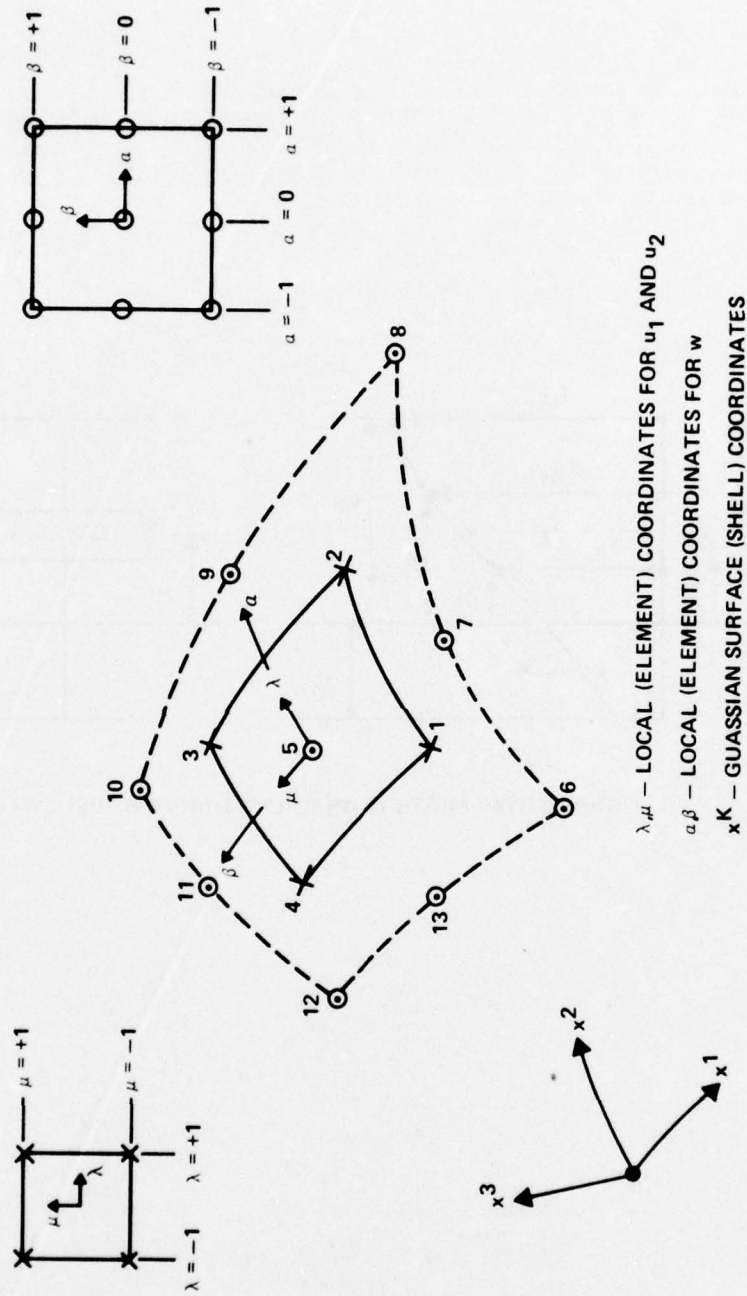


FIGURE 7 SHEFA ELEMENT GEOMETRY

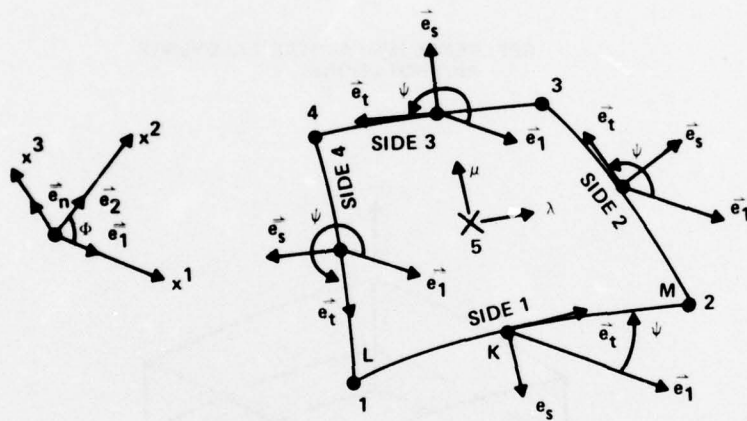
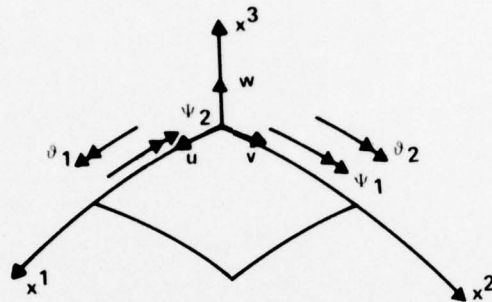
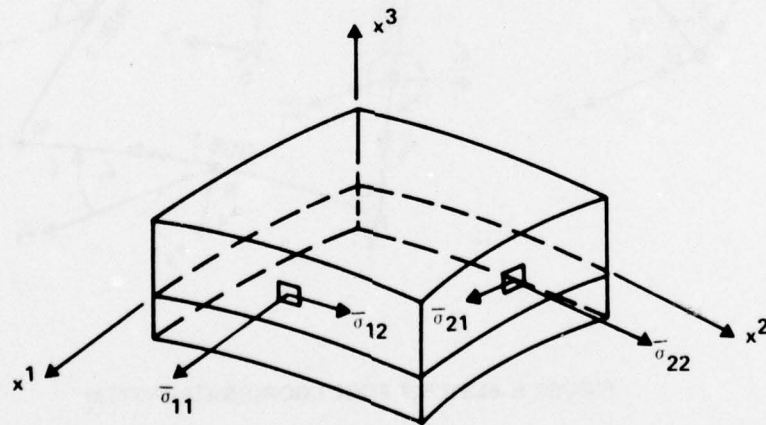


FIGURE 8 ELEMENT EDGE COORDINATE SYSTEM



REFERENCE SURFACE DISPLACEMENTS  
AND ROTATIONS



STRESSES

FIGURE 9 SIGN CONVENTIONS FOR DISPLACEMENTS, ROTATIONS AND STRESSES

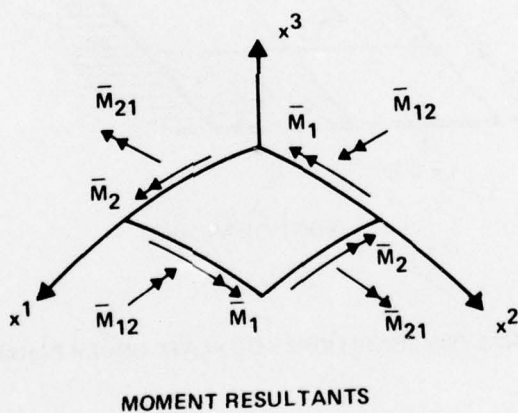
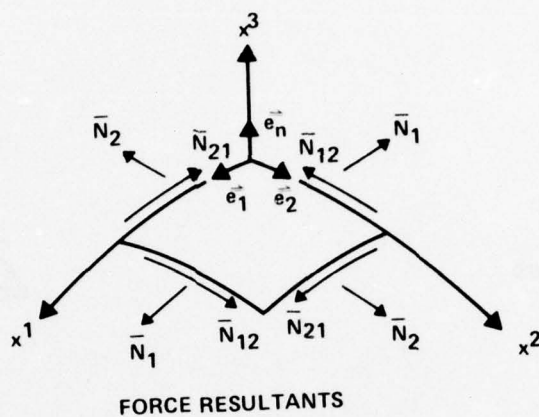


FIGURE 10 SIGN CONVENTIONS FOR FORCE AND MOMENT RESULTANTS ACTING ON REFERENCE SURFACE



MATERIAL PROPERTIES

$$E = 10 \times 10^6 \text{ PSI}$$

$$\nu = 0.3$$

BOUNDARY CONDITIONS  
ON PORTION MESHD

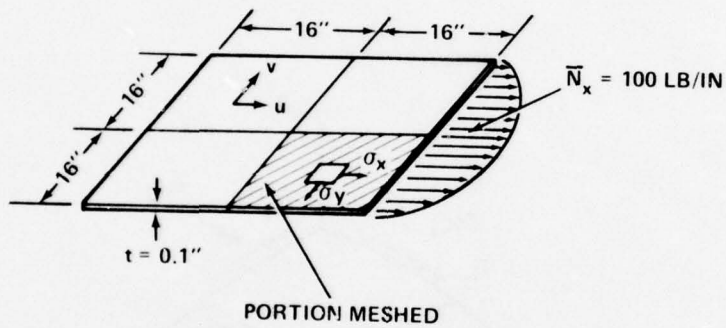
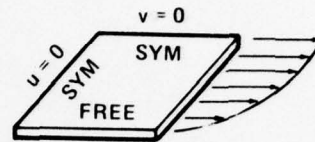


FIGURE 11 ANALYSIS CONDITIONS FOR PLATE UNDER PARABOLIC EDGE LOAD

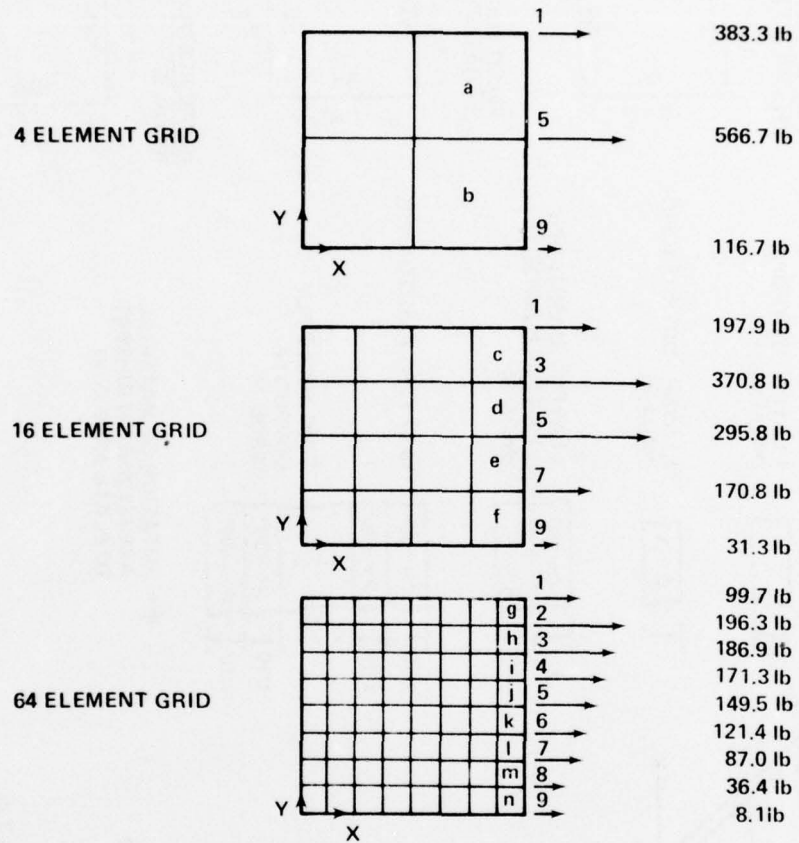
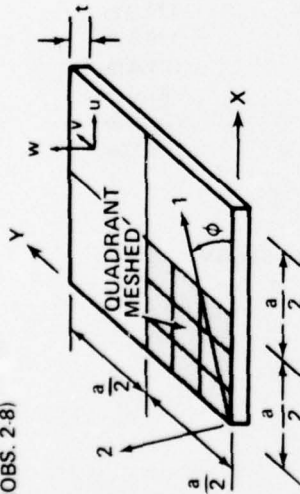


FIGURE 12 MESHES FOR MEMBRANE PLATE STUDY

# BOUNDARY CONDITIONS ON QUADRANT MESHD

## WALL CONSTRUCTIONS

## PLATE GEOMETRY (PROBS. 2,8)



$a = 40$  IN.,  $t = 1.0$  IN.

## LOAD CASES

$P = 10000$  LBS, (PROBS. 3,5)  
= CONCENTRATED LOAD AT  
CENTER OF PLATE  
 $q = 100$  PSI, (PROBS. 2,4,6,7,8)  
= UNIFORM PRESSURE LOAD

## MATERIAL PROPERTIES

ISOTROPIC, (PROBS. 2-5):

$$E = 10^7 \text{ PSI}, \nu = 0.30$$

ORTHOTROPIC, (PROB. 6):

$$E_{11} = 4.338 \times 10^6 \text{ PSI}, \nu_{21} = 0.02$$

$$E_{22} = 0.664 \times 10^6 \text{ PSI}$$

$$G_{12} = 0.8075 \times 10^6 \text{ PSI}$$

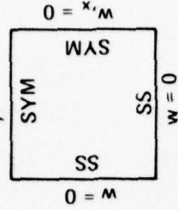
ORTHOTROPIC LAMINAE, (PROBS. 7,8):

$$E_{11} = 10^7 \text{ PSI}, \nu_{12} = 0.25$$

$$E_{22} = G_{12} = 0.25 \times 10^6 \text{ PSI}$$

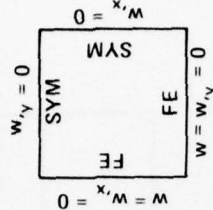
## SIMPLE SUPPORT (SS) (PROBS. 2,3,6,7)

$$w_{,y} = 0$$



## FIXED EDGE (FE) (PROBS. 4,5)

$$w_{,y} = 0$$



## HINGE-RESTRAINED (HR) (PROB. 8)

$$v = w_{,y} = 0$$

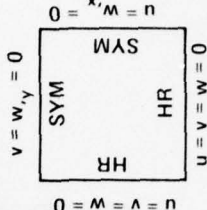


FIGURE 13 SUMMARY OF ANALYSIS CONDITIONS FOR PLATE BENDING PROBLEMS

PLATE BENDING STUDY • 7 x 7 MESH  
SIMPLY SUPPORTED EDGES

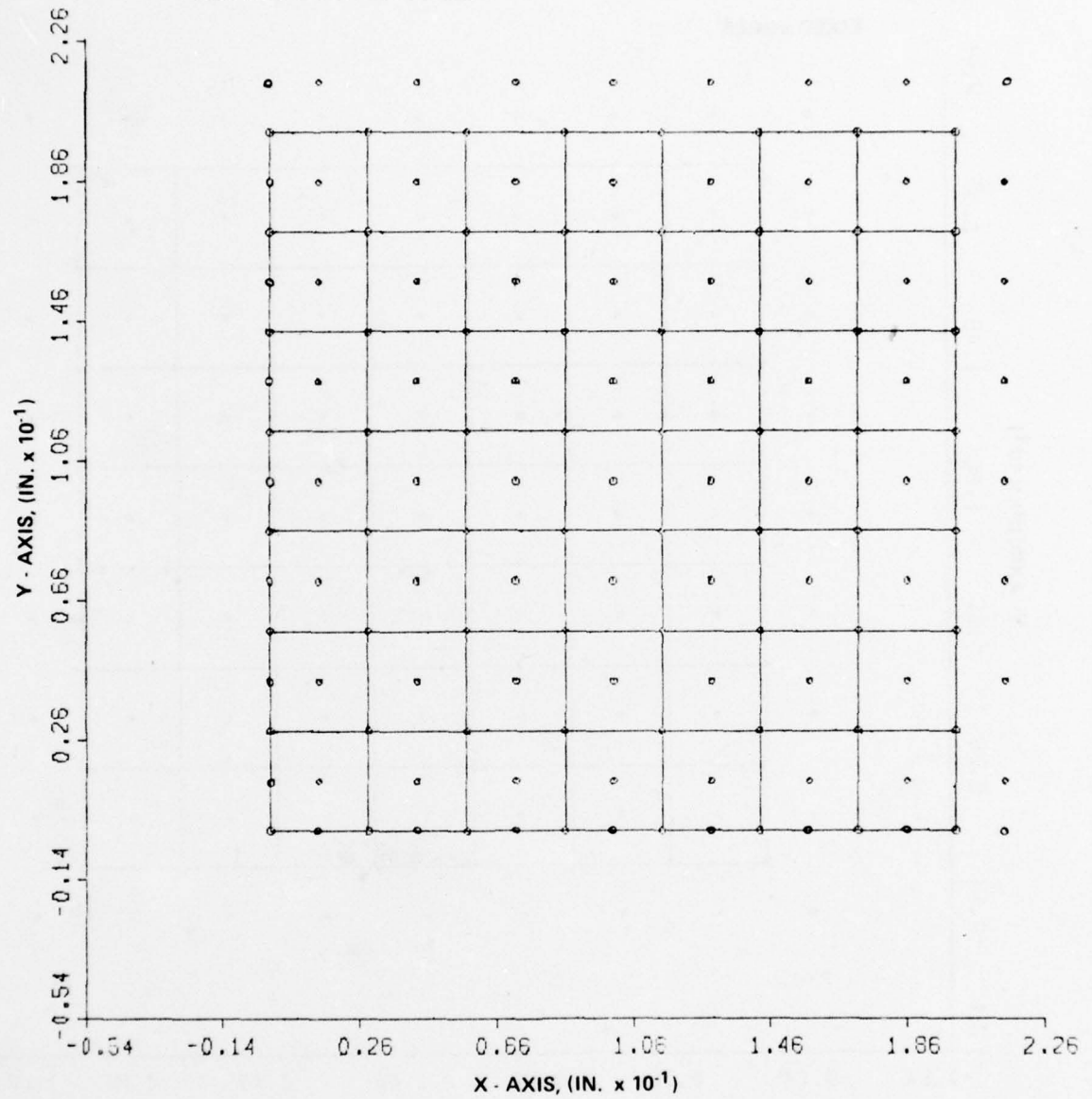


FIGURE 14 TYPICAL MESH FOR PLATE BENDING PROBLEMS WITH SIMPLY SUPPORTED EDGES



## PLATE BENDING STUDY • 7 x 7 MESH

FIXED EDGES

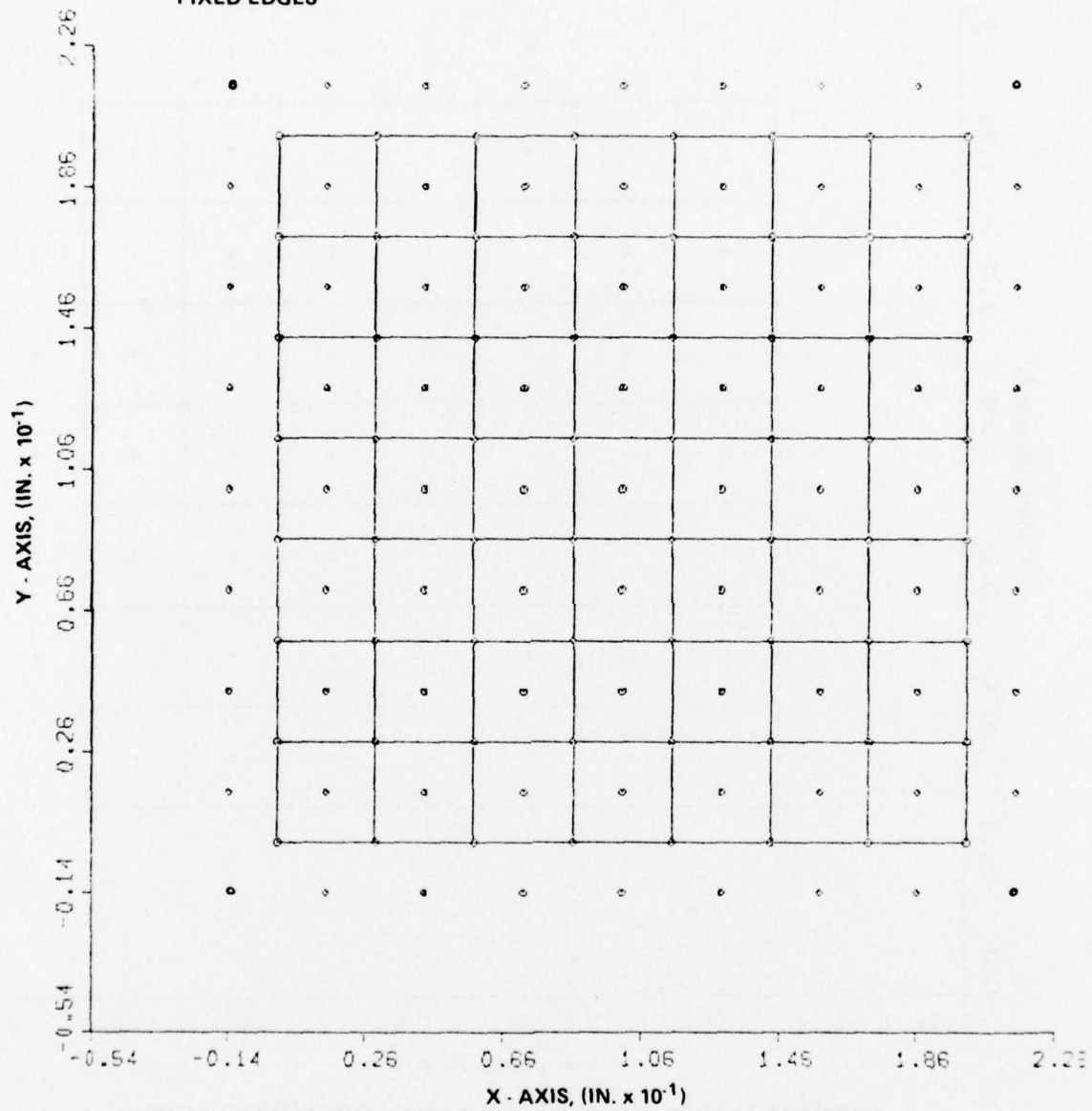


FIGURE 15 TYPICAL MESH FOR PLATE BENDING PROBLEMS WITH FIXED EDGES

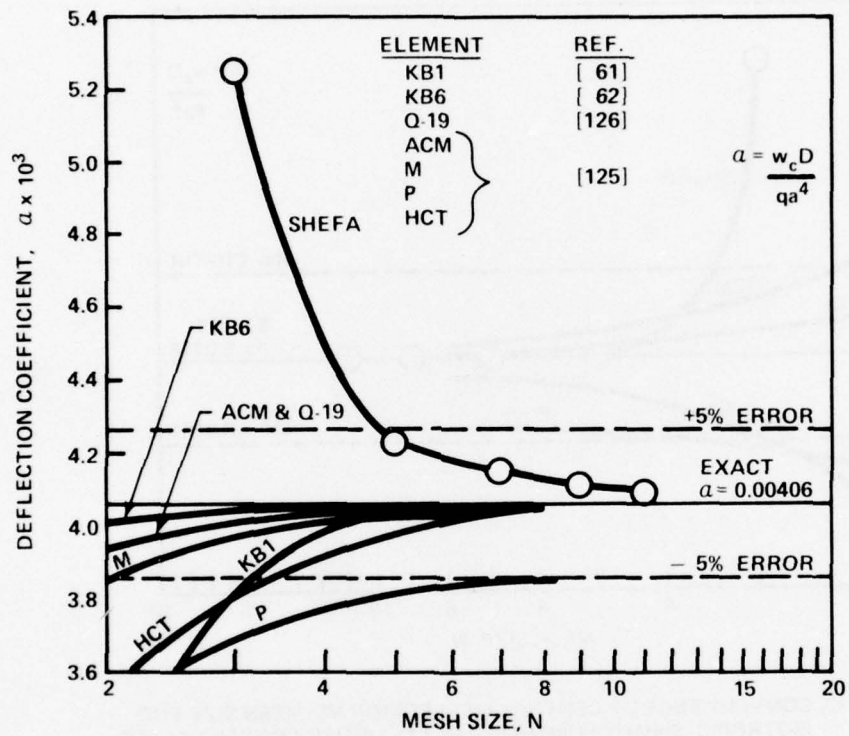


FIGURE 16 CONVERGENCE OF CENTRAL DEFLECTION VS. MESH SIZE FOR ISOTROPIC, SIMPLY-SUPPORTED PLATE UNDER UNIFORM LOAD

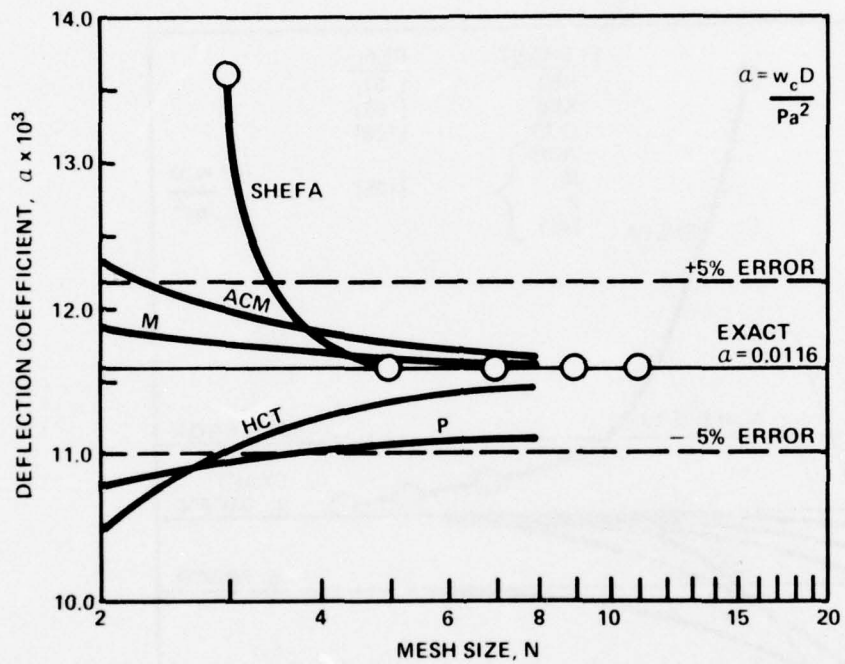


FIGURE 17 CONVERGENCE OF CENTRAL DEFLECTION VS. MESH SIZE FOR ISOTROPIC, SIMPLY-SUPPORTED PLATE UNDER CONCENTRATED LOAD

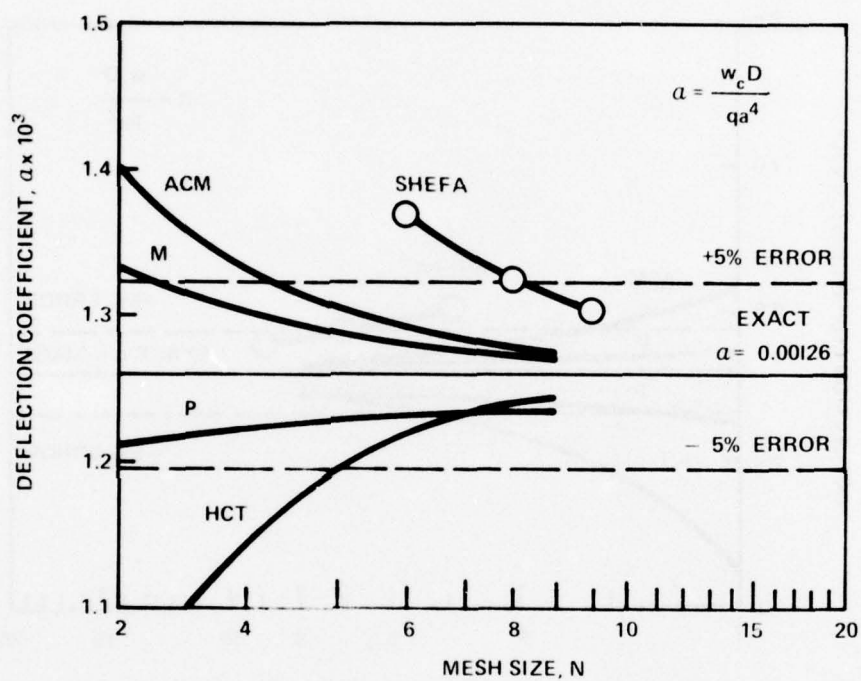


FIGURE 18 CONVERGENCE OF CENTRAL DEFLECTION VS. MESH SIZE FOR ISOTROPIC, CLAMPED PLATE UNDER UNIFORM LOAD



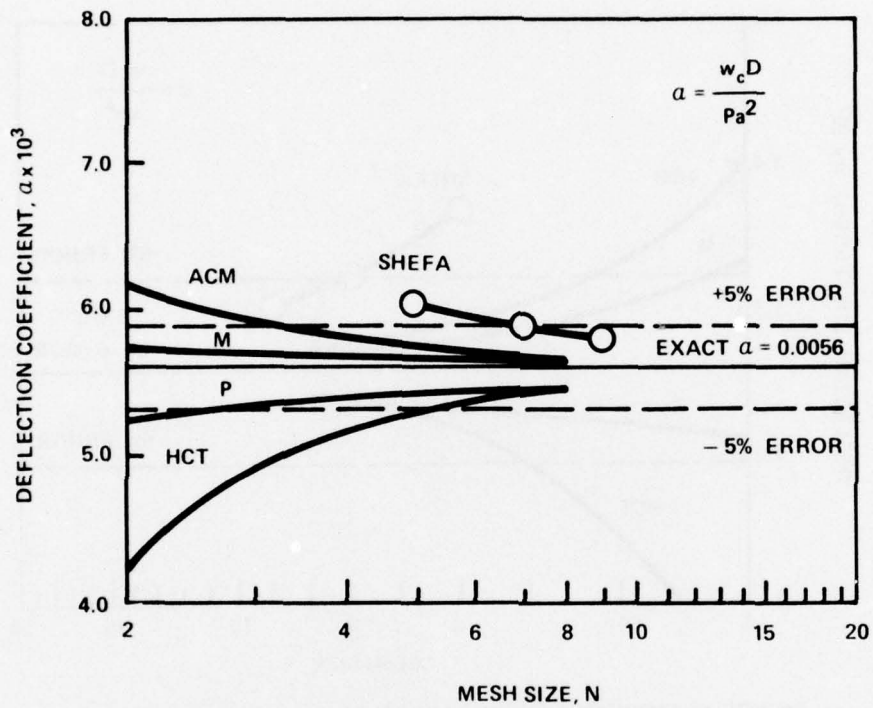


FIGURE 19 CONVERGENCE OF CENTRAL DEFLECTION VS. MESH SIZE FOR ISOTROPIC, CLAMPED PLATE UNDER CONCENTRATED LOAD

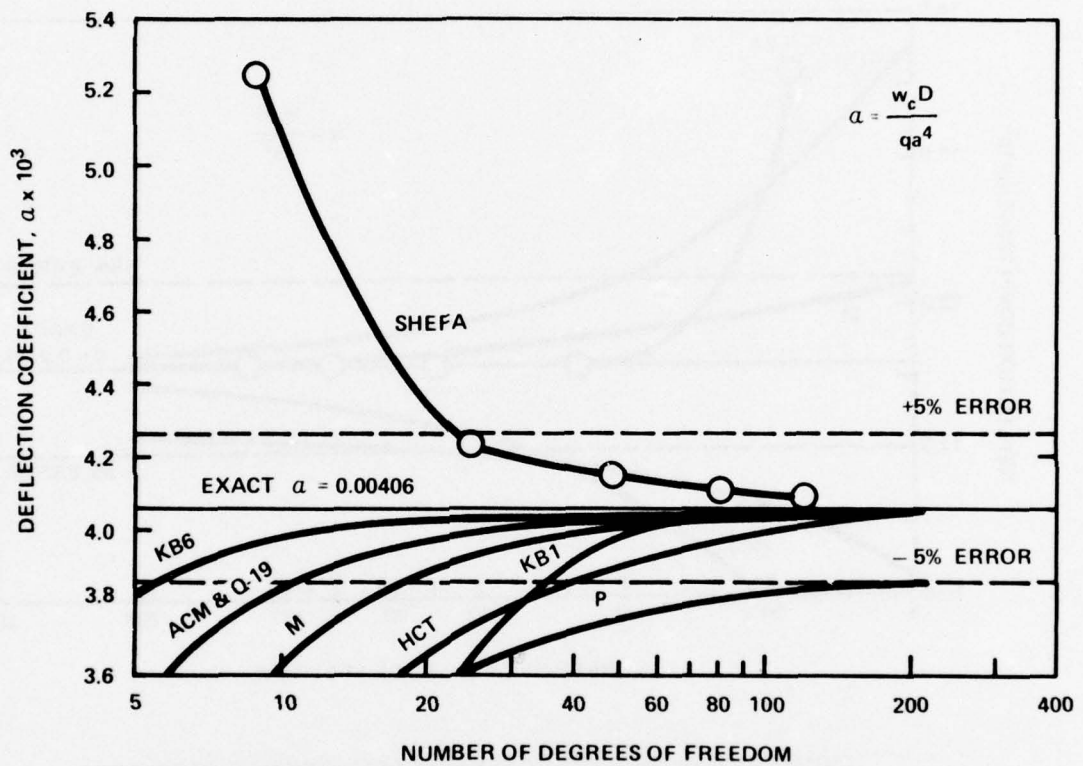


FIGURE 20 CONVERGENCE OF CENTRAL DEFLECTION VS. DEGREES OF FREEDOM FOR ISOTROPIC, SIMPLY-SUPPORTED PLATE UNDER UNIFORM LOAD

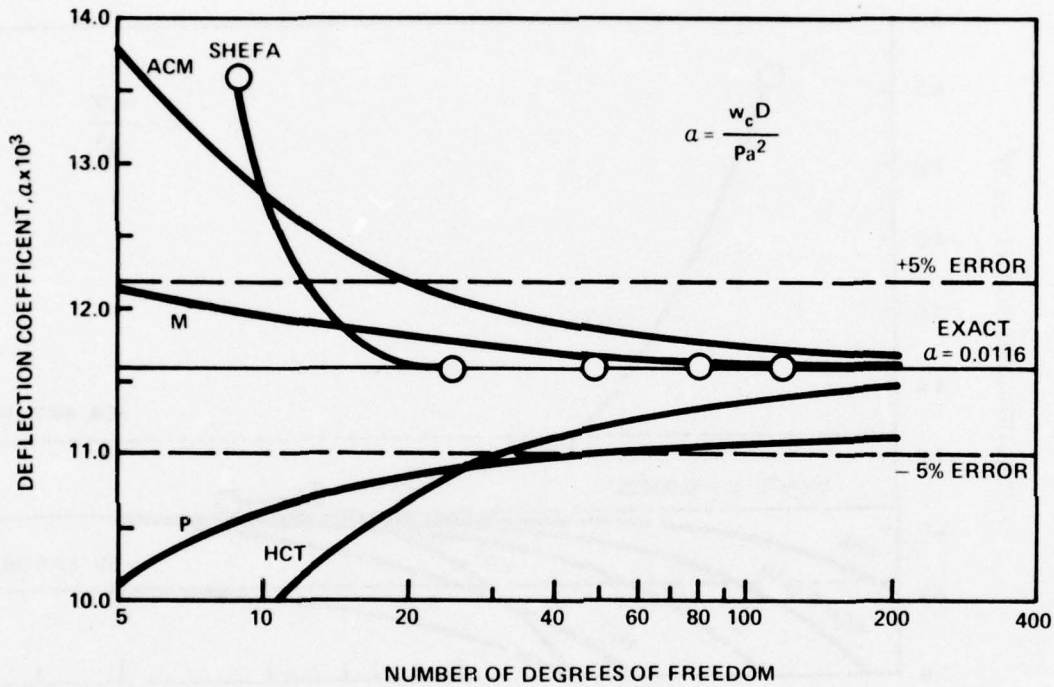


FIGURE 21 CONVERGENCE OF CENTRAL DEFLECTION VS. DEGREES OF FREEDOM FOR ISOTROPIC, SIMPLY-SUPPORTED PLATE UNDER CONCENTRATED LOAD

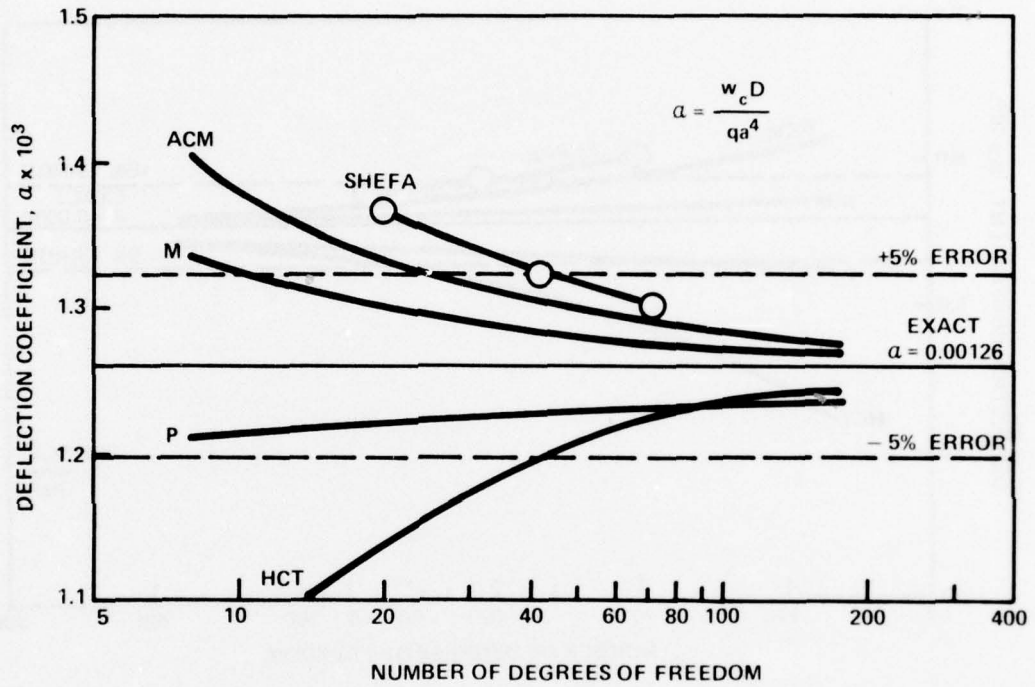


FIGURE 22 CONVERGENCE OF CENTRAL DEFLECTION VS. DEGREES OF FREEDOM FOR ISOTROPIC, CLAMPED PLATE UNDER UNIFORM LOAD



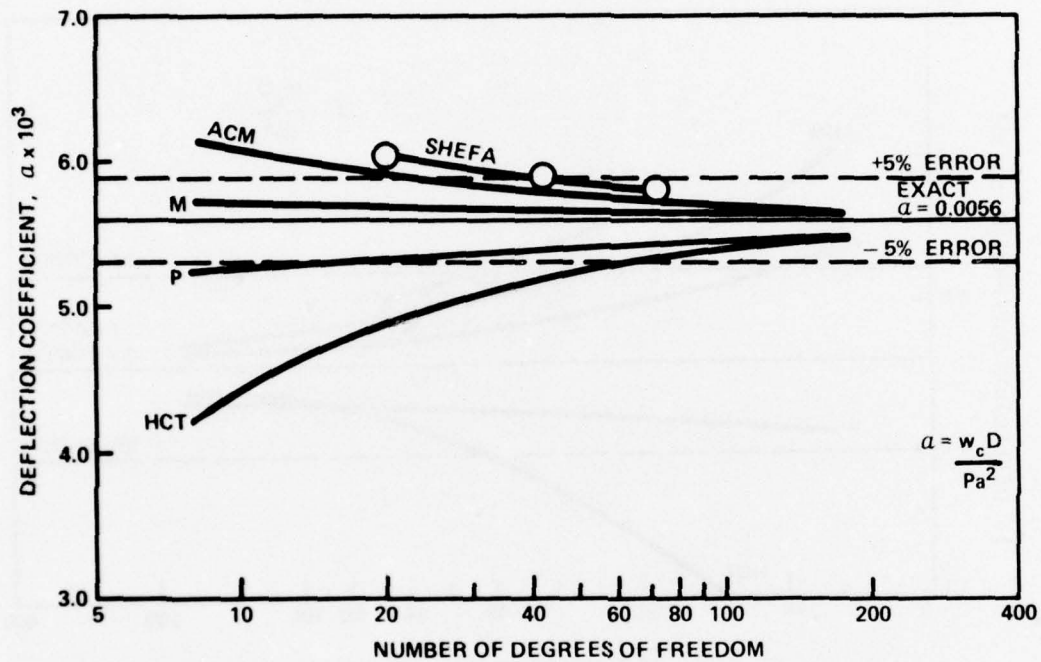


FIGURE 23 CONVERGENCE OF CENTRAL DEFLECTION VS. DEGREES OF FREEDOM FOR ISOTROPIC, CLAMPED PLATE UNDER CONCENTRATED LOAD

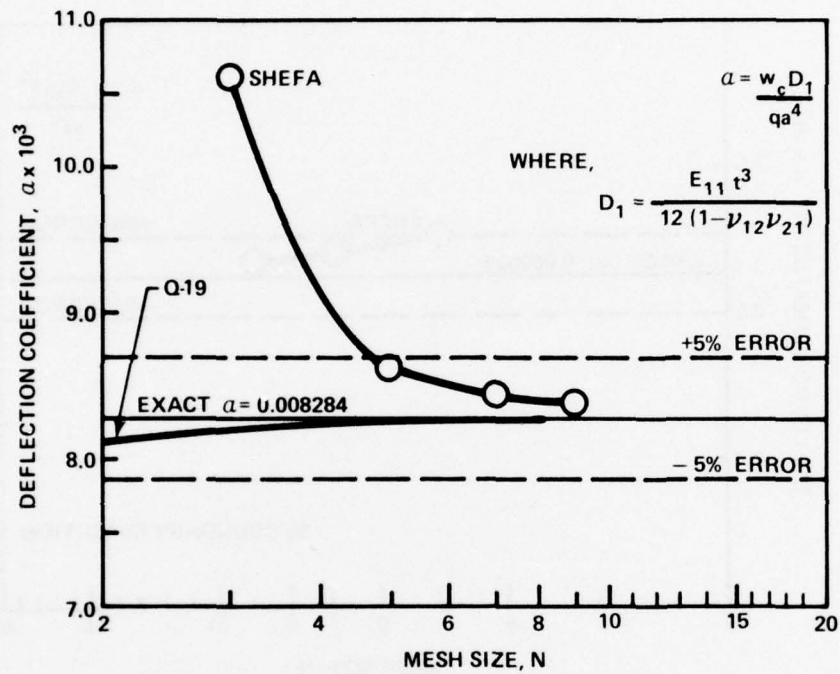


FIGURE 24 CONVERGENCE OF CENTRAL DEFLECTION VS. MESH SIZE FOR SIMPLY SUPPORTED ORTHOTROPIC PLATE UNDER UNIFORM LOAD

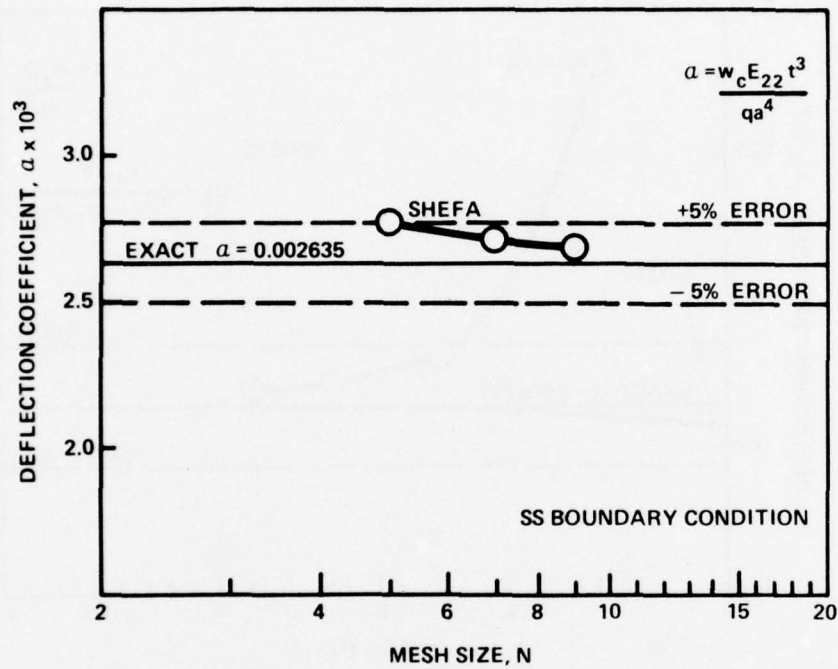


FIGURE 25 CONVERGENCE OF CENTRAL DEFLECTION VS. MESH SIZE FOR ANISOTROPIC PLATE (10 LAYER,  $\pm 30^\circ$  ANGLE-PLY COMPOSITE) UNDER UNIFORM LOAD

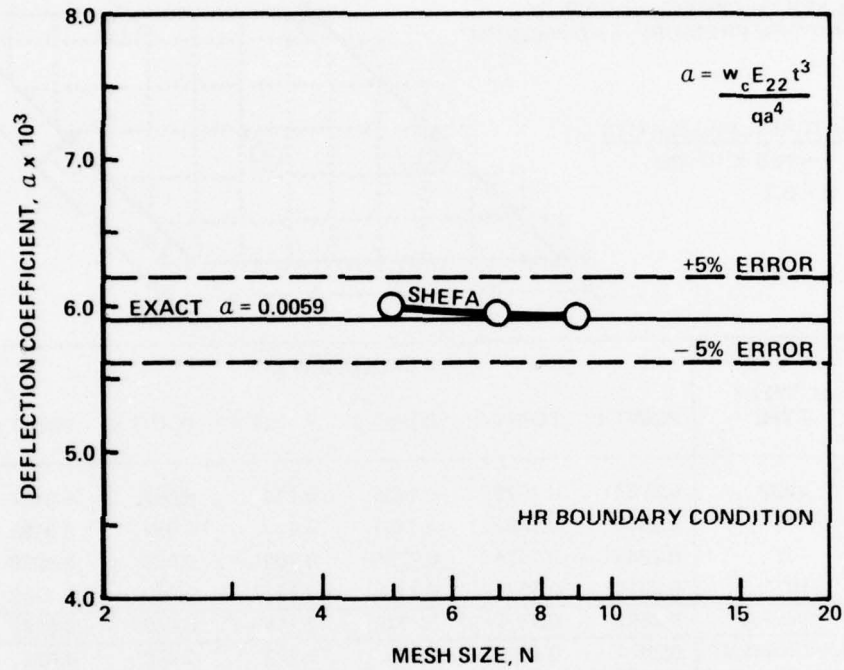


FIGURE 26 CONVERGENCE OF CENTRAL DEFLECTION VS. MESH SIZE FOR ANISOTROPIC PLATE (2 LAYER, CROSS PLY COMPOSITE) UNDER UNIFORM LOAD

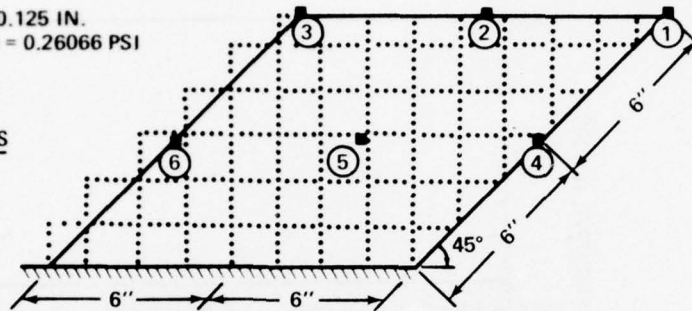


PLATE THICKNESS,  $t = 0.125$  IN.  
UNIFORM PRESSURE,  $q = 0.26066$  PSI

MATERIAL PROPERTIES

$E = 10.5 \times 10^6$  PSI

$\nu = 0.3$



ELEMENT TYPE	DEFLECTION AT					
	POINT 1	POINT 2	POINT 3	POINT 4	POINT 5	POINT 6
ACM	0.2962	0.1979	0.1135	0.114	0.052	0.0197
M	0.2938	0.1965	0.1181	0.113	0.051	0.0198
P	0.2786	0.1874	0.1155	0.108	0.050	0.0210
HCT	0.2814	0.1879	0.1108	0.1112	0.0491	0.0182
SHEFA	0.2853	0.1897	0.1120	0.1159	0.0499	0.0182
EXPERIMENT	0.297	0.204	0.121	0.129	0.056	0.022

FIGURE 27 DEFLECTION OF UNIFORMLY LOADED RHOMBIC CANTILEVER

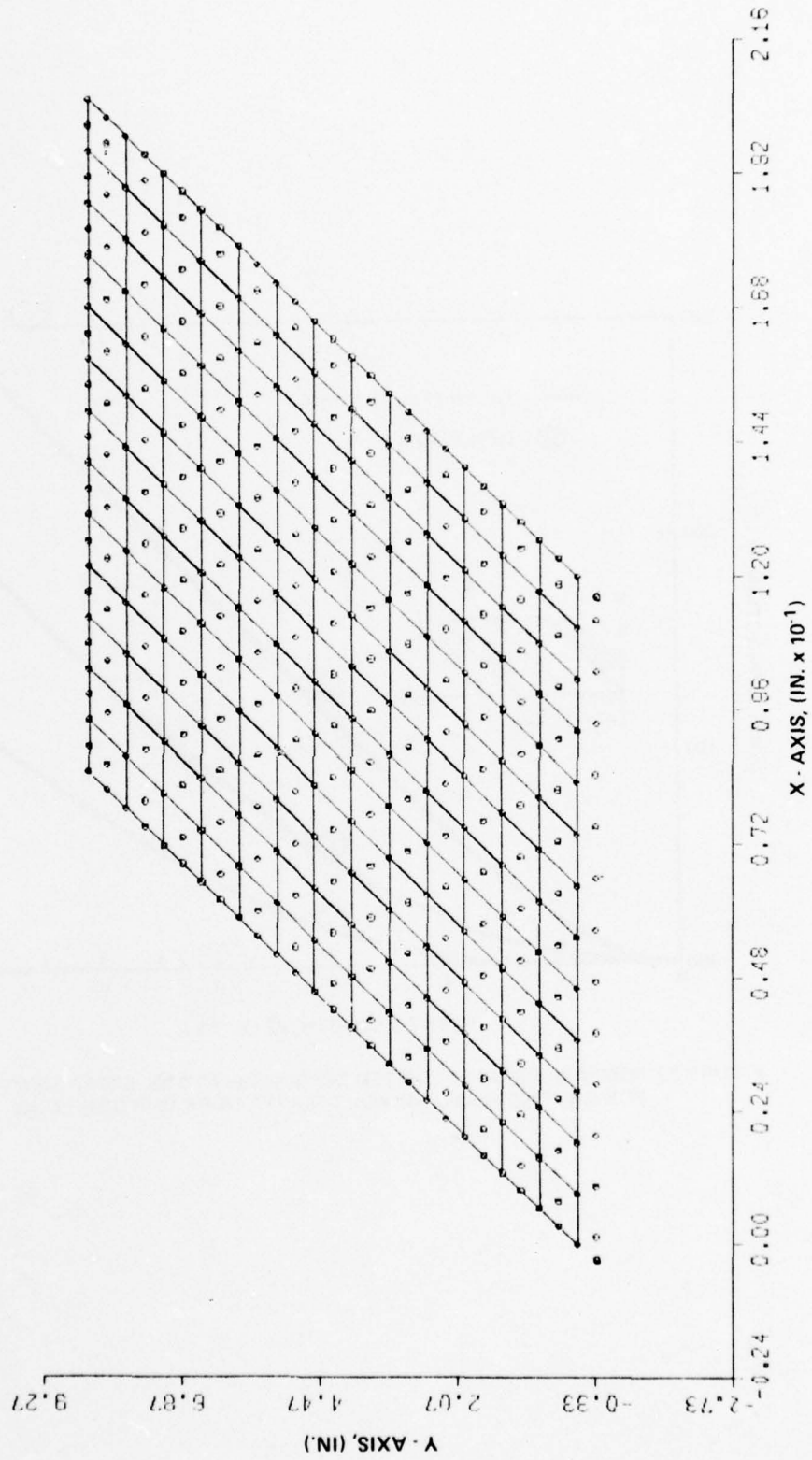


FIGURE 28 CANTILEVERED RHOMBIC PLATE, 13 x 13 MESH

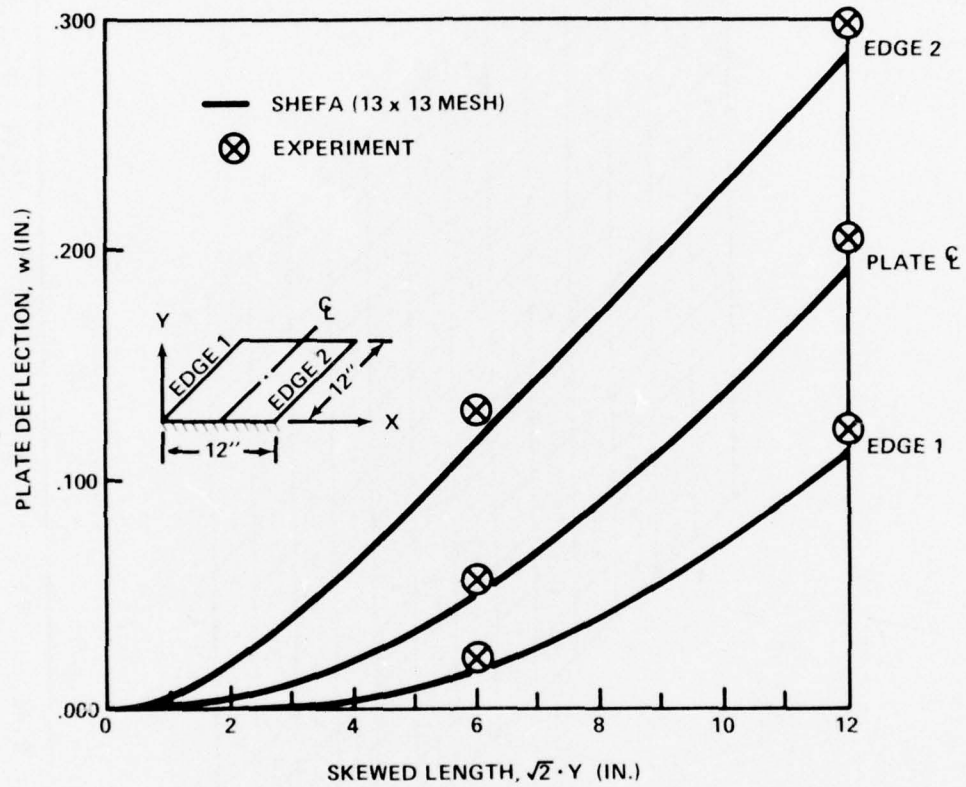
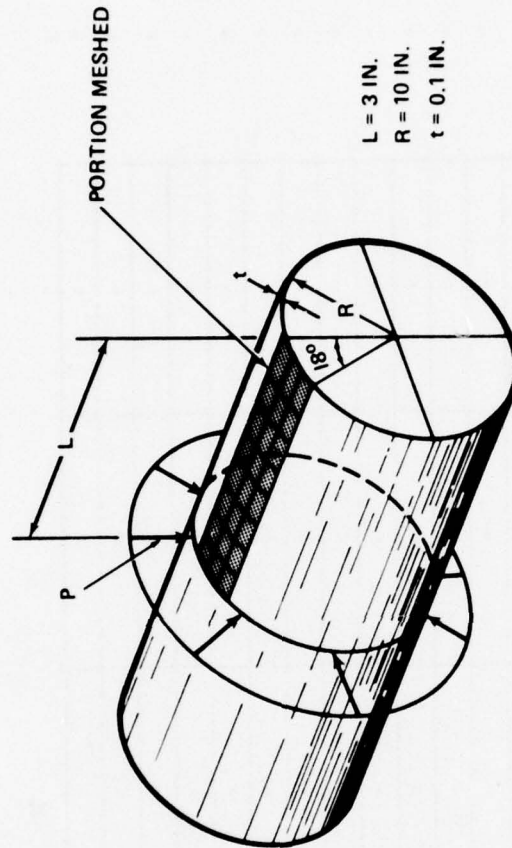


FIGURE 29 COMPARISON OF PREDICTED DISPLACEMENTS VS. EXPERIMENT FOR CANTILEVERED RHOMBIC PLATE UNDER UNIFORM LOAD



**MATERIAL  
PROPERTIES**  
 $E = 10 \times 10^6 \text{ PSI}$   
 $\nu = 0.3$

**BOUNDARY CONDITIONS  
ON PORTION MESHD**

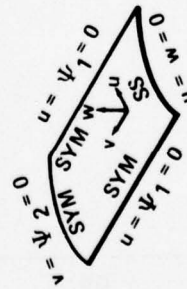


FIGURE 30 SUMMARY OF ANALYSIS CONDITIONS FOR CYLINDRICAL SHELL  
WITH CIRCUMFERENTIAL LINE LOAD



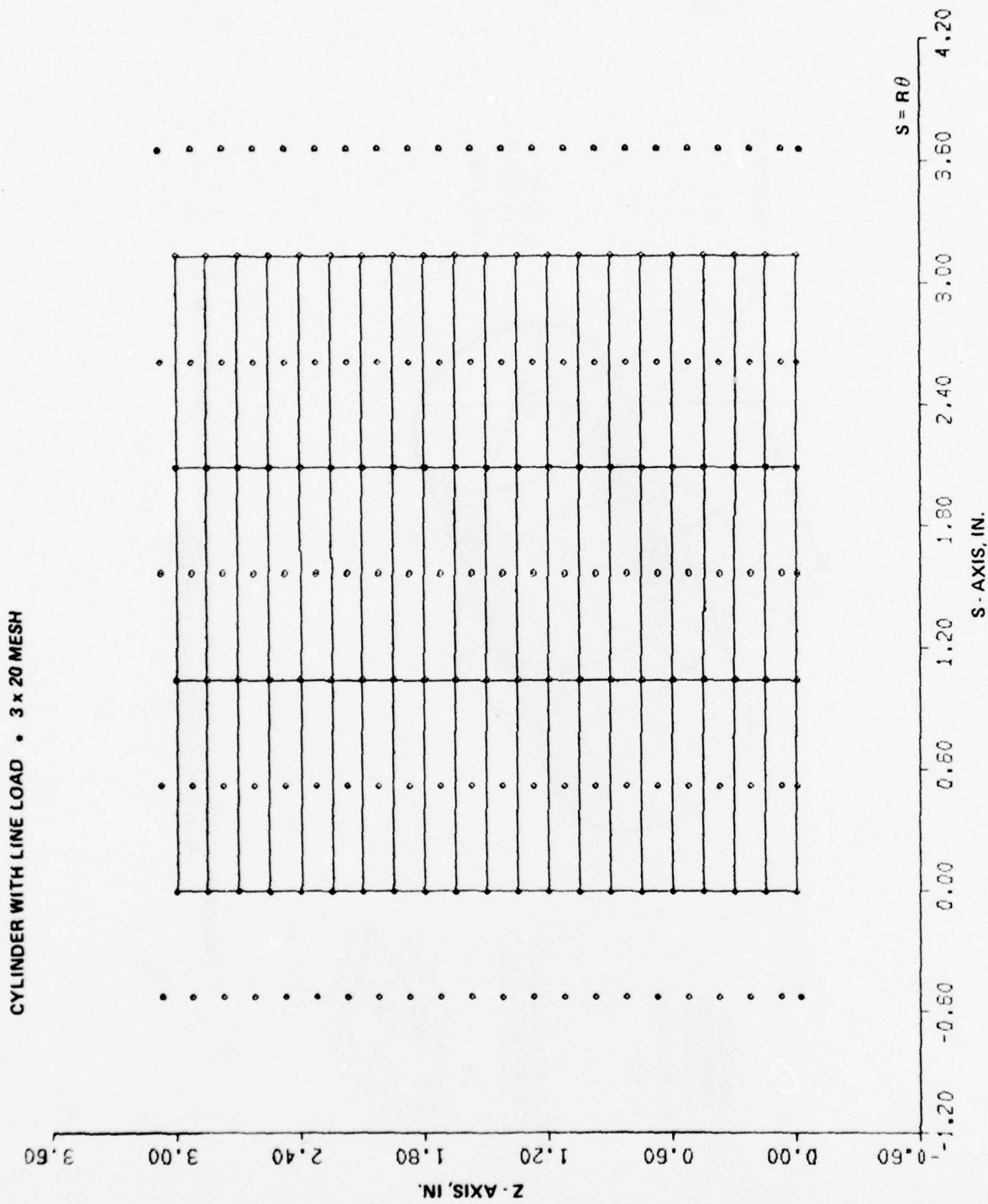


FIGURE 31 TYPICAL MESH FOR CYLINDRICAL SHELL BENDING PROBLEM

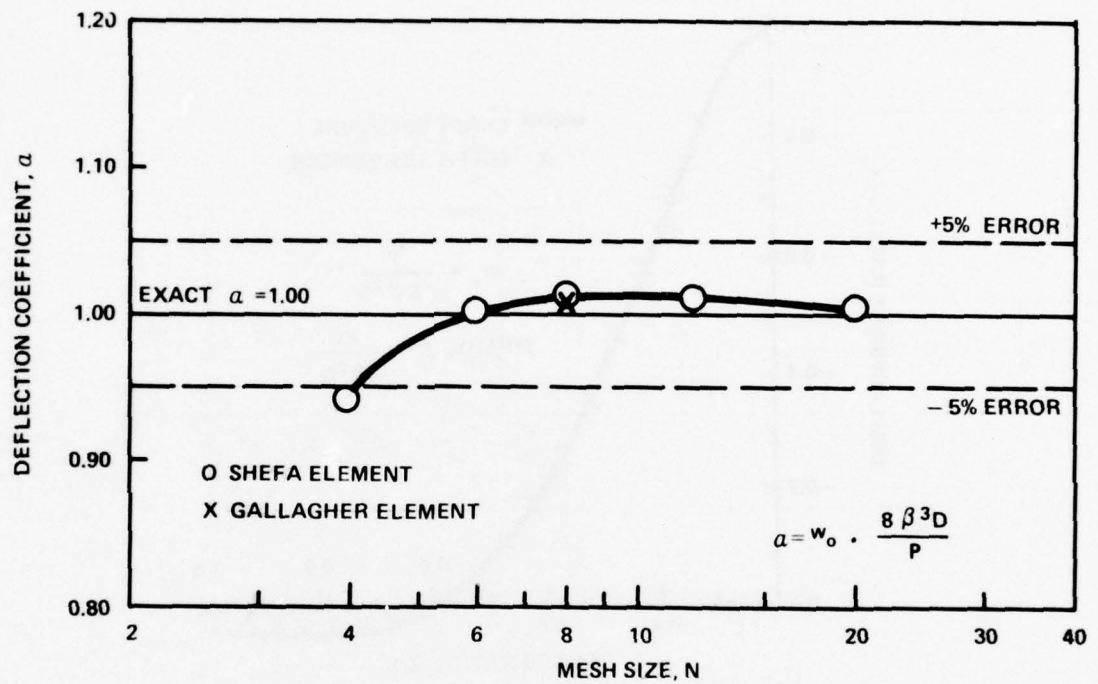


FIGURE 32 CONVERGENCE OF DEFLECTION UNDER LOAD VS. MESH SIZE FOR CYLINDRICAL SHELL WITH A LOAD UNIFORMLY DISTRIBUTED ALONG A CIRCULAR SECTION

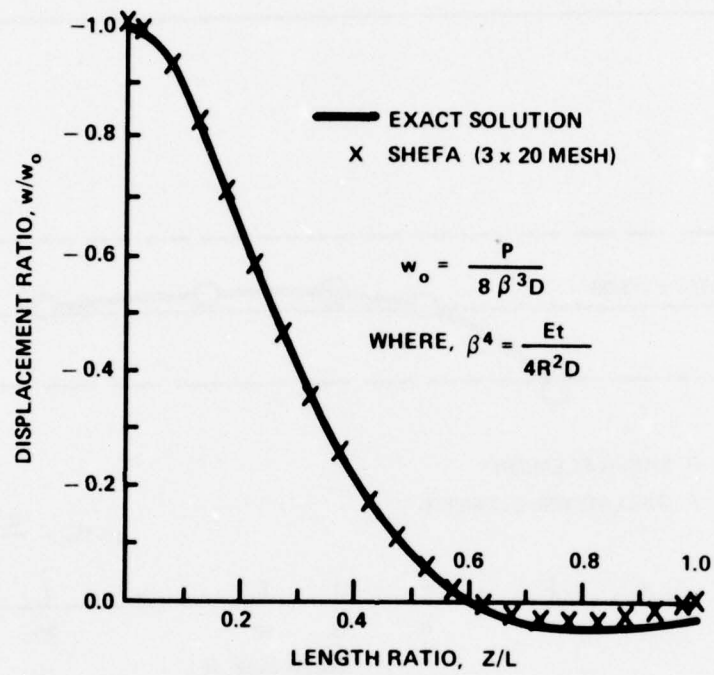


FIGURE 33 DISPLACEMENT DISTRIBUTION FOR CYLINDRICAL SHELL WITH A LOAD UNIFORMLY DISTRIBUTED ALONG A CIRCULAR SECTION

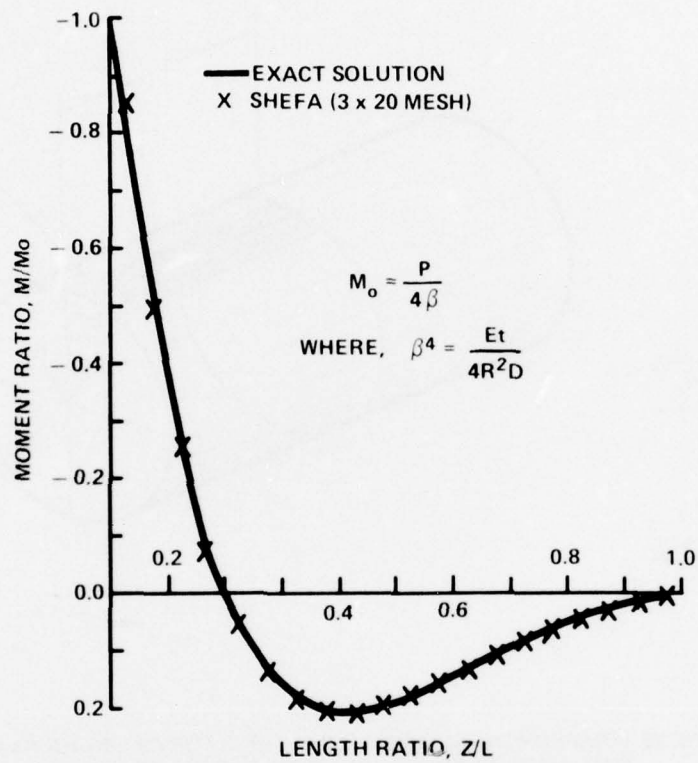


FIGURE 34 MOMENT DISTRIBUTION FOR CYLINDRICAL SHELL WITH A LOAD UNIFORMLY DISTRIBUTED ALONG A CIRCULAR SECTION



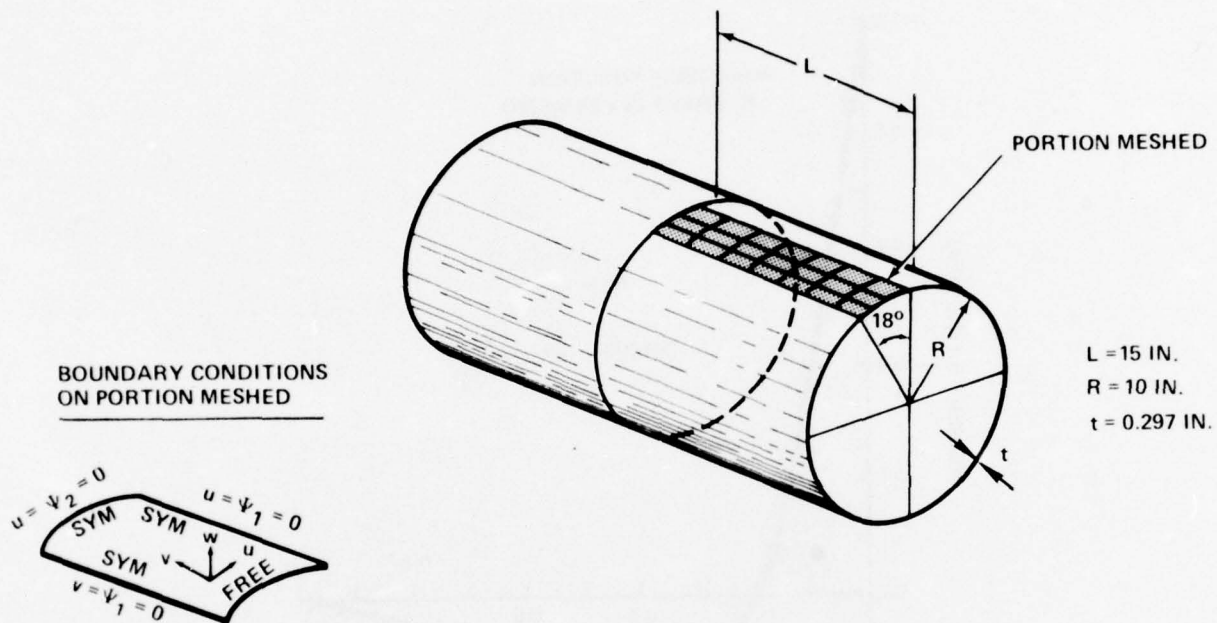


FIGURE 35 SUMMARY OF ANALYSIS CONDITIONS FOR CYLINDRICAL SHELL  
WITH NONLINEAR RADIAL TEMPERATURE GRADIENT

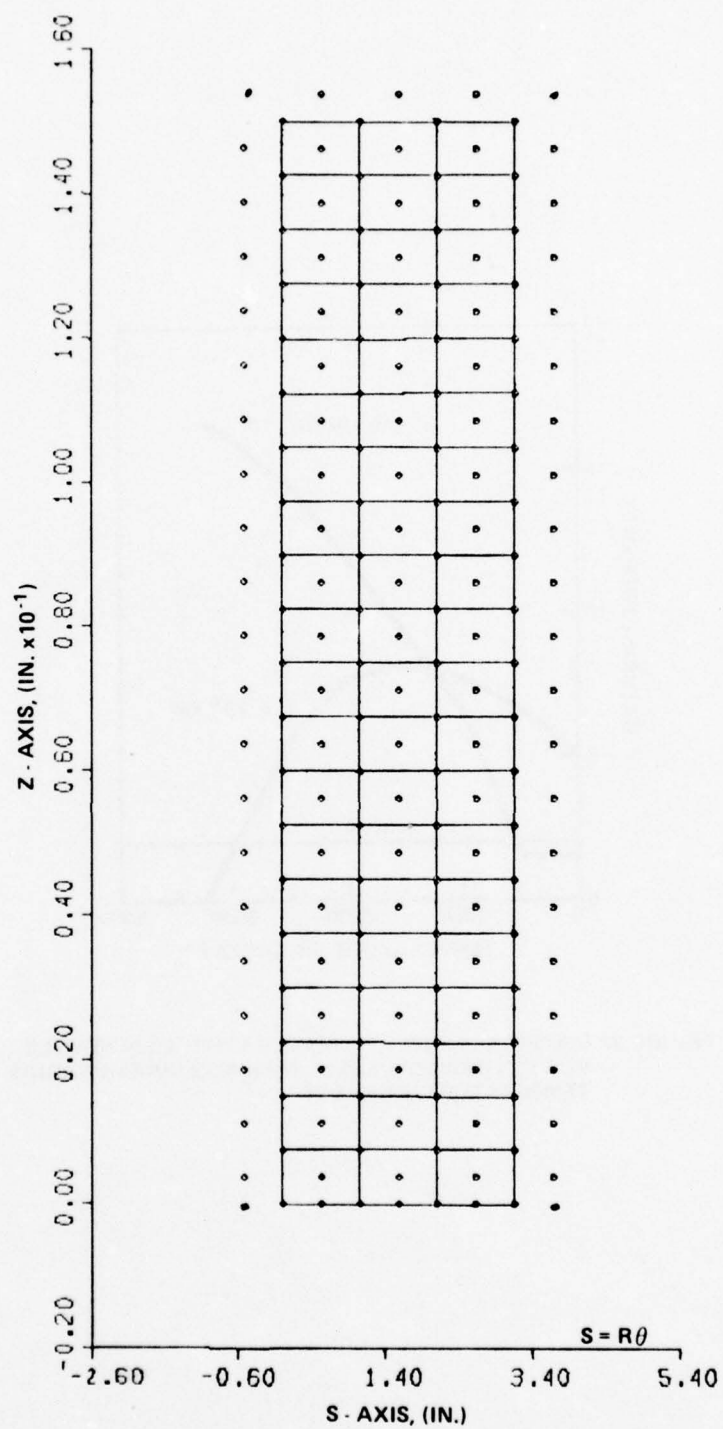


FIGURE 36 CYLINDER WITH NON LINEAR RADIAL TEMPERATURE GRADIENT,  $3 \times 20$  MESH

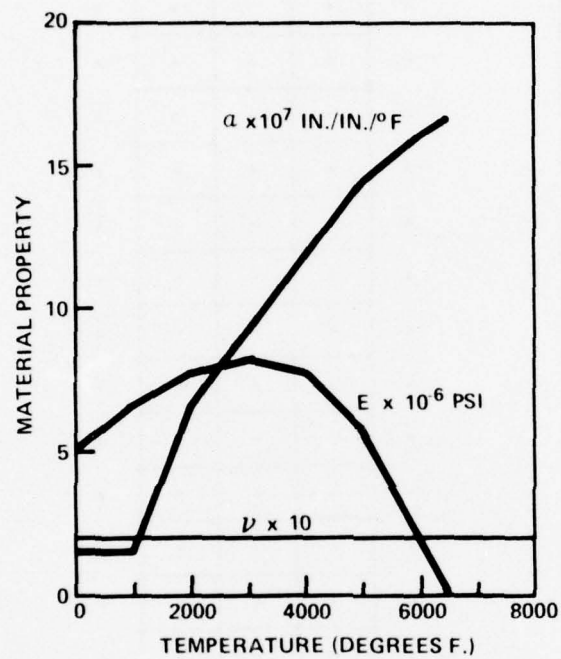


FIGURE 37 MATERIAL PROPERTY TEMPERATURE DEPENDENCE  
FOR CYLINDRICAL SHELL WITH NON LINEAR RADIAL  
TEMPERATURE GRADIENT

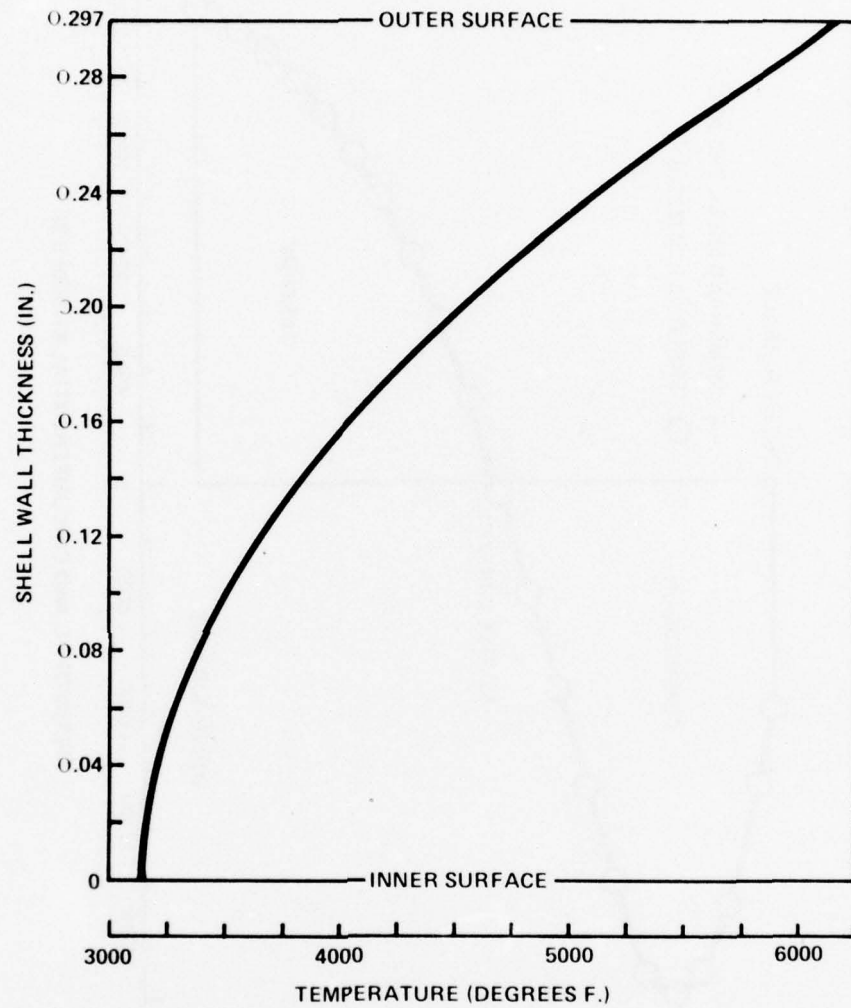


FIGURE 38 TEMPERATURE DISTRIBUTION THROUGH SHELL WALL FOR CYLINDRICAL SHELL WITH NONLINEAR RADIAL TEMPERATURE GRADIENT



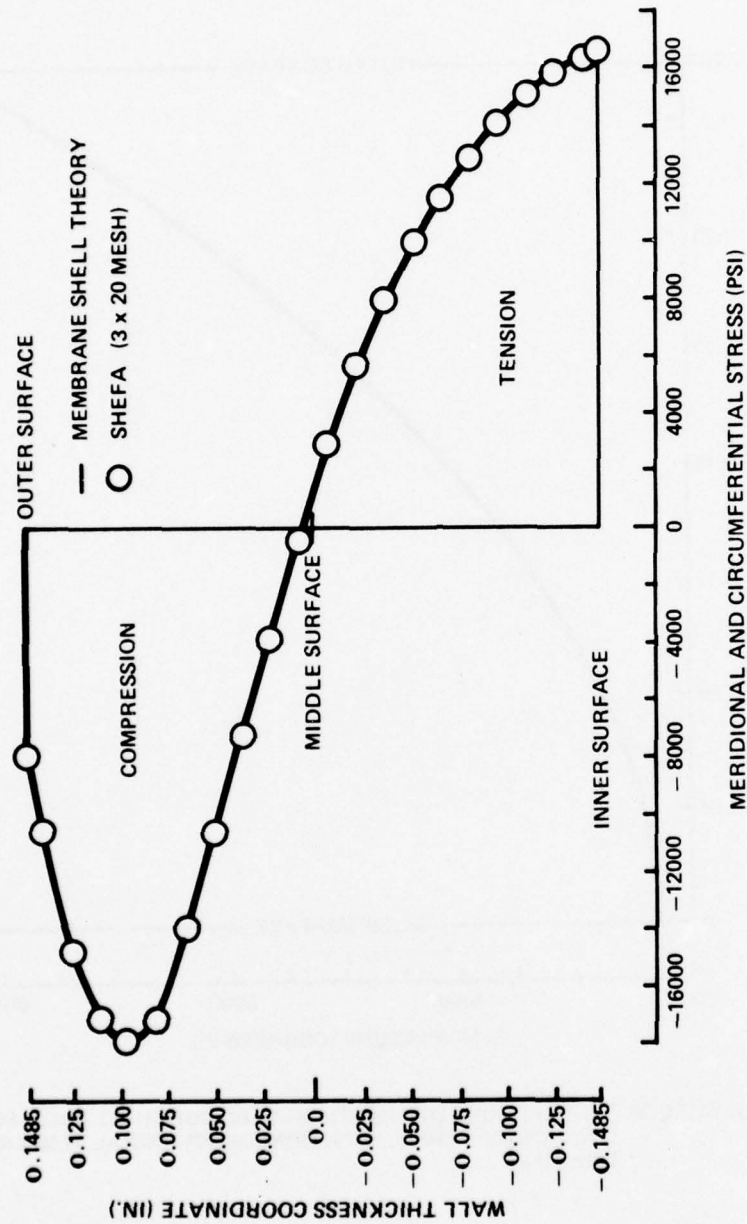


FIGURE 39 STRESS DISTRIBUTION THROUGH SHELL WALL FOR CYLINDRICAL SHELL WITH NON LINEAR RADIAL TEMPERATURE GRADIENT

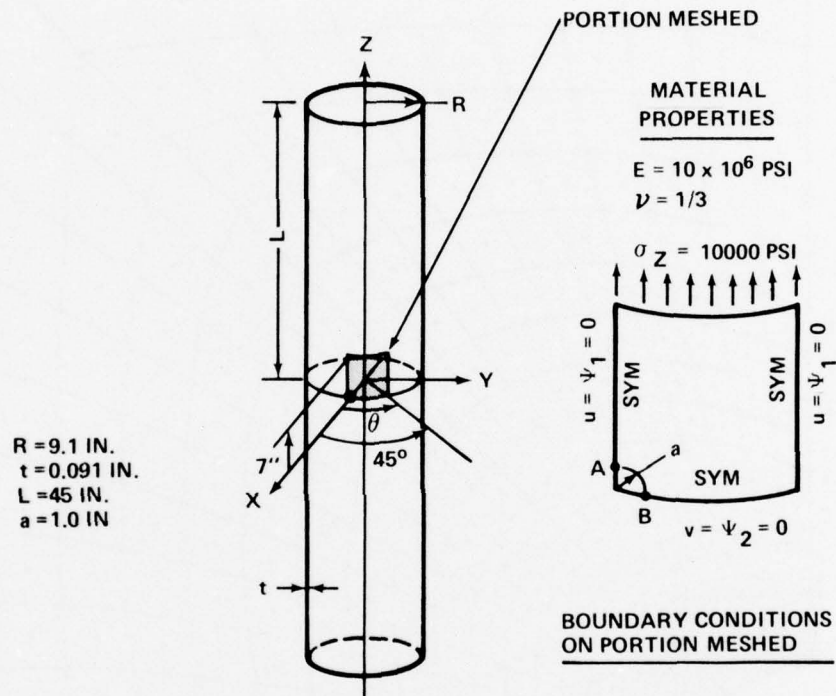


FIGURE 40 SUMMARY OF ANALYSIS CONDITIONS FOR CYLINDRICAL SHELL WITH CIRCULAR CUTOUT LOADED IN TENSION

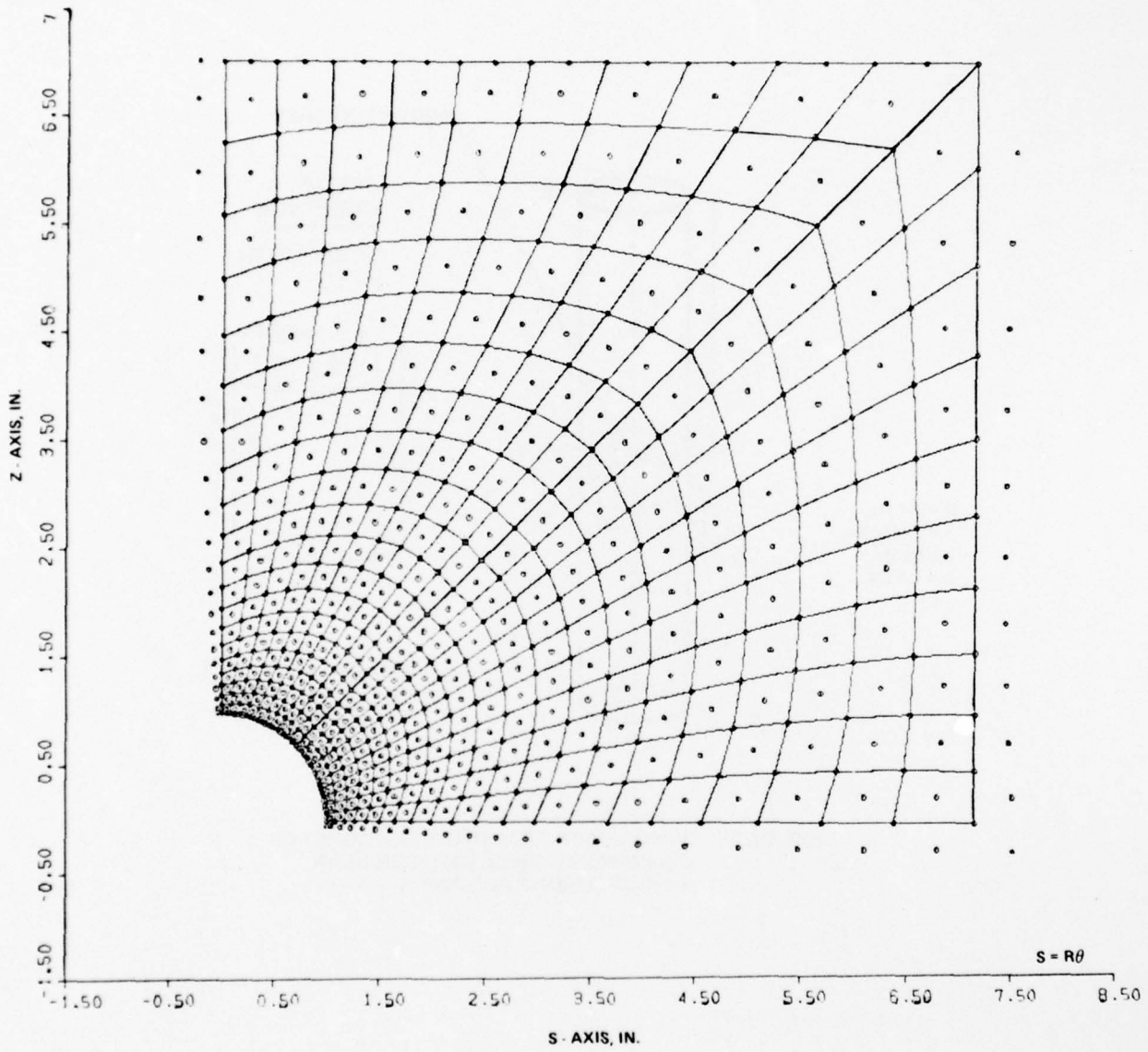


FIGURE 41 CYLINDRICAL SHELL WITH CIRCULAR CUTOUT 20 x 20 MESH

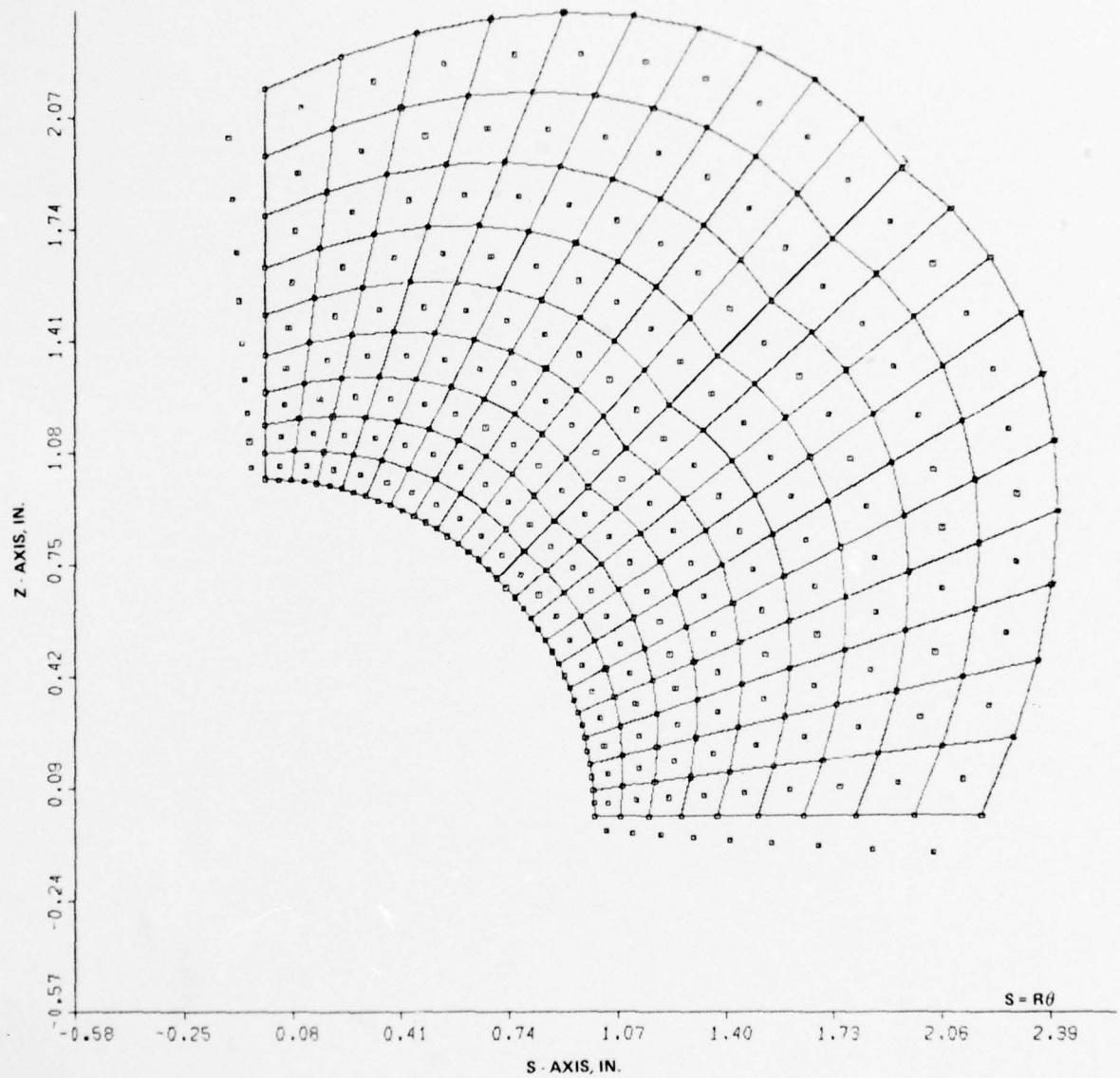


FIGURE 42 CYLINDRICAL SHELL WITH CIRCULAR CUTOUT,  
ENLARGEMENT OF 20 x 20 MESH IN  
VICINITY OF HOLE



## APPENDIX C

## DISCUSSION OF SHAPE FUNCTIONS

In this appendix the linear and quadratic shape functions will be derived in terms of curvilinear interpolating coordinates. The interpolating coordinates are defined at the local element level and are related to the Gaussian surface coordinates through transformations which were derived in Section IV.B.4.

It will be shown that the generalized interpolating procedure used to determine difference relations for arbitrary meshes reduces to the conventional finite difference formulas when the interpolating coordinates and surface coordinates are aligned.

## 1. Derivation of Linear Shape Functions

Let  $\phi(\lambda, \mu)$  be an arbitrary function and expand it in a Taylor's series\* about the centroid of the region shown in Figure C1-a,

$$\begin{aligned}\phi(\lambda, \mu) &= \phi^{\circ} + \lambda \phi,^{\circ}_{\lambda} + \mu \phi,^{\circ}_{\mu} \\ &\quad + \frac{1}{2} (\lambda^2 \phi,^{\circ}_{\lambda\lambda} + 2\lambda\mu \phi,^{\circ}_{\lambda\mu} + \mu^2 \phi,^{\circ}_{\mu\mu}) + O(\Delta)^3 \\ &= \phi^{\circ} + \lambda \phi,^{\circ}_{\lambda} + \mu \phi,^{\circ}_{\mu} + \lambda\mu \phi,^{\circ}_{\lambda\mu} + O(\Delta^2)\end{aligned}\tag{C.1}$$

---

\* The notation  $\phi^{\circ}$  corresponds to  $\phi(0,0)$  and  $\phi,^{\circ}_{\lambda}$  ... corresponds to  $\phi,^{\circ}_{\lambda}(0,0)$ , ...

Recasting in matrix form,

$$\phi(\lambda, \mu) = \{P_1\}^T \{A\} \quad (C.2)$$

where

$$\{P_1\}^T = [1, \lambda, \mu, \lambda\mu] \quad (C.3)$$

$$\begin{aligned} \{A\}^T &= [a_1, a_2, a_3, a_4] \\ &= [\phi^o, \phi^o, \lambda, \phi^o, \mu, \phi^o, \lambda\mu] \end{aligned} \quad (C.4)$$

Evaluating  $\phi(\lambda, \mu)$  at the four discrete points on the boundary of the region,

$$\begin{bmatrix} \phi^1 \\ \phi^2 \\ \phi^3 \\ \phi^4 \end{bmatrix} = \begin{bmatrix} 1 & -1 & -1 & 1 \\ 1 & 1 & -1 & -1 \\ 1 & 1 & 1 & 1 \\ 1 & -1 & 1 & -1 \end{bmatrix} \begin{bmatrix} a_1 \\ a_2 \\ a_3 \\ a_4 \end{bmatrix}$$

or,

$$\{\phi\} = [C] \{A\} \quad (C.5)$$

Solving for the generalized coordinates,

$$\{A\} = [C]^{-1}\{\phi\} \quad (C.6)$$

Substituting (C.6) into (C.2) results in the interpolating equation,

$$\begin{aligned} \phi(\lambda, \mu) &= \{P_1\}^T [C]^{-1} \{\phi\} \\ &= [L(\lambda, \mu)] \{\phi\} \end{aligned} \quad (C.7)$$

where,

$$[C]^{-1} = \frac{1}{4} \begin{bmatrix} 1 & 1 & 1 & 1 \\ -1 & 1 & 1 & -1 \\ -1 & -1 & 1 & 1 \\ 1 & -1 & 1 & -1 \end{bmatrix} \quad (C.8)$$

$$\begin{aligned} [L(\lambda, \mu)] &= [L_1, L_2, L_3, L_4] \\ &= \{P_1\}^T [C]^{-1} \end{aligned} \quad (C.9)$$

Equation (C.9) defines the linear shape functions used in Section IV.B.4 to approximate the tangential displacement fields.

## 2. Interpretation of Generalized Coordinates for Linear Shape Functions

The generalized coordinates associated with the linear shape functions are,

$$\{A\} = [C]^{-1}\{\phi\} \quad (C.10)$$

From (C.10) the following finite difference formulas are obtained,

$$\begin{aligned} a_1 = \phi^o &= \frac{1}{4} (\phi^1 + \phi^2 + \phi^3 + \phi^4) \\ &= [L(o,o)]\{\phi\} \end{aligned} \quad (C.11)$$

$$\begin{aligned} a_2 = \phi_{,\lambda}^o &= \frac{1}{2} \left( \frac{1}{2}(\phi^2 + \phi^3) - \frac{1}{2}(\phi^4 + \phi^1) \right) \\ &= [L_{,\lambda}(o,o)]\{\phi\} \end{aligned} \quad (C.12)$$

$$\begin{aligned} a_3 = \phi_{,\mu}^o &= \frac{1}{2} \left( \frac{1}{2}(\phi^3 + \phi^4) - \frac{1}{2}(\phi^2 + \phi^1) \right) \\ &= [L_{,\mu}(o,o)]\{\phi\} \end{aligned} \quad (C.13)$$

$$\begin{aligned} a_4 = \phi_{,\lambda\mu}^o &= \frac{1}{2} \left( \frac{1}{2}(\phi^3 + \phi^1) - \frac{1}{2}(\phi^4 + \phi^2) \right) \\ &= [L_{,\lambda\mu}(o,o)]\{\phi\} \end{aligned} \quad (C.14)$$

The generalized coordinates thus correspond to the familiar central difference formulas for approximating a variable and its spatial derivatives at the centroid of a square region. When the element boundaries in Figure C1-a coincide with the surface coordinate lines, the mapping plane is undistorted ( $\lambda, \mu$  and  $x^1, x^2$  are aligned) and the interpolating procedure used to determine difference relations for arbitrary meshes



reduces to the conventional finite difference approach using regular, coordinate line meshes.

### 3. Derivation of Quadratic Shape Functions

Let  $\phi(\alpha, \beta)$  be an arbitrary function and expand it in a Taylor's series about the central point labeled 1 of the region shown in Figure C1-b,

$$\begin{aligned}
 \phi(\alpha, \beta) &= \phi^0 + \alpha \phi_{,\alpha}^0 + \beta \phi_{,\beta}^0 \\
 &+ \frac{1}{2} [\alpha^2 \phi_{,\alpha\alpha}^0 + 2\alpha\beta \phi_{,\alpha\beta}^0 + \beta^2 \phi_{,\beta\beta}^0] \\
 &+ \frac{1}{6} [\alpha^3 \phi_{,\alpha\alpha\alpha}^0 + 3\alpha^2\beta \phi_{,\alpha\alpha\beta}^0 + 3\alpha\beta^2 \phi_{,\alpha\beta\beta}^0 + \beta^3 \phi_{,\beta\beta\beta}^0] \\
 &+ \frac{1}{24} [\alpha^4 \phi_{,\alpha\alpha\alpha\alpha}^0 + 4\alpha^3\beta \phi_{,\alpha\alpha\alpha\beta}^0 + 6\alpha^2\beta^2 \phi_{,\alpha\alpha\beta\beta}^0 \\
 &\quad + 4\alpha\beta^3 \phi_{,\alpha\beta\beta\beta}^0 + \beta^4 \phi_{,\beta\beta\beta\beta}^0] + O(\Delta^5) \\
 &= \phi^0 + \alpha \phi_{,\alpha}^0 + \beta \phi_{,\beta}^0 \\
 &+ \frac{1}{2} \alpha^2 \phi_{,\alpha\alpha}^0 + \alpha\beta \phi_{,\alpha\beta}^0 + \frac{1}{2} \beta^2 \phi_{,\beta\beta}^0 \\
 &+ \frac{1}{2} \alpha^2\beta \phi_{,\alpha\alpha\beta}^0 + \frac{1}{2} \alpha\beta^2 \phi_{,\alpha\beta\beta}^0 \\
 &+ \frac{1}{4} \alpha^2\beta^2 \phi_{,\alpha\alpha\beta\beta}^0 + O(\Delta^3) \tag{C.15}
 \end{aligned}$$

Recasting in matrix form,

$$\phi(\alpha, \beta) = \{P_2\}^T \{B\} \tag{C.16}$$

where,

$$\{P_2\}^T = [1, \alpha, \beta, \alpha^2, \alpha\beta, \beta^2, \alpha^2\beta, \alpha\beta^2, \alpha^2\beta^2] \quad (C.17)$$

$$\begin{aligned} \{B\}^T &= [b_1, b_2, \dots, b_9] \\ &= [\phi^\circ, \phi^\circ_{,\alpha}, \phi^\circ_{,\beta}, \frac{1}{2}\phi^\circ_{,\alpha\alpha}, \phi^\circ_{,\alpha\beta}, \frac{1}{2}\phi^\circ_{,\beta\beta}, \\ &\quad \frac{1}{2}\phi^\circ_{,\alpha\alpha\beta}, \frac{1}{2}\phi^\circ_{,\alpha\beta\beta}, \frac{1}{4}\phi^\circ_{,\alpha\alpha\beta\beta}] \end{aligned} \quad (C.18)$$

Evaluating  $\phi(\alpha, \beta)$  at the nine discrete points defined over the region,

$$\begin{bmatrix} \phi^1 \\ \phi^2 \\ \phi^3 \\ \phi^4 \\ \phi^5 \\ \phi^6 \\ \phi^7 \\ \phi^8 \\ \phi^9 \end{bmatrix} = \begin{bmatrix} 1 & 0 & 0 & 0 & 0 & 0 & 0 & 0 & 0 \\ 1 & -1 & -1 & 1 & 1 & 1 & -1 & -1 & 1 \\ 1 & 0 & -1 & 0 & 0 & 1 & 0 & 0 & 0 \\ 1 & 1 & -1 & 1 & -1 & 1 & -1 & 1 & 1 \\ 1 & 1 & 0 & 1 & 0 & 0 & 0 & 0 & 0 \\ 1 & 1 & 1 & 1 & 1 & 1 & 1 & 1 & 1 \\ 1 & 0 & 1 & 0 & 0 & 1 & 0 & 0 & 0 \\ 1 & -1 & 1 & 1 & -1 & 1 & 1 & -1 & 1 \\ 1 & -1 & 0 & 1 & 0 & 0 & 0 & 0 & 0 \end{bmatrix} \begin{bmatrix} b_1 \\ b_2 \\ b_3 \\ b_4 \\ b_5 \\ b_6 \\ b_7 \\ b_8 \\ b_9 \end{bmatrix}$$

or,

$$\{\phi\} = [D] \{B\} \quad (C.19)$$

Solving for the generalized coordinates,

$$\{B\} = [D]^{-1}\{\phi\} \quad (C.20)$$

Substituting (C.20) into (C.16) results in the interpolating equation,

$$\begin{aligned} \phi(\alpha, \beta) &= \{P_2\}^T [D]^{-1} \{\phi\} \\ &= [H(\alpha, \beta)] \{\phi\} \end{aligned} \quad (C.21)$$

where,

$$[D]^{-1} = \frac{1}{4} \begin{bmatrix} 4 & 0 & 0 & 0 & 0 & 0 & 0 & 0 & 0 \\ 0 & 0 & 0 & 0 & 2 & 0 & 0 & 0 & -2 \\ 0 & 0 & -2 & 0 & 0 & 0 & 2 & 0 & 0 \\ -4 & 0 & 0 & 0 & 2 & 0 & 0 & 0 & 2 \\ 0 & 1 & 0 & -1 & 0 & 1 & 0 & -1 & 0 \\ -4 & 0 & 2 & 0 & 0 & 0 & 2 & 0 & 0 \\ 0 & -1 & 2 & -1 & 0 & 1 & -2 & 1 & 0 \\ 0 & -1 & 0 & 1 & -2 & 1 & 0 & -1 & 2 \\ 4 & 1 & -2 & 1 & -2 & 1 & -2 & 1 & -2 \end{bmatrix} \quad (C.22)$$

$$\begin{aligned} [H(\alpha, \beta)] &= [H_1, H_2, \dots, H_9] \\ &= \{P_2\}^T [D]^{-1} \end{aligned} \quad (C.23)$$

Equation (C.23) defines the quadratic shape functions used in Section IV.B.4 to approximate the displacement field for the normal component of deflection.

#### 4. Interpretation of Generalized Coordinates for Quadratic Shape Functions

The generalized coordinates associated with the quadratic shape functions are,

$$\{B\} = [D]^{-1}\{\phi\} \quad (C.24)$$

From (C.24) the following finite difference formulas are obtained,

$$\begin{aligned} b_1 &= \phi^o = \phi^1 \\ &= [H(o,o)]\{\phi\} \end{aligned} \quad (C.25)$$

$$\begin{aligned} b_2 &= \phi^o_{,\alpha} = \frac{1}{2}(\phi^5 - \phi^9) \\ &= [H_{,\alpha}(o,o)]\{\phi\} \end{aligned} \quad (C.26)$$

$$\begin{aligned} b_3 &= \phi^o_{,\beta} = \frac{1}{2}(\phi^7 - \phi^3) \\ &= [H_{,\beta}(o,o)]\{\phi\} \end{aligned} \quad (C.27)$$

$$\begin{aligned} 2b_4 &= \phi^o_{,\alpha\alpha} = (\phi^5 - 2\phi^1 + \phi^9) \\ &= [H_{,\alpha\alpha}(o,o)]\{\phi\} \end{aligned} \quad (C.28)$$

$$\begin{aligned} b_5 &= \phi^o_{,\alpha\beta} = \frac{1}{4}(\phi^2 - \phi^4 + \phi^6 - \phi^8) \\ &= [H_{,\alpha\beta}(o,c)]\{\phi\} \end{aligned} \quad (C.29)$$



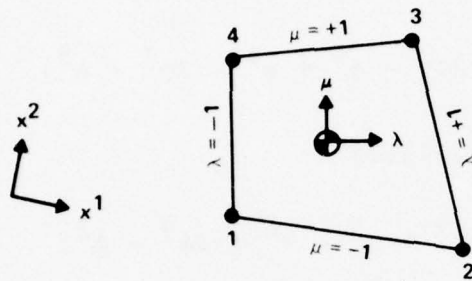
$$\begin{aligned}
 2b_6 = \phi_{,\beta\beta}^o &= (\phi^7 - 2\phi^1 + \phi^3) \\
 &= [H_{,\beta\beta}(o,o)]\{\phi\}
 \end{aligned} \tag{C.30}$$

$$\begin{aligned}
 2b_7 = \phi_{,\alpha\alpha\beta}^o &= \frac{1}{2}(-\phi^2 + 2\phi^3 - \phi^4 + \phi^6 - 2\phi^7 + \phi^8) \\
 &= [H_{,\alpha\alpha\beta}(o,o)]\{\phi\}
 \end{aligned} \tag{C.31}$$

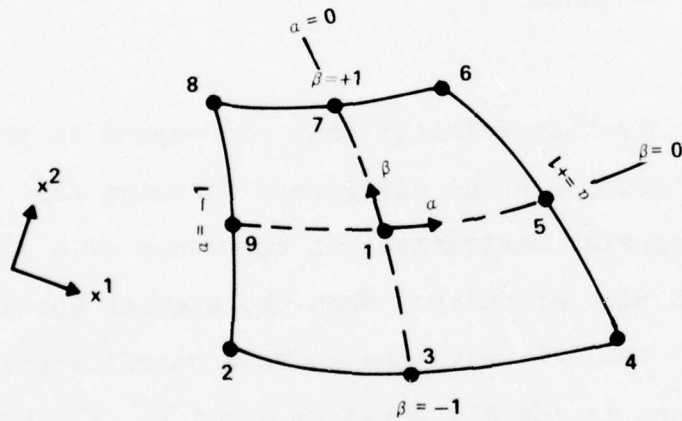
$$\begin{aligned}
 2b_8 = \phi_{,\alpha\beta\beta}^o &= \frac{1}{2}(\phi^4 - 2\phi^5 + \phi^6 - \phi^8 + 2\phi^9 - \phi^2) \\
 &= [H_{,\alpha\beta\beta}(o,o)]\{\phi\}
 \end{aligned} \tag{C.32}$$

$$\begin{aligned}
 4b_9 = \phi_{,\alpha\alpha\beta\beta}^o &= (\phi^2 - 2\phi^3 - \phi^4 + 2\phi^5 + \phi^6 - 2\phi^7 + \phi^8 - 2\phi^9 + 4\phi^1) \\
 &= [H_{,\alpha\alpha\beta\beta}(o,o)]\{\phi\}
 \end{aligned} \tag{C.33}$$

The generalized coordinates thus correspond to the familiar three point central difference formulas for approximating spatial derivatives at the nodes of a square net with a mesh side of unity. When the element boundaries in Figure C1-b coincide with the surface coordinate lines, the mapping plane is not distorted ( $\alpha, \beta$  and  $x^1, x^2$  are aligned) and the interpolating procedure used to determine difference relations for arbitrary meshes reduces to the conventional finite difference approach using regular coordinate line meshes.



A. REGION OVER WHICH LINEAR SHAPE FUNCTIONS ARE DEFINED



B. REGION OVER WHICH QUADRATIC SHAPE FUNCTIONS ARE DEFINED

FIGURE C.1 SHAPE FUNCTION DOMAINS

## APPENDIX D

INVERSE FUNCTIONAL RELATIONSHIP BETWEEN SURFACE  
COORDINATES AND PARAMETRIC INTERPOLATING  
COORDINATES

At a specific point in the shape function domain defined by the surface coordinates,  $x_*^1, x_*^2$ , it is sometimes necessary to know the corresponding values of the curvilinear interpolating coordinates,  $\alpha_*, \beta_*$ , (see Figure D.1). Since the curvilinear interpolating coordinates cannot be explicitly related to the Gaussian surface coordinates for an arbitrary point in the shape function domain, it is necessary to resort to a numerical procedure.

## 1. Newton's Method

Any variable for which a number of discrete values are defined over some domain may be interpolated by the shape function relationship,

$$\phi(\alpha, \beta) = [N_L(\alpha, \beta)]\{\phi_L\} \quad (D.1)$$

where,

$[N_L(\alpha, \beta)]$  = Shape functions

$\{\phi_L\}$  = Discrete values of the variable

$\alpha, \beta$  = Parametric interpolating coordinates

If  $x_*^1, x_*^2$  are the surface coordinates of some point at which it is desired to know the corresponding local coordinates,  $\alpha_*, \beta_*$ , then Newton's method may be employed to solve for  $\alpha_*, \beta_*$ . The method is as follows.

Let the variation of surface coordinates over the element domain be approximated by the shape functions (see Figure D.1),

$$x^1 = [N_L(\alpha, \beta)] \{x_L^1\} \quad (D.2)$$

$$x^2 = [N_L(\alpha, \beta)] \{x_L^2\} \quad (D.3)$$

The nonlinear equations in  $\alpha$  and  $\beta$  for which the roots are desired are then,

$$f_1(\alpha, \beta) = x_*^1 - [N_L]\{x_L^1\} = \Delta x^1 = 0 \quad (D.4)$$

$$f_2(\alpha, \beta) = x_*^2 - [N_L]\{x_L^2\} = \Delta x^2 = 0 \quad (D.5)$$

The iteration is then,

$$\begin{aligned} \alpha_k &= \alpha_{k-1} + \Delta\alpha_k \\ \beta_k &= \beta_{k-1} + \Delta\beta_k \end{aligned} \quad (D.6)$$

The corrections  $(\Delta\alpha_k, \Delta\beta_k)$  are obtained from the equations,



$$\begin{bmatrix} f_{1,\alpha} & f_{1,\beta} \\ f_{2,\alpha} & f_{2,\beta} \end{bmatrix} \begin{Bmatrix} \Delta\alpha \\ \Delta\beta \end{Bmatrix} = \begin{Bmatrix} -f_1 \\ -f_2 \end{Bmatrix} \quad (D.7)$$

or in alternative notation,

$$\begin{bmatrix} x_{,\alpha}^1 & x_{,\beta}^1 \\ x_{,\alpha}^2 & x_{,\beta}^2 \end{bmatrix} \begin{Bmatrix} \Delta\alpha \\ \Delta\beta \end{Bmatrix} = \begin{Bmatrix} \Delta x^1 \\ \Delta x^2 \end{Bmatrix} \quad (D.8)$$

Since,

$$\begin{aligned} f_{1,\alpha} &= -[N_{L,\alpha}]\{x_L^1\} = -x_{,\alpha}^1 \\ f_{1,\beta} &= -[N_{L,\beta}]\{x_L^1\} = -x_{,\beta}^1 \\ f_{2,\alpha} &= -[N_{L,\alpha}]\{x_L^2\} = -x_{,\alpha}^2 \\ f_{2,\beta} &= -[N_{L,\beta}]\{x_L^2\} = -x_{,\beta}^2 \end{aligned} \quad (D.9)$$

Solving (D.8) for the corrections,

$$\Delta\alpha = \frac{1}{J_O^T} [x_{,\beta}^2 \cdot \Delta x^1 - x_{,\beta}^1 \cdot \Delta x^2] \quad (D.10)$$

$$\Delta\beta = \frac{1}{J_O^T} [x_{,\alpha}^1 \cdot \Delta x^2 - x_{,\alpha}^2 \cdot \Delta x^1] \quad (D.11)$$

$$J_O^T = [x_{,\alpha}^1 \cdot x_{,\beta}^2 - x_{,\beta}^1 \cdot x_{,\alpha}^2] \quad (D.12)$$

For any desired point ( $x^1 = x_*^1$ ,  $x^2 = x_*^2$ ) the corresponding local coordinates ( $\alpha = \alpha_*$ ,  $\beta = \beta_*$ ) are determined by the iteration,

$$\begin{pmatrix} \alpha \\ \beta \end{pmatrix}_K = \begin{pmatrix} \alpha \\ \beta \end{pmatrix}_{K-1} + \begin{pmatrix} \Delta\alpha \\ \Delta\beta \end{pmatrix}_K \quad (D.13)$$

The iteration is started with  $\alpha_1 = 0$ ,  $\beta_1 = 0$  and is assumed to converge to the desired values,  $\alpha_*$ ,  $\beta_*$ , when

$$\begin{pmatrix} \alpha \\ \beta \end{pmatrix}_K - \begin{pmatrix} \alpha \\ \beta \end{pmatrix}_{K-1} < \begin{pmatrix} \epsilon \\ \epsilon \end{pmatrix} \quad (D.14)$$

For  $\epsilon = 10^{-6}$  the method usually converges in 3-6 iterations.

## 2. Procedure for Inverse Interpolation of the Linear Shape Functions

For efficiency in programming Newton's method for automatic computation the form will be slightly altered from that previously derived.

The variables  $\Delta x^1$  can be computed as follows,

$$\begin{aligned}
\Delta x^i &= x_*^i - [N_L]\{x_L^i\} \\
&= x_*^i - [P_L]\{A_L^i\} \quad \begin{array}{l} i = 1, 2 \\ L = 1, \dots, 4 \end{array} \quad (D.15)
\end{aligned}$$

where the index  $i$  corresponds to the two surface coordinates, the index  $L$  corresponds to the four labeled nodes of Figure D.1-a and:

$$\{x_L^i\}^T = [x_1^i, x_2^i, x_3^i, x_4^i] \quad (D.16)$$

$$[P_L] = [1, \alpha, \beta, \alpha\beta] \quad (D.17)$$

$$\{A_L^i\}^T = [a_1^i, a_2^i, a_3^i, a_4^i] \quad (D.18)$$

$$\begin{aligned}
a_1^i &= \frac{1}{4}(x_1^i + x_2^i + x_3^i + x_4^i) \\
a_2^i &= \frac{1}{4}(-x_1^i + x_2^i + x_3^i - x_4^i) \\
a_3^i &= \frac{1}{4}(-x_1^i - x_2^i + x_3^i + x_4^i) \\
a_4^i &= \frac{1}{4}(x_1^i - x_2^i + x_3^i - x_4^i) \quad (D.19)
\end{aligned}$$

Substituting (D.17), (D.18) and (D.19) into (D.15),

$$\Delta x^i = x_*^i - a_1^i - a_2^i \alpha - a_3^i \beta - a_4^i \alpha\beta \quad (D.20)$$

The variables  $x_{,\alpha}^i$  and  $x_{,\beta}^i$  are computed as follows,

$$\begin{aligned}
 x_{,\alpha}^1 &= [N_{L,\alpha}]\{x_L^1\} \\
 &= [P_{L,\alpha}]\{A_L^1\}
 \end{aligned}
 \tag{D.21}$$

$$\begin{aligned}
 x_{,\beta}^1 &= [N_{L,\beta}]\{x_L^1\} \\
 &= [P_{L,\beta}]\{A_L^1\}
 \end{aligned}
 \tag{D.22}$$

where,

$$[P_{L,\alpha}] = [0, 1, 0, \beta] \tag{D.23}$$

$$[P_{L,\beta}] = [0, 0, 1, \alpha] \tag{D.24}$$

hence,

$$x_{,\alpha}^1 = a_2^1 + a_4^1 \beta \tag{D.25}$$

$$x_{,\beta}^1 = a_3^1 + a_4^1 \alpha \tag{D.26}$$

The corrections  $\Delta\alpha$  and  $\Delta\beta$  can now be computed by,

$$\Delta\alpha = \frac{1}{J_O^T} [x_{,\beta}^2 \cdot \Delta x^1 - x_{,\beta}^1 \cdot \Delta x^2] \tag{D.27}$$

$$\Delta\beta = \frac{1}{J_O^T} [x_{,\alpha}^1 \cdot \Delta x^2 - x_{,\alpha}^2 \cdot \Delta x^1] \tag{D.28}$$

$$J_O^T = [x_{,\alpha}^1 \cdot x_{,\beta}^2 - x_{,\beta}^1 \cdot x_{,\alpha}^2] \tag{D.29}$$



The iteration for  $\alpha_*$ ,  $\beta_*$  is then,

$$\begin{aligned}\alpha_K &= \alpha_{K-1} + \Delta\alpha \\ \beta_K &= \beta_{K-1} + \Delta\beta\end{aligned}\tag{D.30}$$

### 3. Procedure for Inverse Interpolation of Quadratic Shape Functions

The variables  $\Delta x^i$  are computed as follows,

$$\begin{aligned}\Delta x^i &= x_*^i - [N_L]\{x_L^i\} \\ &= x_*^i - [P_L]\{A_L^i\}\end{aligned}\quad \begin{array}{l} i = 1, 2 \\ L = 1, \dots, 9 \end{array}\tag{D.31}$$

where the index  $i$  corresponds to the two surface coordinates, the index  $L$  corresponds to the nine labeled nodes of Figure D.1-b, and:

$$\{x_L^i\} = [x_1^i, x_2^i, \dots, x_9^i]\tag{D.32}$$

$$[P_L] = [1, \alpha, \beta, \alpha^2, \alpha\beta, \beta^2, \alpha^2\beta, \alpha\beta^2, \alpha^2\beta^2]\tag{D.33}$$

$$\{A_L^i\}^T = [a_1^i, a_2^i, \dots, a_9^i]\tag{D.34}$$

$$a_1^i = x_1^i$$

$$a_2^i = \frac{1}{2}(x_5^i - x_9^i)$$

$$a_3^i = \frac{1}{2}(x_7^i - x_3^i)$$

$$a_4^1 = \frac{1}{2}(x_5^1 - 2x_1^1 + x_9^1)$$

$$a_5^1 = \frac{1}{4}(x_2^1 - x_4^1 + x_6^1 - x_8^1)$$

$$a_6^1 = \frac{1}{2}(x_7^1 - 2x_1^1 + x_3^1)$$

$$a_7^1 = \frac{1}{4}(-x_2^1 + 2x_3^1 - x_4^1 + x_6^1 - 2x_7^1 + x_8^1)$$

$$a_8^1 = \frac{1}{4}(x_4^1 - 2x_5^1 + x_6^1 - x_8^1 + 2x_9^1 - x_2^1)$$

$$a_9^1 = \frac{1}{4}(x_2^1 - 2x_3^1 + x_4^1 - 2x_5^1 + x_6^1 - 2x_7^1 + x_8^1 - 2x_9^1 + 4x_1^1)$$

(D.35)

Substituting (D.33), (D.34) and (D.35) into (D.31),

$$\begin{aligned} \Delta x^1 &= x_*^1 - a_1^1 - a_2^1 \alpha - a_3^1 \beta - a_4^1 \alpha^2 - a_5^1 \alpha \beta - a_6^1 \beta^2 \\ &\quad - a_7^1 \alpha^2 \beta - a_8^1 \alpha \beta^2 - a_9^1 \alpha^2 \beta^2 \end{aligned} \quad (D.36)$$

The variables  $x_{,\alpha}^1$  and  $x_{,\beta}^1$  are computed as follows,

$$\begin{aligned} x_{,\alpha}^1 &= [N_{L,\alpha}]\{x_L^1\} \\ &= [P_{L,\alpha}]\{A_L^1\} \end{aligned} \quad (D.37)$$

$$\begin{aligned} x_{,\beta}^1 &= [N_{L,\beta}]\{x_L^1\} \\ &= [P_{L,\beta}]\{x_L^1\} \end{aligned} \quad (D.38)$$

where,

$$[P_{L,\alpha}] = [0, 1, 0, 2\alpha, \beta, 0, 2\alpha\beta, \beta^2, 2\alpha\beta^2] \quad (D.39)$$

$$[P_{L,\beta}] = [0, 0, 1, 0, \alpha, 2\beta, \alpha^2, 2\alpha\beta, 2\alpha^2\beta] \quad (D.40)$$

hence,

$$x_{,\alpha}^1 = a_2^1 + 2a_4^1\alpha + a_5^1\beta + 2a_7^1\alpha\beta + a_8^1\beta^2 + 2a_9^1\alpha\beta^2 \quad (D.41)$$

$$x_{,\beta}^1 = a_3^1 + a_5^1\alpha + 2a_6^1\beta + a_7^1\alpha^2 + 2a_8^1\alpha\beta + 2a_9^1\alpha^2\beta \quad (D.42)$$

The corrections  $\Delta\alpha$  and  $\Delta\beta$  can now be computed by,

$$\Delta\alpha = \frac{1}{J_O^T} [x_{,\beta}^2 \cdot \Delta x^1 - x_{,\beta}^1 \cdot \Delta x^2] \quad (D.43)$$

$$\Delta\beta = \frac{1}{J_O^T} [x_{,\alpha}^1 \cdot \Delta x^2 - x_{,\alpha}^2 \cdot \Delta x^1] \quad (D.44)$$

$$J_O^T = [x_{,\alpha}^1 \cdot x_{,\beta}^2 - x_{,\beta}^1 \cdot x_{,\alpha}^2] \quad (D.45)$$

The iteration for  $\alpha_*$ ,  $\beta_*$  is then,

$$\alpha_K = \alpha_{K-1} + \Delta\alpha$$

$$\beta_K = \beta_{K-1} + \Delta\beta \quad (D.46)$$

## 4. SUBROUTINE LISTING

```

      SUBROUTINE ISOINV(ICASE,X1S,X2S,ELNO,LS,MS,AS,BS,IPRINT)
C*****
C**
C**  SUBROUTINE FOR DETERMINING THE INVERSE FUNCTIONAL RELATIONSHIP
C**  BETWEEN ISOPARAMETRIC INTERPOLATING COORDINATES AND SPATIAL
C**  COORDINATES USING A NEWTON - RAPHSOIN ITERATION METHOD
C**  *****      R J EDWARDS      *   DEC 1974
C**
C**  X1S , X2S = SPATIAL COORDINATES INPUT TO SUBROUTINE
C**  ELNO = ELEMENT NUMBER
C**  LS , MS = LINEAR INTERPOLATING COORDINATES CORRESPONDING TO
C**           X1S , X2S
C**  AS , BS = QUADRATIC INTERPOLATING COORDINATES CORRESPONDING TO
C**           X1S , X2S
C**
C**  ICASE = -1 RETURN LS = LAMBDA-STAR , MS = MU-STAR
C**  ICASE = +1 RETURN AS = ALPHA-STAR , BS = BETA-STAR
C**  ICASE = 0 RETURN BOTH LS , MS AND AS , BS
C**
C**  IPRINT = 0 , DO NOT PRINT SUMMARY DATA
C**  IPRINT = 1 , PRINT SUMMARY DATA
C**
C*****
      COMMON/ISODAT/ CX1(13),CX2(13),IGX(13)
      REAL LS,MS,LI,MI
      DATA EPS,ILN/0.000001/, ITLIM/30/
      IF(ICASE) 100,100,200
C*****
C**
C*  ITERATION FOR INVERSE INTERPOLATION OF BI-LINEAR SHAPE FUNCTIONS
C**
C*****
100 CONTINUE
      X1 =CX1(1)
      X2 =CX1(2)
      X3 =CX1(3)
      X4 =CX1(4)
      Y1 =CX2(1)
      Y2 =CX2(2)
      Y3 =CX2(3)
      Y4 =CX2(4)
      A1 = 0.25*( X1 + X2 + X3 + X4)
      A2 = 0.25*(-X1 + X2 + X3 - X4)
      A3 = 0.25*(-X1 - X2 + X3 + X4)
      A4 = 0.25*( X1 - X2 + X3 - X4)
      B1 = 0.25*( Y1 + Y2 + Y3 + Y4)
      B2 = 0.25*(-Y1 + Y2 + Y3 - Y4)
      B3 = 0.25*(-Y1 - Y2 + Y3 + Y4)
      B4 = 0.25*( Y1 - Y2 + Y3 - Y4)
      LS = 0.0
      MS = 0.0

```



```

      IT = 0
110  LI = LS
      MI = MS
      DELX1 = X1S - A1 - A2*LI - A3*MI - A4*LI*MI
      DELX2 = X2S - B1 - B2*LI - B3*MI - B4*LI*MI
      X1L = A2 + A4*MI
      X1M = A3 + A4*LI
      X2L = B2 + B4*MI
      X2M = B3 + B4*LI
      DETJ = X1L*X2M - X1M*X2L
      IF(ABS(DETJ).LT.EPSILN) GO TO 130
      DETJI = 1.0/DETJ
      DELL = DETJI * (X2M*DELX1 - X1M*DELX2)
      DELM = DETJI * (X1L*DELX2 - X2L*DELX1)
      LS = LI + DELL
      MS = MI + DELM
      ADELL = ABS(DELL)
      ADELM = ABS(DELM)
      IT = IT + 1
      IF(IT-ITLIM) 120,120,150
C**
C***** CONVERGENCE TEST
120 IF(ADELL.GT.EPSILN .OR. ADELM.GT.EPSILN) GO TO 110
C**
      GO TO 200
130 WRITE(6,1000) (CX1(I),I=1,13),(CX2(I),I=1,13),X1L,X1M,X2L,X2M,DETJ
      RETURN
150 WRITE(6,2000) ELNO,X1S,X2S,LI,MI,LS,MS,X1L,X1M,X2L,X2M,DETJ,
1      DELL,DELM
      IF(IT.LT.(ITLIM+4)) GO TO 110
      RETURN
200 IF(IPRINT) 201,201,202
202 WRITE(6,5000) ELNO,X1S,X2S,IT,LS,MS
201 IF(ICASE) 300,251,251
C*****
C**
C* ITERATION FOR INVERSE INTERPOLATION OF BI-QUADRATIC SHAPE FUNCTIONS
C**
C*****
251 CONTINUE
      X1 =CX1(5)
      X2 =CX1(6)
      X3 =CX1(7)
      X4 =CX1(8)
      X5 =CX1(9)
      X6 =CX1(10)
      X7 =CX1(11)
      X8 =CX1(12)
      X9 =CX1(13)
      Y1 =CX2(5)
      Y2 =CX2(6)
      Y3 =CX2(7)
      Y4 =CX2(8)
      Y5 =CX2(9)

```

```

Y6 =CX2(10)
Y7 =CX2(11)
Y8 =CX2(12)
Y9 =CX2(13)
X12 = 2.*X1
X32 = 2.*X3
X52 = 2.*X5
X72 = 2.*X7
X92 = 2.*X9
Y12 = 2.*Y1
Y32 = 2.*Y3
Y52 = 2.*Y5
Y72 = 2.*Y7
Y92 = 2.*Y9
C1 = X1
C2 = 0.50*(X5-X9)
C3 = 0.50*(X7-X3)
C4 = 0.50*(X5-X12+X9)
C5 = 0.25*( X2 - X4 + X6 - X8)
C6 = 0.50*( X7 - X12 + X3)
C7 = 0.25*(-X2 + X32 - X4 + X6 - X72 + X8)
C8 = 0.25*( X4 - X52 + X6 - X8 + X92 - X2)
C9 = 0.25*( X2 - X32 + X4 - X52 + X6 - X72 + X8 - X92) + X1
D1 = Y1
D2 = 0.50*(Y5-Y9)
D3 = 0.50*(Y7-Y3)
D4 = 0.50*(Y5 - Y12 + Y9)
D5 = 0.25*(Y2 - Y4 + Y6 - Y8)
D6 = 0.50*(Y7 - Y12 + Y3)
D7 = 0.25*(-Y2 + Y32 - Y4 + Y6 - Y72 + Y8)
D8 = 0.25*( Y4 - Y52 + Y6 - Y8 + Y92 - Y2)
D9 = 0.25*( Y2 - Y32 + Y4 - Y52 + Y6 - Y72 + Y8 - Y92) + Y1
AS = 0.0
BS = 0.0
IT = 0
210 AI = AS
BI = BS
A2 = AI*AI
B2 = BI*BI
AB = AI*BI
A2B = A2*BI
AB2 = AI*B2
A2B2 = A2*B2
TA = 2.0*AI
TB = 2.0*BI
TAB = 2.0*AB
TAB2 = 2.0*AB2
TA2B = 2.0*A2B
DELX1 = X1S - C1 - C2*AI - C3*BI - C4*A2 - C5*AB - C6*B2
1      - C7*A2B - C8*AB2 - C9*A2B2
DELX2 = X2S - D1 -D2*AI - D3*BI -D4*A2 - D5*AB - D6*B2
1      - D7*A2B - D8*AB2 - D9*A2B2
X1A =C2 + C4*TA + C5*BI + C7*TAB + C8*B2 + C9*TAB2
X1B = C3 + C5*AI + C6*TB + C7*A2 + C8*TAB + C9*TA2B

```

```

X2A = D2 + D4*TA + D5*BI + D7*TAB + D8*B2 + D9*TA2B
X2B = D3 + D5*AI + D6*TB + D7*A2 + D8*TAB + D9*TA2B
DETJ = X1A*X2B - X1B*X2A
IF(ABS(DETJ).LT.EPSILN) GO TO 230
DETJI = 1.0/DETJ
DELA = DETJI * (X2B*DELX1 - X1B*DELX2)
DELB = DETJI * (X1A*DELX2 - X2A*DELX1)
AS = AI + DELA
BS = BI + DELB
ADELA = ABS(DELA)
ADELB = ABS(DELB)
IT = IT + 1
IF(IT-ITLIM) 220,220,250
C**
C***** CONVERGENCE TEST
220 IF(ADELA.GT.EPSILN .OR. ADELB.GT.EPSILN) GO TO 210
C**
GO TO 300
230 WRITE(6,3000) (CX1(I),I=1,13),(CX2(I),I=1,13),X1A,X1B,X2A,X2B,DETJ
RETURN
250 WRITE(6,4000) ELNO,X1S,X2S,AI,BI,AS,BS,X1A,X1B,X2A,X2B,DETJ
1 DELA,DELB
IF(IT.LT.(ITLIM+4)) GO TO 210
RETURN
300 IF(IPRINT) 301,301,302
302 WRITE(6,6000) ELNO,X1S,X2S,IT,AS,BS
301 RETURN
1000 FORMAT(1H0,/,/,5X,67HTHE DETERMINANT OF THE INVERSION MATRIX (JACOB
1IAN) IS EQUAL TO ZERO ,
2 //7X,8HX1(I) = ,1PE15.6,/,15X,6E15.6,
3 ///7X,8HX2(I) = ,1PE15.6,/,15X,6E15.6,
4 ///5X,6HX1L = ,E20.8,5X,6HX1M = ,E20.8,5X,6HX2L = ,E20.8,
5 /,5X,6HX2M = ,E20.8,5X,7HDETJ = ,E20.8,/)
3000 FORMAT(1H0,/,/,5X,67HTHE DETERMINANT OF THE INVERSION MATRIX (JACOB
1IAN) IS EQUAL TO ZERO ,
2 //7X,8HX1(I) = ,1PE15.6,/,15X,6E15.6,
3 ///7X,8HX2(I) = ,1PE15.6,/,15X,6E15.6,
4 ///5X,6HX1A = ,E20.8,5X,6HX1B = ,E20.8,5X,6HX2A = ,E20.8,
5 /,5X,6HX2B = ,E20.8,5X,7HDETJ = ,E20.8,/)
5000 FORMAT(1H0,/,/,5X,69HTHE ITERATION TO FIND LAMBDA, MU CONVERGED WIT
1H THE FOLLOWING RESULTS,
2 //5X,9HEL.NO. = ,18,5X,6HX1S = ,1PE15.6,5X,6HX2S = ,1PE15.6,
3 //5X,12HITERATION = ,15,5X,9HLAMBDA = ,E15.6,5X,5HMU = ,E15.6,/)
6000 FORMAT(1H0,/,/,5X,69HTHE ITERATION TO FIND ALPHA,BETA CONVERGED WIT
1H THE FOLLOWING RESULTS,
2 //5X,9HEL.NO. = ,18,5X,6HX1S = ,1PE15.6,5X,6HX2S = ,1PE15.6,
3 //5X,12HITERATION = ,15,5X,8HALPHA = ,E15.6,5X,7HBETA = ,E15.6,/)
2000 FORMAT(1H0,4X,49HTHE ITERATION TO FIND LAMBDA, MU DID NOT CONVERGE
1 //5X,9HEL.NO. = ,18,5X,6HX1S = ,1PE15.6,5X,6HX2S = ,1PE15.6,
2 //5X,5HLI = ,E20.8,5X,5HMI = ,E20.8,5X,
3 /5X,5HLS = ,E20.8,5X,5HMS = ,E20.8,
4 //5X,6HX1L = ,E20.8,5X,6HX1M = ,E20.8,5X,
5 /5X,6HX2L = ,E20.8,5X,6HX2M = ,E20.8,5X,7HDETJ = ,E20.8,
6 //5X,9HDEL(L) = ,E20.8,5X,9HDEL(M) = ,E20.8,/)

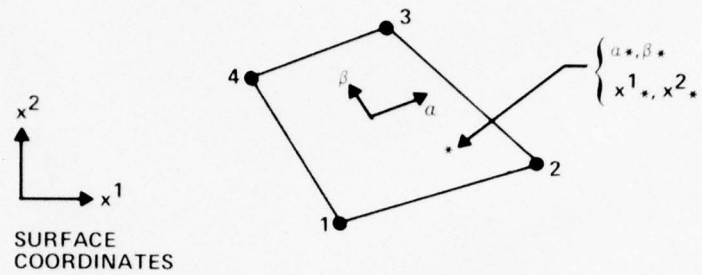
```

```

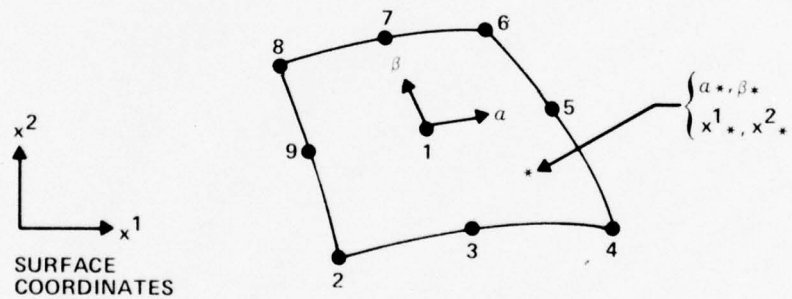
4000 FORMAT(1H0,4X,49HTHE ITERATION TO FIND ALPHA,BETA DID NOT CONVERGE
1 //5X,9HDEL.NO. = ,18,5X,6HX1S = ,1PE15.6,5X,6HX2S = ,1PE15.6,
2 //5X,5HAI = ,E20.8,5X,5HBI = ,E20.8,5X,
3 //5X,5HAS = ,E20.8,5X,5HBS = ,E20.8,
4 //5X,6HX1A = ,E20.8,5X,6HX1B = ,E20.8,5X,
5 //5X,6HX2A = ,E20.8,5X,6HX2B = ,E20.8,5X,7HDETJ = ,E20.8,
6 //5X,9HDEL(A) = ,E20.8,5X,9HDEL(B) = ,E20.8,/)
END

```





A. LINEAR SHAPE FUNCTION DOMAIN



B. QUADRATIC SHAPE FUNCTION DOMAIN

FIGURE D.1 SHAPE FUNCTION DOMAINS

## APPENDIX E

## SHELL REFERENCE SURFACE GEOMETRIES

The tensors necessary to describe the geometry and deformation of the shell reference surface are presented in this Appendix for several classes of shell surfaces. The equations for a conical reference surface are developed in detail to demonstrate the practical utilization of the general tensor formulation of Chapter II. The equations for cylindrical and spherical surfaces and those for flat plates in both polar and rectangular coordinates are only summarized since the detailed development closely parallels that of the conical surface example.

## 1. Conical Shell Geometry

Gridpoints on the shell reference surface are defined in the cylindrical coordinate system\* (see Figure E.1),

$$\left\{ \begin{matrix} x^1 \\ x^2 \\ x^3 \end{matrix} \right\}_G = \left\{ \begin{matrix} R \\ \theta \\ Z \end{matrix} \right\} \quad (E.1)$$

---

\*The coordinate system subscripts G, B and S refer to grid-point coordinates, basic coordinates and surface coordinates respectively.

The cone angle  $\alpha$  and base radius  $R_B$  are also specified. The following geometrical parameter may then be calculated,

$$L = \frac{R_B}{\tan \alpha} \quad (E.2)$$

At an arbitrary point P on the shell reference surface,

$$\begin{matrix} \left\{ \begin{matrix} x^1 \\ x^2 \\ x^3 \end{matrix} \right\} \\ B \end{matrix} = \begin{matrix} \left\{ \begin{matrix} X \\ Y \\ Z \end{matrix} \right\} \\ B \end{matrix} = \begin{matrix} \left\{ \begin{matrix} R \cos \theta \\ R \sin \theta \\ Z \end{matrix} \right\} \\ B \end{matrix} = \begin{matrix} \left\{ \begin{matrix} (L-x^2) \tan \alpha \cos x^1 \\ (L-x^2) \tan \alpha \sin x^1 \\ Z \end{matrix} \right\} \\ B \end{matrix} \quad (E.3)$$

where the Gaussian surface coordinates are,

$$\begin{matrix} \left\{ \begin{matrix} x^1 \\ x^2 \\ x^3 \end{matrix} \right\} \\ S \end{matrix} = \begin{matrix} \left\{ \begin{matrix} \theta \\ \varphi \\ z \end{matrix} \right\} \\ S \end{matrix} \quad (E.4)$$

The position vector of point P is,

$$\begin{aligned} \vec{r} &= x^K \vec{I}_K \\ &= (L-Z) \tan \alpha \cos \theta \vec{I}_1 \\ &\quad + (L-Z) \tan \alpha \sin \theta \vec{I}_2 + Z \vec{I}_3 \end{aligned} \quad (E.5)$$

The base vectors of the surface coordinates are then,

$$\vec{a}_\alpha = \vec{r}_{,\alpha} \quad (\text{E.6})$$

hence,

$$\begin{aligned} \vec{a}_1 &= -R \sin\theta \vec{I}_1 + R \cos\theta \vec{I}_2 \\ \vec{a}_2 &= -\tan\alpha \cos\theta \vec{I}_1 - \tan\alpha \sin\theta \vec{I}_2 + (1) \vec{I}_3 \end{aligned} \quad (\text{E.7})$$

The metric tensor is given by,

$$a_{\alpha\beta} = \vec{a}_\alpha \cdot \vec{a}_\beta \quad (\text{E.8})$$

hence,

$$\begin{aligned} a_{11} &= R^2 \\ a_{12} &= a_{21} = 0 \\ a_{22} &= \frac{1}{\cos^2\alpha} \end{aligned} \quad (\text{E.9})$$

The metric tensor, its determinant and the associated metric tensor are thus,



$$a_{\alpha\beta} = \begin{bmatrix} R^2 & 0 \\ 0 & \frac{1}{\cos^2 \alpha} \end{bmatrix} \quad (\text{E.10})$$

$$a = |a_{\alpha\beta}| = \frac{R^2}{\cos^2 \alpha} \quad (\text{E.11})$$

$$a^{\alpha\beta} = \begin{bmatrix} \frac{1}{R^2} & 0 \\ 0 & \cos^2 \alpha \end{bmatrix} \quad (\text{E.12})$$

The incremental arc lengths in the base vector directions are,

$$dS_1 = A_1 dx^1 = R d\theta \quad (\text{E.13})$$

$$dS_2 = A_2 dx^2 = \frac{1}{\cos \alpha} dz \quad (\text{E.14})$$

and the incremental arc length on the shell reference surface is,

$$\begin{aligned} dS^2 &= a_{\alpha\beta} dx^\alpha dx^\beta \\ &= (R d\theta)^2 + \left( \frac{1}{\cos \alpha} dz \right)^2 \end{aligned} \quad (\text{E.15})$$

The unit vectors in the base vector directions are,

$$\vec{e}_\alpha = \frac{\vec{a}_\alpha}{A_\alpha} \quad (\text{no sum}) \quad (\text{E.16})$$

thus,

$$\vec{e}_1 = -\sin\theta \vec{I}_1 + \cos\theta \vec{I}_2 \quad (\text{E.17})$$

$$\vec{e}_2 = -\sin\alpha \cos\theta \vec{I}_1 - \sin\alpha \sin\theta \vec{I}_2 + \cos\alpha \vec{I}_3 \quad (\text{E.18})$$

The unit normal vector is,

$$\begin{aligned} \vec{e}_n &= \vec{e}_1 \times \vec{e}_2 \\ &= \cos\alpha \cos\theta \vec{I}_1 + \cos\alpha \sin\theta \vec{I}_2 + \sin\alpha \vec{I}_3 \end{aligned} \quad (\text{E.19})$$

The transformation relating unit vectors in surface coordinates and unit vectors in basic coordinates is then,

$$\begin{Bmatrix} \vec{e}_1 \\ \vec{e}_2 \\ \vec{e}_n \end{Bmatrix} = [T_{SB}] \begin{Bmatrix} \vec{I}_1 \\ \vec{I}_2 \\ \vec{I}_3 \end{Bmatrix} \quad (\text{E.20})$$

where,

$$[T_{SB}] = \begin{bmatrix} -S_{\theta} & C_{\theta} & 0 \\ -S_{\alpha}C_{\theta} & -S_{\alpha}S_{\theta} & C_{\alpha} \\ C_{\alpha}C_{\theta} & C_{\alpha}S_{\theta} & S_{\alpha} \end{bmatrix} \quad (E.21)$$

$$\begin{aligned} C_{\alpha} &= \cos\alpha, & S_{\alpha} &= \sin\alpha \\ C_{\theta} &= \cos\theta, & S_{\theta} &= \sin\theta \end{aligned} \quad (E.22)$$

Conversely,

$$\begin{aligned} \begin{Bmatrix} \vec{I}_1 \\ \vec{I}_2 \\ \vec{I}_3 \end{Bmatrix} &= [T_{SB}]^{-1} \begin{Bmatrix} \vec{e}_1 \\ \vec{e}_2 \\ \vec{e}_n \end{Bmatrix} \\ &= [T_{SB}]^T \begin{Bmatrix} \vec{e}_1 \\ \vec{e}_2 \\ \vec{e}_n \end{Bmatrix} \end{aligned} \quad (E.23)$$

since,

$$[T_{SB}]^T [T_{SB}] = [I] \quad (E.24)$$

where  $[I]$  is the identity matrix.

It follows that the transformation relating shell displacement components to basic displacement components is,

$$\begin{Bmatrix} u_{\theta} \\ u_S \\ u_n \end{Bmatrix} = [T_{SB}] \begin{Bmatrix} u_X \\ u_Y \\ u_Z \end{Bmatrix} \quad (\text{E.25})$$

and conversely,

$$\begin{Bmatrix} u_X \\ u_Y \\ u_Z \end{Bmatrix} = [T_{SB}]^T \begin{Bmatrix} u_{\theta} \\ u_S \\ u_n \end{Bmatrix} \quad (\text{E.26})$$

The Christoffel symbols of the second kind are defined by,

$$\Gamma_{\beta\alpha}^{\alpha} = a^{\alpha\lambda} (\vec{a}_{\lambda} \cdot \vec{a}_{\beta,\alpha}) \quad (\text{E.27})$$

where,

$$\begin{aligned} \vec{a}_{1,1} &= -R \cos\theta \vec{I}_1 - R \sin\theta \vec{I}_2 \\ \vec{a}_{1,2} &= \vec{a}_{2,1} = \tan\alpha \sin\theta \vec{I}_1 - \tan\alpha \cos\theta \vec{I}_2 \\ \vec{a}_{2,2} &= 0 \end{aligned} \quad (\text{E.28})$$



hence,

$$\begin{aligned}
 \Gamma_{11}^1 &= a^{11}(\vec{a}_1 \cdot \vec{a}_{1,1}) + a^{12}(\vec{a}_2 \cdot \vec{a}_{1,1}) \\
 &= 0 \\
 \Gamma_{12}^1 &= a^{11}(\vec{a}_1 \cdot \vec{a}_{1,2}) + a^{12}(\vec{a}_2 \cdot \vec{a}_{1,2}) \\
 &= -\frac{\tan \alpha}{R} = \Gamma_{21}^1 \\
 \Gamma_{22}^1 &= a^{11}(\vec{a}_1 \cdot \vec{a}_{2,2}) + a^{12}(\vec{a}_2 \cdot \vec{a}_{2,2}) \\
 &= 0 \\
 \Gamma_{11}^2 &= a^{21}(\vec{a}_1 \cdot \vec{a}_{1,1}) + a^{22}(\vec{a}_2 \cdot \vec{a}_{1,1}) \\
 &= R \sin \alpha \cos \alpha \\
 \Gamma_{12}^2 &= a^{21}(\vec{a}_1 \cdot \vec{a}_{1,2}) + a^{22}(\vec{a}_2 \cdot \vec{a}_{1,2}) \\
 &= 0 = \Gamma_{21}^2 \\
 \Gamma_{22}^2 &= a^{21}(\vec{a}_1 \cdot \vec{a}_{2,2}) + a^{22}(\vec{a}_2 \cdot \vec{a}_{2,2}) \\
 &= 0
 \end{aligned} \tag{E.29}$$

The covariant form of the initial curvature tensor is defined by,

$$b_{\alpha\beta} = \vec{e}_n \cdot \vec{a}_{\alpha,\beta} \tag{E.30}$$

hence,

$$\begin{aligned}
 b_{11} &= -R \cos \alpha \\
 b_{21} &= b_{12} = 0 \\
 b_{22} &= 0
 \end{aligned} \tag{E.31}$$

The mixed form of the initial curvature tensor is defined by,

$$b_{\alpha}^{\rho} = a^{\rho\beta} b_{\alpha\beta} \quad (\text{E.32})$$

or in matrix form,

$$\begin{bmatrix} b_1^1 & b_2^1 \\ b_1^2 & b_2^2 \end{bmatrix} = \begin{bmatrix} a^{11} & a^{12} \\ a^{21} & a^{22} \end{bmatrix} \mathbf{x} \begin{bmatrix} b_{11} & b_{12} \\ b_{21} & b_{22} \end{bmatrix} \quad (\text{E.33})$$

hence,

$$b_{\alpha}^{\rho} = \begin{bmatrix} -\frac{\cos\alpha}{R} & 0 \\ 0 & 0 \end{bmatrix} \quad (\text{E.34})$$

The covariant derivatives of the covariant initial curvature tensor are,

$$b_{\alpha\beta} |_{\lambda} = b_{\alpha\beta,\lambda} - \Gamma_{\alpha\lambda}^{\mu} b_{\mu\beta} - \Gamma_{\beta\lambda}^{\mu} b_{\alpha\mu} \quad (\text{E.35})$$

or in matrix form,

$$\begin{aligned}
 \begin{bmatrix} b_{11}|_{\lambda} & b_{12}|_{\lambda} \\ b_{21}|_{\lambda} & b_{22}|_{\lambda} \end{bmatrix} &= \begin{bmatrix} b_{11,\lambda} & b_{12,\lambda} \\ b_{21,\lambda} & b_{22,\lambda} \end{bmatrix} - \\
 &\begin{bmatrix} \Gamma_{1\lambda}^1 & \Gamma_{1\lambda}^2 \\ \Gamma_{2\lambda}^1 & \Gamma_{2\lambda}^2 \end{bmatrix} \begin{bmatrix} b_{11} & b_{12} \\ b_{21} & b_{22} \end{bmatrix} - \\
 &\begin{bmatrix} b_{11} & b_{12} \\ b_{21} & b_{22} \end{bmatrix} \begin{bmatrix} \Gamma_{1\lambda}^1 & \Gamma_{2\lambda}^1 \\ \Gamma_{1\lambda}^2 & \Gamma_{2\lambda}^2 \end{bmatrix}
 \end{aligned}
 \tag{E.36}$$

thus,

$$b_{\alpha\beta}|_1 = \begin{bmatrix} 0 & -\sin\alpha \\ -\sin\alpha & 0 \end{bmatrix} \tag{E.37}$$

$$b_{\alpha\beta}|_2 = \begin{bmatrix} -\sin\alpha & 0 \\ 0 & 0 \end{bmatrix} \tag{E.38}$$

The covariant derivatives of the mixed initial curvature tensor are,

$$b_{\beta}^{\alpha}|_{\lambda} = a^{\alpha\mu} b_{\beta\mu}|_{\lambda} \tag{E.39}$$

or in matrix form,

$$\begin{bmatrix} b_1^1|_\lambda & b_2^1|_\lambda \\ b_1^2|_\lambda & b_2^2|_\lambda \end{bmatrix} = \begin{bmatrix} a^{11} & a^{12} \\ a^{21} & a^{22} \end{bmatrix} \begin{bmatrix} b_{11}|_\lambda & b_{12}|_\lambda \\ b_{21}|_\lambda & b_{22}|_\lambda \end{bmatrix} \quad (\text{E.40})$$

hence,

$$b_\beta^\alpha|_1 = \begin{bmatrix} 0 & -\frac{\sin\alpha}{R^2} \\ -\sin\alpha \cos^2\alpha & 0 \end{bmatrix} \quad (\text{E.41})$$

$$b_\beta^\alpha|_2 = \begin{bmatrix} -\frac{\sin\alpha}{R^2} & 0 \\ 0 & 0 \end{bmatrix} \quad (\text{E.42})$$

A concise summary of the above analytical development for the conical shell geometry is contained in Table E.1.

## 2. Cylindrical Shell Geometry

Gridpoint coordinates on the shell reference surface are defined in the cylindrical system (see Figure E.2),

$$\begin{Bmatrix} x^1 \\ x^2 \\ x^3 \end{Bmatrix} = \begin{Bmatrix} R \\ \theta \\ z \end{Bmatrix} \quad (\text{E.43})$$

G



At an arbitrary point P on the shell reference surface,

$$\begin{matrix} \left\{ \begin{matrix} x^1 \\ x^2 \\ x^3 \end{matrix} \right\} \\ B \end{matrix} = \begin{matrix} \left\{ \begin{matrix} X \\ Y \\ Z \end{matrix} \right\} \\ B \end{matrix} = \begin{matrix} \left\{ \begin{matrix} R \cos \theta \\ R \sin \theta \\ Z \end{matrix} \right\} \\ B \end{matrix} = \begin{matrix} \left\{ \begin{matrix} R \cos x^1 \\ R \sin x^1 \\ x^2 \end{matrix} \right\} \\ B \end{matrix} \quad (E.44)$$

where the Gaussian surface coordinates are,

$$\begin{matrix} \left\{ \begin{matrix} x^1 \\ x^2 \\ x^3 \end{matrix} \right\} \\ S \end{matrix} = \begin{matrix} \left\{ \begin{matrix} \theta \\ \phi \\ z \end{matrix} \right\} \\ S \end{matrix} \quad (E.45)$$

The position vector of point P is,

$$\begin{aligned} \vec{r} &= x^K \vec{I}_K \\ &= R \cos \theta \vec{I}_1 + R \sin \theta \vec{I}_2 + Z \vec{I}_3 \end{aligned} \quad (E.46)$$

Proceeding as in the conical shell example, the equations summarized in Table E.2 are obtained.

### 3. Spherical Shell Geometry

Gridpoint coordinates on the shell reference surface are defined in the spherical system (see Figure E.3).

$$\left\{ \begin{matrix} x^1 \\ x^2 \\ x^3 \end{matrix} \right\}_G = \left\{ \begin{matrix} R \\ \theta \\ \phi \end{matrix} \right\} \quad (\text{E.47})$$

At an arbitrary point P on the shell reference surface,

$$\left\{ \begin{matrix} x^1 \\ x^2 \\ x^3 \end{matrix} \right\}_B = \left\{ \begin{matrix} X \\ Y \\ Z \end{matrix} \right\} = \left\{ \begin{matrix} R \sin \theta \cos \phi \\ R \sin \theta \sin \phi \\ R \cos \theta \end{matrix} \right\} = \left\{ \begin{matrix} R \sin x^1 \cos x^2 \\ R \sin x^1 \sin x^2 \\ R \cos x^1 \end{matrix} \right\} \quad (\text{E.48})$$

where the Gaussian surface coordinates are,

$$\left\{ \begin{matrix} x^1 \\ x^2 \\ x^3 \end{matrix} \right\}_S = \left\{ \begin{matrix} \theta \\ \phi \\ z \end{matrix} \right\} \quad (\text{E.49})$$

The position vector of point P is,

$$\begin{aligned} \vec{r} &= x^K \vec{I}_K \\ &= R \sin \theta \cos \phi \vec{I}_1 + R \sin \theta \sin \phi \vec{I}_2 + R \cos \theta \vec{I}_3 \end{aligned} \quad (\text{E.50})$$

Proceeding as in the conical shell example, the equations summarized in Table E.3 are obtained.

## 4. Plate Geometry in Polar Coordinates

Gridpoint coordinates on the plate reference surface are defined in the cylindrical system (see Figure E.4),

$$\begin{pmatrix} x^1 \\ x^2 \\ x^3 \end{pmatrix}_G = \begin{pmatrix} R \\ \theta \\ z_P \end{pmatrix} \quad (\text{E.51})$$

At an arbitrary point P on the plate reference surface,

$$\begin{pmatrix} X^1 \\ X^2 \\ X^3 \end{pmatrix}_B = \begin{pmatrix} X \\ Y \\ z_P \end{pmatrix} = \begin{pmatrix} R \cos \theta \\ R \sin \theta \\ z_P \end{pmatrix} = \begin{pmatrix} x^1 \cos x^2 \\ x^1 \sin x^2 \\ z_P \end{pmatrix} \quad (\text{E.52})$$

where the Gaussian surface coordinates are,

$$\begin{pmatrix} x^1 \\ x^2 \\ x^3 \end{pmatrix}_S = \begin{pmatrix} R \\ \theta \\ z \end{pmatrix} \quad (\text{E.53})$$

The position vector of point P is,

$$\begin{aligned}\vec{r} &= x^K \vec{I}_K \\ &= R \cos \theta \vec{I}_1 + R \sin \theta \vec{I}_2 + z_P \vec{I}_3\end{aligned}\quad (E.54)$$

Proceeding as in the conical shell example, the equations summarized in Table E.4 are obtained.

### 5. Plate Geometry in Cartesian Coordinates

Gridpoint coordinates on the plate reference surface are defined in the Cartesian system (see Figure E.5),

$$\begin{pmatrix} x^1 \\ x^2 \\ x^3 \end{pmatrix}_G = \begin{pmatrix} X \\ Y \\ z_P \end{pmatrix} \quad (E.55)$$

At an arbitrary point P on the plate reference surface,

$$\begin{pmatrix} x^1 \\ x^2 \\ x^3 \end{pmatrix}_B = \begin{pmatrix} X \\ Y \\ z_P \end{pmatrix} = \begin{pmatrix} x^1 \\ x^2 \\ z_P \end{pmatrix} \quad (E.56)$$

where the Gaussian surface coordinates are,



$$\left\{ \begin{matrix} x^1 \\ x^2 \\ x^3 \end{matrix} \right\}_S = \left\{ \begin{matrix} X \\ Y \\ Z \end{matrix} \right\} \quad (\text{E.57})$$

The position vector of point P is,

$$\begin{aligned} \vec{r} &= x^K \vec{I}_K \\ &= X \vec{I}_1 + Y \vec{I}_2 + Z \vec{I}_3 \end{aligned} \quad (\text{E.58})$$

Proceeding as in the conical shell example, the equations summarized in Table E.5 are obtained.

AD-A034 788 NAVAL SURFACE WEAPONS CENTER WHITE OAK LAB SILVER SP--ETC F/G 13/13  
A GENERALIZED FINITE DIFFERENCE ELEMENT FOR THE THERMOELASTIC S--ETC(U)  
JUN 76 R J EDWARDS

NAVAL SURFACE WEAPONS CENTER WHITE OAK LAB SILVER SP--ETC F/G 13/13  
A GENERALIZED FINITE DIFFERENCE ELEMENT FOR THE THERMOELASTIC S--ETC(U)  
JUN 76 R J EDWARDS

NSWC/WOL/TR-76-66

NL

AD  
A034788

AD  
A034788

1000

DATE  
FILMED  
2-77

DATE  
FILMED  
2-77

TABLE E.1

SUMMARY OF CONICAL SHELL GEOMETRYSURFACE COORDINATES:

$$\begin{Bmatrix} x^1 \\ x^2 \\ x^3 \end{Bmatrix} = \begin{Bmatrix} \theta \\ z \\ z \end{Bmatrix}$$

INCREMENTAL ARC LENGTHS:

$$\begin{Bmatrix} dS_1 \\ dS_2 \\ dS \end{Bmatrix} = \begin{Bmatrix} Rd\theta \\ dZ/\cos\alpha \\ \sqrt{(Rd\theta)^2 + (dZ/\cos\alpha)^2} \end{Bmatrix}$$

METRIC TENSORS:

$$a_{\alpha\beta} = \begin{bmatrix} R^2 & 0 \\ 0 & \frac{1}{\cos^2\alpha} \end{bmatrix} \quad a^{\alpha\beta} = \begin{bmatrix} \frac{1}{R^2} & 0 \\ 0 & \cos^2\alpha \end{bmatrix} \quad a = |a_{\alpha\beta}| = \frac{R^2}{\cos^2\alpha}$$

CHRISTOFFEL SYMBOLS:

$$\Gamma_{\alpha\beta}^1 = \begin{bmatrix} 0 & -\frac{\tan\alpha}{R} \\ -\frac{\tan\alpha}{R} & 0 \end{bmatrix}, \quad \Gamma_{\alpha\beta}^2 = \begin{bmatrix} R \sin\alpha \cos\alpha & 0 \\ 0 & 0 \end{bmatrix}$$

CURVATURE TENSORS:

$$b_{\alpha\beta} = \begin{bmatrix} -R \cos\alpha & 0 \\ 0 & 0 \end{bmatrix} \quad b_{\beta}^{\alpha} = \begin{bmatrix} -\frac{\cos\alpha}{R} & 0 \\ 0 & 0 \end{bmatrix}$$

COVARIANT DERIVATIVES OF CURVATURE TENSORS:

$$b_{\alpha\beta|1} = \begin{bmatrix} 0 & -\sin\alpha \\ -\sin\alpha & 0 \end{bmatrix}, \quad b_{\alpha\beta|2} = \begin{bmatrix} -\sin\alpha & 0 \\ 0 & 0 \end{bmatrix}$$

$$b_{\beta|1}^{\alpha} = \begin{bmatrix} 0 & -\frac{\sin\alpha}{R^2} \\ -\sin\alpha \cos^2\alpha & 0 \end{bmatrix}, \quad b_{\beta|2}^{\alpha} = \begin{bmatrix} -\frac{\sin\alpha}{R^2} & 0 \\ 0 & 0 \end{bmatrix}$$

COORDINATE TRANSFORMATIONS:

$$\begin{Bmatrix} u_{\theta} \\ u_S \\ u_n \end{Bmatrix} = [T_{SB}] \begin{Bmatrix} u_X \\ u_Y \\ u_Z \end{Bmatrix}, \quad \begin{Bmatrix} u_X \\ u_Y \\ u_Z \end{Bmatrix} = [T_{SB}]^T \begin{Bmatrix} u_{\theta} \\ u_S \\ u_n \end{Bmatrix}$$

WHERE,

$$[T_{SB}] = \begin{bmatrix} -\sin\theta & \cos\theta & 0 \\ -\sin\alpha \cos\theta & -\sin\alpha \sin\theta & \cos\alpha \\ \cos\alpha \cos\theta & \cos\alpha \sin\theta & \sin\alpha \end{bmatrix}$$

TABLE E.2  
SUMMARY OF CYLINDRICAL SHELL GEOMETRY

SURFACE COORDINATES:

$$\begin{Bmatrix} x^1 \\ x^2 \\ x^3 \end{Bmatrix} = \begin{Bmatrix} \theta \\ z \\ z \end{Bmatrix}$$

INCREMENTAL ARC LENGTHS:

$$\begin{Bmatrix} dS_1 \\ dS_2 \\ dS \end{Bmatrix} = \begin{Bmatrix} R d\theta \\ dz \\ \sqrt{(R d\theta)^2 + (dz)^2} \end{Bmatrix}$$

METRIC TENSORS:

$$a_{\alpha\beta} = \begin{bmatrix} R^2 & 0 \\ 0 & 1 \end{bmatrix}, \quad a^{\alpha\beta} = \begin{bmatrix} 1/R^2 & 0 \\ 0 & 1 \end{bmatrix}, \quad a = |a_{\alpha\beta}| = R^2$$

CHRISTOFFEL SYMBOLS:

$$\Gamma_{\alpha\beta}^1 = \Gamma_{\alpha\beta}^2 = \begin{bmatrix} 0 & 0 \\ 0 & 0 \end{bmatrix}$$

CURVATURE TENSORS:

$$b_{\alpha\beta} = \begin{bmatrix} -R & 0 \\ 0 & 0 \end{bmatrix}, \quad b_{\beta}^{\alpha} = \begin{bmatrix} -1/R & 0 \\ 0 & 0 \end{bmatrix}$$

COVARIANT DERIVATIVES OF CURVATURE TENSORS:

$$b_{\alpha\beta|1} = b_{\alpha\beta|2} = b_{\beta|1}^{\alpha} = b_{\beta|2}^{\alpha} = \begin{bmatrix} 0 & 0 \\ 0 & 0 \end{bmatrix}$$

COORDINATE TRANSFORMATIONS:

$$\begin{Bmatrix} u_{\theta} \\ u_z \\ u_n \end{Bmatrix} = [T_{SB}] \begin{Bmatrix} u_X \\ u_Y \\ u_Z \end{Bmatrix}, \quad \begin{Bmatrix} u_X \\ u_Y \\ u_Z \end{Bmatrix} = [T_{SB}]^T \begin{Bmatrix} u_{\theta} \\ u_z \\ u_n \end{Bmatrix}$$

WHERE,

$$[T_{SB}] = \begin{bmatrix} -\sin\theta & \cos\theta & 0 \\ 0 & 0 & 1 \\ \cos\theta & \sin\theta & 0 \end{bmatrix}$$



TABLE E.3

SUMMARY OF SPHERICAL SHELL GEOMETRYSURFACE COORDINATES:

$$\begin{pmatrix} x^1 \\ x^2 \\ x^3 \end{pmatrix} = \begin{pmatrix} \theta \\ \phi \\ z \end{pmatrix}$$

INCREMENTAL ARC LENGTHS:

$$\begin{pmatrix} dS_1 \\ dS_2 \\ dS \end{pmatrix} = \begin{pmatrix} Rd\theta \\ R \sin \theta d\phi \\ \sqrt{(Rd\theta)^2 + (R \sin \theta d\phi)^2} \end{pmatrix}$$

METRIC TENSORS:

$$a_{\alpha\beta} = \begin{bmatrix} R^2 & 0 \\ 0 & R^2 \sin^2 \phi \end{bmatrix}, \quad a^{\alpha\beta} = \begin{bmatrix} \frac{1}{R^2} & 0 \\ 0 & \frac{1}{R^2 \sin^2 \phi} \end{bmatrix}, \quad a = |a_{\alpha\beta}| = R^4 \sin^2 \phi$$

CHRISTOFFEL SYMBOLS:

$$\Gamma_{\alpha\beta}^1 = \begin{bmatrix} 0 & 0 \\ 0 & -\sin \theta \cos \theta \end{bmatrix}, \quad \Gamma_{\alpha\beta}^2 = \begin{bmatrix} 0 & \cot \theta \\ \cot \theta & 0 \end{bmatrix}$$

CURVATURE TENSORS:

$$b_{\alpha\beta} = \begin{bmatrix} -R & 0 \\ 0 & -R \sin^2 \theta \end{bmatrix}, \quad b_{\beta}^{\alpha} = \begin{bmatrix} -\frac{1}{R} & 0 \\ 0 & -\frac{1}{R} \end{bmatrix}$$

COVARIANT DERIVATIVES OF CURVATURE TENSORS:

$$b_{\alpha\beta|1} = b_{\alpha\beta|2} = b_{\beta|1}^{\alpha} = b_{\beta|2}^{\alpha} = \begin{bmatrix} 0 & 0 \\ 0 & 0 \end{bmatrix}$$

COORDINATE TRANSFORMATIONS:

$$\begin{pmatrix} u_{\theta} \\ u_{\phi} \\ u_n \end{pmatrix} = [T_{SB}] \begin{pmatrix} u_X \\ u_Y \\ u_Z \end{pmatrix}, \quad \begin{pmatrix} u_X \\ u_Y \\ u_Z \end{pmatrix} = [T_{SB}]^T \begin{pmatrix} u_{\theta} \\ u_{\phi} \\ u_n \end{pmatrix}$$

WHERE,

$$[T_{SB}] = \begin{bmatrix} \cos \theta \cos \phi & \cos \theta \sin \phi & -\sin \theta \\ -\sin \phi & \cos \phi & 0 \\ \sin \theta \cos \phi & \sin \theta \sin \phi & \cos \theta \end{bmatrix}$$

TABLE E.4

SUMMARY OF PLATE GEOMETRY IN POLAR COORDINATESSURFACE COORDINATES:

$$\begin{Bmatrix} x^1 \\ x^2 \\ x^3 \end{Bmatrix} = \begin{Bmatrix} r \\ \theta \\ z \end{Bmatrix}$$

INCREMENTAL ARC LENGTHS:

$$\begin{Bmatrix} dS_1 \\ dS_2 \\ dS \end{Bmatrix} = \begin{Bmatrix} dR \\ R d\theta \\ \sqrt{(dR)^2 + (R d\theta)^2} \end{Bmatrix}$$

METRIC TENSORS:

$$a_{a\beta} = \begin{bmatrix} 1 & 0 \\ 0 & R^2 \end{bmatrix}, \quad a^{a\beta} = \begin{bmatrix} 1 & 0 \\ 0 & \frac{1}{R^2} \end{bmatrix}, \quad a = |a_{a\beta}| = R^2$$

CHRISTOFFEL SYMBOLS:

$$\Gamma_{a\beta}^1 = \begin{bmatrix} 0 & 0 \\ 0 & -R \end{bmatrix}, \quad \Gamma_{a\beta}^2 = \begin{bmatrix} 0 & \frac{1}{R} \\ \frac{1}{R} & 0 \end{bmatrix}$$

CURVATURE TENSORS:

$$b_{a\beta} = b_{\beta}^a = \begin{bmatrix} 0 & 0 \\ 0 & 0 \end{bmatrix}$$

COVARIANT DERIVATIVES OF CURVATURE TENSORS:

$$b_{a\beta|1} = b_{a\beta|2} = b_{\beta|1}^a = b_{\beta|2}^a = \begin{bmatrix} 0 & 0 \\ 0 & 0 \end{bmatrix}$$

COORDINATE TRANSFORMATIONS:

$$\begin{Bmatrix} u_r \\ u_\theta \\ u_n \end{Bmatrix} = [T_{sb}] \begin{Bmatrix} u_x \\ u_y \\ u_z \end{Bmatrix}, \quad \begin{Bmatrix} u_x \\ u_y \\ u_z \end{Bmatrix} = [T_{SB}]^T \begin{Bmatrix} u_r \\ u_\theta \\ u_n \end{Bmatrix}$$

WHERE,

$$[T_{SB}] = \begin{bmatrix} \cos \theta & \sin \theta & 0 \\ -\sin \theta & \cos \theta & 0 \\ 0 & 0 & 1 \end{bmatrix}$$

TABLE E.5

SUMMARY OF PLATE GEOMETRY IN CARTESIAN COORDINATESSURFACE COORDINATES:

$$\begin{Bmatrix} x^1 \\ x^2 \\ x^3 \end{Bmatrix} = \begin{Bmatrix} X \\ Y \\ Z \end{Bmatrix}$$

INCREMENTAL ARC LENGTHS:

$$\begin{Bmatrix} dS_1 \\ dS_2 \\ dS \end{Bmatrix} = \begin{Bmatrix} dX \\ dY \\ \sqrt{(dX)^2 + (dY)^2} \end{Bmatrix}$$

METRIC TENSORS:

$$a_{\alpha\beta} = \begin{bmatrix} 1 & 0 \\ 0 & 1 \end{bmatrix}, \quad a^{\alpha\beta} = \begin{bmatrix} 1 & 0 \\ 0 & 1 \end{bmatrix}, \quad a = |a_{\alpha\beta}| = 1$$

CHRISTOFFEL SYMBOLS:

$$\Gamma_{\alpha\beta}^1 = \Gamma_{\alpha\beta}^2 = \begin{bmatrix} 0 & 0 \\ 0 & 0 \end{bmatrix}$$

CURVATURE TENSORS:

$$b_{\alpha\beta} = b_{\beta}^{\alpha} = \begin{bmatrix} 0 & 0 \\ 0 & 0 \end{bmatrix}$$

COVARIANT DERIVATIVES OF CURVATURE TENSORS:

$$b_{\alpha\beta|1} = b_{\alpha\beta|2} = b_{\beta}^{\alpha}|_1 = b_{\beta}^{\alpha}|_2 = \begin{bmatrix} 0 & 0 \\ 0 & 0 \end{bmatrix}$$

COORDINATE TRANSFORMATIONS:

$$\begin{Bmatrix} u_X \\ u_Y \\ u_n \end{Bmatrix} = \begin{bmatrix} 1 & 0 & 0 \\ 0 & 1 & 0 \\ 0 & 0 & 1 \end{bmatrix} \begin{Bmatrix} u_X \\ u_Y \\ u_Z \end{Bmatrix}$$

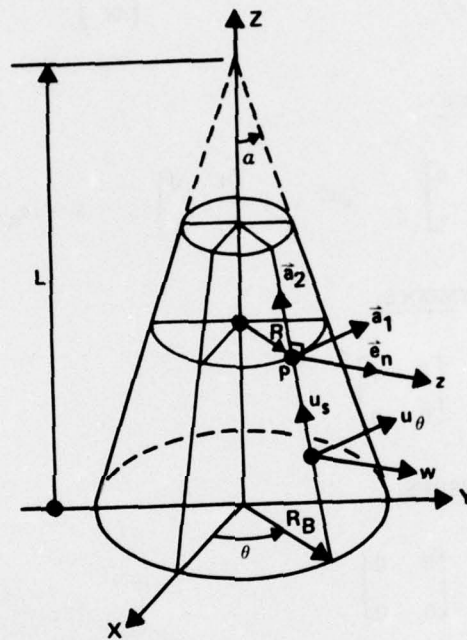


FIGURE E.1 CONICAL REFERENCE SURFACE



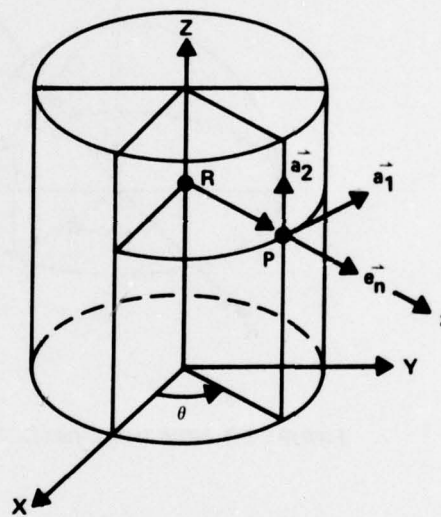


FIGURE E. 2 CYLINDRICAL REFERENCE SURFACE

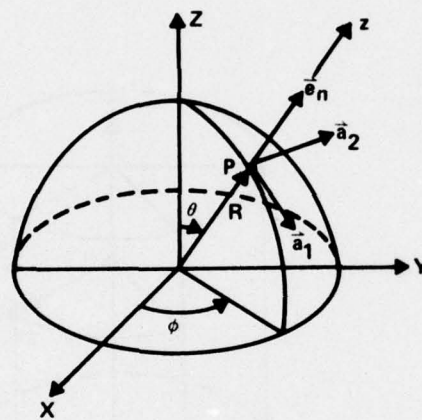


FIGURE E.3 SPHERICAL REFERENCE SURFACE

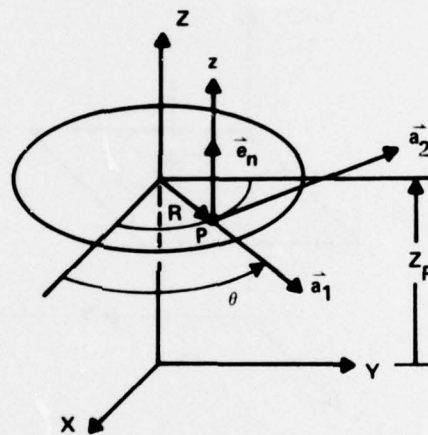


FIGURE E.4 PLATE REFERENCE SURFACE IN POLAR COORDINATES

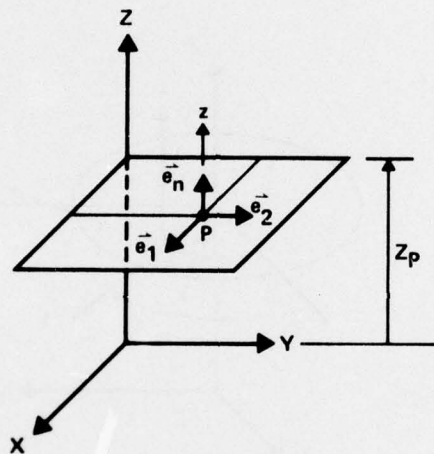


FIGURE E.5 PLATE REFERENCE SURFACE IN CARTESIAN COORDINATES



## REFERENCES

1. Melosh, R. J., "Development of the Stiffness Method to Define Bounds on Elastic Behavior of Structures," Ph.D. Thesis, University of Washington, Seattle, Washington, 1962.
2. McLay, R. W., "An Investigation Into the Theory of the Displacement Method of Analysis for Linear Elasticity," Ph.D. Thesis, University of Washington, Seattle, Washington, 1963.
3. Fraeijis de Veubeke, B. M., Editor, "Matrix Methods of Structural Analysis," AGARDograph 72, Pergamon Press Limited, Oxford, 1964.
4. Key, S. W., "A Convergence Investigation of the Direct Stiffness Method," Ph.D. Thesis, University of Washington, Seattle, Washington, 1966.
5. Johnson, M. W., Jr. and McLay, R. W., "Convergence of the Finite Element Method in the Theory of Elasticity," J. Applied Mechanics, Ser. E, Vol. 35, No. 2, 1968.
6. Dunne, P. C., "Complete Polynomial Displacement Fields for Finite Element Method," Aeron. J. Roy. Soc., Vol. 72, 1968.
7. Arantes e Oliveira, E. R. de, "Completeness and Convergence in the Finite Element Method," Proc. 2D Conf. Matrix Methods Struct. Mech., AFFDL-TR-68-150, Dec. 1969.
8. Hartung, R. F., "An Assessment of Current Capability for Computer Analysis of Shell Structures," AFFDL-TR-71-54, Apr. 1971.
9. Hartung, R. F. and Ball, R. E., "A Comparison of Several Computer Solutions to Three Structural Shell Analysis Problems," AFFDL-TR-73-15, Apr. 1973.
10. Oden, J. T., "Finite Elements of Non-Linear Continua," McGraw Hill Book Company, New York, 1972.
11. Argyris, J. H. and Kelsey, S., "Energy Theorems and Structural Analysis," Butterworths Scientific Publications, London, 1960.

12. Turner, M. J., Clough, R. W., Martin, H. C. and Topp, L. J., "Stiffness and Deflection Analysis of Complex Structures," J. Aeronaut. Sci., Vol. 23, Sep. 1956.
13. Clough, R. W., "The Finite Element Method in Plane Stress Analysis," J. Structural Division, ASCE, Proceedings of 2nd Conference on Electronic Computation, 1960.
14. Gallagher, R. H., "A Correlation Study of Methods of Matrix Structural Analysis," AGARDograph 69, Pergamon Press Limited, Oxford, 1964.
15. Przemieniecki, J. S., Et.Al., Editors, "Matrix Methods in Structural Mechanics - Proceedings of the Conference Held at Wright-Patterson Air Force Base, Ohio 26-28 October 1965," AFFDL-TR-66-80, Nov. 1966.
16. Berke, L., Et.Al., Editors, "Proceedings of the Second Conference on Matrix Methods in Structural Mechanics," AFFDL-TR-68-150, Dec. 1969.
17. Rowan, W. H. and Hackett, R. M., Editors, "Proceedings of the Symposium on Application of Finite Element Methods in Civil Engineering, Vanderbilt University, November 13-14, 1969," American Society of Civil Engineers, 1969.
18. Fraeijis de Veubeke, B. M., Editor, "Proceedings of IUTAM Symposium on High-Speed Computing of Elastic Structures," Liege, Belgium, Aug. 1970.
19. Hartung, R. F., Editor, "Computer Oriented Analysis of Shell Structures - Proceedings of a Conference Held at Lockheed Missiles and Space Company, Palo Alto, California, August 10-14, 1970," AFFDL-TR-71-79, Jun. 1971.
20. Bader, R. M., Et.Al., Editors, "Proceedings of the Third Conference on Matrix Methods in Structural Mechanics," AFFDL-TR-71-160, Dec. 1973.
21. Fenves, S. J., Et.Al., Editors, "Numerical and Computer Methods in Structural Mechanics - Proceedings of the Conference Held at Urbana, Illinois, September 8-10, 1971," Academic Press, Inc., New York, 1973.

22. Pilkey, W., Et.Al., Editors, "Structural Mechanics Computer Programs: Surveys, Assessments and Availability (Proceedings of a Symposium Held at the University of Maryland, June 1974)," University Press of Virginia, Charlottesville, 1974.
23. Zienkiewicz, O. C. and Cheung, Y. K., "The Finite Element Method in Structural and Continuum Mechanics," McGraw Hill Publishing Company Limited, London, 1968.
24. Zienkiewicz, O. C., "The Finite Element Method in Engineering Science," McGraw Hill Publishing Company Limited, London, 1971.
25. Oden, J. T., Clough, R. W., and Yamamoto, Y., Editors, "Advances in Computational Methods in Structural Mechanics and Design (Proceedings of 2nd U.S.-Japan Seminar on Matrix Methods of Structural Analysis and Design)," University of Alabama Press, Huntsville, Alabama, 1972.
26. Gallagher, R. H., "Finite Element Analysis: Fundamentals," Prentice-Hall, Inc., Englewood Cliffs, New Jersey, 1974.
27. Fung, Y. C., "Foundations of Solid Mechanics," Prentice Hall, Inc., Englewood Cliffs, New Jersey, 1965.
28. Irons, B. M., "Engineering Application of Numerical Integration in Stiffness Method," AIAA Journal, Nov. 1966.
29. Ergatoudis, I., Irons, B. M. and Zienkiewicz, O. C., "Curved, Isoparametric Quadrilateral Elements for Finite Element Analysis," Int. J. Solids Structures, Vol. 4, 1968.
30. Zienkiewicz, O. C., "Isoparametric and Allied Numerically Integrated Elements - A Review," Numerical and Computer Methods in Structural Mechanics, Academic Press Inc., 1973.
31. Ahmad, S., Irons, B. M. and Zienkiewicz, O. C., "Curved Thick Shell and Membrane Elements with Particular Reference to Axisymmetric Problems," Proc. 2nd. Conf. Matrix Methods Struct. Mech., AFFDL-TR-68-150, Dec. 1969.



32. Ahmad, S., Irons, B. M. and Zienkiewicz, "Analysis of Thick and Thin Shell Structures by Curved Finite Elements," Int. J. Num. Methods in Eng., Vol. 2, 1970.
33. Gallagher, R. H., "Analysis of Plate and Shell Structures," Proc. Symp. Application Finite Element Method in Civil Engr., ASCE, 1969.
34. Gallagher, R. H., "Applications of Finite Element Analysis," Proc. 2nd U.S.-Japan Seminar on Matrix Methods Struct. Anal. and Design, Univ. Alabama Press, Huntsville, 1972.
35. Melosh, R. J. and Christiansen, H. N., "Structural Analysis and Matrix Interpretive System (SAMIS) Program: Technical Report," JPL Technical Memorandum No. 33-311, Nov. 1966.
36. Lang, T. E., "Structural Analysis and Matrix Interpretive System (SAMIS) User Report," JPL Technical Memorandum No. 33-305, Mar. 1967.
37. McNeal, R. H., Editor, "The NASTRAN Theoretical Manual," NASA SP-221(01), Dec. 1972.
38. McCormick, C. W., Editor, "The NASTRAN User's Manual," NASA SP-222(01), Jun. 1972.
39. Batt, J. R. and Jordan, S., "MAGIC III: An Automated General Purpose System for Structural Analysis-Vol. I: Engineer's Manual," AFFDL-TR-72-42, Jul. 1972.
40. Jordan, S., and Batt, J. R., "MAGIC III: An Automated General Purpose System for Structural Analysis-Vol. II: User's Manual," AFFDL-TR-72-42, Jul. 1972.
41. Bathe, K. J. and Wilson, E. L., "Thick Shells," Structural Mechanics Computer Programs: Surveys, Assessments and Availability, University Press of Virginia, Charlottesville, 1974.
42. Pawsey, S. F. and Clough, R. W., "Improved Numerical Integration of Thick Shell Finite Elements," Int. J. Num. Methods in Eng., Vol. 3, 1971.
43. Zienkiewicz, O. C., Taylor, R. L. and Too, J. M., "Reduced Integration Techniques in General Analysis of Plates and Shells," Int. J. Num. Methods in



44. Wilson, E. L., Taylor, R. L., Doherty, W. P. and Ghaboussi, J., "Incompatible Displacement Models," Numerical and Computer Methods in Structural Mechanics," Academic Press, Inc., 1973.
45. Clough, R. W. and Johnson, C. P., "A Finite Element Approximation for the Analysis of Thin Shells," Int. J. of Solids Structures, Vol. 4, 1968.
46. Mebane, P. M. and Stricklin, J. A. "Implicit Rigid Body Motion in Curved Finite Elements," AIAA Journal, Vol. 9, No. 2, Feb. 1971.
47. Fonder, G. and Clough, R. W., "Explicit Addition of Rigid-Body Motions in Curved Finite Elements," AIAA Journal, Vol. 11, No. 3, Mar. 1973.
48. Stanton, E. L., "A Design Study for the Addition of Higher Order Parametric Discrete Elements to NASTRAN," NASA TM X-2637, Sep. 1972.
49. Stanton, E. L. and Palacol, E. L., "Anisotropic Parametric Plate Discrete Elements," McDonnell Douglas Astronautics Co. Paper WD 1656, Mar. 1972.
50. Dawe, D. J., "Curved Finite Elements in the Analysis of Shell Structures," Vol. 5, Part J, Proc. First Int. Conf. on Struct. Mech. in Reactor Technology, Berlin, 1971.
51. Bogner, F., Fox R. and Schmit, L., "A Cylindrical Shell Discrete Element," AIAA Journal, Vol. 5, No. 4, Apr. 1967.
52. Cantin, R. and Clough, R., "A Curved Cylindrical Shell Discrete Element," AIAA Journal, Vol. 6, No. 5, May 1968.
53. Olson, M. and Lindberg, G., "Vibration Analysis of Cantilevered Curved Plates Using a New Cylindrical Shell Finite Element," Proc. 2nd Conf. Matrix Methods Struct. Mech., AFFDL-TR-68-150, Dec. 1969.
54. Yang, T. Y. and Kim, H. W., "Asymmetrical Bending and Vibration of a Conical Shell Finite Element," Purdue Univ. Tech. Report No. 73-5-2, May 1973.
55. Connor, J. and Brebbia, C., "Stiffness Matrix for Shallow Rectangular Shell Element," Proc. ASCE, J. Engr. Mech. Div., No. EM2, Apr. 1968.

56. Bergan, P. G. and Clough, R. W., "Large Deflection Analysis of Plates and Shallow Shells Using the Finite Element Method," Int. J. Num. Methods in Engr., V. 5, 1973.
57. Gallagher, R. H., "The Development and Evaluation of Matrix Methods for Thin Shell Structural Analysis," Ph.D. Thesis, State University of New York, Buffalo, New York, 1966.
58. Gallagher, R. H. and Yang, H., "Elastic Instability Predictions for Doubly Curved Shells," Proc. 2nd. Conf. Matrix Methods Struct. Mech., AFFDL-TR-68-150, Dec. 1969.
59. Greene, B., Jones, R. and Strome, D., "Dynamic Analysis of Shells Using Doubly-Curved Finite Elements," Proc. 2nd Conf. Matrix Methods Struct. Mech., AFFDL-TR-68-150, Dec. 1969.
60. Wempner, G., Oden, J. T. and Kross, D., "Finite Element Analysis of Thin Shells," Proc. ASCE, J. Engr. Mech. Div., No. EM6, Dec. 1968.
61. Key, S. W. and Beisinger, Z., "The Analysis of Thin Shells With Transverse Shear Strains by the Finite Element Method," Proc. 2nd Conf. Matrix Methods Struct. Mech., AFFDL-TR-68-150, Dec. 1969.
62. Key, S. W. and Beisinger, Z. E., "SLADE: A Computer Program for the Static Analysis of Thin Shells," Sandia Laboratories Report No. SC-RR-69-369, Nov. 1970.
63. Jones, R. F., "Shell and Plate Analysis by Finite Elements," Proc. ASCE, J. Struct. Div., No. ST5, May 1973.
64. Utku, S., "Stiffness Matrices for Thin Triangular Elements of Nonzero Gaussian Curvature," AIAA Journal Vol. 5, No. 9, Sep. 1967.
65. Strickland, G. and Loden, W., "A Doubly-Curved Triangular Shell Element," Proc. of 2nd Conf. on Matrix Methods in Struct. Mech., AFFDL-TR-68-150, Dec. 1969.
66. Bonnes, G., Dhatt, G., Giroux, Y. and Robichaud, L., "Curved Triangular Elements for the Analysis of Shells," Proc. of 2nd Conf. on Matrix Methods in Struct. Mech., AFFDL-TR-68-150, Dec. 1969.

67. Cowper, G. R., Lindberg, G. M. and Olson, M., "A Shallow Shell Finite Element of Triangular Shape," Int. J. Solids Structures, Vol. 6, Aug. 1970.
68. Dhatt, G., "Numerical Analysis of Thin Shells by Curved Triangular Elements Based on Discrete-Kirchoff Hypothesis," Proc. Symp. Application Finite Element Methods in Civil Engr., ASCE, 1969.
69. Argyris, J. H. and Scharpf, D., "The SHEBA Family of Shell Elements for the Matrix Displacement Method," Aeronaut. J., Oct. 1968.
70. Cowper, G. R., Lindberg, G. M. and Olson, M. D., "Comparison of Two High-Precision Triangular Finite Elements for Arbitrary Deep Shells," Proc. 3rd Conf. on Matrix Methods in Struct. Mech., AFFDL-TR-71-160, Dec. 1973.
71. Dupuis, G. and Goel, J., "A Curved Finite Element for Thin Elastic Shells," Int. J. Solids and Structures, Vol. 6, 1970.
72. Thomas, G. and Gallagher, R. H., "A Triangular Thin Shell Finite Element: Linear Analysis," NASA CR-1972.
73. Bushnell, D., "Thin Shells," Structural Mechanics Computer Programs: Surveys, Assessments and Availability, University Press of Virginia, Charlottesville, 1974.
74. Yates, D. N., Sable, W. W. and Vinson, T. J., "The DAISY Code," Numerical and Computer Methods in Structural Mechanics, Academic Press Inc., 1973.
75. Meijers, P., "Review of the ASKA Program," Numerical and Computer Methods in Structural Mechanics, Academic Press, Inc., 1973.
76. Chu, S. L., "Analysis and Design Capabilities of STRUDL Program," Numerical and Computer Methods in Structural Mechanics, Academic Press Inc., 1973.
77. Ayres, D. J., "Elastic-Plastic and Creep Analysis Via the MARC Finite Element Computer Program," Numerical and Computer Methods in Structural Mechanics, Academic Press Inc., 1973.



78. Courant, R., Friedrichs, K. and Lewy, H., "On the Partial Difference Equations of Mathematical Physics," Math. Ann., Vol. 100, 1928.
79. Forsythe, G. E. and Wasow, R. W., "Finite-Difference Methods for Partial Differential Equations," John Wiley and Sons, Inc. New York, 1960.
80. McNeal, R. H., "An Asymmetrical Finite Difference Network," Quart. Appl. Math., Vol. 11, 1953.
81. Williams, D., "An Introduction to the Theory of Aircraft Structures," Edward Arnold Publishers, Ltd., London, 1960.
82. Griffen, D. S. and Kellogg, R. B., "A Numerical Solution for Axially Symmetrical and Plane Elasticity Problems," Int. J. Solids Structures, Vol. 3, 1967.
83. Havner, K. S. and Stanton, E. L., "On Energy-Derived Difference Equations in Thermal Stress Problems," J. Franklin Inst., Vol. 284, Aug. 1967.
84. Bushnell, D. and Almroth, B. O., "Finite-Difference Energy Method for Nonlinear Shell Analysis," Computer Oriented Analysis of Shell Structures, AFFDL-TR-71-79, Jun. 1971.
85. Almroth, B. O., Brogan, F. A. and Pittner, E. V., "Buckling Analysis of Segmental Orthotropic Cylinders Under Nonuniform Stress Distribution," Lockheed Missiles and Space Company Report M-77-65-4, Vol. VIII, Jul. 1965.
86. Almroth, B. O. and Brogan, F. A., "Buckling of Cylinders with Cutouts," AIAA Journal, Vol. 8, No. 2, Feb. 1970.
87. Brogan, F. A., Forsberg, K. and Smith, S., "Experimental and Analytical Investigation of the Dynamic Behavior of a Cylinder with a Cutout " AIAA Paper No. 68-318, AIAA/ASME 9th Structures, Structural Dynamics and Materials Conference, Apr. 1968.
88. Brogan, F. A. and Stern, P., "Analysis of Stiffened Shells with Cutouts," Lockheed Missiles and Space Company Report N-3M-69-1, 1969.



89. Almroth, B. O., Brogan, F. A. and Marlowe, M. B.,  
"Collapse Analysis for Elliptic Cones," AIAA  
Journal, Vol. 9, Jan. 1971.
90. Almroth, B. O., Brogan, F. A. and Zele, F.,  
"Nosetip Design Analysis and Test (NDAT)  
Program-User's Manual for the STAGS Computer  
Code," SAMSO-TR-71-95, Dec. 1970.
91. Almroth, B. O., Brogan, F. A., Meller, E. and  
Zele, F., "User's Manual for the STAGS Computer  
Code," Lockheed Missiles and Space Company  
Report D266611, Apr. 1972.
92. Almroth, B. O., Brogan, F. A. and Marlowe, M. B.,  
"Collapse Analysis for Shells of General Shape,  
Volume I: Analysis," AFFDL-TR-71-8, Vol. I,  
Aug. 1972.
93. Almroth, B. O., Brogan, F. A., Meller, E., Zele, F.  
and Petersen, H. T., "Collapse Analysis for Shells  
of General Shape, Volume II: User's Manual  
for the STAGS-A Computer Code," AFFDL-TR-71-8,  
Vol. II, Mar. 1973.
94. Brogan, F. A. and Almroth, B. O., "Practical  
Methods for Elastic Collapse Analysis for  
Shell Structures," AIAA Paper No. 71-359,  
AIAA/ASME 12th Structures, Structural Dynamic  
and Materials, Conference, Apr. 1971.
95. Almroth, B. O. and Brogan, F. A., "Bifurcation  
Buckling as an Approximation of the Collapse  
Load for General Shells," AIAA Journal  
Vol. 10, Apr. 1972.
96. Almroth, B. O., Brogan, F. A. and Marlowe, M. B.,  
"Stability Analysis of Cylinders with Circular  
Cutouts," AIAA Journal, Vol. 11, Nov. 1973.
97. Almroth, B. O. and Felippa, C. A., "Structural  
Stability," Structural Mechanics Computer  
Programs: Surveys, Assessments and Availability,  
University Press of Virginia, Charlottesville,  
1974.
98. Almroth, B. O., Bushnell, D. and Sobel, L. H.,  
"Buckling of Shells of Revolution with Various  
Wall Constructions, Vol. 1 - Numerical Results,"  
NASA CR-1049, May 1968.

99. Bushnell, D., Almroth, B. O. and Sobel, L. H.,  
"Buckling of Shells of Revolution with Various  
Wall Constructions, Vol. 2 - Basic Equations  
and Method of Solution," NASA CR-1050, May 1968.
100. Bushnell, D., Almroth, B. O. and Sobel, L. H.,  
"Buckling of Shells of Revolution with Various  
Wall Constructions, Vol. 3-User's Manual for  
BOSOR," NASA CR-1051, May 1968.
101. Almroth, B. O. and Bushnell, D., "Computer Analysis  
of Various Shells of Revolution," AIAA Journal,  
Vol. 6, Oct. 1968.
102. Bushnell, D., "Nonlinear Analysis for Axisymmetric  
Elastic Stresses in Ring-Stiffened, Segmented  
Shells of Revolution," Proc. AIAA/ASME 10th  
Structures, Structural Dynamics and Materials  
Conference, New Orleans, Louisiana, Apr. 1969
103. Bushnell, D., "Analysis of Buckling and Vibration  
of Ring-Stiffened, Segmented Shells of  
Revolution," Int. Journal Solids Structures,  
Vol. 6, 1970.
104. Bushnell, D., "Stress, Buckling and Vibration  
of Prismatic Shells," AIAA Journal,  
Vol. 9, Oct. 1971.
105. Bushnell, D., "Analysis of Complex Shells of  
Revolution Under Combined Mechanical and  
Thermal Loads," AIAA Journal, Vol. 9  
Mar. 1971.
106. Bushnell, D., "Stress, Stability and Vibration of  
Complex Branched Shells of Revolution:  
Analysis and User's Manual for BOSOR4,"  
Lockheed Missiles and Space Company Report  
D243605, Mar. 1972.
107. Bushnell, D., "Effect of Ring Out-of-Plane Bending  
Stiffness on Thermal Buckling Prediction for  
Ring-Stiffened Cylinders," AIAA Journal,  
Vol. 9, Aug. 1972.
108. Bushnell, D., "Nonsymmetric Buckling of Cylinders  
with Axisymmetric Thermal Discontinuities,"  
AIAA Journal, Vol. 11, Sep. 1973.
109. Bushnell, D., "Evaluation of Various Analytical Models  
for Buckling and Vibration of Stiffened Shells,"  
AIAA Journal, Vol. 11, Sep. 1973.

110. Johnson, D. E., "A Difference-Based Variational Method for Shells," Int. Journal Solids Structures, Vol. 6, 1970.
111. Jensen, P. S., "Finite Difference Techniques for Variable Grids," Computer Oriented Analysis of Shell Structures, AFFDL-TR-71-79, Jun. 1971.
112. Forsberg, K. J., "An Evaluation of Finite Difference and Finite Element Techniques for Analysis of General Shells," Proc. IUTAM Conf. on High Speed Computing of Elastic Structures, Liege, Belgium, Aug. 1970.
113. Loden, W. A., "User's Manual for the REXBAT Program," Lockheed Missiles and Space Company Report 6-80-70-24, Aug. 1970.
114. Bushnell, D., "Finite Difference Energy Models Versus Finite Element Models: Two Variational Approaches in One Computer Program," Numerical and Computer Methods in Structural Mechanics, Academic Press Inc., 1973.
115. Green, A. E. and Zerna, W., "Theoretical Elasticity," Clarendon Press, Oxford, 1954.
116. Sokolnikoff, I. S., "Tensor Analysis, Theory and Applications to Geometry and Mechanics of Continua," John Wiley and Sons, Inc., New York, 1951.
117. Sanders, J. L., Jr., "Nonlinear Theories for Thin Shells," Harvard University Technical Report No. 10, Feb. 1961.
118. Oden, J. T., "Calculation of Stiffness Matrices for Finite Elements of Thin Shells of Arbitrary Shape," AIAA Journal, May 1968.
119. Langhaar, H. L., "Energy Methods in Applied Mechanics," John Wiley and Sons, Inc., New York, 1962.
120. Zudans, Z., "New Formulation and Evaluation of Elastic Shell Theory," Ph.D. Thesis, University of Pennsylvania, Philadelphia, Pennsylvania, 1966.
121. Reuter, R. C., Jr., "Concise Property Transformation Relations for an Anisotropic Lamina," J. Composite Materials, Apr. 1971.



122. Rivello, R. M., "Theory and Analysis of Flight Structures," McGraw Hill Book Company, New York, 1969.
123. Archer, J. S., "Consistent Mass Matrix for Distributed Mass Systems," Proc. ASCE, Vol. 89, Aug. 1963.
124. Timoshenko, S. and Goodier, J. N., "Theory of Elasticity," McGraw-Hill Book Company, New York, 1951.
125. Clough, R. W. and Tocher, J. L., "Finite Element Stiffness Matrices for Analysis of Plate Bending," Matrix Methods in Structural Mechanics, AFFDL-TR-66-80, Nov. 1966.
126. Rai, I. S. and Sandhu, R. S., "Finite Element Analysis of Anisotropic Plates Using Q-19 Element," AFFDL-TR-74-120, Part I, Oct. 1974
127. Clough, R. W. and Fellippa, C. A., "A Refined Quadrilateral Element for Analysis of Plate Bending," 2D Conf. Matrix Methods Struct. Mech., AFFDL-TR-68-150, Dec. 1969.
128. Timoshenko, S. and Woinowsky-Krieger, S., "Theory of Plates and Shells," McGraw-Hill Book Company, New York, 1959.
129. Lekhnitski, S. G., "Anisotropic Plates," Gordon and Breach, Science Publishers, New York, 1968.
130. Fortier, R. C., "A Study Into the Behavior of Unsymmetrically Layered Anisotropic Plates," Ph.D. Thesis, Northeastern University, Boston, Massachusetts, 1972
131. Gilliam, P. "Thermal Stresses in an Orthotropic, Nonhomogeneous Thin Shell of Revolution," TRW Inc., Informal Technical Memorandum, Mar. 1972.
132. Van Dyke, P., "Stresses About a Circular Hole in a Cylindrical Shell," AIAA Journal, Vol. 3, No. 9, Sep. 1965.
133. Lekkerkerker, J. G., "Stress Concentration Around Circular Holes in Cylindrical Shells," Proc. Eleventh Int. Congress Applied Mechanics, Springer-Verlag, Berlin, 1964.



## DISTRIBUTION LIST

	<u>Copies</u>
AVCO Corporation 201 Lowell Street Wilmington, Massachusetts 01887 Attn: Dr. D. E. Johnson	1
Dr. A. A. Pallone	1
Advanced Ballistic Missile Defense Agency Commonwealth Building 1300 Wilson Boulevard Arlington, Virginia 22209 Attn: Mr. V. Kupelian	1
Aeronautical Research Associates of Princeton, Inc. 50 Washington Road Princeton, New Jersey 08540 Attn: Dr. T. McDonough	1
Aerospace Corporation P.O. Box 92957 Los Angeles, California 90009 Attn: Mr. D. Geiler	1
Mr. R. Hallse	1
Mr. J. McClelland	1
Dr. E. Meyer	1
Mr. R. Mortensen	1
Army Ballistic Research Laboratories Aberdeen Proving Ground, Maryland 21005 Attn: Dr. W. J. Gillich	1
Dr. N. J. Huffington, Jr.	1
Mr. E. Quigley	1
Army Materials and Mechanics Research Center Watertown, Massachusetts 92172 Attn: Mr. J. F. Dignam	1
Aerotherm-Acurex Corporation 485 Clyde Avenue Mountain View, California 94040 Attn: Dr. D. Baker	1
Air Force Flight Dynamics Laboratory Wright Patterson Air Force Base, Ohio 45433 Attn: Mr. R. Bader	1
MR. J. Johnson	1

NSWC/WOL/TR 76-66

Air Force Materials Laboratory	
Wright-Patterson Air Force Base, Ohio 45433	
Attn: Mr. T. Cooper (MXA)	1
Dr. W. Kessler (MBC)	1
Mr. C. Pratt (MXS)	1
Mr. D. Schmidt (MBC)	1
Air Force Office of Scientific Research	
Building 410	
Bolling Air Force Base, Washington, D.C. 20332	
Attn: Mr. W. J. Walker	1
Air Force Weapons Laboratory	
Kirtland Air Force Base	
Albuquerque, New Mexico 87117	
Attn: LTCOL D. Ericson	1
Battelle Columbus Laboratories	
505 King Avenue	
Columbus, Ohio 43201	
Attn: Dr. M. Lemcoe	1
Dr. H. D. Moran	1
Mr. B. R. Noton	1
Office of the Chief of Naval Operations	
Department of the Navy	
Washington, D. C. 20350	
Attn: Mr. R. Blaise (OP-620E)	1
Office of the Chief of Naval Research	
800 North Quincy Street	
Arlington, Virginia 22217	
Attn: Dr. N. Perrone (Code 439)	1
Office of the Chief of Research and Development	
Department of the Army	
Washington, D. C. 20310	
Attn: Dr. J. Bryant (DARS-ARS-PM)	1
Defense Documentation Center	
Cameron Station	
Alexandria, Virginia 22314	12
Director, Defense Nuclear Agency	
Washington, D. C. 20305	
Attn: Mr. J. Moulton	1
Effects Technology, Inc.	
P.O. Box 30400	
5383 Hollister Avenue	
Santa Barbara, California 93105	
Attn: Mr. J. Green	1
Dr. R. F. Parisse	1

Embassy of Australia  
1601 Massachusetts Avenue  
Washington, D. C. 20036  
Attn: Dr. G. A. Morgan 1

General Electric Company  
Re-entry & Environment Systems Division  
Valley Forge Space Center  
P.O. Box 8555  
Philadelphia, Pennsylvania 19101  
Attn: Mr. A. Garber 1  
Mr. H. R. Minnich 1

ITT Research Institute  
10 West 35th Street  
Chicago, Illinois 60616  
Attn: Mr. S. Bortz 1

The Johns Hopkins University  
Applied Physics Laboratory  
8621 Georgia Avenue  
Silver Spring, Maryland 20910  
Attn: Mr. W. Caywood 1  
Mr. R. M. Rivello 1

Kaman Sciences Corporation  
1700 Garden of the Gods Road  
Colorado Springs, Colorado 80907  
Attn: Mr. F. Barberra 1

Lockheed Missiles & Space Company, Inc.  
3251 Hanover Street  
Palo Alto, California 94304  
Attn: Dr. D. Bushnell 1  
Dr. R. F. Hartung 1

Lockheed Missiles & Space Company, Inc.  
P.O. Box 504  
1111 Lockheed Way  
Sunnyvale, California 94088  
Attn: Mr. A. Mietz 1  
Mr. R. Teter 1

Los Alamos Scientific Laboratory  
Los Alamos, New Mexico 87544  
Attn: Dr. J. Taylor 1

Martin-Marietta Corporation  
Orlando Division  
P.O. Box 5837  
Orlando, Florida 32805  
Attn: Mr. G. Fotieo 1  
Mr. L. Kinnaird 1

Materials Sciences Corporation  
Blue Bell Office Campus  
Merion Towle Building  
Blue Bell, Pennsylvania 19422  
Attn: Dr. W. Rosen

1

McDonnell Douglas Astronautics Company  
5301 Bolsa Avenue  
Huntington Beach, California 92647  
Attn: Mr. L. Greszczuk  
Mr. J. Jortner  
Dr. J. C. Peck  
Dr. R. Reck  
Mr. F. Stone

1  
1  
1  
1  
1

McDonnell Douglas Astronautics Company  
1136 Washington Boulevard  
St. Louis, Missouri 63166  
Attn: Mr. R. L. Johnson

1

NASA Goddard Space Flight Center  
Greenbelt, Maryland  
Attn: Dr. J. B. Mason  
Dr. W. Case

1  
1

NASA Langley Research Center  
Hampton, Virginia 23665  
Attn: Dr. R. Anderson (MS-188)  
Dr. P. Cooper (MS-208)  
Dr. A. K. Noor (MS-362)  
Dr. J. P. Raney  
Mr. W. B. Stephens (MS-190)  
Dr. D. Weidman (MS-188C)

1  
1  
1  
1  
1  
1

National Aeronautics and Space Administration  
Scientific and Technical Information Facility  
P.O. Box 33  
College Park, Maryland 20740

1

Commander, Naval Air Systems Command  
Department of the Navy  
Washington, D. C. 20361  
Attn: Mr. W. Volz (AIR-320C)

1

Director, Naval Research Laboratory  
Washington, D. C. 20375  
Attn: Dr. P. Mast  
Dr. I. Wolock

1  
1



Commander  
 Naval Air Development Center  
 Warminster, Pennsylvania 18974  
 Attn: Dr. T. Hess 1  
       Dr. S. L. Huang 1  
       Dr. R. K. Lobb 1  
       Mr. T. Neu 1

Commander  
 David W. Taylor Naval Ship Research &  
 Development Center  
 Bethesda, Maryland 20034  
 Attn: Dr. B. Cuthill 1  
       Dr. G. Everstine 1  
       Mr. M. Hurwitz 1  
       Dr. R. F. Jones 1  
       Mr. J. McKee 1  
       Mr. P. Matula 1

Chief of Naval Material  
 Department of the Navy  
 Arlington, Virginia 20360  
 Attn: Dr. R. Allgier (MAT-0321) 1  
       Mr. S. Jacobson (MAT-03422) 1

Naval Postgraduate School  
 Monterey, California 93940  
 Attn: Dr. R. Ball 1

Commander  
 Naval Weapons Center  
 China Lake, California 93557  
 Attn: Mr. E. L. Jeter 1  
       Mr. J. Serpanos 1

Commander, Naval Sea Systems Command  
 Department of the Navy  
 Washington, D. C. 20362  
 Attn: Mr. M. Kinna (SEA-0352) 1  
       Mr. S. Marcus (SEA-03B0) 1  
       Mr. L. Pasiuk (SEA-03513) 1  
       Mr. G. Sorkin (SEA-035) 1

Commander  
 Naval Underwater Systems Center  
 New London, Connecticut 06320  
 Attn: Mr. A. Carlson 1

Nuclear Regulatory Commission 7920 Norfolk Avenue Bethesda, Maryland 20014 Attn: Dr. S. Klein (LMFBR)	1
Oak Ridge National Laboratory P.O. Box X Oak Ridge, Tennessee 37830 Attn: Dr. W. P. Eatherly	1
Philco-Ford Corporation Aeronutronic Division Ford Road Newport Beach, California 92663 Attn: Mr. W. Smallwood	1
Prototype Development Associates, Inc. 1740 Garry Avenue, Suite 201 Santa Ana, California 92705 Attn: Dr. J.G. Crose	1
Dr. J. McDonald	1
Dr. D. McGovern	1
Mr. J. Schutzler	1
Dr. E. Stanton	1
R & D Associates 525 Wilshire Boulevard Santa Monica, California 90403 Attn: Dr. A. Field	1
Sandia Laboratories P.O. Box 5800 Albuquerque, New Mexico 87115 Attn: Dr. S. Key	1
Dr. T. G. Priddy	1
SMU Institute of Technology Civil and Mechanical Engineering Dept. Dallas, Texas 75275 Attn: Dr. R. M. Jones	1
Office of the Secretary of Defense Director of Defense Research & Engineering Pentagon Washington, D. C. 20301 Attn: Mr. J. Persh (OAD/ET)	1
Director, Strategic Systems Project Office (PM-1) Department of the Navy Washington, D. C. 20376 Attn: SP-272	1

Southern Research Institute	
2000 Ninth Avenue, South	
Birmingham, Alabama 35205	
Attn: Mr. J. Koenig	1
Dr. C. D. Pears	1
Space & Missile System Organization	
Worldway Postal Center	
P.O. Box 92960	
Los Angeles, California 90045	
Attn: MAJ L. Hudak	1
MAJ J. McCormack	1
Project Manager, Trident Systems Project (CNM-PM2)	
Department of the Navy	
Washington, D. C. 20360	
Attn: Mr. J. L. Crone (PM-2-001)	1
TRW Systems Group	
One Space Park Boulevard	
Redondo Beach, California 90200	
Attn: Mr. J. Bird	1
Mr. A. Hausrath	1
Mr. R. Winje	1
University of California at Los Angeles	
Mechanics and Structures Department	
Los Angeles, California 90024	
Attn: Dr. S. B. Dong	1
University of Delaware	
Mechanical and Aerospace Engineering Dept.	
Newark, Delaware 19711	
Attn: Dr. J. R. Vinson	1
University of Maryland	
College Park, Maryland	
Attn: Dr. B. Berger (ENME)	1
Dr. P. Cuniff (ENME)	1
Dr. B. Donaldson (ENAE)	1
Dr. W. Fournery (ENME)	1
Dr. C. Heins (ENCE)	1
Dr. H. G. Schaeffer (ENAE)	1
Dr. W. Walston (ENME)	1
Dr. W. B. Widhelm (BSAD)	1
Dr. J. Yang (ENME)	1
Weiler Research, Inc.	
2672 Bayshore Frontage Road, Suite 524	
Mountain View, California 94040	
Attn: Dr. F. Weiler	1



TO AID IN UPDATING THE DISTRIBUTION LIST  
FOR NAVAL SURFACE WEAPONS CENTER, WHITE  
OAK LABORATORY TECHNICAL REPORTS PLEASE  
COMPLETE THE FORM BELOW:

TO ALL HOLDERS OF NSWC/WOL/TR 76-66  
by R. J. Edwards, Code WA-21

DO NOT RETURN THIS FORM IF ALL INFORMATION IS CURRENT

---

A. FACILITY NAME AND ADDRESS (OLD) (Show Zip Code)

---

NEW ADDRESS (Show Zip Code)

---

B. ATTENTION LINE ADDRESSES:

---

C.

☐ REMOVE THIS FACILITY FROM THE DISTRIBUTION LIST FOR TECHNICAL REPORTS ON THIS SUBJECT.

---

D.

NUMBER OF COPIES DESIRED \_\_\_\_\_



DEPARTMENT OF THE NAVY  
NAVAL SURFACE WEAPONS CENTER  
WHITE OAK, SILVER SPRING, MD. 20910

OFFICIAL BUSINESS  
PENALTY FOR PRIVATE USE, \$300

POSTAGE AND FEES PAID  
DEPARTMENT OF THE NAVY  
DOD 316



COMMANDER  
NAVAL SURFACE WEAPONS CENTER  
WHITE OAK, SILVER SPRING, MARYLAND 20910

ATTENTION: CODE WA-21